UNIVERSITY OF LIVERPOOL

Aqueous Phase Hydrogenation of

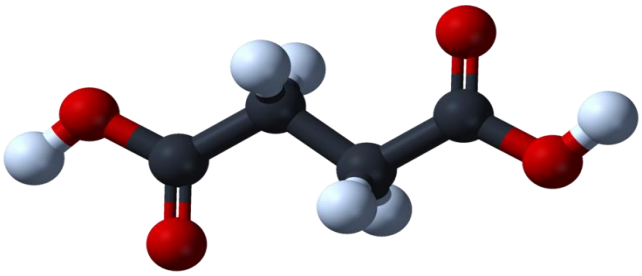

Succinic Acid

Using Mono- and Bi-metallic Ruthenium-Based Catalysts

Thesis submitted in accordance with the requirements of the University of Liverpool for the degree of Doctor of Philosophy

Ali Habib Bashal

March 2018

Acknowledgements

In the name of God, the Most Merciful

I would like to thank firstly Almighty God for giving me the opportunity and strength to do my research. Then there are many people who have supported me throughout my work at the University of Liverpool. Initially, I would like to express my wholeheartedly thanks to my supervisor, Professor Lopez-Sanchez for his hospitality, care, help, and guidance throughout this research. Tony, you are one of the secrets of my many achievements. I am grateful to both of my co-supervisors, professor Greeves and Dr. Priecel for their scientific help and unflinching support.

I want to thank every member of Professor Lopez-Sanchez group, past and present. To Monica, Joel, Azam, Nadiah, Liqaa, and Hammed, I owe them a great deal of gratitude for their help and supports, especially the first three, they're awesome. To Aldo and Scott my officemates, for their encouragement – it's been a pleasure! To David and Javier for their pleasant company outside of the university and making my time such an enjoyable and instructive inside the university. A very special thanks to Marco for his advice and motivation. Apart from JALS group members, I would like to thank Professors Kozhevnikov and Arnolds for their support while taking the introduction to catalysts and spectroscopy modules respectively. To my brother, Ahmad for his enormous help. To Dr. Deawson and Dr. Demmah for their help on characterizing my samples by TEM. Steven Moss is thanked for his massive help in HPLC analysis.

To my entire family for their patience and passion, I owe them every breath especially my father, Mr. Habib, and Mum. To all my teachers including Dr. Seraj, Dr. Awad, Dr. Muslim, and special appreciations goes to U.M.Mahdi Al-Tebir. Lastly, I would like to thank everyone who supported me in any way throughout my academic life and beyond. "And beware of a day in which you will be brought back to God. Then every soul shall be recompensed fully for what it has earned, and they will not be wronged." (Quran, Surah-Al Baqarah, Chapter 2: 281).

ABSTRACT

Most of the succinic acid hydrogenation in the literature have been done in high reaction conditions and with a help of organic solvent instead of a green solvent such as a water. Therefore, one of the main objectives of this study is to develop catalytic systems to improve reaction rates for the hydrogenation of succinic acid in water at mild reaction condition, also to find a promoter to affect the catalyst activity so that selectivity to 1,4-butanediol can be achieved.

The increasing social concern about environmental problems and energy demand have urged scientists to put their attention on the catalytic conversion of renewable biomass to produce various chemicals. Carboxylic acids, i.e., succinic acid can be obtained *via* fermentation of biomass. To produce significant chemicals from bio-renewable and low-cost carboxylic acids is highly desirable. The hydrogenation of carboxylic acids suffers from lack of selectivity so an active catalyst is needed to overcome those unwelcomed issues.

Diols have a massive demand in the plastic industries due to their use as monomers to produce polyesters. Diols are considered a significant product amongst other products (lactones and cyclic ethers). It is hard to target diols since undesired-straight chain alkanes, acids, and, alcohols are produced by over-hydrogenation and C-C cleavage reactions which affect the selectivity. The choice of a catalyst under suitable experimental conditions would shift the selectivity to the diols. Therefore, to fulfil the necessity towards these diols, more efficient catalysts have been developed in this thesis. We demonstrated the significance of the support in the hydrogenation of succinic acid using different metals. The potential of tin as a promoter towards the formation of diols from the hydrogenation of succinic acid and other biomass-derived acids was successfully achieved.

Liquid-phase hydrogenation of succinic acid was carried out over different reactors, high-pressure conventional batch and microwave reactors.

In the conventional reactor, the reaction conditions were optimized by varying the hydrogen pressure and reaction temperature to maximize the conversion of succinic acid and to avoid undesirable hydrogenolysis. Increasing the reaction pressure enhanced the hydrogenation activity and improved the yield of alcohols. Increasing temperature raised the rate of the reaction but negatively impacted the yield of the alcohols.

The location of Ru nanoparticles on carbon nanotubes (CNTs), as well as the support's properties, had significant effects on the catalytic performance. We have demonstrated that the catalytic performance of Ru catalysts is strongly support-dependent. CNTs were found to increase the reactivity of all tested supported metals (Ru, Pt, and Pd) in the hydrogenation of succinic acid in both reactors systems. However, the use of CNTs as supports for Ru produced significantly superior rates of reaction as compared to other supports such as activated carbon, silica or Al_2O_3. 5% Ru/CNT proved to be the best catalyst for this reaction and, at mild conditions (150 °C, 50 bar hydrogen), delivered 95.4 % conversion of succinic acid after 11 h in water. Furthermore, we reported for the first time that the use of pressurized microwave reactors resulted in a 3-fold reduction of the reaction time compared to the conventional heating reactor (pressure autoclave).

All catalysts were characterized by X-ray diffraction, temperature programmed reduction, electron microscopy, CO chemisorption and X-ray photoelectron spectroscopy to be able to understand the relationship between the structure-activity and selectivity. Based on the XPS results, it is suggested that the electronic promotional effect along with the high accessibility of pores in the carbon nanotubes seem to be responsible for the finer activity of the catalyst. No sign of crystalline phases of metallic Ru in all reduced Ru based catalysts was observed, suggesting that the Ru nanoparticles are too small to be characterized by XRD. Linked to XRD, analysis of the TEM images showed that Ru catalysts (AC and CNT-based) and Pt/CNT were well dispersed while Pd/CNT exhibited a bimodal distribution showing agglomeration to big particles between 6 and 13 nm apart from the small 2±0.7 nm nanoparticles.

On the other hand, the selectivity towards a single product remained an issue in both reactors but even more in the microwave reactor where less optimization work was carried out. At the completion of the reaction, the conventional reactor gave a combined yield of alcohols (1, 4-butanediol, *n*-propanol, *n*-butanol) of ~40 % whereas in the microwave reactor the yield drops to 18.2 %.

Future work will determine the reasons behind this, but at this stage, we could hypothseze that the local hot spots could be responsible. Therefore, as the second objective of this thesis, we worked towards the selectivity to 1,4-butanediol. A wide range of Ru/Sn bimetallic catalysts were prepared on carbon and CNTs and tested. We found that Sn could substantially increase selectivity at iso-conversion levels as compared to the monometallic analogue. The incorporation the Sn into the Ru-based catalyst (2% Sn-5% Ru/CNT) results showed the almost complete elimination of the unwanted C-C cleavage reactions, thus the percentage of C-C cleavage products obtained decreased from 100 % to 7.7 % in which the yield of 1,4-butanediol increased from 4 to ~80 %. Based on XPS and TPR results, envision the formation of a new type of active site, potentially Ru-Sn alloy on CNT which has a high impact to produce diols from the hydrogenation of different carboxylic acids.

The third objective of this thesis was to explore the activity of the Ru-Sn/CNT system to other hydrogenation reactions attempting to further capitalize in a combined higher selectivity offered by Ru-Sn while enhancing reactivity using CNTs as support. The system was very efficient in the production of adipic acid, caprolactone, and 1,6-hexanediol from the hydrogenation of cis,cis-muconic acid at 200 °C. High selectivity for these products was accomplished by altering the hydrogen pressure for the hydrogenation reaction. Also, the levulinic acid hydrogenation was successfully performed towards to 1,4-pentanediol using the same system.

Table of Contents

List of Figures

List of Tables

List of Schemes

List of Abbreviations

1,6-HDA	1,6-hexanediamine
2-Pyrr	2-Pyrrolidone
2-MTHF	2-methyltetrahydrofuran
AA	Adipic acid
ACAC	Acetylacetonate
BJH	Barrett-Joyner-Halenda
BET	Brunauer–Emmett–Teller
BDO	1,4-Butanediol
ECL	Caprolactone
DOE	Department of Energy
E. Coli	Escherichia Coli
GBL	Gamma-butyrolactone
GVL	Gamma-valerolactone
HAP	Hydroxyapatite
HDO	1,6-Hexanediol
HMF	5-Hydroxymethylfurfural
JCPDS	Joint Committee on Powder Diffraction Standards
ktpa	kilo tonnes per annum
LA	Levulinic acid
ccMA	cis,cis-Muconic acid
M.A.	Maleic Acid
M.Anh.	Maleic Anhydride
NMP	N-Methyl-2-Pyrrolidone
NPs	Nano-particles
PA	Pressure autoclave
PBT	Polybutylene terephthalate
PDO	1,4-pentanediol
PTMEG	Polytetramethylene ether glycol
PVC	Polyvinyl chloride
PVP	Polinylpyrrolidone
S	Selectivity
SA	Succinic Acid
THF	Tetrahydrofuran
TCA	Tricarboxylic acid
Y	Yield

CHAPTER 1

INTRODUCTION

Chapter 1: Introduction

This section contains some basic background information about catalysis and catalyst characterization techniques. Also, we summarise the previous literature on the hydrogenation of biomass-based acids.

1.1 Catalysis

1.1.1 Definition of Catalysis

The term catalysis was defined by Baron J. J. Berzelius in 1835.[1] In a catalytic role, the purpose of a catalyst is to increase the rate of reaction. The catalyst remains unchanged or consumed by a chemical reaction.[2] The catalyst will not allow a thermodynamically impossible reaction to proceed; thus, it does not affect the thermodynamics of a particular reaction. A catalyst lowers the activation energy, which is essential to initiate a chemical reaction *via* producing an alternative reaction pathway.[3] This effect is best understood using the potential energy diagram shown in **Figure 1.1**.

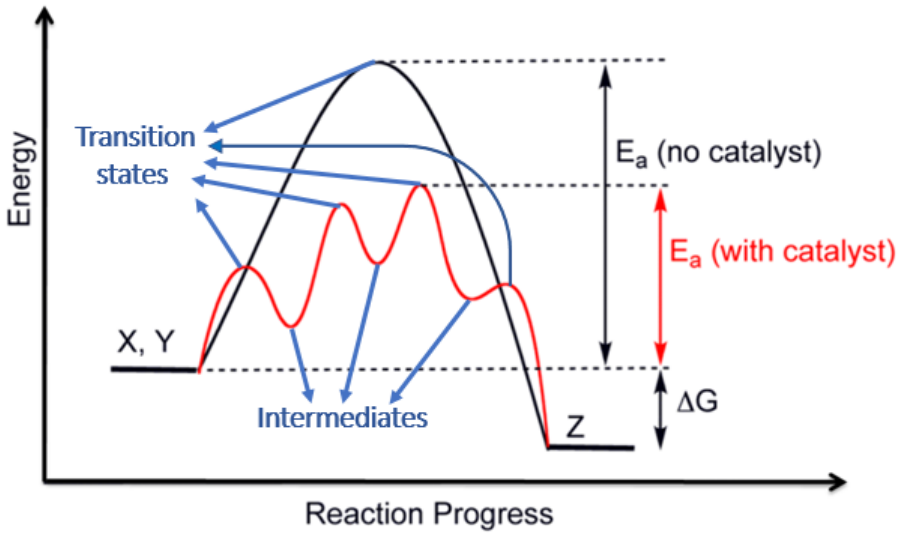

Figure 1.1. The effect of a catalyst on the activation energy of a reaction. X and Y represent the reactants and Z represents the product.[4]

Different transition state and intermediates are not found in non-catalysed reaction. Most of the chemical reactions that take place in human organisms are carried out by natural catalysts, known as enzymes. Catalysis plays a vital role in our life.[2]

1.1.2 Importance of the Catalysts and Hydrogen in Chemical Production

The majority of the products such as chemicals, pharmaceuticals, drinks, and foods that are being consumed in our daily life have been produced using at least a catalyst at some stage.[2] Catalysts are widely used in the chemical industry to decrease energy consumption and increase manufacture rate. A valuable and comprehensively applicable method for the reduction of chemical substances is catalytic hydrogenation. Molecular hydrogen (H_2) is a potential energy carrier in the green and clean energy-based economy, mostly to meet the demands of chemical processes, such as these required in a bio-refinery.[5] Currently, hydrogen is produced in large quantities by natural gas steam reforming.

1.1.3 Types of Catalysis

There are three types of catalysts, i.e., heterogeneous, homogeneous and enzymatic catalysts.[6]

- Homogeneous and Enzymatic Catalysts

A homogeneous catalyst is present in an identical phase (either liquid or gas) as the reactants and products. Enzymatic catalysts are a subgroup of homogeneous catalysis in which biological units are responsible for the catalysis.[7] The separation processes in homogeneous catalysis have to be enhanced since they are sometimes uneconomic and/or technically unachievable.[2]

Some of the homogeneous catalysts, e.g., sulfuric acid, require handling in corrosion-proof facilities whereas heterogeneous catalysts are non-corrosive in standard reactor units.[7] Under these circumstances, there is an increasing need for heterogeneous catalytic-driven processes where a catalyst is in the different phase from the reactants, typically solid.

- Heterogeneous Catalysts

Heterogeneous catalysts are easier to separate and recycle from the gas and/or liquid reactants and products. However, control of heterogeneous processes is complicated.[7,8] The heterogeneous catalytic reactions take place on the surface by breaking and forming bonds between the atoms of the catalyst surface and the reacting species.

1.1.4 The Surface Area of the Catalyst

The larger the surface area of the catalyst is, the greater the contact between the reactant and active sites. Thus, the rate of the reaction increase. This phenomenon has been shown by Ross for the situation of the reaction **A**+**B** → **P** as it is shown in **Figure 1.2**.[9]

A series of gas-phase collisions of molecules **A** and **B** occurred before approaching the solid catalyst. Molecule **A** arrives at the active surface, i.e., (metal crystallite embedded within a pore) when it reaches the solid (pore mouth). In fact, molecule **A** has to diffuse down the pore and will collides with both gas-phase molecules and with the walls of the pore; the relevant number of surface collisions depends on the reaction conditions (temperature and pressure) as well as those relative to gas-phase collisions will then correspond to the pore diameter.[9]

- What is Happening in the Catalyst Pores?

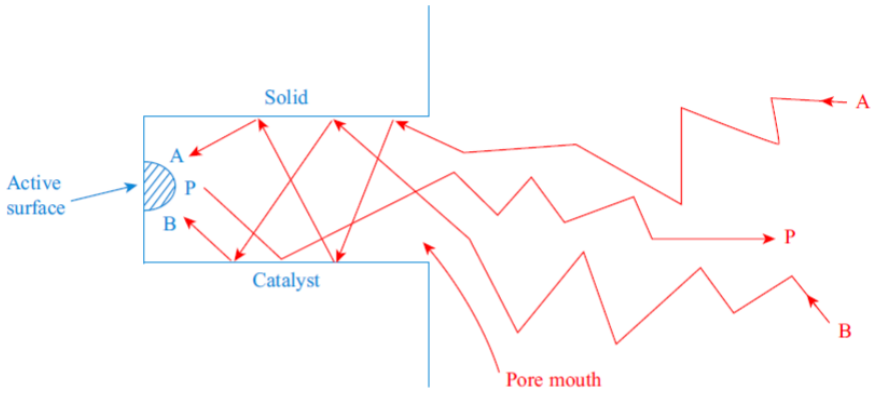

Figure 1.2. Schematic illustration the chemistry that happen at catalyst pore. Adopted directly from Ross book.[9]

Once adsorbed on the active surface, seven different steps are required to complete the process as presented in **Figure 1.3**.[8] In the first step, the diffusion of the reactants from a bulk fluid to the catalyst particle takes place, then in the second step the diffusion of the reactants over the catalyst intra-particle pores take place. Step (3) the adsorption of the reactants on the catalytic surface and step (4) reaction on the surface whereas steps 5, 6, and 7 including desorption and the diffusions of products.

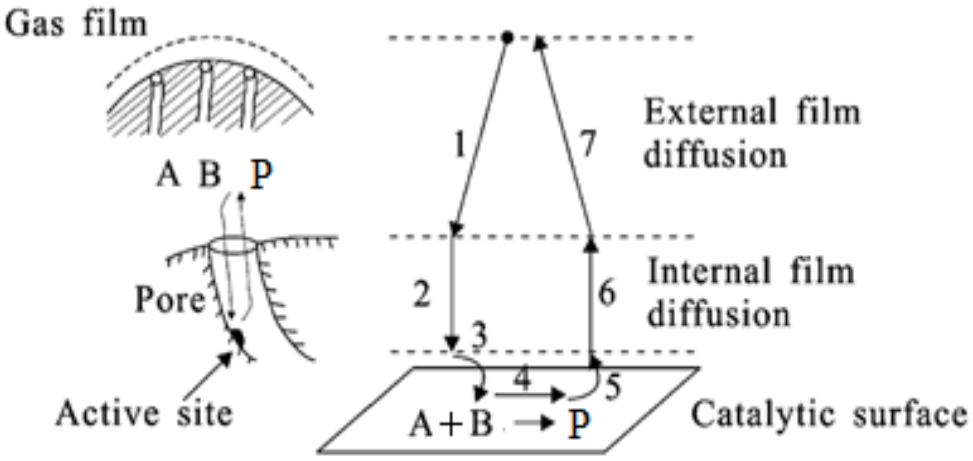

Figure 1.3. Steps in heterogeneous catalysis reaction. Adopted directly from Lin et al.[7] *and Bartholomew et al.*[10]

- What is Happening Inside the Catalyst Pores?

Molecule **A** can react with the corresponding species following from the diffusion and adsorption of molecule **B** to give adsorbed product **P**; **P** then desorbs and diffuse out from of the pore and away from the surface. Through the catalyst intra-particle pores (step six) the products diffuse into the bulk fluid (step seven).[8] The rate of the reaction may still depend on the rate of adsorption of **A** or **B**, by desorption of product **P** or on the surface reaction of **A** with **B**; nevertheless, the rate may be equally affected by the rates of diffusion (from or to) the surface and (out or into) of the pore. Therefore, for the highly active catalytic surface, the catalyst must have an easily accessible outer and inner surface.[9]

1.1.5 Heterogeneous Catalyst Components

The three main components of a heterogeneous catalyst are active sites, promoter, and the support.

1.1.5.1. Active Sites

The term of the active site in a heterogeneous catalyst can be visualized as the set of atoms that directly catalyses a given reaction. To improve the catalyst properties, it is important to understand the structure of the active site.[11] The activity of the catalyst depends on the active phase which is constituted of one or more chemical species. The active sites could be sensitive to the reaction conditions, as they are often dispersed in a support.[2]

1.1.5.2. The Promoter

The modifiers (additives) adjust the performance of real industrial catalysts.

When a modifier enhances the catalyst activity in terms of reaction rate per site, it is called a promoter. A promoter can be a second metal, non-inert support, oxide or other additive, which can vary the electronic and the geometric structure of the metal surface.[12] In most cases, not only high activity but also high selectivity is desired. The selectivity to some desired products can be improved by adding substances that limit unwanted reactions.[13]

- ## Bimetallic Catalysts

The term of bimetallic catalyst comes from combining the monometallic catalyst, which consists of a single metal element as the active component, with a second metal element. The chemical and electronic properties of bimetallic catalysts are regularly different from those of monometallic catalyst.[14] Long *et al.*[15] elucidated the difference in catalytic performances, concluding that they are caused by the change in electronic configuration structure of the metal crystallites upon adding the second metal element although their promotion effect can simply be the consequence of merely improving the dispersion of the metal so that active sites are more isolated. The promoter could help to avoid the deactivation of the catalyst. In methane combustion, for instance, it has been reported the activity of Pd/Al_2O_3 increased after introducing a prompter (Pt). The Pd catalysts exhibited larger particles growth than their bimetallic counterparts, which decrease the Pd dispersion and suppressed the catalytic activity.[16,17]

The advantages of bimetallic catalysts over monometallic catalysts in enhancing catalytic performance has received much attention from the chemical industry.[14] In many cases, bimetallic catalysts can be used to increase selectivity to a specific product. This will be discussed in Chapter 4.

1.1.5.3. Support

Supports are materials which play an essential role in heterogeneous catalysis by improving the dispersion of the active phase and therefore enhancing the contact between the catalyst active phase and the reaction substrate. The support in a heterogeneous catalyst will typically have high surface area, and suitable porosity. To enhance the heterogeneous catalyst's performance and stability, we could concentrate on the morphology and pores size of the selected support materials.[18]

The catalyst supports, i.e., silica, titania, alumina, and zirconia, are materials on which active metal nanoparticles are formed or deposited.[19] Matatov-Meytal and Sheintuch,[20] addressed that the primary functions of support which are: increasing the surface area, decreasing sintering, and improving the chemical stability of the catalytic material.[2] The interactions between the support's surface, solvent, and metal precursor during an impregnation step strongly affect the metal dispersion.[21] The surface area of the support should be large, which results in a high dispersion of an active phase. Highly porous support also might be useful to increase the rate of the reaction.[8]

Carbon has attracted much attention as a support due to its high surface area.[22,21] Catalysts supported on carbon have been used successfully in the liquid phase hydrogenation of succinic acid,[23] dehydrogenation of cyclohexane,[24] and many other reactions.[22,25]

1.1.5.3.1. Activated Carbon as a Support

The "activated" carbon (AC) used as support is mainly derived from naturally occurring materials such as coal, wood, and peat having a complex porous structure and the resulting high surface area may exceed 1000 m^2/g.[26] AC has the highest surface area compared to alumina, silica, zeolite, and carbon nantubes.[25,27] AC is extensively used for purification and separation of liquid phase mixtures.[28]

Aksoylu *et al.*[29] suggested that AC has all the essential characteristics to be used as a catalyst support.[29] In the past, limited applications of carbon as a catalyst support were reported because of the lack of understanding of numerous aspects related to AC in supported catalysts. Further investigations have allowed a determination of all the chemical and physical characteristics of carbon material, especially for AC (porosity and surface area).[30] Depending on the preparation conditions and feedstock, an extreme degree of different porosity of AC can be established.

- ## Activated Carbon Structure

The AC structural heterogeneity is due to of the presence of micropores, mesopores, and macropores with different shapes and sizes. Furimsky addressed that the wood-derived AC possesses a sizeable macroporous structure (>50 nm), while the coal-based AC can adsorb high molecular weight substances due to its suitable mesoporosity (2−50 nm), whereas microporous AC (<2 nm) can be prepared from the nut-shells.[31] **Figure 1.4** presents 3 different (pore size) of carbon, the microporous, mesoporous, and macroporous structure.[29]

The morphology of the supports are considered to be the significant factors in promoting a high dispersion of nanoparticles, influencing the performance of the catalyst.[32] Recently, carbon nanotubes (CNTs) have been shown as essential materials for catalysts as a support.[33] CNTs based catalysts appear to compete with activity of AC based catalyst although CNTs have less surface area.[34]

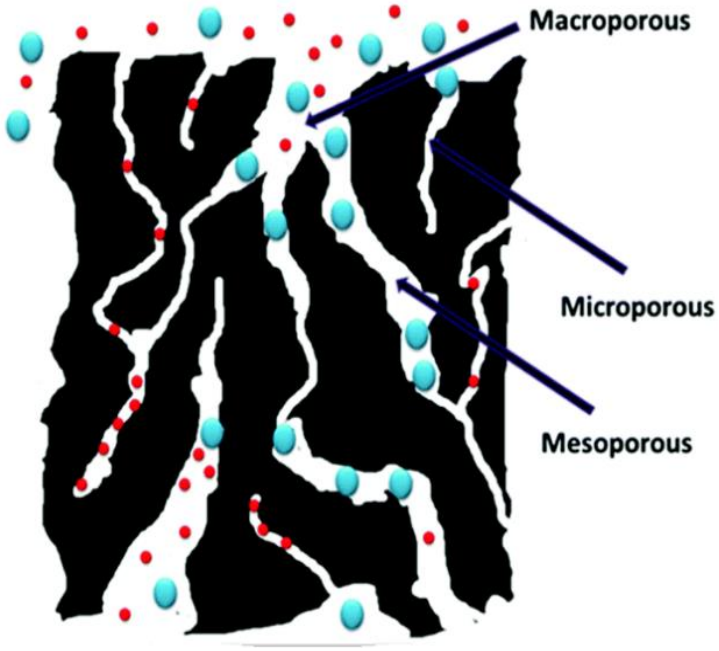

Figure 1.4. A structural scheme for an activated carbon, which contains highly disordered micropores, mesoporous, and macropores. Adopted directly from Li et al.[35]

1.1.5.3.2. Carbon Nanotubes as Catalyst Support

In the last decade, much attention has been given to carbon-derived nano-structured materials. The new forms of carbon such as carbon nanofibers and CNTs have revealed a great potential as catalyst supports.[36] CNTs were firstly synthesised by Davis, Slawson, and Rigby in 1953,[37] and their physical properties mainly resembled those of graphene. In graphene, carbon atoms are tightly organised in a regular sp^2-bonded atomic-scale honeycomb (hexagonal) pattern. Moreover, this pattern is a basic structure for other sp^2 carbon bonded materials (allotropes) such as carbon nanotubes and fullerenes.[36] Graphene known as the "mother" of all allotropes, as shown in **Figure 1.5**, where it is observed that graphite is stacked graphene, fullerenes are wrapped graphene, and nanotubes are rolled graphene.[25]

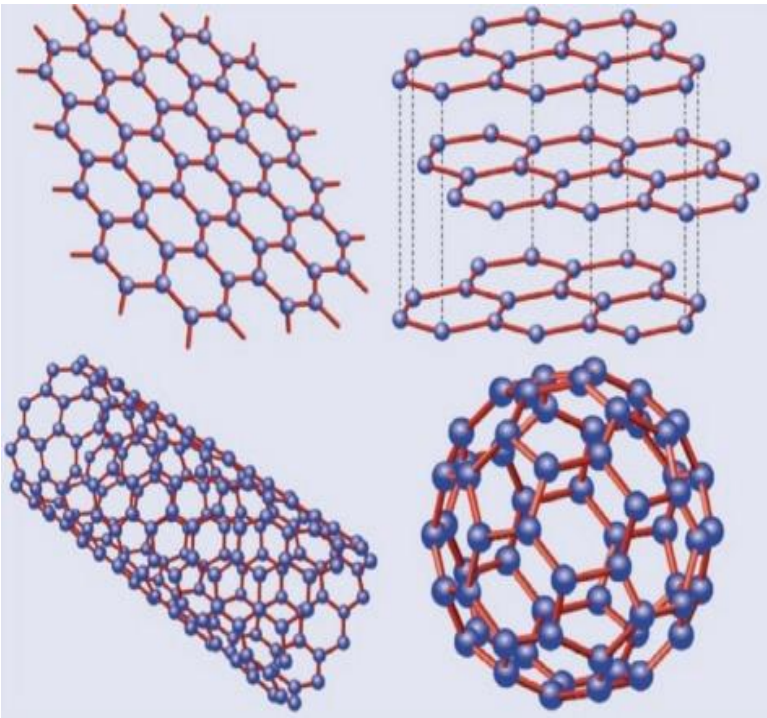

Figure 1.5. Carbon allotropes. Top left: Graphene; Top right: Graphite (stacked graphene); bottom left: nanotube (rolled graphene); bottom right: fullerene (graphene wrapped up in bucky-balls). Adopted directly from Castro Neto.[38]

CNTs can be subdivided into two classes: single-walled nanotubes (SWCNTs) and multi-walled nanotubes (MWCNTs).[39] The SWCNTs have diameters between 0.4 and 2 nm while the MWCNTs have diameters between 2–100 nm.[40] The interlayer spacing between graphitic layers in MWCNTs is 0.34 nm.[41] These concentric nanotubes are held together with relatively weak van der Waals bonding.[25] The walls of CNTs are shaped by a hexagonal lattice of carbon atoms. Each atom is connected to three neighbouring atoms, forming sp^2 bonding. Thus, the nanotubes are stronger than diamond since the diamond structure has weaker sp^3 bonds.[42]

1.1.5.3.2.1. Production of Carbon Nanotubes

Several methods have been used for the synthesis of CNTs. We will discuss the main techniques along with some of the benefits and drawbacks of each technique for manufacturing CNTs.

The primary three systems are arc discharge, laser ablation, which is considered a physical process, and chemical vapor deposition, which is a chemical process.[42]

- Arc Discharge

The arc discharge is the simplest and most widespread method to manufacture CNTs which was prepared by Lijima in 1991. However, it required very high processing temperature (3000–4000 °C), which can lead to CNTs with few structural defects.[42]

- Laser ablation

The laser-ablation (vaporisation) has been used to produce CNTs.[43] In a high-temperature reactor, the pulsed laser was used to strike at a graphite target in the presence of a small amount of cobalt, nickel in the presence of inert gas such as helium which vaporizes graphite target.[44] As vaporised carbon condenses, the nanotubes grow on the cooler surfaces of the reactor and, to collect the nanotubes, a water-cooled surface is used.[45] The production of CNTs with this method gives pure CNTs in high yield compared to the arc discharge method. However, the evaporation of the carbon source is quite limiting, and this prevents the scale-up to industrial manufacture.[42,46]

- Chemical Vapour Deposition

Chemical vapor deposition (CVD) is one of the most common technique to synthesise CNTs when aiming to control large-scale production. Several hydrocarbon sources have been studied for growing CNTs; such as acetylene, methane, and carbon monoxide.[47] A gas flow of the reactant such as ethylene is passed over transition metals like nickel, cobalt, and iron under inert gas at atmospheric pressure at ~700 °C.[45] Because of the saturation of carbon atoms on the metal particle site, the carbon precipitates, which then forms CNTs.

Among other synthesis methods, CVD is comparatively less energy intensive, which prompts a promising path to manufacture CNTs. Owing to a high purity of the CNTs, CVD is an economical and practical technique for their commercial production.[39,46] The comparisons between these methods are presented in **Table 1.1.**

Table 1-1. Comparisons of three major CNT synthesis techniques.[36]

Technique	Purity	Y, %	SWCNT/MWCNT	T, °C	Scalability
Arc discharge	Low purity but high quality	~60	Both	~4000	Laboratory-scale
Laser ablation	Relatively high	~90	SWCNT > MCWNT	~1200	Laboratory-scale
CVD	High	~90	MWCNT > SWCNT	500–700	Large-scale

Note: Y, yield; CNT, carbon nanotube; CVD, chemical vapor deposition; MWCNT, multiwall carbon nanotube; SWCNT, single-walled carbon nanotube Temp, temperature.

CNTs have turned out to be one of the most dynamic fields within nanotechnology and nanoscience due to their extraordinary properties which make them appropriate for numerous potential applications including electronic devices, reinforced materials, hydrogen storage, and catalysis.[48,49]

CNTs can be an attractive alternative to conventional supports for many reasons, including thermal stability; and the absence of microporosity (for MWCNT) which can eventually affect the catalytic activity.[25] Moreover, one of an important element in which the MWCNTs are considered to be a good support for catalysts is their inherently mesoporous structure. Their pore sizes allow for diffusion, reaction and desorption of chemical species.[50]

1.1.5.4. Catalysts Preparations Methods

The synthesis method has an impact on the structure, composition, morphology, dispersion, and the performance of the catalyst.[51] In order to achieve high performance and minimize the cost of the catalyst, high dispersion of the metal nanoparticles on a support needs to be accomplished.[52] Most of the preparation methods need filtering and washing, and some of those procedures are time-consuming and cause loss of noble metals.

Some methods also require the use of polymers or surfactants as stabilizers, but the elimination processes for these materials becomes problematic.[51] The impregnation method is one of the most common procedures employed,[18] which is a straightforward preparation method involving an impregnation step followed by a reduction with no need of washing or filtering steps.

Due to the ease and simplicity to control metal loading, this is a well-established catalyst preparation procedure. In this method, the volume of a solution including a precursor of an active phase of the catalyst is loaded on the solid support.

If the volume of the solution used is either less or equal to the pore volume of the support, the technique is described as “incipient wetness”. On the other hand, when an excess of solution is used, the technique is referred as “wet impregnation” where the excess solvent is removed by drying.[53]

1.2. State of the Art in the Catalytic Hydrogenation of Biomass Derived Acids

For over hundred years, chemical manufacturers have been using petroleum, coal, and natural gas to deliver the majority of industrial products, such as methane, ethylene, and alcohols.[54] Unfortunately, the burning of fossil resources increases the levels of CO_2 concentration in the earth atmosphere which has a direct effect on our global climate.[55] The emissions of carbon dioxide (CO_2), diminishing fossil supplies and unstable prices of the petro-derived raw materials have resulted with an urge to develop green and sustainable processes that can produce chemicals at a low cost, and an environmentally-friendly safe manner using renewable feedstocks.[56]

Nature offers a variety of plant resources, which represents a broad range of biomass feedstocks.[57] In ecology, biomass is the mass of living biological organisms in a specific area at a given time, and it contains microorganisms, animals or plants.[58] Biomass feedstocks can be categorised into: sugars (e.g., glucose, starch, etc.), lignocellulosic or woody biomass, triglycerides (e.g., vegetable oil), and living organisms. Lignocellulosic biomass is a source of carbon which could be used to manufacture renewable chemicals and liquid fuels.[59] Moreover, it is an inexpensive, abundant, and rapid growing form of biomass. Lignocellulose consists of three key building blocks (polymers): cellulose, hemicellulose and lignin,[7] as displayed in **Figure 1.13**

Cellulose is a long-chain structural component of glucose monomers connected by β-(1,4)-glycosidic bonds.[60] Hemicellulose is a polymer based on hexose (D-galactose, D-glucose, D-mannose) and pentose sugars (L-arabinose and D-xylose), whereas lignin is a polymer derived from coumaryl, coniferyl, and sinapyl alcohols.[60,61] Typically, lignocellulosic biomass contains around 35–50 % of cellulose, 25–30 % of hemicellulose, and 15–30 % of lignin.[62]

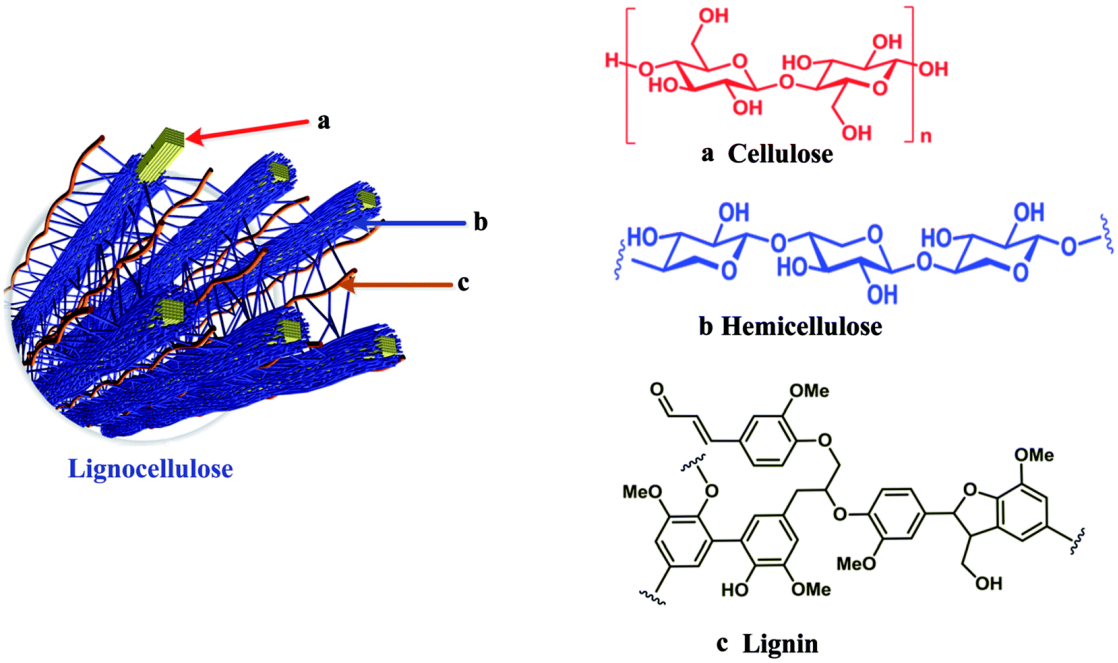

Figure 1.6. Lignocellulosic biomass, (a) cellulose, (b) hemicellulose and (c) lignin. Adopted directly from Sebayang et al.[60]

On an industrial scale, the enzymatic hydrolysis of starch is used to yield glucose.[63] The U.S. Department of Energy (DOE) identified sugars as an accessible chemical derived from the resultant biochemical transformations of lignocellulosic biomass (**Figure 1.14**).[64]

Catalytic conversion of the compounds (building blocks) mentioned above can give a variety of new chemicals. Specifically, hydrogenation of succinic acid (SA), levulinic acid (LA) and cis, cis-muconic acid (MA) are studied in the present work.

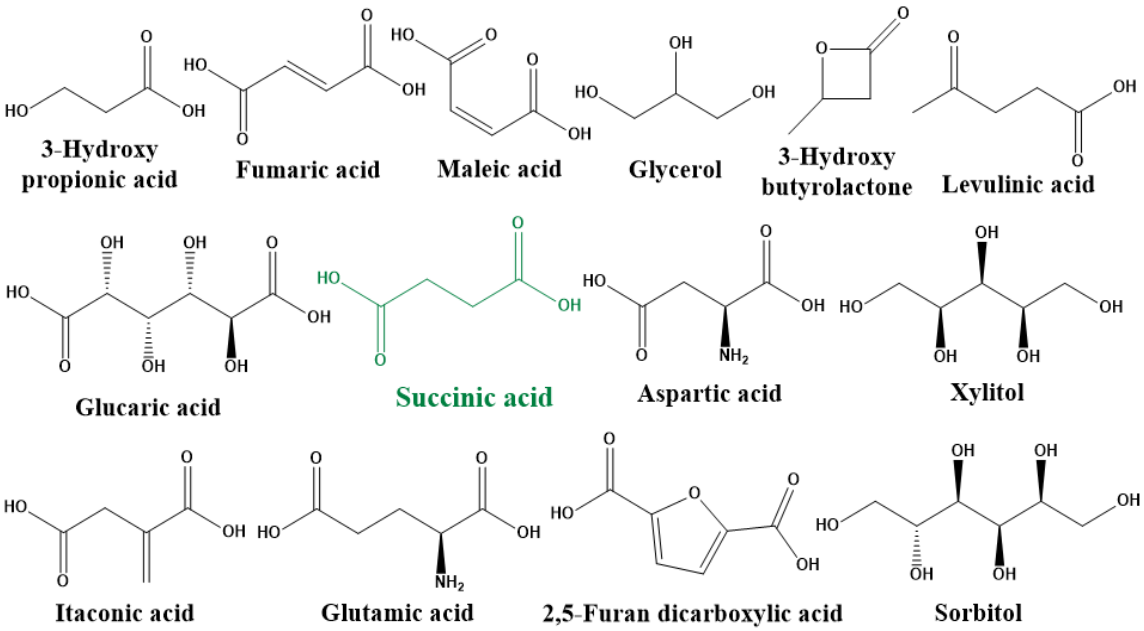

Figure 1.7. Department of Energy's top bio-based products from bio-refinery carbohydrates. Adopted from Werpy et al.[64]

1.2.1. Succinic Acid

Dicarboxylic acids are particularly well-known chemicals which can be manufactured by the biological and chemical treatment of biomass.[65] The ability to produce significant dicarboxylic acids from inexpensive and renewable biomass is exceptionally desirable.[66] Succinic acid is one of the most critical dicarboxylic acids. The name is derived from the Latin name "succinum" which means amber. Georgius Agricola isolated SA for the first time in 1546 *via* distillation of amber.[67] Very often succinic acid is also called amber or butanedioic acid.

Succinic acid is an odourless, colourless solid, soluble in water at room temperature. It plays a significant role in the metabolisms of numerous organisms.[68] Succinic acid is typically used in the food industry as it does not represent any health hazard on human metabolism as an additive.[69] Currently, the chemical industry mainly produces succinic acid from an oil. However, a fermentation route from biomass is a promising alternative.

1.2.1.1. Oil based Succinic Acid Production

Succinic acid is predominately manufactured from fossil resources by petrochemical processes. **Scheme 1.1** displays the oxidation of butane to maleic anhydride, followed by hydrogenation to succinic anhydride and further hydrolysis to succinic acid.

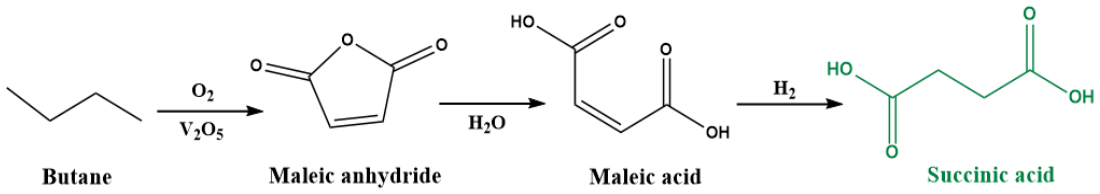

Scheme 1.1. Petroleum-derived of succinic acid.

Another possible route is *via* the hydration of maleic anhydride to maleic acid, followed by subsequent hydrogenation into SA.[70] The petrochemical process is a well-established technology which permits the manufacture of SA with insufficient yields.[71] However, SA synthesis from fossil resources might become unfavourable because of unstable oil prices manufacture of SA could be achieved through fermentation. Currently, there are several companies which commercialise bio-succinic acid using different organisms such as Myriant (USA), BioAmber (Canada), Reverdia (Netherlands), BASF-Purac JV (Spain) and Succinity (Germany).[72,73]

Using the DuPont license, BioAmber is scaling up the bio-succinic acid production in China in a joint venture with South Korean CJ CheilJedang Corporation to multi-ton capacity.[74,75] Some of the critical facts on microbial succinate fermentation are summarised in **Table 1.3**.[72]

Table 1-2. Industrial production of Succinic acid from biomass feedstock. Adopted from Becker et al.[72]

Company	Annual production capacity (plant site) [t/a]	Organism	Feedstock
Succinity	10,000 (Spain)	Basfia succiniciproducens	Glycerol
Myriant	13,600 (USA)	E. coli	Sorghum
BioAmber	3,000 (France, demonstration plant)	E. coli, Candida krusei	Corn
Reverdia	10,000 (Italy)	Saccharomyces cerevisiae	Starch

Bio-based SA production technology involves a fermentation step followed by recovery and purification steps. In the fermentation process, succinic acid is manufactured by microorganisms such as *Escherichia coli* and *A. succinogenes* using glucose as a fermentation feedstock.[64] The last steps consist of the elimination of impurities and conversion of succinate salts into a free acid form, followed by refining SA to its necessary purity, and crystallisation.[76]

Based on **Scheme 1.2**, during succinic acid manufacture, one mole of glucose and two moles of CO_2 are used to create two moles of succinic acid. The production of SA by these processes is beneficial as well since CO_2 is required as another substrate by microorganisms.[67]

This process is, therefore, a green process. Bio-succinate has been used successfully in pharmaceutical applications as well as a flavouring enhancer for low-sodium food.[77]

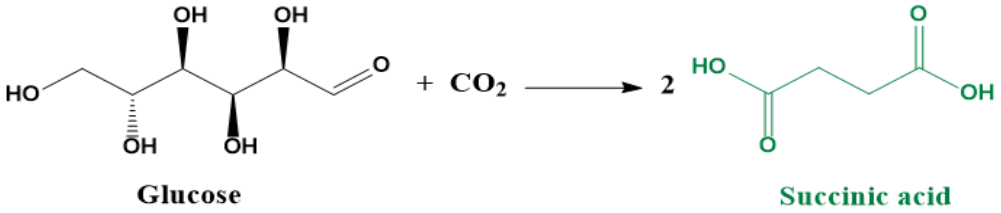

Scheme 1.2. Synthetic scheme of bio-based SA by fermentation.

Succinic acid has a variety of uses in industries such as food, chemicals, and plastics, besides, a wide range of derivatives can be produced from it. In the year 2011, the price of petroleum-based succinic acid was around USD 2,600 per metric tonnes whereas the bio-based succinic acid was nearly USD 3,000 per metric tonnes. However, the cost of bio-based succinic acid decreased to USD 2,860 per metric tonnes in 2013 onwards.[73] The global succinic acid market is expected to progressively grow at a compound annual growth rate of about 27.4 %, and it might reach $1.8 billion in 2025.[69]

Succinic acid could be an economical intermediate for the manufacture of numerous commodity chemicals. The market of succinic acid could be even broader if the production costs were lowered.[78] The most important group of possible succinic acid derivatives contains molecules synthesised *via* hydrogenation: tetrahydrofuran (THF), γ-butyrolactone (GBL) and 1, 4-butanediol (BDO). Beside these derivatives, there are other products which could be produced from succinic acid, such as 2-pyrrolidone, succinimide, maleic acid, butyric acid, butanol, and propanol.[79] **Figure 1.15** shows the potential routes to intermediates and specialty chemicals from succinic acid.[80]

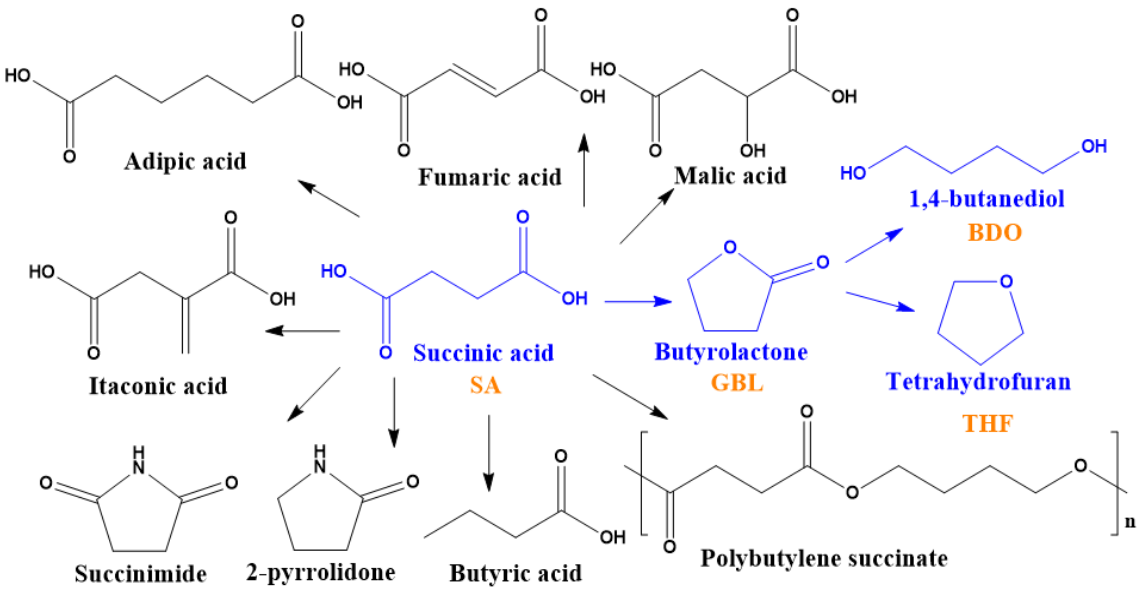

Figure 1.8. Potential uses of bio-based Succinic acid. Adapted from Berezina et al. [80]

1.2.1.2. Reduced Derivatives of Succinic Acid

Some of the reduced derivatives of succinic acid such as GBL, BDO, and THF are produced from maleic anhydride. In the future, succinic acid may replace maleic anhydride to manufacture these chemicals.[81] This has motivated researchers all over the world to investigate different catalysts and reaction conditions to make these transformations feasible.

1.2.1.2.1. γ-Butyrolactone

GBL is a lactone (cyclic ester) which finds applications as a common solvent for polymers, stain remover, and paint stripper.[82] Many researchers have accomplished yields higher than 90 % GBL, specifically from the hydrogenation of maleic anhydride and succinic anhydride.[83,84] GBL is also manufactured chemically by the cyclic dehydrogenation of BDO.

Table 1.4 displays the catalytic data reported in the literature that targets GBL selectivity in the hydrogenation of succinic acid.

Table 1-3. Overview of the results of the hydrogenation of succinic acid to GBL from literature.

Entry	Catalyst	T, °C	Solvent	t, h	p,H_2 bar	X,SA %	S,GBL %	Comments	Ref
1	4%Re/C	240	H_2O	10	80	91	59	S_{BDO}=4 S_{THF}=33 PS=2	[85]
2	0.6%Re/C	200	1,4-Dioxane	7	80	73.1	88.7	S_{BDO}=7.7 S_{THF}=3.6 TOF=25	[86]
3	5%Ru/C	240	1,4-Dioxane	8	60	90	74	S_{BDO}=6 S_{THF}=8 PS=2.4	[87]
4	0.1%Pd/ zirconia	200	H_2O	33	100	34	99	S_{BDO}=NA S_{THF}=NA PS=0.8 TOF=714	[88]
5	10%Pd/ SBA-15	250	Ethanol+ H_2O	8	100	65	39	S_{BDO}=36 S_{THF}=25 PS=6.1 TOF=4.3	[89]
6	1%Pd/SiO_2-NH_2	240	1,4-Dioxane	4	60	100	94	PS=1.1 TOF=47	[90]

Note: T, temperature; P, hydrogen pressure; t, time; X, conversion (%); S, selectivity (%); PS, metal particle size (nm); NA, not available; TOF, turnover frequencies (h^{-1}).

The **Table 1.4** shows that the hydrogenation of succinic acid depends on the choice of noble metal, support, and solvent. 1,4-dioxane was preferred as a solvent in the hydrogenation of succinic acid to GBL. The authors obtained good activity in shorter reaction times when compared to the reaction in aqueous solution due to the higher solubility of hydrogen in 1,4-dioxane.[91] Di *et al.* [85] performed the reaction in water using 4 % Re/C and they achieved low selectivity to GBL (59 %) after 10 h at 240 °C and 80 bar H_2 whereas another study accomplished 88 % selectivity to GBL at a lower temperature (200 °C) and in 7 h reaction time with the use of 1,4-dioxane as solvent (Table 1.4, entries 1 and 2).[86]

The use of Ru based catalysts in the hydrogenation of succinic acid mainly produced GBL, which was then further converted to 1,4-butanediol and THF to a lesser extent.[81] Pd catalysts showed high selectivity to GBL, no matter which support was used. At low reaction temperatures, Pd is inactive for most hydrogenation reactions including aromatic rings,[92] likewise, in the hydrogenation of succinic acid. As shown in **Table 1.1**, the reaction requires high temperature and high hydrogen pressure when using H_2O. Zhang *et al.*[88] performed the reaction 200 °C and 100 bar to be able to achieve 34 % of succinic acid and 99 % selectivity for GBL using 0.1 % Pd/ zirconia (Table 1.4, entry 4).[88] The study also concluded that as the Pd loading increased (0.2, 0.5, and 1 %), the conversion increased, whereas selectivity for GBL decreased.

The size of Pd particles could be highly affected by different pore size in the mesoporous support materials. Chung *et al.*[89] synthesized Pd catalysts supported on mesoporous silica (MCM-41 and SBA-15). The authors found that large Pd particles were prepared on small pore size support (MCM-41), however, using SBA-15 which has larger pores prompted the formation of smaller Pd particles and improved the catalytic activity. 10 % Pd/SBA-15 was able to convert 65 % of succinic acid and the selectivity to GBL was close to 40 % at 250 °C and 100 bar of H_2 (Table 1.4, entry 5).[89]

One of the elements which could be responsible for low activity in Pd catalyst is the agglomeration of Pd particles. The interaction between the Pd particles and the support can affect the catalytic properties of Pd catalysts by affecting the particle size. [90,93] The Sol-gel method was better for preparing Pd catalyst than other conventional methods such as impregnation. [94] You *at el.*[90] successfully prepared Pd/SiO_2-NH_2 with Pd average size of 1.1 nm by utilizing 3-(2-aminoethyl amino) propyltrimethoxysilane (AAPTS) as stabiliser agent. The stabilizer strengthens the interface between the support and Pd particles which leads to highly dispersed particles and prevents agglomerations. The study found 94 % selectivity to GBL with 100 % SA conversion using 1% Pd/SiO_2-NH_2 at 60 bar hydrogen pressure and 240 °C high reaction temperature (Table 1.4, entry 6).

Palladium particles supported on alumina xerogel were synthesized in small sizes and high dispersion compared to using AC as a support in which it affect the reactivity of a given catalyst.[94] Pd seems to be a selective catalyst to produce GBL in the hydrogenation of succinic acid. However, Pd catalysts might need further improvement to be more active in mild reaction conditions since most of previous works have been done in very harsh reaction conditions which could not be suitable for demanding industries.

1.2.1.2.2. Tetrahydrofuran

THF is an important organic solvent, which is used a precursor of a series of polymers, such as tetrahydrothiophene, polytetramethylene ether glycol (PTMEG), polyurethane elastomers, and polyvinyl chloride (PVC).[23,95,96] Currently, THF can be manufactured by several petrochemical processes such as the hydrogenation of maleic anhydride,[97] oxidation of butadiene,[98] and dehydration of BDO.[99] The most commonly used industrial process involves the acid-catalysed dehydration of BDO, with yield higher than 90 %.[99] Therefore, finding a green platform that can substitute these feedstock is attractive.[100] In 2017 the global THF market has exceeded 800 thousand tons, according to a report by global industry analysts, Inc.[101]

Succinic acid can readily be produced by fermenting biomass in biorefineries, therefore, the production of THF from this source has attracted much attention recently.[23,102,103] THF is one of the last products in the consecutive reaction pathway of SA hydrogenation and offers some challenges regarding selectivity and reaction time. **Table 1.5** summarises the catalytic data reported in the literature which targets THF production from succinic acid hydrogenation reaction.

Table 1-4. Overview of the results of the hydrogenation of succinic acid to THF from literature.

Entry	Catalyst	Solvent	T, °C	p(H_2) bar	t, h	X(SA) %	S(THF) %	Comments	Ref
1	5%Ru/ Starbon®	Ethanol/ H_2O	100	10	24	90	60	S_{GBL}=30 S_{BDO}=10 PS=NA	104
2	5%Ru/C	1,4-Dioxane	240	80	4	91	50.9	S_{GBL}= 36 S_{BDO}=8 PS= 3.5	23
3	5%Re/C	1,4-Dioxane	240	80	8	100	38	S_{GBL}= 27 S_{BDO}=4.5 PS= 3.9	105

Note: T, temperature; P, hydrogen pressure; t, time; X, conversion (%); S, selectivity (%); PS, metal particle size (nm); NA, not available; TOF, turnover frequencies (h^{-1}).

Various Starbon® supported metal catalysts have been used by Luque *et al*.[104] for the hydrogenation of SA using ethanol/H_2O as solvent (the role of ethanol in the reaction is unclear). Ru supported on Starbon® favoured the formation of THF from succinic acid where the reaction was performed at 100 °C, 10 bar H_2 pressure, and long reaction times (24 h). 90 % SA conversion and 60 % selectivity for THF was accomplished (Table 1.5, entry 1).

Hong *et al*.[23] pre-graphitized ruthenium–carbon (Ru–XC) catalysts at temperatures (200–400 °C) and prepared them via a single-step surfactant-templating method. The reaction was performed at 240 °C and 80 bar H_2 pressure. The results were affected by the pre-graphitization temperature in which different Ru particles size were obtained. The smallest Ru particle size (ca. 3.5 nm) catalyst exhibited the highest THF yield (46 %) in 4 h reaction time at (91 %) of SA conversion (Table 1.5, entry 2).

The same group later prepared Re catalysts supported on H_2SO_4-treated mesoporous carbons by incipient wet impregnation with different acid concentrations up to 1. The Re(0.4)-MC showed the highest surface area and the lowest particle size for Re. However, Re catalyst showed less selectivity for THF, the study achieved 38 % selectivity to THF at 100 % conversion with the 0.4 M treated catalyst. (Table 1.5, entry 3).[105]

1.2.1.2.3. 1, 4-Butanediol

In the biomass refinery, the hydrogenation of carboxylic acids to their corresponding diol or alcohols is considered to be one of the most significant chemical reaction.[65] Selective hydrogenation of fermented biomass based acids such as lactic acid, acetic acid, and succinic acid can produce 1,2-propanediol, ethanol, and BDO respectively. 1,4-butanediol is a valuable 4-carbon, straight-chain alcohol.[106] BDO is a significant commodity chemical used to manufacture over 2.5 million tons of valuable polymers annually.[107] BDO is expected to have a future demand and in February 2017 a report by Grand View Research Inc. indicated that the BDO global market is expected to reach USD 12.6 billion by 2025.[108]

BDO is an important starting material for the synthesis of fine chemicals such as THF.[109-111] Dehydrogenation of BDO in the presence of a Ru catalyst gives GBL whereas at high temperature in the presence of phosphoric acid gives THF. GBL can be further converted to pyrrolidin-2-one and N-methyl-pyrrolidone, which are useful organic solvents. These chemicals are broadly used in fibres, films, plastics, and artificial leather.[103,111]

Important polymers could be also produced from BDO such as polybutylene terephthalate (PBT), polyethers, polyurethanes, and other polyesters.[112] PBT possesses good thermal stability and great mechanical properties, which makes it suitable for the automotive and electrical industries.[113] Within the plastics industry, adipic acid (AA) is one of the main building blocks with a market of around 3 million tons per year. Using rhodium-based catalysts, the catalytic carboxylation of BDO to AA has been reported.[75] The reaction is well-studied (1970) and it is achieved at 175 °C and 48 bar of CO, which yields about 74 % of AA at 100 % BDO conversion.[75]

There are five well-known chemical based processes for manufacturing BDO which are summarised in **Scheme 1.3**. The 'Reppe Process' named after the chemist Walter Reppe is one of the earliest technologies to produce BDO (Scheme 1.3 A).[111]

The Reppe process consists of using ruthenium and rhodium catalysts. Formaldehyde and acetylene are used as feedstock in this multi-stage process.[110,114] However, the process suffers numerous disadvantages, such as the hazardous nature of formaldehyde and acetylene.

The second process is called the Lyondell process, where the starting raw material is propylene oxide. It is converted to allyl alcohol, followed by its hydro-formylation into 4-hydroxybutyraldehyde. This is hydrogenated to BDO during the last step (Scheme 1.3 B).[111]

The third process is the butadiene acetoxylation, patented by Mitsubishi-Kasei (Scheme 1.3 C). The reaction between acetic acid and butadiene in the presence of oxygen, gives 1,4-diacetoxy-2-butene which upon catalytic hydrogenation *via* saturated intermediate is further hydrolysed to BDO.[111] Butane is the starting material for the fourth and fifth processes to produce BDO (Scheme 1.3 D).

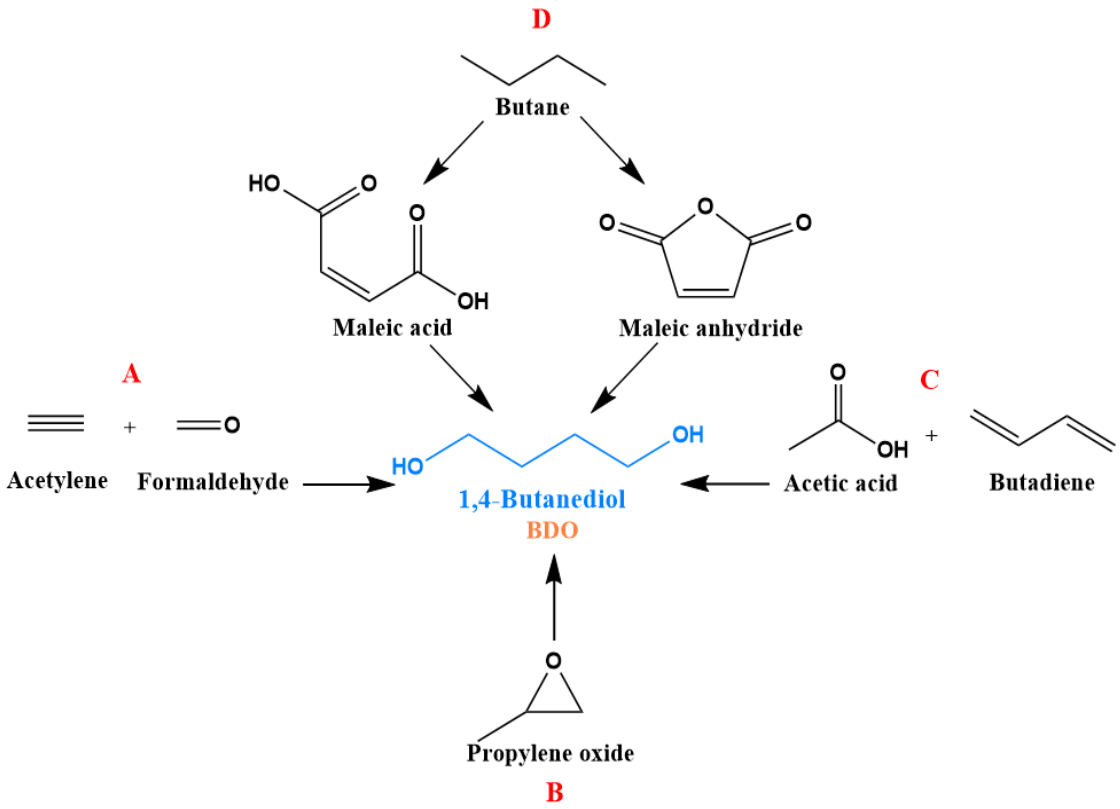

Scheme 1.3. Chemical routes to produce BDO. Adopted from Lee et al.[111]

In the fourth route, selective oxidation of butane to maleic anhydride takes place in the gas phase using vanadium oxide or vanadium phosphorous oxides as catalysts after reaction with methanol, BDO can be produced throughout the reduction of the resulting dimethyl maleate.[111]

The last recognised chemical process is the Davy McKee process, which is based on the esterification of maleic acid and its subsequent hydrogenation.[111] Hydrogenation of maleic anhydride is another common process available in industry and one of abundant method to produce BDO.[115] Maleic anhydride is hydrogenated to succinic anhydride, which is converted to GBL, and finally BDO is formed by further hydrogenation of GBL.[116]

Due to the increase of succinic acid production in the bio-refinery process, direct hydrogenation of SA might be soon the economical chemical process to produce BDO. **Figure 1.15** shows the hydrogenation pathways of SA (highlighted in blue colour) which have been suggested in previous studies.[87,94] The first step is the hydrogenation of SA to produce GBL, followed by the consecutive hydrogenation of GBL to give BDO or THF depending on the reaction conditions. **Table 1.6** summarises the catalytic data reported in the previous literature on hydrogenation of succinic acid to BDO.

Luque and co-workers,[104] used a Starbon®, polysaccharide-derived mesoporous materials, as a support for different precious metal catalysts to hydrogenation of succinic acid at mild reaction conditions (100 °C, 10bar H_2 pressure, 24h). They used 3:5 mixtures of ethanol in water as solvent where the role of ethanol in the reaction is unclear. Pt/Starbon® and Rh/Starbon® exhibited high selectivity to produce BDO.[104] The maximum selectivity to BDO was 90 % and 85 % over Rh/Starbon® and Pt/ Starbon® respectively (Table 1.6, entry 1 and 2). Apart from Luque report, no other study has accomplished high selectivity for BDO using monometallic catalysts and in mild reaction conditions. Ru/Starbon® displayed high selectivity for THF.

Also, Ru catalyst supported on carbon showed 34 % selectivity for BDO (Table 1.6, entry 4). The reaction was performed in harsh reaction conditions (240 °C, 60 bar). The study detected by-products which might be due to C-C cleavage. Ru based catalysts seem to be unselective for BDO.

Bimetallic catalysts have shown more selectivie to BDO in some reports.[86,117,118] Re-modified precious metal catalysts were successfully studied for hydrogenation of SA to BDO by many researchers.[81,106,118]

Table 1-5. Overview of the results of the hydrogenation of SA to BDO from literature.

Entry	Catalyst	T °C	Solvent	P,H_2 bar	t, h	X,SA %	S,BDO %	Comments	Ref
1	5%Rh/ Starbon®	100	Ethanol +H_2O	10	24	60	90	S_{GBL}=10 PS=8.5 TOF=6	104
2	5%Pt/ Starbon®	100	Ethanol +H_2O	10	24	78	85	S_{GBL}=30//S_{THF}=60 PS= 9.7 TOF=13	104
3	5%Ru/ Starbon®	100	Ethanol +H_2O	10	24	10	10	S_{GBL}=30//S_{THF}=60 PS=2.7 TOF=10	104
4	5%Ru/C	240	1,4-Dioxane	60	8	8	34	S_{GBL}=19//S_{THF}=5 $S_{by\text{-}products}$=42 PS=2.7	87
5	2%Re-2%Pd/C	160	H_2O	150	77	100	66	S_{GBL}=32//S_{THF}=15 $S_{by\text{-}products}$ =42 PS=2.7	119
6	4%Re–2%Ru/C	160	H_2O	150	51	100	62	S_{GBL}=0//S_{THF}=NA PS=2;15-60nm	119
7	2.6%Re–2.2%Pd /TiO_2	160	H_2O	150	48	100	83	S_{GBL}=10//S_{THF}=NA PS=NA	106
8	0.3%Re–0.3%Ru/C	200	1,4-Dioxane	80	7	100	71	S_{GBL}=18//S_{THF}=10 PS=5.1 TOF= 61.2	86
9	2%Pd–5%FeO_x/C	200	H_2O	50	50	100	70	S_{GBL}=9//S_{THF}=8 PS=4.4	120

Note: T, temperature; P, hydrogen pressure; t, time; X, conversion (%); S, selectivity (%); PS, metal particle size (nm); NA, not available; TOF, turnover frequencies (h^{-1}).

Minh *et al*.[119] reported that Ru and Pd monometallic catalysts supported on carbon are less selective to BDO. However, when Re was added to those monometallic catalysts, the reactivity and selectivity improved. At the same reaction conditions, the formation of BDO increased and achieved selectivity up to 66 % (77 h) and 62 % (51 h) for Re-Pd/C and Re-Ru/C respectively (Table 1.6, entry 5 and 6). The study used very high hydrogen pressure (150 bar) and a very long reaction time to achieve these results.

The same group used TiO_2 instead of carbon to support Re-Pd catalyst and at the same reaction conditions (160 °C and 150 bar) increased the selectivity for BDO to 83 % (42 h) in short reaction time.[106] Due to the low solubility of H_2 in water, high hydrogen pressure is needed to produce BDO in high yield (Table 1.6, entry 7).

Kang *et al*.[86] studied the activity of the Re–Ru/C bimetallic catalyst for succinic acid hydrogenation in 1,4-dioxane. 0.3% Re-0.3% Ru/C displayed the best catalytic activity for BDO production with 71 % selectivity at 100 % conversion of succinic acid. Thanks to the high solubility of hydrogen in 1,4-dioxane since the reaction was done in 7 h reaction time with less severe reaction conditions (80 bar H_2 pressure and 200 °C).[86] The role of Re was not clarified in those reports due to the similar metal atomic sizes. Re can be miscible with other metals such as Ru, Pt, and Pd which complicated the characterisation results.[86,121] The combination of rhenium and noble metals caused difficulty in structural and chemical analysis (Table 1.6, entry 8).

Non-precious-iron is cheaper than Re and recently, Fe was successfully used as a promoter for Pd catalysts not only to enhance the activity but also to tune the selectivity (Table 1.6, entry 9).[122] Liu *et al*.[122] carried out the reaction in water with Pd catalysts modified with FeO_x. Doping Pd with Fe improved the dispersion of the Pd particles which increased the activity of the catalyst. FeO_x acted as a Lewis acid sites on the catalysts which enhance dehydration activity.

Due to the high acidity of the Pd catalyst after introducing Fe, 70 % selectivity of BDO was obtained full conversion of SA. The reaction was performed under the relatively mild conditions of 200 °C and 50 bar H_2 but still in long reaction time (50 h).[122]

Apart from Luque *et al*.[104] study where they did not use any promoter, using a promoter, i.e., Re and FeO_x seems to be significant to promote the formation of BDO. The high cost, and the difficulty to characterizing Re based catalysts and a long reaction time that Fe was required to increase the selectivity for BDO, opened an opportunity to develop better catalytic system where high selectivity to BDO can be achieved in short reaction time.

1.2.2. Levulinic Acid

Levulinic acid (LA) is a short-chain fatty acid having and an acidic carboxyl group and a ketone carbonyl group, also known as 4-oxo-pentanoic acid. LA is one of highly demanding chemical since according to a study by Grand View Research, Inc., the global levulinic acid market demand is expected to reach 3,820 tons by 2020.[123]

LA can be produced in a decent yield at both semi-industrial scale and laboratory scale by acid hydrolysis of lignocellulosic biomass *via* heterogeneous or homogeneous catalysts.[124] levulinic acid is used as a food flavouring agent, solvent, and starting material for the preparation of a variety of chemicals and pharmaceutical compounds.[125]

Reduction of levulinic acid is done using noble metal catalysts, i.e., Pt, Pd, Au, and Ru, which show high selectivity to γ-valerolactone.[59,126] However, depending on the reaction conditions and the catalyst, different products could also be produced from the catalytic hydrogenation of levulinic acid.

The catalytic hydrogenation of levulinic acid involves a two-step sequence: hydrogenation of levulinic acid to 4-hydroxypentanoic acid (4-HPA) followed by dehydration to form GVL, as shown in **scheme 1.4** along with other useful compounds that can derive from levulinic acid.[126] GVL is hydrogenated to 1,4-pentanediol (PDO), which dehydrates to 2-methyltetrahydrofuran (2-MTHF).[63] GVL can be used as fuel.[127] Thus, extensive research has been focused on converting levulinic acid to GVL.

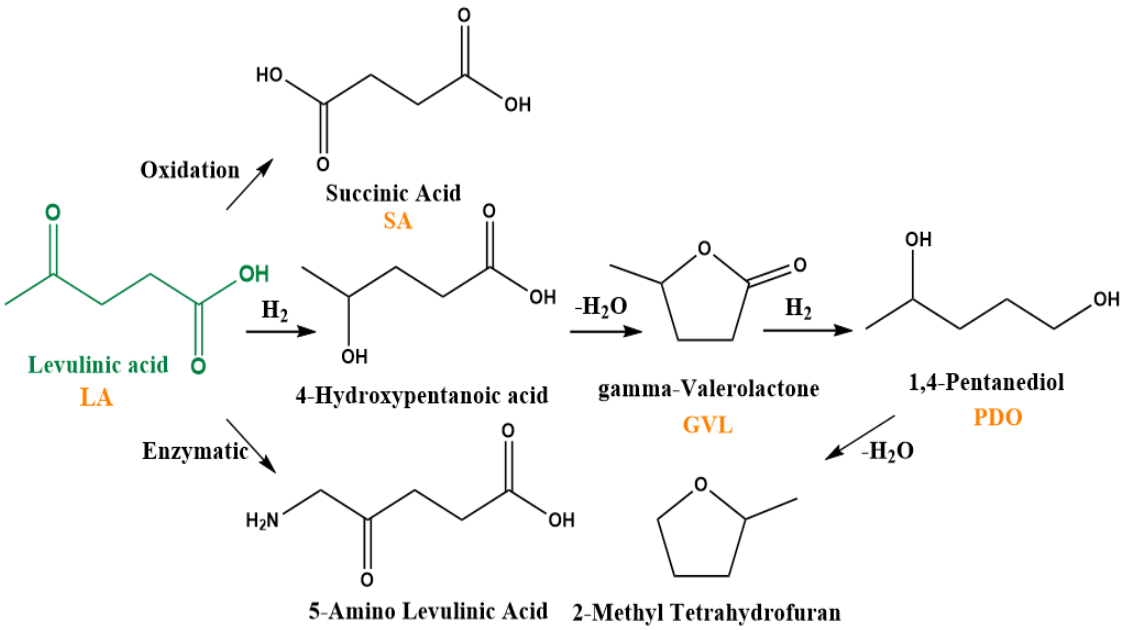

Scheme 1.4. Useful compounds derived from LA. Adopted from Balla et al. [128]

PDO is another highly valuable product from LA, which has huge potential as a monomer for the production of polyesters.[65] There are few studies focusing on producing PDO from LA. A possible explanation is the high stability of the lactone ring structure in GVL, which inhibits the sequential hydrogenation process.[129] On the other hand, the formation of PDO depends on the reaction temperature. At higher temperatures, consecutive conversion of PDO into 2-MTHF and alcohols such as 1-pentanol, 2-pentanol, and 1-butanol takes place.[130]

Table 1.7 presents the catalytic data reported in previous studies which target PDO from LA. Until 2013, only homogenous organometallic catalysts based on $Ru(acac)_3$ and a Bis(diphenylphosphinoethyl) phenylphosphine (triphos) ligand have been reported for the hydrogenation of LA to PDO with excellent performance.[30] At 140 °C and under 150 bar of H_2 pressure, Corbel-Demailly *et al*.[130] used 3 different catalysts to study this reaction in an aqueous medium. They found that Ru/C is a more active catalyst than Pd/C. Promoting these catalysts with Re resulted in high activity for the hydrogenation of LA to PDO. 1.9% Ru-3.6% Re/C produced 82 % selectivity to PDO at 100 % LA conversion (Table 1.7, entry 1).[130]

Table 1-6. Overview of the results of the hydrogenation of LA to PDO from literature.

Entry	Catalyst	Sol	T °C	p(H_2) bar	t, h	X,LA %	S, PDO %	Comments	Ref
1	1.9%Ru–3.6%Re/C	H_2O	140	150	28	100	82	S_{GVL}=0 S_{others}= 18 PS=2	[130]
2	4%Rh–MoOx/SiO_2	H_2O	80	60	6	100	70	S_{GVL}=1.1 $S_{by\text{-}products}$= 28.9 PS= 4.3	[131]
3	4%Pt–0.49%Mo/HAP	H_2O	130	50	12	100	93	S_{GVL}= trace $S_{by\text{-}products}$=4 PS= 3.2	[132]

Note: Sol;solvent, T, temperature; P, hydrogen pressure; t, time; X, conversion (%); S selectivity (%); PS, metal particle size; NA, not available; by-products: 2-pentanol, 1-pentanol, 2-methyl-tetrahydrofuran, and alkanes.

Li *et al.*[65] first reported the selective aqueous phase hydrogenation of levulinic acid to PDO using Mo-modified Rh/SiO_2 catalyst (Table 1.7, entry 2).The selectivity was 1.1 % (PDO) when 4% Rh/SiO_2 was used. However, Mo-modified Rh/SiO_2 catalyst increased the selectivity of PDO to 70 % using 10 wt. % levulinic acid aqueous solution.

Mizugaki *et al.*[132] developed a hydroxyapatite-supported platinum–molybdenum (Pt-Mo/HAP) bimetallic catalyst for the hydrogenation of LA to PDO using water as solvent under mild conditions (130 °C and 50 bar H_2 pressure) at a levulinic acid/catalyst weight ratio of 1.2. The Pt–Mo/HAP system produced 93 % of selectivity to PDO at 100 % LA conversion (Table 1.7, entry 3).[132]

Mo species encourage the hydrogenation steps acting as Lewis acid sites activating the carbonyl group of GVL.[132] The long reaction times and expensive noble metals required to achieve PDO in high yields suggest that developing a low cost, greener, and more efficient system for the synthesis of 1, 4-pentanediol from LA is challenging matter but highly desirable.

1.2.3. cis,cis-Muconic Acid

cis,cis-Muconic acid (ccMA) is a di-unsaturated dicarboxylic acid with six carbon atoms. ccMA is a promising oxygen-rich platform molecule that can be manufactured from sugar.[133] ccMA is synthesised from glucose by fermentation using yeast (*Saccharomyces cerevisiae*) or metabolically engineered bacteria (*Escherichia coli, Pseudomonas putida*).[134]

ccMA might appeared as a promising platform molecule to produce highly industrial demanding molecules, i.e. adipic acid (AA), caprolactam, and hexamethylenediamine. These chemicals are fundamental building blocks for the production of nylon-6,6, polyurethanes and polyesters (**Figure 1.16**).[135] Due to the high industrial importance of adipic acid, ccMA might be used to produce bio-renewable adipic acid in high scale in near future.

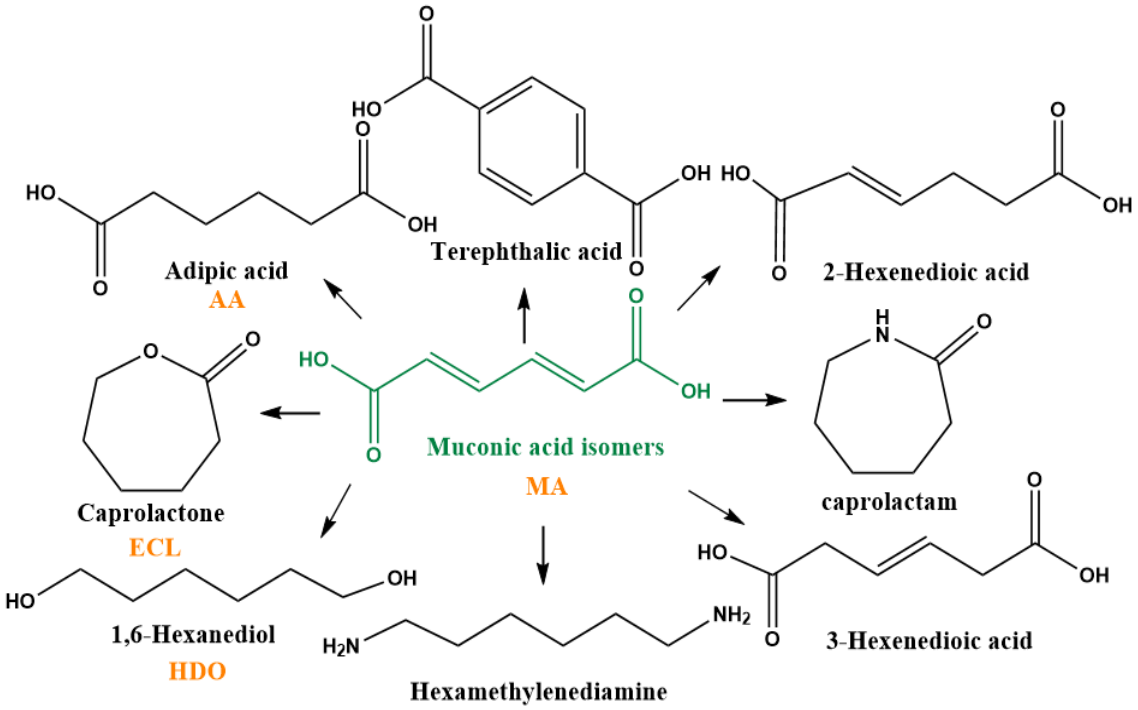

Figure 1.9. Value added products obtained from Bio-based MA. Adopted from Matthiesen et al.[135]

1.2.3.1. Hydrogenation of Muconic Acid to Adipic Acid

Adipic acid is one of today's most important building blocks in the plastics industry with a market of around 3 million tons per year. Every year, 2.6×10^6 tons are mostly used for the production of nylon 6,6.[72] **Scheme 1.5** shows the use of adipic acid along with 1,6-hexanediamine (1,6-HDA) in the production of polyamide (PA 6,6 or Nylon 6,6).

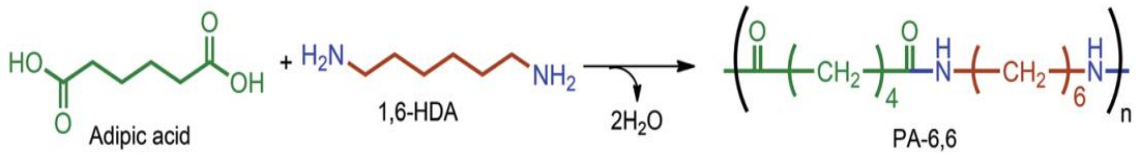

Scheme 1.5. The Production of PA 6,6. Adopted directly from Isikgor et al.[136]

Nylon 6,6 is mainly used to produce fibres (fishing lines, tires, carpets, home furnishing, parachutes, luggage, and resins.[137] Nylon resins are used in electrical connectors, auto parts, and items such as gears and self-lubricating bearings.[138] Adipic acid is also used for manufacturing jams, gelatines, and polyurethanes.[139] The present market price is $1500–$1700 per ton and its foremost producers are Rhodia, Invista, DuPont, BASF and Ascend.[75]

Benzene is the commercial petrochemical source for adipic acid.[140] Therefore, production of AA *via* environmentally friendly pathways is desired. The most recent bio-renewable ways towards adipic acid are from sugars. The routes include pathways *via* glucaric acid, 5-hydroxymethylfurfural and MA. **Figure 1.17** summarises both the alternative bio-renewable routes in light blue and the conventional petro-based routes towards AA in gray.[75]

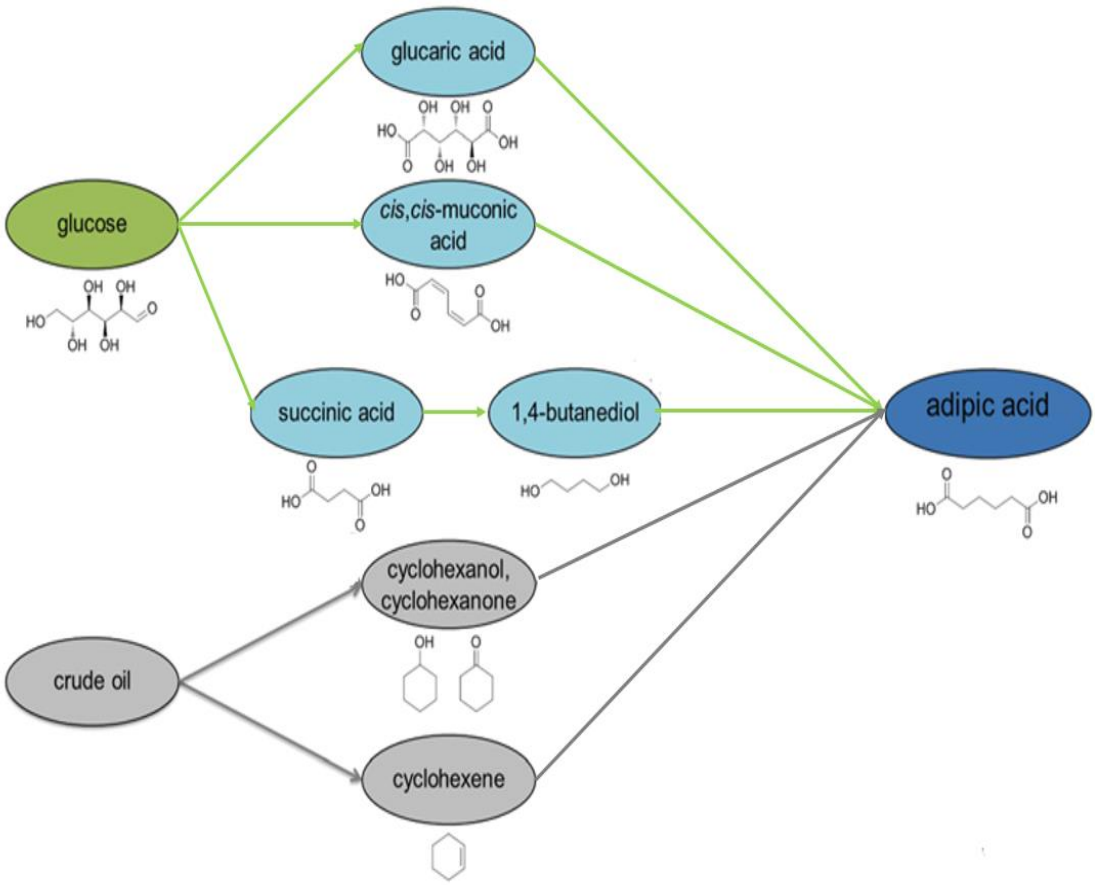

Figure 1.10. The production routes to adipic acid, showing bio-based feedstock (green), bio-based platform chemicals (light blue), and existing petro-based routes (grey). Adopted directly from Beerthuis et al.[75]

Rennovia developed a two-step heterogeneous catalytic route for the synthesis of adipic acid from glucose. In the process, glucose was aerobically oxidised to glucaric acid and Adipic acid was manufactured by hydro-deoxygenation with 89 % yield.[140] Adipic acid can also be formed from glucose through a chemo-catalytic conversion of the bio-based precursor ccMA as shown in **Scheme 1.6**.

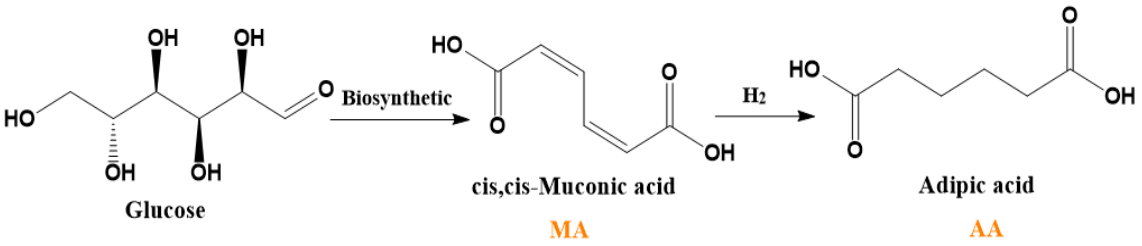

Scheme 1.6. Two-step process for the conversion of D-glucose to AA via the formation of ccMA. Adopted from Beerthuis et al.[75]

ccMA can be easily hydrogenated into adipic acid under relatively mild conditions typically using noble metal supported catalysts in water or ethanol.[141] Only a few reports can be found in the literature on the reaction of ccMA to AA, there are summarised in **Table 1.8**.

Table 1-7. Overview of the results on the hydrogenation of ccMA to AA from literature.

Entry	Catalyst	Solvent	T, ˚C	p,H_2bar	t, min	X,ccMA %	Y,AA %	Comments	Ref
1	10% Pt/C	H_2O	25	34	150	100	97	PS=NA	[142]
2	5% Pd/C	Ethanol	24	4	3	>97	>94	PS=NA	[134]
3	1% Rh/AC	Ethanol	25	25	35	100	99.8	PS=2.03	[143]
4	14.2% Ni/Al_2O_3	H_2O	60	10	300	100	99.4	PS=NA	[139]

Note: T, temperature; P, hydrogen pressure; t, time; X, conversion; PS, metal particle size; Y, yield; NA, not available.

Niu and co-workers,[142] were the first to investigate the hydrogenation of ccMA under Pt supported on active carbon catalysts, with 10 wt. % of metal (Table 1.8, entry 1). With H_2 pressure (34 bar) and after 150 minutes of reaction time a 97 % yield of AA was achieved.[142]

Vardon *et al*.[134] performed a catalyst screening experiment to find highly active materials for ccMA hydrogenation at low pressure and temperature. The group used commercial noble metal catalysts including Pd, Pt, and Ru supported on carbon. They reported that Pd/C was by far the most active catalyst (Table 1.8, entry 2). Under 4 bar hydrogen pressure, room temperature, and using ethanol as a solvent, they obtained >94 % yield of AA after <3 minutes of reaction time.[134]

The same group tested platinum group metals catalysts (e.g. Pt, Ru, Pd, Rh) supported on silica and activated carbon.[143] The study has found that Pd and Rh were both active compared to Ru and Pt. However, 1 % Rh/AC showed the best catalytic activity due to high dispersion of Rh on AC, and the high surface area compared to another tested catalyst (Table 1.8, entry 3). 99.8 % yield of adipic acid was achieved in 35 min using ethanol at mild conditions (25 °C, 25 bar H_2 pressure).[143]

These days, preparing new catalysts system where less expensive catalyst is more desired. One of the most element that could be alternative to noble metals in hydrogenation reaction is nickel (Ni). Ni is ten times cheaper than Pt.[139] Scelfo *et al*.[139] used less expensive Ni-based catalyst and milder reaction conditions to hydrogenate ccMA to adipic acid. The group prepared efficient Ni-based catalysts through the incipient-wetness impregnation method and performed the reaction in water (Table 1.8, entry 4). The study concluded that 14.2 % Ni/Al_2O_3 could be a potential substitute for supported noble metal catalysts for the hydrogenation of ccMA. Full ccMA conversion with 99.8 % yield of adipic acid was achieved under 10 bar H_2 pressure, 60 °C, and 5 hours reaction time.[141]

Hydrogenation of ccMA to AA is relatively easy to curry out in comparison with the production of other products such as 1,6-hexanediol. Therefore, developing highly efficient catalytic hydrogenation systems with less expensive is highly recommended to fulfill the industrial demands.

1.2.3.2. Hydrogenation of Muconic Acid to Caprolactone

Caprolactone (ECL) is used to manufacture polymers for industrial applications such as polycaprolactone and polyglecaprone 25.[136] There is a significant application of polycaprolactone as a biomaterial with a specific focus on medical devices.[144] Another significant industrial application of ECL is the production of caprolactam, which has been broadly used in the polymer industry with a yearly manufacture of about 4 million tons.[145]

In fact, the majority of ECL is used for the commercial manufacture of caprolactam, of which around 90 % is processed to nylon-6, and the leftover 10 % is utilized for the production of other plastics.[136]

In 1974, Takahashi *et al*.[146] prepared caprolactam after reacting ammonium hydroxide with ECL in the presence of ammonium sulfonate. Caprolactam nowadays is manufactured at large scale from cyclohexanone.[147] However, when using extremely aggressive reagents, the unwanted ammonium sulphate is formed as by-product, making this process unfavourable for the production of caprolactam.[147]

Therefore, finding alternative routes is highly desired. Buntara *et al*.[145] were the first group to propose a route to produce bio-derived caprolactam specifically from HMF. However, they used many steps to achieve their goal. They firstly started from HMF to HDO and then to ECL. In their process, HDO was firstly oxidised to its corresponding monoaldehyde, which cyclised to lactol, followed by the dehydrogenation of the lactol, which yielded ECL. Further amination of ECL gives caprolactam.[145]

Scheme 1.7 shows the synthetic route for the conversion of HMF, *via* 1,6-hexanediol, into caprolactam. This bio-route from HMF still needs some improvement to increase the yield and reduce the cost.[136] Also, the HMF route to caprolactam is limited by the yield of HDO, as the yield of bio-based HDO is not high enough when using HMF as feedstock (ca. 57.8 %).

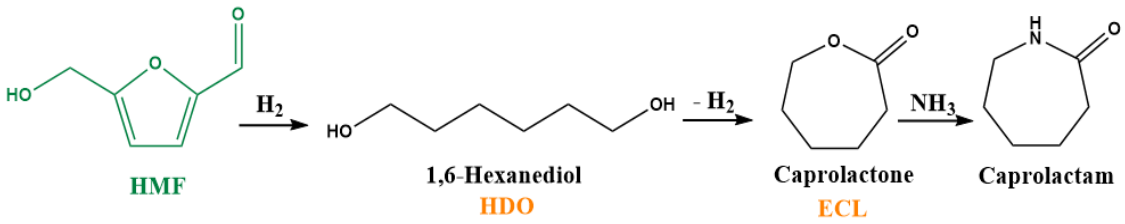

Scheme 1.7. Synthetic routes for the conversion of HMF into caprolactam. Adopted from Buntara et al.[145]

Silva *et al*.[148] produced ECL from the hydrogenation of dimethyl adipate in 1,4-dioxane over a Ru-Sn/TiO_2 catalyst under comparatively harsh conditions (255 °C and 50 bar). The study reports a low conversion of 21 % and low selectivity to ECL (22 %).[148]

Bio-derived ccMA can be a potential alternative to HMF and dimethyl adipate for the manufacture of ECL which could further be used for the synthesis of caprolactam. We will show the first example to produce ECL from hydrogenation of ccMA in one pot.

1.2.3.3. Hydrogenation of Muconic Acid to 1, 6-Hexanediol

1,6-hexanediol (HDO) is a versatile diol with two primary hydroxyl groups. HDO is widely used in the production of polyesters, polyurethane elastomers for adhesives, coatings, and polymeric plasticisers.[149]

Compared with the polyesters commonly synthesised from ethylene glycol such as polyethylene terephthalate (PET), polyesters made from 1,6-hexanediol have better properties in terms of hydrolytic stability, flexibility, and caustic resistance. HDO can be produced from HMF and used as an intermediate to produce other valuable polymers such as PA-6,6 and *Ethernacoll.*

In 2000, the worldwide manufacture of HDO was close to 33,000 tons per year.[150] At the present time, most of the 1,6-HDO production is obtained from petrochemical sources via multiple reactions, including cyclohexane oxidation or the hydrogenation of adipic acid.[151] As much attention has been paid to biomass refinery, finding a biomass derived route for the synthesis of HDO is desired. Hydrogenation of adipic acid or its esters, and hydrogenation of HMF are also potential routes to 1,6-HDO.[151] HMF is one of the chemicals that can be produced also from glucose or fructose. Several homogeneous or heterogeneous catalysts including zirconium phosphate supported Pd, Rh–ReOx/SiO_2, RuSn/TiO_2, and Cu–Zn–Al catalyst have been successfully prepared HDO.[150,152,153]

Various useful chemicals have been successfully produced from HMF such as 2,5-furandicarboxylic acid, 2,5-diformylfuran, SA, LA and 2,5-dimethylfuran.[152] **Table 1.9** below summarises the production of 1,6-HDO from HMF *via* catalytic hydrogenation which are reported in previous studies.

Table 1-8. Overview of the results on the hydrogenation of HMF to 1, 6-HDO from literature.

Entry	Catalyst	T, °C	Solvent	t, h	p,H_2 bar	X,HMF %	S,HDO %	Comments	Ref
1	Rh–ReOx/SiO_2	180	H_2O	20	80	100	73	HDO produced throughout HTO	[150]
2	Pd/ zirconium-phosphate	140	Ethanol	21	FA	96.9	43	Y_{HDN}=15.2 $Y_{by\text{-}products}$=19.1 PS=11.9	[152]
3	Pd/SiO_2+Ir-ReOx/SiO_2	100	H_2O/THF	24	70	100	57.8	Y_{hexane}= 9 $Y_{hexanol}$=24	[154]

Note: T, temperature; P, hydrogen pressure; t, time; X, conversion; PS, metal particle size; S, selectivity; Y, yield; (%) NA, not available; by-products, HDN, 2,5-hexandion; HTO, 1, 2, 6-hexanetriol; FA, formic acid; others: methyl furfural, tetrahydrofuran-dimethanol, and 2,5-dimethylfuran.

The selective production of 1,6-hexanediol from HMF however is difficult to accomplish, as there are several competing compounds that can be formed along with HDO, as shown in **Scheme 1.8.** Buntara *et al.*[150] reported two to five-step process to synthesise HDO from HMF. HDO was formed from HMF throughout 1,2,6-hexanetriol, the study has achieved 73 % selectivity for HDO in the reaction conditions of 18 °C and 80 bar (Table 1.9, entry 1). Alternatively, using formic acid as a hydrogen source, the one-pot conversion of HMF to HDO was developed by Tuteja *et al*.[152] The study reported 43 % yield for HDO (HMF conv. 96.9 %) over Pd/zirconium phosphate (ZrP) catalyst after 21 h reaction time at 140 °C (Table 1.9, entry 2).[152] The study claimed that the acidity of the support surface speeded up the cleavage of C-O bond in a furan ring

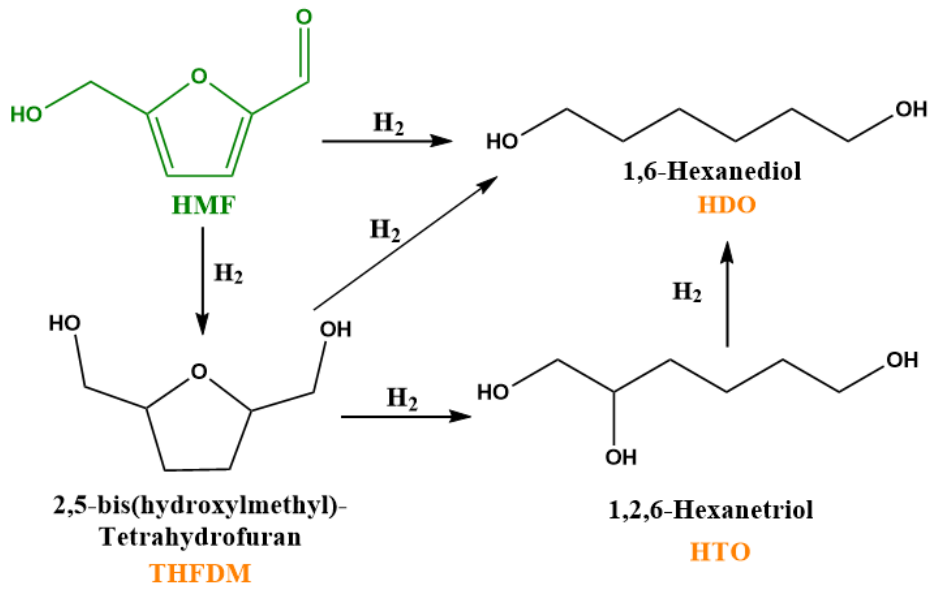

Scheme 1.8. Hydrogenation of HMF to HDO. Adopted from Buntara et al.[145]

In 2015, Xiao *et al*.[154] used Pd/SiO_2 + Ir–ReOx/SiO_2 to synthesise HDO. 57.8 % yield of HDO from biomass-derived (HMF) was obtained using a solution of 40 % water and 60 % tetrahydrofuran with reaction conditions of 100 °C and 70 bar H_2 (Table 1.9, entry 3).[154] The study reveals that high hydrogen pressure was beneficial to the formation of 1,6-HDO by decreasing the formation of hexane and hexanol. 1,6-HDO formation was affected by use of the reaction solvent.

At volume ratio 2:3 H_2O and THF significantly improved the yield of HDO. However, the study indicated that the reason for the enhancement in activity is still uncertain. Finding another path to produce HDO is highly desirable. To the present date the yield of bio-based 1, 6-hexanediol is modest when using HMF as feedstock (ca. 57.8 %). Bio-derived ccMA could offer an alternative to producing 1,6-hexanediol.

1.3. Thesis Outline

It is difficult to hydrogenate the succinic acid, due to the low electrophilicity of the carbonyl carbon. Based on the literature, this reaction was done in mostly in high temperature and pressure and using 1,4-dioxane. 1,4-dioxane was used in the literature as it is an effective solvent, since the reaction proceeded fast compared to using water. Water is a green, abundant, and safe solvent compared to alcohols and especially 1,4-dioxane which is toxic and succinic acid is produced by fermentation as an aqueous solution so using water would be an ideal. Therefore, an improvement in this process, such as the use of low temperatures and pressures or the introduction of a reactive metal-based catalyst, are needed.

In view of this, we decided to compare the activity of Pd, Pt and Ru nanoparticles supported in different supports to establish their relative activity and application when using water as solvent in succinic acid hydrogenation. Additionally, we show for the first time that the use of carbon nanotubes and microwave reactor, can increase the rate of reaction for Pd, Pt and Ru in this reaction. Promoting Ru/CNT with tin was also successfully accomplished in this study since we could have enhanced the formation of 1,4-butanediol by reducing hydrogenolysis by-products.

The thesis is arranged into seven chapters and one Appendix as follows:

In Chapter 1, Introduction, background about catalysis, carbon nanotubes, and measurement techniques. The chapter also contains an overview of the importance of biomass as a suitable replacement for fossil source in the production of chemicals. The catalytic transformations of biomass-derived succinic acid, muconic acid and levulinic acid to important chemicals and diols are reviewed.

In Chapter 2, the experimental section is covered. The catalysts' preparation methods, the experimental steps, and performance of characterisation techniques are described.

In Chapter 3, the catalytic performance of Ru supported on CNT is assessed in the liquid-phase hydrogenation of succinic acid for the first time. To find optimum reaction conditions, different parameters, i.e., temperature, pressure and metal loading on the catalytic activity of Ru catalyst were studied. Reaction pathways are suggested and a recyclability of the Ru/CNT catalyst is described.

In Chapter 4, a different Sn loadings (1,1.5,2,2.5, and 5 %) in 5% Ru-X% Sn catalysts were prepared using CNTs and AC as supports to compare their intrinsic activities and selectivity to diols in the hydrogenation of different bio-based acids such as succinic acid, levulinic acid, and cis,cis-muconic acid.

Chapter 5, the liquid-phase hydrogenation of cis,cis-muconic acid has been studied using selective catalysts (Pd, Ru, and Ru-Sn) to produce three valuable products: adipic acid, caprolactone, and 1,6-hexanediol.

In Chapter 6, the effect of a microwave reactor in the hydrogenation of succinic acid using various catalysts with different supports such as Ru, Pd, Pt, and Re supported on different supports were examined also for first time. The results are compared to the conventional heating reactor (pressure autoclave). The levulinic acid hydrogenation in microwave using best catalyst was reported as well.

Finally, Chapter 7 presents the conclusions of this PhD thesis, together with proposed directions towards future work.

CHAPTER 2

Experimental

Materials and Methods

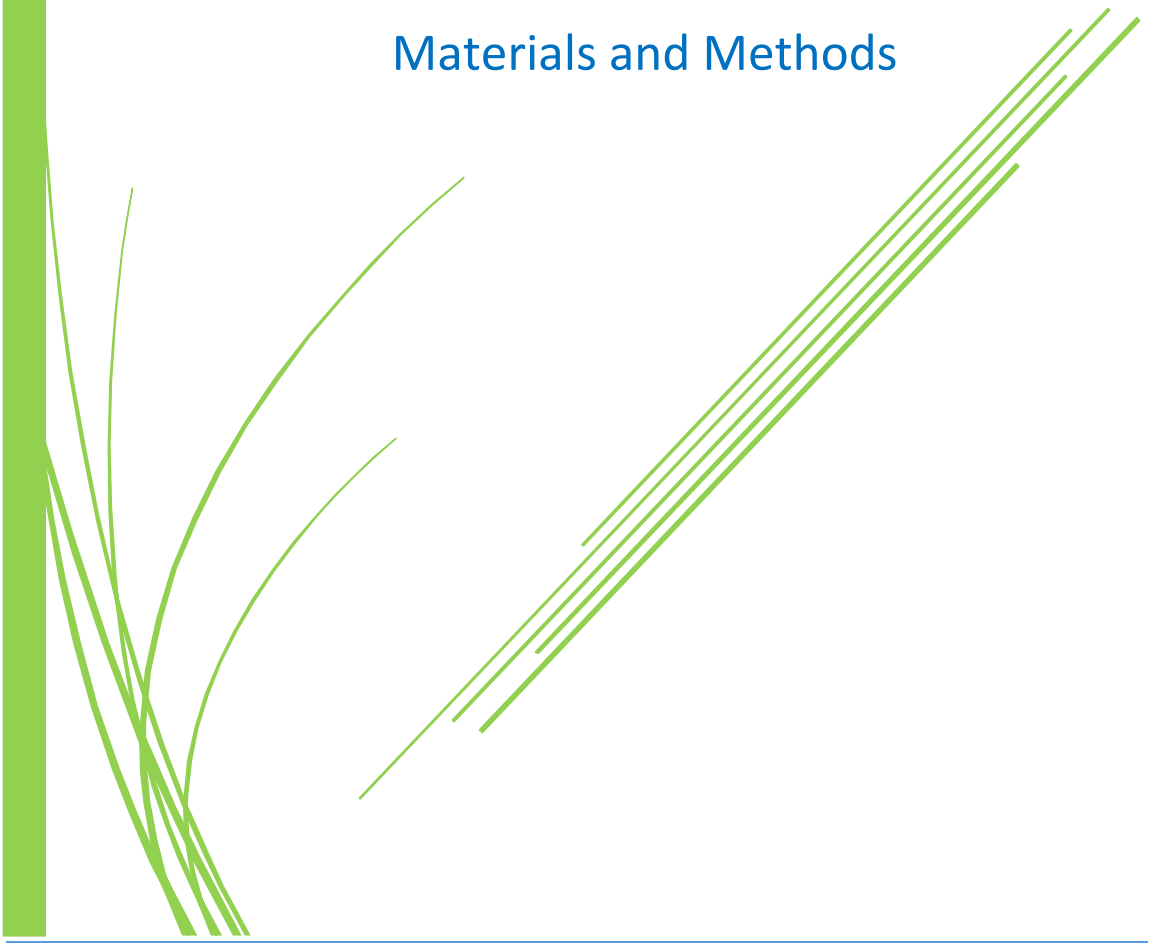

Chapter 2: Experimental: Materials and Methods

The purity, source of materials, the catalyst preparation procedure, and catalytic performance processes are described. We also introduce the instrumental setup of numerous characterisation techniques that have been used to characterise the catalysts that were used.

2.1. Chemicals – Source and Purity

Multi-walled carbon nanotubes (CNTs) typically with 6-8 tube walls, outside diameter 10 nm, inside diameter 4.5 nm and length of 4 µm with a purity of (95 %) were purchased from Sigma-Aldrich Chemicals. Activated carbon (NORIT®SX PLUS) was received as a research sample from CABOT Corporation. Ultra-pure deionised water (18.2 MΩ) was used as a solvent for all tests. H_2 and % N_2 were supplied by BOC ((certified as ultra-high quality (UHP)) N_2 was used to purge the reactor before performing the reaction and H_2 was used to reduce the catalysts and to perform the reactions. The chemicals listed in.

Table 2.1 were used without further purification and bought from Sigma Aldrich except for GBL, gamma alumina and tin chloride which were purchased from Alfa Aesar, methanol from Fisher Scientific, and ccMA acid from ACROS.

Table 2-1. List of chemicals, and their purity.

Chemicals	Purity (%)	Chemicals	Purity (%)	Chemicals	Purity (%)
succinic acid	≥99.0	levulinic acid	98	$PdCl_2$	≥99.9
1,4-butanediol	99.0	1,4-pentanediol	99	$RuCl_3 \cdot xH2O$	99.98
γ-butyrolactone	99	γ-valerolactone	99	SiO_2	99.8
propionic acid	99.5	cis,cis-muconic acid	98	n-propanol	99.5
butyric acid	≥99.0	Adipic acid	99	1,6-hexanediol	99
methanol	99.8	ε-Caprolactone	97	$H_2PtCl_6 \cdot xH_2O$	≥99.9

2.2. Carbon Nanotubes Purification

In all CNTs supported catalysts, the CNTs were washed with water to remove loosely bound impurities (ca. 0.6% Fe and 0.3% Co were found as major impurities after washing, mostly as particles grown within the tube pore) which have been reported in the literature.[155] The method is as follows: (1) Distilled water (300 mL) was added to a 500 mL beaker and stirred (300 rpm) on a hotplate using a magnetic stirrer bar. (2) 1 g of pristine CNT (from Sigma-Aldrich) was then added. (3) The mixture (suspension) was left to stir for 4 h at room temperature. (5) The mixture was filtered using a Büchner funnel and washed with 1000 mL of distilled water. (6) The washed CNT was placed onto a watch glass (covered with aluminum foil) and dried in the vacuum oven overnight at 80 °C. The following day, the CNT was ready to be used for the catalyst preparation.

2.3. Catalysts Preparation

2.3.1. Monometallic Catalysts Preparation

The catalysts were synthesised *via* the impregnation method, the method has been developed by our research group, Mai at el.[156] as follows: (1) an appropriate amount of metal salt was placed in a 12-mL vial and dissolve it using 3 mL of deionised water.

(2) The solution was mixed for 10 min on a hot plate with continuous stirring at room temperature and the solution turned black with a Ru precursor, dark brown with a Pd precursor, dark green with a Re precursor, and yellow with a Pt precursor.

(3) A small amount (200 µl) of the resulting solution was added dropwise using a single channel pipette to 1 g of support, the support previously placed in the mortar, so all the surface was covered with the drops.

(4) After each addition, the support and the metal solution were thoroughly ground with a pestle. The solvent was removed by drying in the oven at 120 °C for 5 min.

(5) Step four was repeated until all the metal salt solution was consumed, followed by the addition of 0.5 mL of fresh deionised water to clean the vial that had a metal salt solution and this was added also onto the support.

(6) The mortar with the prepared catalyst was covered with aluminium foil with small holes and placed in an oven overnight at 120 °C.

(7) Before testing the catalysts, all of them were reduced in a Carbolite horizontal tube furnace (schematic diagram of this furnace is shown in (**Figure 2.1**) under H_2 flow (60 mL min^{-1}) at 400 °C with a heating rate of 5 °C min^{-1} for 4 h.

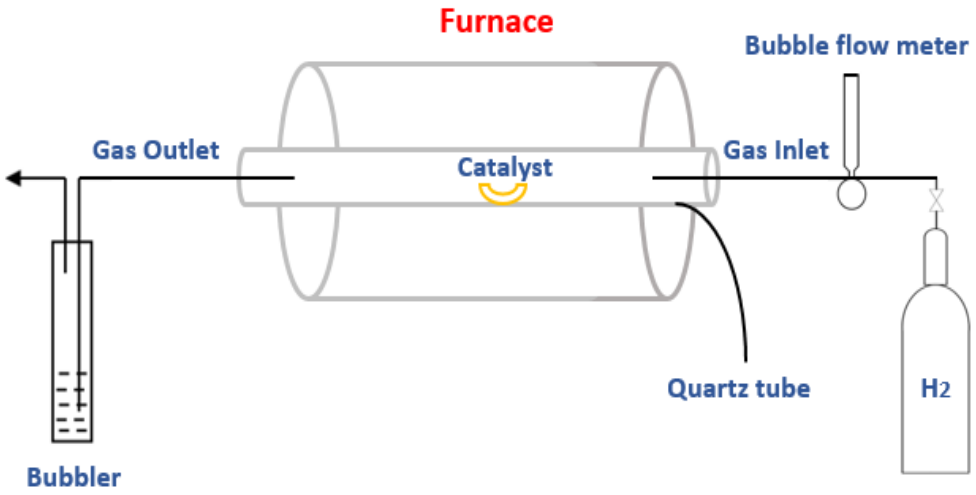

Figure 2.1. Schematic diagram of the furnace that used in this work

2.3.2. Preparation of 5% Ru/unwashed CNT (Chapter 3)

Pristine CNT was used directly without the water washing step. To prepare the catalyst, we applied the same procedure that was used in the monometallic catalysts preparation Section (2.3.1).

2.3.3. Preparation of Ru Supported Inside of CNT (5% Ru (IN) CNT) (Chapter 3)

According to the process reported in the literature,[157] 5% Ru(IN)CNT was prepared by;(1) dissolving 0.1026 g of $RuCl_3$ in 10 mL of acetone followed by the addition of 1 g of CNT where the latter looked like a paste. (2) The mixture (paste) was then placed into an ultrasonic bath for 0.5 h to obtain a homogeneous dispersion. The ultrasonic treatment was required to force the Ru salt to enter the CNT channels by the aid of capillary action.

This treatment also helped to remove the air and permit the migration of the Ru salt solution into the CNT channels.[158]

(3) The mixture (paste) was heated in air at 1 °C/min up to 110 °C, held at 110 °C for 11 h to remove residual (4) Before testing the 5% Ru(IN)CNT it was also reduced under H_2 flow (60 mL min^{-1}) at 400 °C with a heating rate of 5 °C min^{-1} for 4 h.

2.3.4. Bimetallic (Ru-Sn) Catalysts Preparation (Chapter 4)

An appropriate amount of ruthenium (0.1026 g of $RuCl_3$) and tin salts (depending on the loading) were dissolved together in 3 mL of methanol due to tin chloride being insoluble in water (the colour of the solution was black). The catalyst was prepared from the resultant solution using the same synthetic procedure for a monometallic catalyst.

2.4. Techniques for Catalyst Characterization

To acquire valuable information about a given catalyst, such as the structure, surface area, number of active sites, optimum reduction temperature, and chemical states of the metal, different instrumental techniques were applied. In this section, the corresponding analytical techniques are described.

2.4.1. X-Ray in Characterization Techniques

X-rays are a form of electromagnetic radiation. The energy that comes from X-ray photons is significantly higher than that of light. When a given specimen is hit by a monochromatic beam of X-ray photons, three phenomena may happen which are scatter, fluorescence, and absorption.

There are three essential X-ray methods based on these fundamental phenomena: the scattering effect, which is the basis of X-ray diffraction, the absorption technique, which is the basis of the radiographic analysis, and the fluorescence impact, which is the foundation of X-ray fluorescence. X-ray techniques play a crucial role in providing information on the elemental composition and structure of matter.

2.4.2. X-Ray Diffraction (XRD)

- Theory

X-ray powder diffraction is one of the main characterisation techniques used for solid materials. X-ray diffraction crystallography is an analytical technique based on the principle of diffraction, which is mainly used to provide information regarding the crystallinity of unknown crystalline materials such as minerals and inorganic compounds, as well as to provide the crystalline phases present.

This principle is built on the fact that each crystalline solid has its sole fingerprint of x-ray intensity.[159] The peaks in an x-ray diffraction pattern are associated with the atomic distances. When the material is crystalline, incident x-ray beam interacts with the atoms that organized in a repeated pattern. When the incident wave hits the atom at a random angle, an interference of the reflected waves might be destructive or constructive.[160] In other words, interference patterns formed by excited atoms when single wavelength x-rays hit a crystal lattice. It should be noted that numerous patterns will interfere with one to another and cancel each other out. This phenomenon is called destructive interference, as shown in **Figure 2.2**, whereas at the right angle and distance these patterns can be in-phase with each other and constructive interference could happen (**Figure 2.3**).[161]

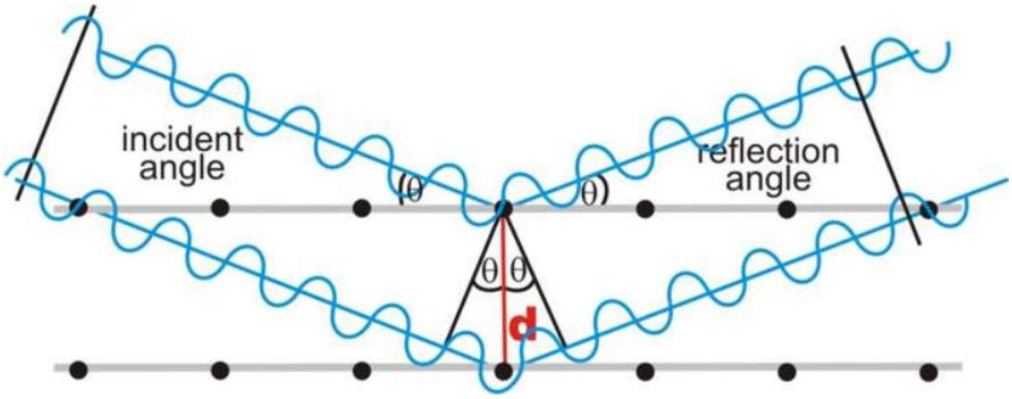

Figure 2.2. Destructive interference of reflected waves. Adopted directly from web page (Bragg's Law of Diffraction).[160]

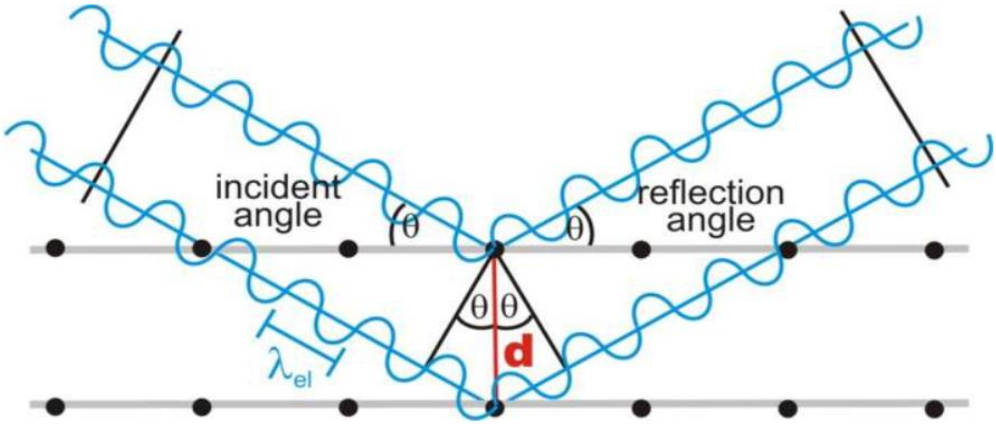

Figure 2.3. Constructive Interference of reflected waves Adopted directly from web page (Bragg's Law of Diffraction).[160]

To attain constructive interference, the pathway variance between the two incidents and the scattered waves, which is 2dsinθ, should be a multiple of the wavelength λ. The equation below is known as the Bragg equation, which gives the relation between interplanar distance d and diffraction angle θ. It should be noted that each mineral has a set of unique d-spacing pattern.[159]

$$2d\sin\theta = n\lambda \qquad \text{Equation 2.1}$$

From the equation, **d** is the interplanar crystal spacing, **θ** is the angle of incidence or reflection of the x-ray beam, **n** is the order of the diffraction (1, 2,…), and **λ** is the x-ray wavelength in **Å**.

- Experimental

The measurements were conducted using a Panalytical X'Pert PRO HTS X-ray diffractometer using Cu Kα radiation (λ = 0.154 nm). Prior to XRD studies, all catalysts were reduced in flowing H_2 at (400 °C for 4 h). The powder diffraction patterns were recorded in the 2θ range of 4° to 90° for 60 min.

2.4.3. X-Ray Photoelectron Spectroscopy (XPS)

- Theory

X-ray photoelectron spectroscopy (XPS) is a surface characterisation method that provides valuable information on the elemental composition and electronic state of the elements that are in the catalyst.[162]

The X-rays used in this instrument are either magnesium Kα or aluminum Kα with energies of 1253.6 eV and 1486.7 eV, respectively.[163] When an X-ray beam with known energy hits the atoms, it causes a discharge of the inner shell electrons, so the energy of those electrons can be measured. The difference in the energy of ejected electrons and the hitting X-ray gives the binding energy (BE) of the electron to the atom. Moreover, the kinetic energy of the emitted electron and the photon energy along with the work function can be used to calculate the binding energy of the electron. The obtained value can determine the chemical state of specific elements or atomic composition of a sample.[164]

The measured kinetic energy, KE is given by (Equation 2.2):

$$KE = h\nu - BE - \phi \qquad \text{Equation 2.2}$$

Where BE is the binding energy of the atomic orbital from which the ejected electron originates, **hv** is the energy of the photon (**h** is Planck's constant and **v** is the frequency of the exciting radiation), and **ϕ** is the work function of the spectrometer. XPS can be utilized to detect and determine the concentration of the elements at the surface since each element has a unique set of binding energies.[163]

- Experimental

X-ray photoelectron spectroscopy (XPS) spectra were recorded on an ESCALAB 250 spectrometer and Al Kα radiation (1486 eV) was used as the X-ray source. The C 1s peak for C-C/C-H in 5%Ru/AC at 284.8 eV was used as a standard for the charge correction. Binding energy maxima was determined by fitting the peaks with an asymmetric line-shape function. XPS measurements were performed at the A*STAR, institute of chemical and engineering sciences, in Singapore.

2.4.4. Electron Microscopy

- Theory

Until now, the most widely used tool for analysis features sizes above 1 µm is optical (light) microscopy, which happens to be the oldest microscopy technique. However, electron microscopy techniques such as transmission electron microscopy (TEM) and scanning electron microscopy (SEM) are the best choice for smaller sizes (<50 nm).[165]

SEM is based on scattered electrons and offers as high as 2 million magnifications whereas TEM is based on a transmitted electron and has up to 50 million magnifications. **Figure 2.4** displays the schematic diagram showing the most critical parts in a light microscope and transmission electron microscope.

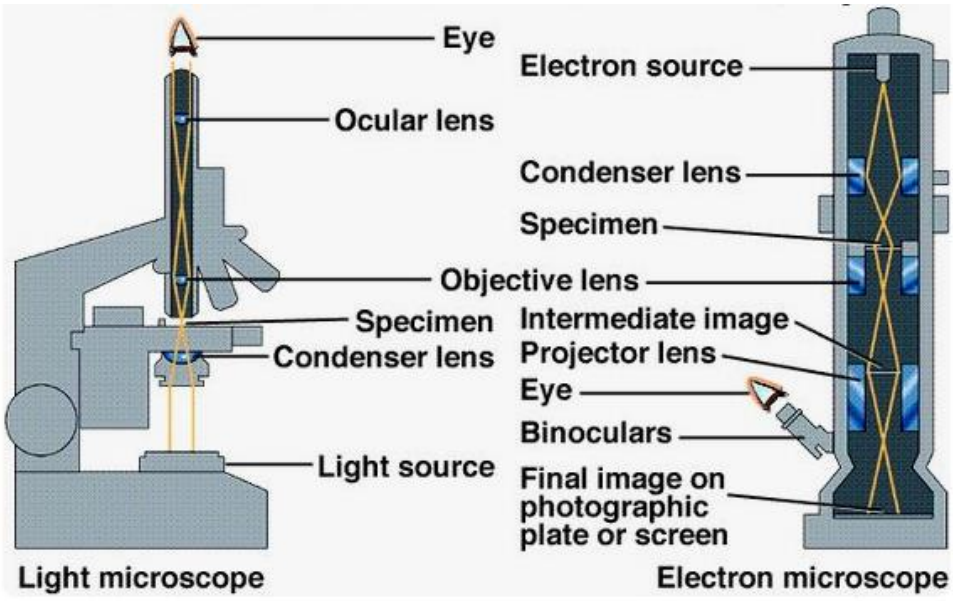

Figure 2.4. Schematic diagram of light microscope and electron microscope. Adopter directly from a web page (Comparison between light microscope and electron microscope).[166]

The design of a transmission electron microscope is like that of an optical microscope. Electrons of high energy (>100 kV) and electromagnetic lenses are used in TEM instead of photon and glass lenses which are used in an optical microscope.

In TEM, all the information come from electron-sample interaction.[167] The reason behind calling it “transmission” electron microscopy is that the electron beam passes an electron-transparent specimen and is detected below a grid to form images, using a set of lenses which is projected onto a fluorescent screen/CCD camera.[167]

The given resolution of 0.2 nm is 1,000 times larger than a light microscope provides and around 500,000 times more than that of a human eye. TEM produces high resolution and magnification imaging down to an atomic level which provides information such as morphology, crystal structure, and particle size distribution.[168]

- Experimental

The microstructure and morphology of the catalysts were examined by JEOL JEM 3010 TEM operating at 300 kV voltage. Prior to the microscopy examination, each sample was dispersed in methanol and deposited on the 300 mesh Cu holey carbon TEM grid. Particle size distributions of metal nanoparticles are based on the counting of at least 100 particles. TEM measurements were performed in the Nano investigation Centre of the University of Liverpool.

2.4.5. Chemisorption

- Theory

In supported catalysts, the active metal phase may exist as clusters on the surface of the support, where it provides as active sites for the reaction. During a reaction, only a portion of the total metal loading is exposed to reactant molecules, which reflects a percentage of the amount of metal.[169] The number of exposed atoms may be obtained from chemisorption techniques as they measure an amount of gas adsorbed on the metal at monolayer coverage. Knowing the stoichiometry of a chemisorption reaction is fundamental to determine an accurate metal dispersion.[170]

The pulse method is used to determine how many gas molecules are present on a catalyst surface.[169] The adsorbate gas (H_2 or CO) should be selected depending on the catalyst. The selected gas should have minimum adsorption on the support of the given catalyst and the interaction with the metal should be irreversible.[169]

In the pulse chemisorption method, the reduced catalyst is flushed with inert gas, i.e., helium at elevated temperature to remove any adsorbed H_2 gas which was previously used to reduce the catalyst. Then, a known volume of adsorbate gas is injected as pulses in a flow of inert gas until the saturation of the catalyst surface is obtained.[169] **Figure 2.5** shows the adsorption plot, where the first five peaks were indicating that there is an amount of CO have been adsorbed and the last two peaks displayed the same area which is an indication of saturation.

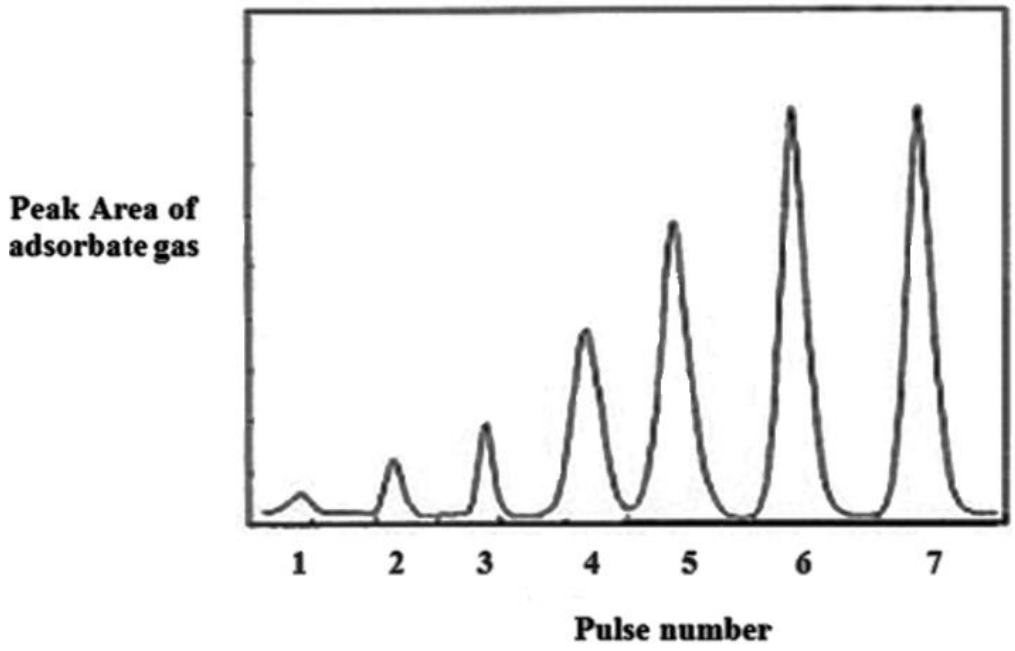

Figure 2.5. A plot of peak area vs pulse number of adsorbate gas (CO or H_2). Adapted directly from a web page (chemisorption).[169]

By calculating the difference between the volume of each pulse and the portion of adsorbate not adsorbed, the quantity of gas adsorbed is obtained.[169] The volume of the active chemisorbed gas (usually 10 % CO in helium) is calculated by the volume injected, $\mathbf{V_{inj}}$ and from the area, under the peaks, as follows;

$$\mathbf{V_{ads}}\left(\mathbf{STP}, \frac{\mathbf{cm^3}}{\mathbf{g}}\right) = \frac{\mathbf{V_{inj}}}{\mathbf{m}} \times \sum_{\mathbf{i=1}}^{\mathbf{n}} \left[\, \mathbf{1} - \frac{\mathbf{A_i}}{\mathbf{A_f}} \,\right] \qquad \text{Equation 2.3}$$

where **STP** is standard temperature and pressure (273 K and 1 atm), **m** is a mass of the sample (g), $\mathbf{A_i}$ is the area of the peak **i**, and $\mathbf{A_f}$ is the area of the last peak.

The schematic diagram of equipment for pulse chemisorption is given in **Figure 2.6**.

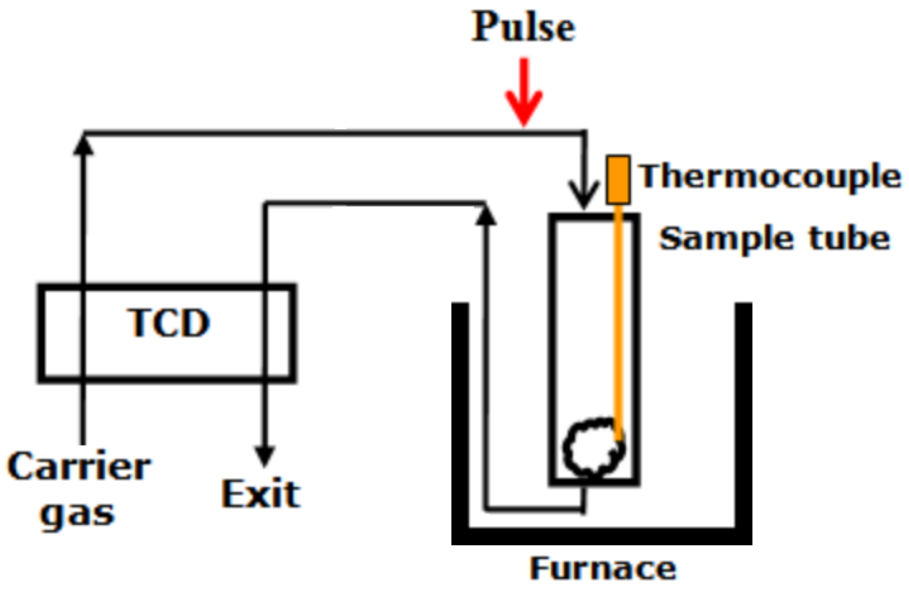

Figure 2.6. Schematic diagram of equipment for pulse chemisorption. Adapted directly from a web page (Catalyst characterization-Chemisorption).[169]

The percentage of metal dispersion, **D** (%) could also be calculated based on adsorbent gas as defined in the following formula:

$$D_{CO} = \frac{SF.A_r.CHS_{CO}}{L_{Me}} \qquad \text{Equation 2.4}$$

where **SF** is the chemisorption stoichiometric factor, $\mathbf{A_r}$ is metal relative atomic weight (g mol^{-1}), $\mathbf{CHS_{CO}}$ is the number of moles chemisorbed per gram of catalyst (mol g^{-1}), and $\mathbf{L_{Me}}$ is the metal loading (%).

- Experimental

The metal dispersion was determined from the amount of CO chemisorbed on the metal sites and was measured by the pulse CO chemisorption (carried out also with the same equipment and detector as in TPR and TPD).

The samples were placed in a quartz U-tube reactor, purged by flowing helium for 30 min followed by reduction of the catalysts with H_2/N_2 stream for 4 h at 400 °C. After the reduction, the reactor was cooled to 35 °C and CO pulses were repeated until the metal surface was saturated with CO. The dispersion of metals was calculated using the Equation 1.4.

2.4.6. Thermal Analysis

- Theory

Thermal analysis is a method in which the physical property of a material is measured as a function of temperature. The reactions studied as a function of temperature were desorption, reduction, and oxidation.[171] In this section, some background information will be discussed.

2.4.6.1. Temperature Programmed Desorption (TPD)

A widely used technique to characterise the basicity and acidity of solid samples is temperature-programmed desorption. Carbon dioxide (CO_2) is used to determine basic sites whereas ammonia (NH_3) is used as a probe molecule to determine acidic sites.[172] In CO_2-TPD/NH_3-TPD, desorption peaks reflect the quantity of basic/acidic sites existing on the catalyst while the desorption temperature relates to strength of adsorption of CO_2/NH_3 with the adsorbent.

- Experimental

Temperature programmed desorption of CO_2 (TPD-CO_2) and NH_3 (TPD-NH_3) were used to determine the basicity and acidity properties of a given catalyst respectively. In a typical setup, 0.1 g of catalyst was packed in a quartz U-tube reactor and pre-treated in-situ under helium flow at 150 °C for 30 min to remove any impurities that might be present on the surface of the catalyst such as water. Then, the sample was cooled down to 50 °C for CO_2 and 150 °C for NH_3. The adsorption of NH_3 was performed at 150 °C whereas the adsorption of CO_2 was carried out at 50 °C for 30 min. After saturation, helium was flushed for 30 min at the same temperature to remove the physisorbed NH_3 or CO_2. The peak area of the desorbed NH_3 or CO_2 was measured by integrating the peaks and calibrating the mass signal of standard NH_3/He and CO_2/He gases, respectively. Before the TPD measurement, the catalysts were reduced in hydrogen flow at 400 °C for 4 h. Supports were treated in a nitrogen flow at 400 °C for 4 h therefore, deconvolution was only considered at temperature below 400 °C.

2.4.6.2. The Temperature-Programmed Reduction (TPR)

Temperature-programmed reduction (TPR) is used to find the most efficient reduction conditions for the catalysts, but also reflect metal support interaction. Moreover, in a complex system, i.e., bimetallic catalysts, it is possible to determine an alloy formation or the promoter effects.[173] The first TPR profile was reported by Robertson *et al*.[174] for nickel and nickel-copper catalysts. In this technique, the catalyst is submitted to a programmed temperature rise and reducing gas mixture (usually H_2 diluted in inert gas, i.e., N_2, Ar) is flowed over the sample.

The following equation represents the reaction between metal oxide M_xO_y and hydrogen to produce a pure metal (M).[173]

$$M_xO_{y\,(solid)} + H_2 \longrightarrow M_{(solid)} + H_2O \qquad \text{Equation 2.5}$$

In this method, the prepared catalyst is reduced by hydrogen gas, which is diluted in an inert gas. As reduction starts, hydrogen is consumed and quantified by TCD. At the end of the reduction, no more H_2 is consumed and the thermal conductivity of the gas from the catalyst returns to the baseline.[175]

- Experimental

The TPR profiles were obtained after the pre-treatment by flowing 5 % H_2/N_2 gas mixture (50 mL/min) through 0.05 g of the fresh catalyst (the catalyst was loaded in a U-shaped quartz reactor) while increasing the temperature from ambient temperature to 700 °C with a heating rate of 10 °C/min. Liquid nitrogen/alcohol slush trap between cell and detector was used during the process to condense unwanted water vapour.

Temperature-programmed reduction (TPR), Temperature programmed desorption (NH_3-TPD & CO_2-TPD) and CO-chemisorption were performed in Micromeritics AutoChem 2920 II instrument equipped with a thermal conductivity detector (TCD) (**Figure 2.7**).

Figure 2.7. Micromeritics Autochem II 2920

2.4.7. Texture and Porosity

- Theory

Surface area is a significant property in the behavior of a catalyst. It can be determined from physical gas adsorption on the surface.[176] In this method, the inert gas is adsorbed by a given amount of catalyst over a wide range of relative pressures at a constant temperature. The quantity of gas that adsorbed at a certain constant temperature is referred to an adsorption isotherm.[177] These isotherms could be classified into six types as shown in **Figure 2.8**, which was proposed by the IUPAC.[178]

Each type of physisorption isotherms are different and they give an indication for different adsorbent materials. Type I isotherm gives an indication of microporous adsorbents whereas Type II and Type III isotherm would indicate macroporous or non-porous adsorbents. Type III isotherm propose a weak adsorbent–adsorbate interactions and there is no Point B so from this isotherm there is no identifiable monolayer formation. Type IV and Type V isotherms are a mark of mesoporous adsorbents whereas the latter isotherm shape is like Type III isotherm and proposes also the weak adsorbent–adsorbate interactions. The last isotherm (Type VI) would give an indication of a highly uniform surface (layer-by-layer adsorption).[176,179]

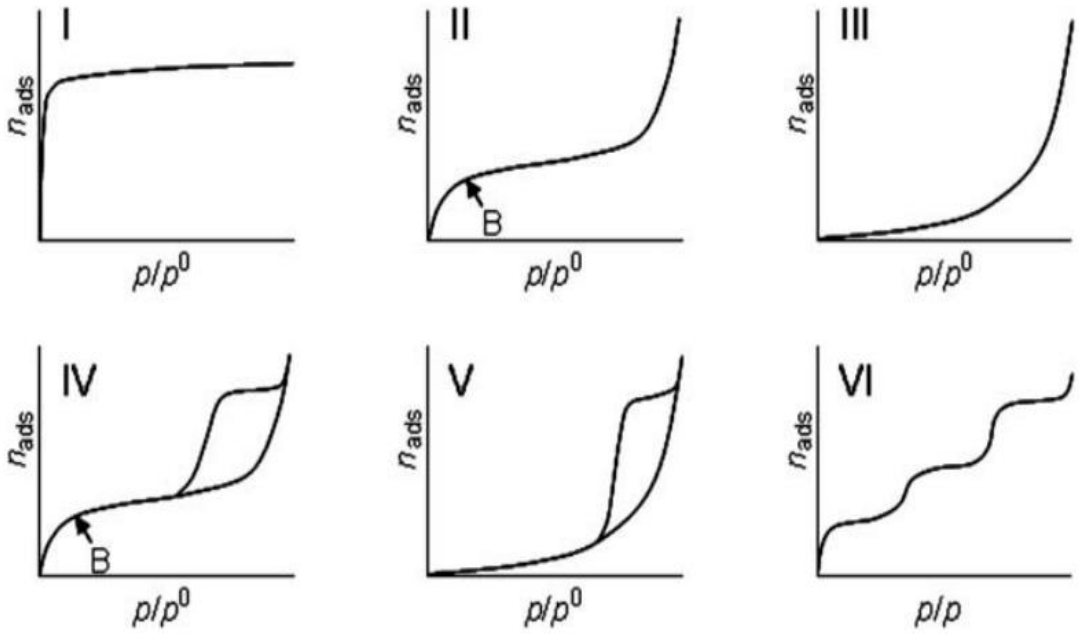

Figure 2.8. Different types adsorption isotherm. Type I: microporous, type II: macroporous or non-porous, type III: macroporous or non-porous with weak interaction, type VI: mesoporous, type V: mesoporous with weak interaction, and type VI: layer-by-layer adsorption. Adopted directly from Claudia Weidenthaler.[176]

To assess the surface area of a material, the number of molecules in a monolayer of the adsorbate must be known. The volume correlated to point B is assumed to be that of the monolayer, however, the point B is difficult to be determined. Consequently, to evaluate the monolayer capacity of a given adsorbent, numbers of models have been developed.[176] The model based on an adsorption of the monolayer of gas on the surface of a solid is the Langmuir model whereas multilayer adsorption is contemplated by the BET method which is a method developed by Brunauer, Emmett, and Teller.[180] The BET theory, an extension of the Langmuir model which is based on the model of monolayer–multilayer adsorption. The BET method is a universal method for the evaluation of surface areas using *via* a BET Equation 2.6.[176]

$$\frac{1}{V_a\left(\frac{P_0}{P}-1\right)} = \frac{(C-1)}{V_m C} \times \frac{P}{P_0} + \frac{1}{V_m C} \qquad \text{Equation 2.6}$$

Where **p** is the partial pressure of adsorbate; $\mathbf{p_0}$ is the saturated pressure of the adsorptive at – 196 °C and the BET constant **C** is related to the strength of the interaction between the gas and the solid, $\mathbf{V_a}$ is the volume of $\mathbf{N_2}$ gas adsorbed at a given relative pressure ($\mathbf{p/p_o}$), and $\mathbf{V_m}$ is the volume of gas adsorbed in a monolayer. To determine the surface area using the BET equation, at least three data points are required, in the $\mathbf{p/p_0}$ range 0.025 to 0.30.

The monolayer capacity $\mathbf{V_m}$ can be calculated by the following equation: where **S** is the slope, and **i** is the **y**-intercept.

$$V_m = \frac{1}{s+i} \qquad \text{Equation 2.7}$$

The following Equation (2.8) used to identify the total surface area which could be found after calculating $\mathbf{V_m}$, the volume of gas adsorbed in a monolayer on the sample.

$$S = \frac{V_m \times N \times a}{m \times 22400} \qquad \text{Equation 2.8}$$

where **S** is the specific surface area (m^2/g), **N** is the Avogadro constant, **m** is the mass of the test powder (g), **a** is the area covered by one nitrogen molecule (0.162 nm^2), and the constant number 22,400 is the molar volume of $\mathbf{N_2}$ (mL mol^{-1}) under standard conditions.[181]

To evaluate the pore size distribution, the Kelvin equation is used by the Barrett–Joyner–Halenda (BJH) method. The Kelvin equation combined with a standard isotherm is required for this calculation (Equation 2.9).[176]

$$\ln(p/p^0) = -2\gamma V_m / \mathrm{RT}(r_p - t_c) \qquad \text{Equation 2.9}$$

Where surface tension **γ** of the bulk fluid and the molar liquid volume $\mathbf{V_m}$, $\mathbf{t_c}$ the thickness of the adsorbed multilayer film and $\mathbf{r_p}$ is the pore radius.[179]

- Experimental

The surface area of catalysts and pore volume can be calculated using nitrogen sorption. Prior to analyses, all samples were degassed overnight at 300 °C before physisorption experiments to remove any impurities present on the surface. Nitrogen physisorption isotherms of catalysts and supports were measured on a Quantachrome NOVA 4200e analyser (**Figure 2.9**) at -196 °C using the relative pressures range 0.05-0.99.

The total pore volume was taken at the adsorption point of 0.99 p/p_0. The pore size distribution was measured by Barrett-Joyner-Halenda (BJH) method from desorption branch of the isotherm where the specific surface areas were estimated by Brunauer–Emmett–Teller (BET) equation from adsorption branch points between 0.05 and 0.3 p/p_0. Prior to the investigation, supports were heat-treated in a nitrogen flow at 400 °C for 4 h and metal-containing catalysts were reduced in hydrogen flow at 400 °C for 4 h.

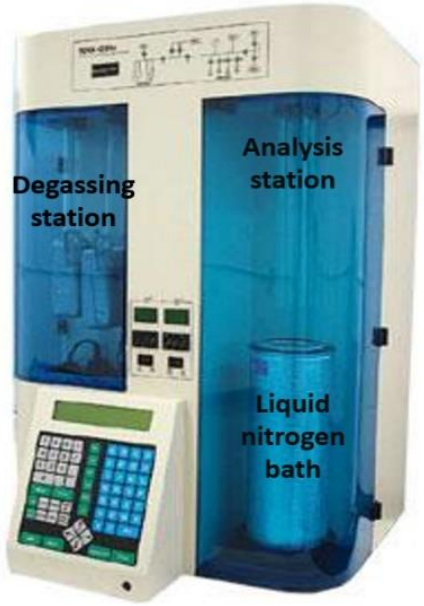

Figure 2.9. Surface area and porosity analyzer Quantachrome Nova 4200.

2.5. Catalytic Activity Measurement (Reactors)

2.5.1. Pressure Autoclave reactor

The catalytic reactions were performed using high-pressure reactors pressure autoclave (Stainless Steel, Parr Instrument Company) at an agitation speed of 1000 rpm. The reactor is shown in schematic diagram (**Figure 2.10**).

An amount of a starting material (carboxylic acid) was dissolved under continuous stirring in water as a solvent, total volume was maintained to be 25 mL. After complete dissolution, 0.5 mL of the acid solution was taken to be used as a blank (time zero point) and this sample was analysed by HPLC.

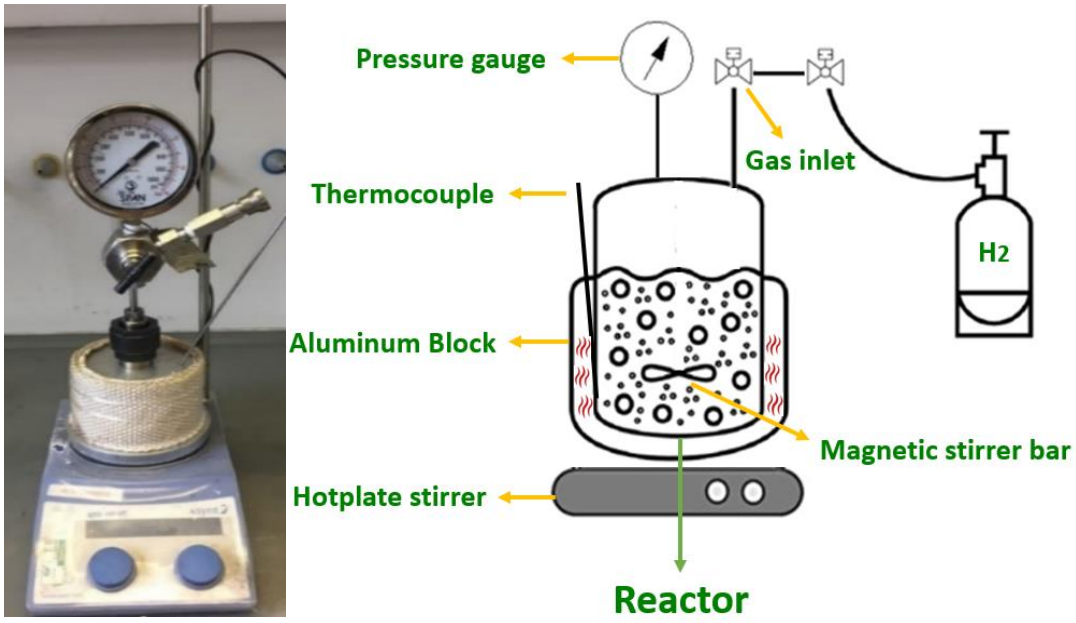

Figure 2.10. Schematic diagram and picture of pressure autoclave reactor.

The remaining solution was placed in an autoclave reactor (pressure vessel reactor or Parr stirred reactor) to start the reaction. An amount of catalyst was added with a magnetic bar into the vessel then it was purged 3 times with N_2 to remove air from the system. The vessel was heated to 150 °C, then the autoclave was pressurised with H_2 to the desired pressure after taking into the consideration the vapour pressure of water. The temperature of the reaction was controlled using thermocouple. At the end of a reaction (both reactors), the autoclave was cooled down using ice and then H_2 (overhead gas) was released and a sample was taken to be analysed by HPLC.

2.5.2. Parr Stirred Reactors

An accurate amount of a substrate and catalyst was added into an autoclave ((stainless steel Parr 4590 series reactor (50 mL) equipped with an overhead gas entrainment stirrer)) and the total volume was maintained at 25 mL. The reactor was purged with nitrogen several times to remove air and heated up to the desired temperature at an agitation speed of 1000 rpm. The temperature in the reactor was controlled by a temperature controller using a thermocouple. Then, the autoclave was pressurised with H_2 to the desired pressure after taking into the consideration the vapour pressure of water. **Figure 2.11** shows the schematic diagram of Parr reactor.

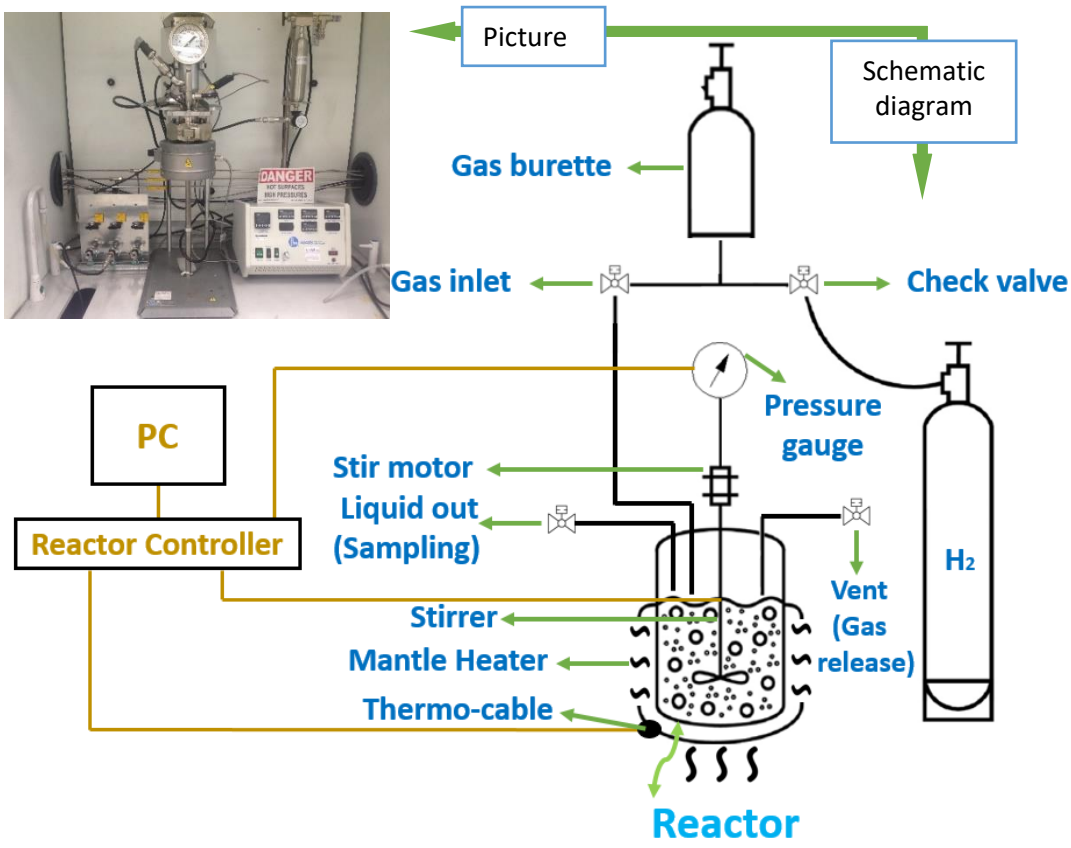

Figure 2.11 Schematic diagram of Parr reactor (Parr Instrument Company). 50 mL stainless-steel autoclave equipped with a thermocouple and overhead stirrer.

2.5.3. Microwave Chemistry

- Background

Sustainable (green) chemistry has been the subject of extensive studies during the last decade since chemical innovation has to meet both economic and environmental goals simultaneously.[182] The principles of green chemistry have prompted the development of cleaner and less energy-consuming chemical processes,[183] and the need of energy during the heating and cooling steps during the reaction and purification and the waste generated in any process are the primary detrimental effects to the environment.[183,184]

Microwaves are used in spacecraft communication, food processing, remote sensing, but most frequently in domestic heating. Recently, microwave heating has been used as a replacement for the conventional laboratory heating.[185] Microwave radiation has lower frequencies (3×10^{10} Hz and 6×10^{8} Hz) and longer wavelengths (0.5 to 50 cm) than visible light. Thus, electric charges should oscillate at that frequency to generate electromagnetic waves.[185] Electromagnetic pulse is the source of heating and microwave irradiation provides rapid and selective heating.[186]

Microwave chemistry is based on the principle of electromagnetic radiation absorption where molecules absorb radiation (electromagnetic energy) and then converted to thermal energy.[185] To transform the microwave energy into heat the dielectric substance must expose to microwave radiation.[185] The mechanisms behind the work of dielectric heating are shown in **Figure 2.12.**

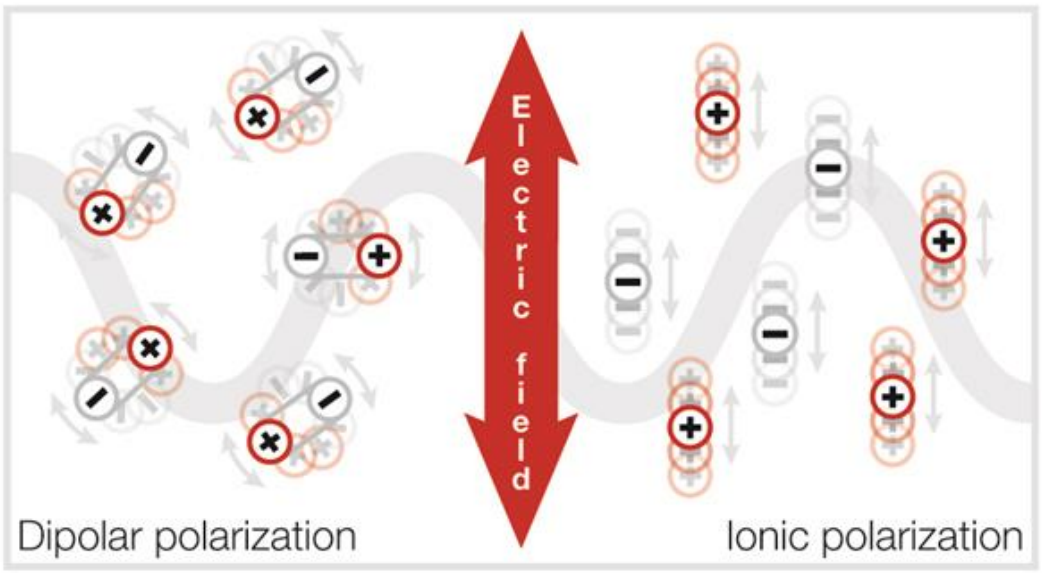

Figure 2.12 Two different dielectric heating mechanisms: dipolar polarization and ionic conduction where dipoles swing and ions move respectively in the microwave field. Adopted directly from web page (Microwave-assisted synthesis).[187]

Dipolar polarization and ionic conduction are the two effects which cause heating in the microwave. In dipolar polarization, the substance should has a dipole moment when irradiated with microwaves to be able to generate heat.[188] Because of the swing back and forth in the microwave field, and the dipoles align to the swing field. This phenomenon causes rotation and then friction, which ends up eventually in heat energy.[188] The same situations occur in ionic conduction, but now charged particles (ions) swing back and forth, which causes collisions with near molecules or atoms and this ends up creating heat.[188]

The heating by microwave-assisted synthesis is direct "molecular" heating of the reaction mixture (Table 2.2, entry 1) where no need to initial heating of the vessel surface is needed. On the contrary, conventional mantel synthesis (pressure autoclave) needs first to heat the reaction vessel surface before heating the content of the reaction vessel as shown in Table 2.2, entry 2, which takes longer time.[187]

Table 2-2 Graphical design of introduction of heat and temperature distribution in a reaction mixture for conventional and microwave heating. Adopted directly from web page (Microwave-assisted synthesis).[187]

Entry	Heat Source	Heat Introduction	Temperature Distributions
1	Microwave heating	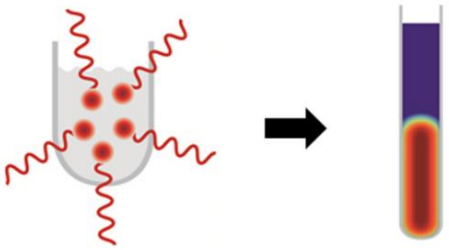	
2	Conventional heating	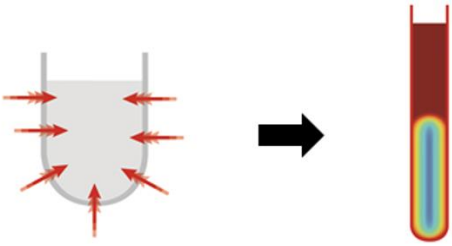	

Taking these two different systems into consideration, one study indicated that using microwaves as an energy source in chemical transformations would save much energy (up to 85-fold) than using conventional media.[183] Therefore, microwave chemistry can be a strong contributor to green chemistry. Microwave irradiation would entitle a widespread range of applications across different industries such as biotechnology, plastics, chemicals petroleum, and pharmaceuticals.[189]

- Experimental

We tested our using catalysts in a high-pressure microwave reactor. A new concept in microwave instrumentation was created by Milestone Inc. A new Milestone SynthWAVE single Reaction Chamber Microwave Synthesizer (Catalog Number 1223) was used (**Figure 2.12**).

SynthWAVE can perform single or multiple reactions at temperatures up to 300 °C and pressures to 199 bar. The SynthWAVE designed for safe and reproducible scale-up of microwave-enhanced chemical reactions and using the SynthWAVE is incredible easy.

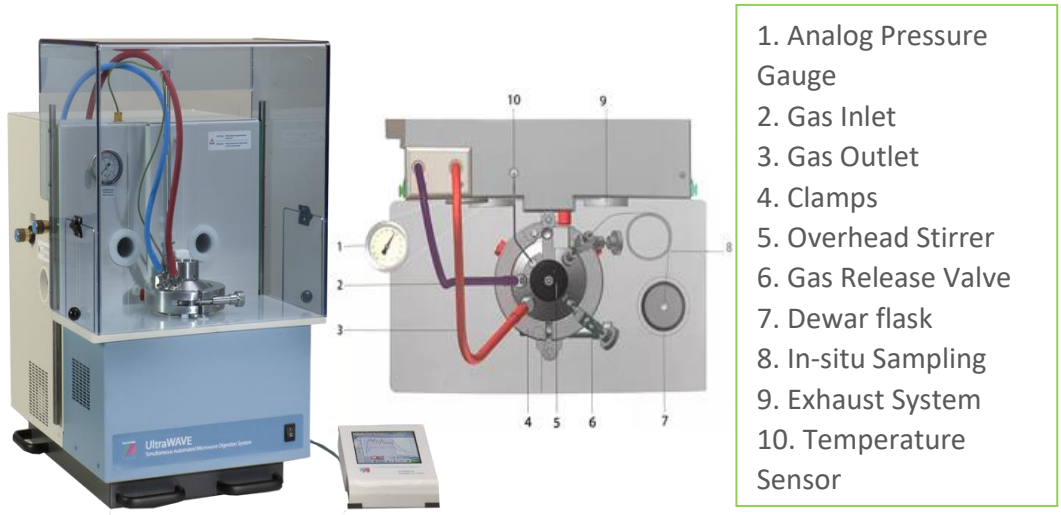

Figure 2.12. SynthWAVE high-pressure microwave picture (left), SynthWAVE reactor (right).

The procedure is described as follows: (1) after switching on the unit and logging in to the system, the program was set to the desired pressure and temperature. (2) Water was loaded into a 1000 mL of the polytetrafluoroethylene (PTFE) vessel, which was then placed in the SynthWAVE cavity.

(3) 5 vials were charged with acid solutions (e.g. SA or LA) and with the catalysts accordingly. (4) The vials were capped and held in a rack in the PTFE vessel.
(5) The rack was centred in the cavity, hung in the reactor and the reactor closed. (6) For enhanced security, the clamp was secured from outside manually as well. (7) Using a pressure regulator, the reactor was loaded with nitrogen gas several times to remove air, stirring commenced and hydrogen was pressurised to the desired pressure.
The program is automatically started to heat up to the desired temperature (e.g. 3 min to reach 150 °C). At the end of the reaction, the reactor started to cool down using recirculating chiller and the H_2 pressure was slowly released. Cool down step would take up to 40 min in the reaction (depending on the reaction temperature).

2.6. Product Analysis (HPLC)

The reaction mixtures were determined and quantified using high-performance liquid chromatography (HPLC) after filtered using 0.22 µm syringe membrane filter. Calibration curves of the reaction products were constructed using an external standard method. The calibration plots showed a linear response for each chemical and the calibration profiles of the all products can be found in Appendix. After each reaction, the product mixture was sampled and syringe-filtered and analysed by using HPLC, Agilent 1200 Series, (Santa Clara, CA, USA). The HPLC was equipped with an inline degasser, quaternary pump, an auto-sampler, a refractive index detector (RID) and a Varian Metacarb 67H column (300 x 6.5 mm), using an aqueous solution (mobile phase) of sulphuric acid (2.8 mM) at a flow rate of 0.8 mL min^{-1} at 30 °C.

2.7. Calculated Formulas

Conversion of succinic acid (**X**), selectivity (**S**), yields of the products (**Y**), dispersion of the metallic phase (**D**) and carbon mass balance (**CMB**) were calculated as follows:

Equation 2.10

$$\boldsymbol{X}\ (\%) = \frac{initial\ concentration\ of\ succinic\ acid\ -\ final\ concentration\ of\ succinic\ acid}{initial\ concentration\ of\ succinic\ acid} \times 100$$

Equation 2.11

$$S\ (\%) = \frac{concentration\ of\ product}{initial\ concentration\ of\ succinic\ acid\ -\ final\ concentration\ of\ succinic\ acid} \times 100$$

Equation 2.12

$$Y\ (\%) = \frac{concentration\ of\ product}{initial\ concentration\ of\ succinic\ acid} \times 100$$

Equation 2.13

$$CMB(\%) = \frac{total\ mole\ of\ products\ and\ unreacted\ substrate}{initial\ moles\ of\ substrate} \times 100$$

CHAPTER 3

Selective Hydrogenation of Succinic Acid in Water by Pd,Pt, and Ru Catalysts Supported on Activated Carbon and Carbon Nanotubes

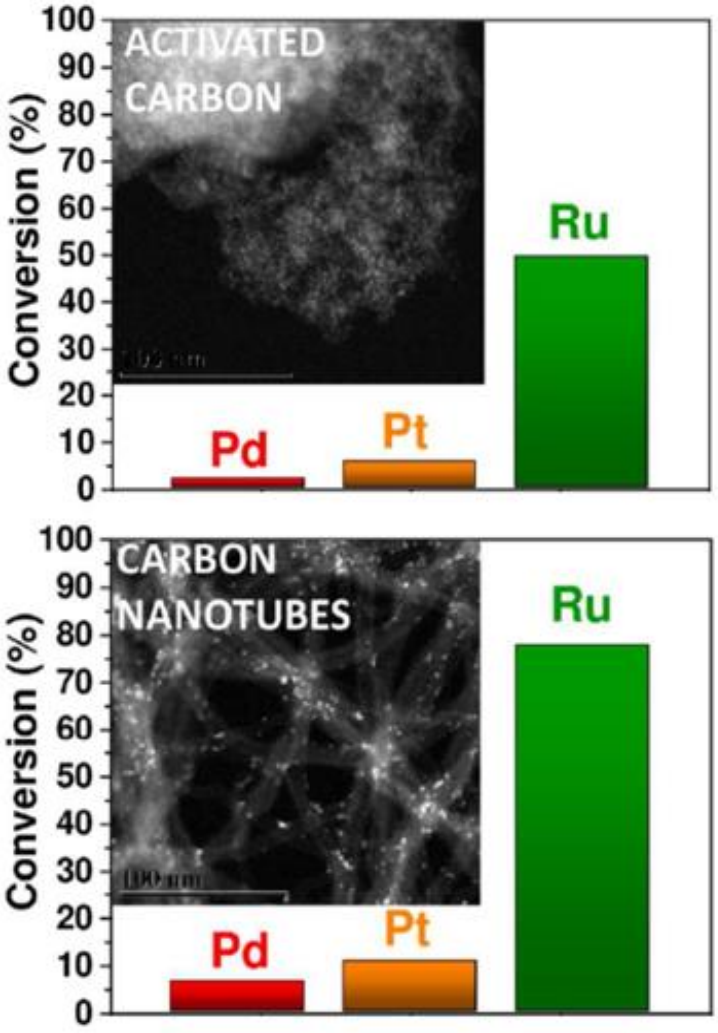

CHAPTER 3: Selective Hydrogenation of Succinic Acid in Water by Pd, Pt, and Ru Catalysts Supported on Activated Carbon and Carbon Nanotubes

3.1. Introduction

Succinic Acid (SA), a biomass-based dicarboxylic acid, is an essential molecule used for pharmaceutical products and biodegradable plastics.[78] Green-feedstock succinic acid can replace maleic anhydride to produce a variety of chemicals via hydrogenation processes, i.e., γ-butyrolactone (GBL), 1,4-butanediol (BDO), and tetrahydrofuran (THF) due to increased production in biorefineries.[190] However, improvements in this process, such as the use of low temperatures and pressures or the introduction of a reactive metal-based catalyst, are needed. It is difficult to hydrogenate the SA, due to the low electrophilicity of the carbonyl carbon.[191]

Based on a literature reports, the reaction medium plays an essential role in reactivity in the hydrogenation of SA. Mostly, 1,4-dioxane was used in previous reports as it is an effective solvent, since the reaction proceeded fast compared to using water. Zhang *et al.*[88] converted 72 % of succinic acid after 33 h in water over 2% Ru/C with 66 % selectivity to GBL at 180 °C and high hydrogen pressure (150 bar). While Hong *et al*.[87] obtained 90 % conversion in 8h using 1, 4-dioxane over 5% Ru/C at 240 °C and 80 bar hydrogen pressure and selectivity to GBL was 74 %. Moreover, Luque *et al*.[104] achieved 90 % conversion of SA over 5% Ru/C and 60, 30 and 10 % selectivities to THF, GBL and BDO, respectively. The study used 3:5 mixtures of ethanol in water as a solvent at mild conditions and long reaction time (100 °C, 10 bar, 24 h), although the role of ethanol in the reaction is uncertain. Water is a green, abundant, and safe solvent compared to alcohols and especially 1,4-dioxane which is toxic.[192,193] Also, succinic acid is produced by fermentation as an aqueous solution,[100] so using water would be an ideal. The hydrogenation of SA is composed of various reaction steps, as shown in **Scheme 3.1**.

The first step in the hydrogenation pathway is the hydrogenation of SA to produce GBL. Subsequently, GBL is hydrogenated to give BDO or THF depending on the reaction conditions applied. THF could be obtained directly from the acid catalysed dehydration of BDO.[194] Undesired straight-chain alkanes, alcohols and acids are produced by over hydrogenation and hydrogenolysis reactions. Thus, getting a specific product from succinic acid hydrogenation is not straightforward, as there is a wide range of possible hydrogenation products.

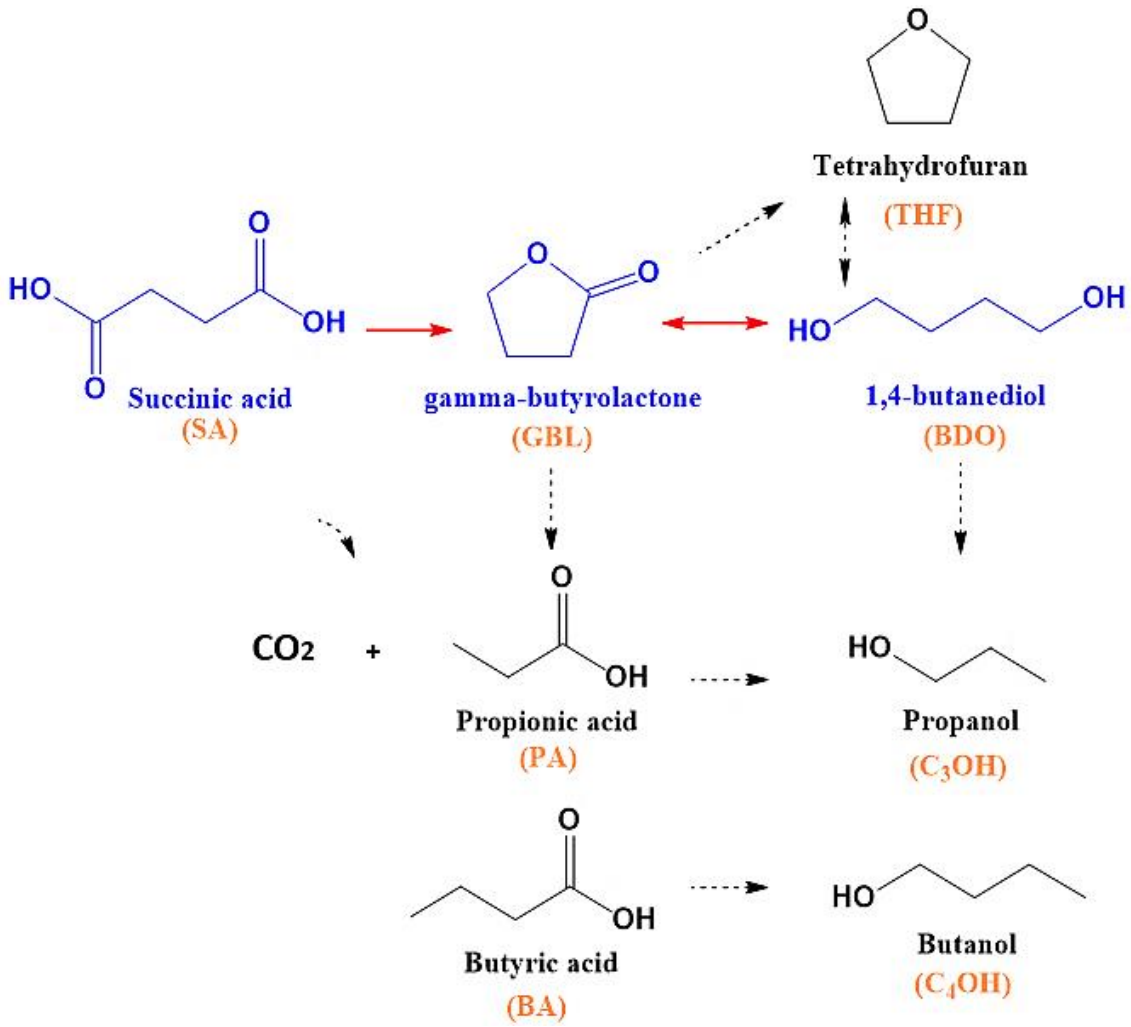

Scheme 3.1 Suggested scheme for the hydrogenation of succinic acid.

It should be noticed here that if the catalyst was able to produce just GBL in abundant content, BDO would be readily formed from a further hydrogenation of GBL. However, if hydrogenolysis of SA, GBL, and BDO to propionic acid, butyric acid, and primary C_3/C_4 alcohol respectively have happened, then gaining BDO in high yield is not possible. Therefore, finding a suitable noble metal that can hydrogenate first carboxylic acid, promote cyclisation to GBL, and then further hydrogenate GBL to BDO is important.

Ru is renowned as a highly active catalyst in both homogeneous and heterogeneous systems.[195,196] Michel, and Gazellot concluded that Ru catalysts have superior activity compared to other precious metals in aqueous solution, but the reason is still under investigation.[197] In heterogeneous catalytic processes, carbon has attracted attention to be used as a support due to its properties, which can be tailored to specific purposes.[22]

Activated carbon (AC) is commonly used as a support in catalytic systems due to the high surface area, well-developed porosity, and stability at elevated temperatures.[198,199] However, in the last decade, new forms of carbon such as carbon nanotubes (CNTs) have been discovered and demonstrated to be a potential catalyst support.[45]

CNTs were first observed by Davis, Slawson, and Rigby in 1953[37] and have become increasingly popular owing to their unique structural properties, such as electrical conductivity, porosity or specific metal-support interactions.[200,201] CNTs are capable to enhance a dispersion of the active phase.[202,203] Liao *et al.*[204] showed that the activity of Pd nanoparticles was improved by supported on CNTs in a hydrogenation of levulinic acid to γ-valerolactone. Also for the same reaction, Teixeira *et al.*[156] showed that the activity of molybdenum carbide nanoparticles supported on CNTs increased.

Ru catalysts with various supports have been widely studied.[196,205] CNT supported Ru showed excellent performance in various types of reactions, such as syngas conversion,[206] dehydrogenation/hydrogenation,[201,207] NH_3 decomposition,[208] and hydroformylation.[209]

A significant application of Ru catalysts is in the hydrogenation of biomass feedstock to various chemicals.[205,210,211] Additionally, the deposition of Ru particles on or in CNT channels may enhance the performance of the catalyst. One study has demonstrated higher activity of Ru/CNT in ammonia synthesis when Ru particles dispersed on the outside of CNTs compared to a catalyst where the particles located inside the channels.[212] However, Ran *et al.*[213] have observed an opposite trend in cellobiose hydrogenation since the catalyst activity increased when Ru particles were dispersed inside of the CNTs, and this might be due to an enrichment of the reactant in the channels.[214] In addition, increasing the selectivity to a specific product was also achieved with confined Pt nanoparticles within CNTs in the hydrogenation of cinnamaldehyde showing an improvement in selectivity to cinnamyl alcohol.[215,216] This may be due to a curvature of the channels which may alter molecular adsorption on an active phase and this modifies the catalytic activity/selectivity of the reaction outcome.[215] Rossi *et al*.[217] reported that it is easy to fill the tubes with a liquid due to the action of capillary forces since the walls inside the CNTs channels are hydrophilic. Wang *et al*.[157] showed that Ru particles can also be loaded into CNTs channels using an ultrasonication-assisted impregnation method. High purity is one of the requirements for optimal performance of CNTs in their numerous applications.[218]

Often as-prepared CNTs contain significant amounts of impurities, from the use of metal catalysts, such as Fe, Co, and metal alloys (e.g., Fe-Co) during the synthesis.[219,220] Amorphous carbon could also be present either along the walls of the graphitic tubes or twisted within them.[221] The presence of these impurities and amorphous carbon could change the electrical properties of the CNTs.[220] Since CNTs have such a wide variety of potential applications, it is vital to remove residual metals and various impurities to gain more control of their properties. Chemical oxidation, thermal oxidation, chromatography, centrifugation, filtration and many other methods have been investigated to wash CNTs.[218] These techniques, however, have high thermal budgets and are time-consuming.[221]

Therefore, future research is needed to find an efficient, cheap, and easy way to wash the nanotubes (with water) which causes no damage to the nanotubes.

Herein, the catalytic performance of Ru supported on CNTs is assessed in the hydrogenation of SA in liquid-phase for the first time. The primary goal of this study was to find an active and selective catalyst for the hydrogenation of succinic acid. Therefore, in this chapter we investigate the effect of different parameters such as Ru loading, temperature, supports and hydrogen pressures on catalytic activity and selectivity. The catalytic activity and selectivity of 5% Ru(IN)CNT where Ru particles were deposited inside CNT was assessed.

Ru catalyst supported on unwashed-CNTs (5% Ru/unwashed-CNT) was also evaluated and compared with washed-CNTs (5% Ru/CNT). For comparison, the activity of different metal nanoparticles i.e., Pd and Pt supported on activated carbon and CNTs were also evaluated to establish their relative activity in succinic acid hydrogenation. Finally, recycling tests were performed to assess the reproducibility of the washed-CNT supported Ru catalyst (5% Ru/CNT) during liquid phase hydrogenation of succinic acid reaction.

3.2. Experimental

All catalysts used in this chapter were prepared by incipient wetness impregnation whereas Ru(IN)CNT was prepared following Wang *et al*.[157] work as described in Chapter 2. Ruthenium loading in all catalysts was fixed at 5 wt. % unless otherwise mentioned. Water-washed CNTs were used to prepare virtually all the catalysts whereas 5% Ru-unwashed CNT (The washing steps were shown in Chapter 2). Furthermore, 5% Ru/CNT refers to washed-CNT supported 5% Ru catalyst. 5% Ru/CNT also refers to 5% Ru(Mix)/CNT (Ru particles are dispersed inside and outside of the CNTs).

3.3. Results and Discussion

The AC and CNT supported Ru catalysts and Pd/Pt supported on CNT were characterised by different methods and assessed in liquid phase hydrogenation of succinic acid.

3.3.1. Characterization of Catalysts

3.3.1.1. Powder X-Ray Diffraction Analysis

The XRD patterns of unwashed-CNTs, water washed-CNTs, AC, and the corresponding Ru catalysts are presented in Figure 3.1 whereas 5% Ru(IN)/CNT, 5% Ru/CNT, 7%Ru/CNT, and 10% Ru/CNT are shown in Figure 3.2. By comparing the XRD results of CNTs before and after washing step, there is no change in the characteristic diffraction peaks of CNTs after the water pre-treatment which suggests that the structure of CNTs was not destroyed or changed by the washing step.

As the carbon nanotubes have different orientations to the incident X-ray beam, a statistical distribution of carbon nanotubes is expected. As a result, the critical features of the X-ray diffraction pattern of CNTs are similar to those of graphite.[222] Almost all the XRD patterns of Ru catalysts lack a diffraction peak for Ru except for 5% Ru/AC sample (Figure 3.1) where a peak for Ru (101) at 44° was shown (JCPDS 001-1253). However, the presence of Ru is confirmed, in most of other samples cases, by other characterisation methods (e.g. TEM), suggesting that the Ru particles are outside of the detection limits of XRD, most likely due to their small size and highly dispersed nature.

In all CNT-based diffractograms, peaks at 25.7°, 42.7°, and 78.5° were indexed as (002), (100), and (110) reflections for graphite structure, respectively[223,224] (JCPDS 00-001-0640).

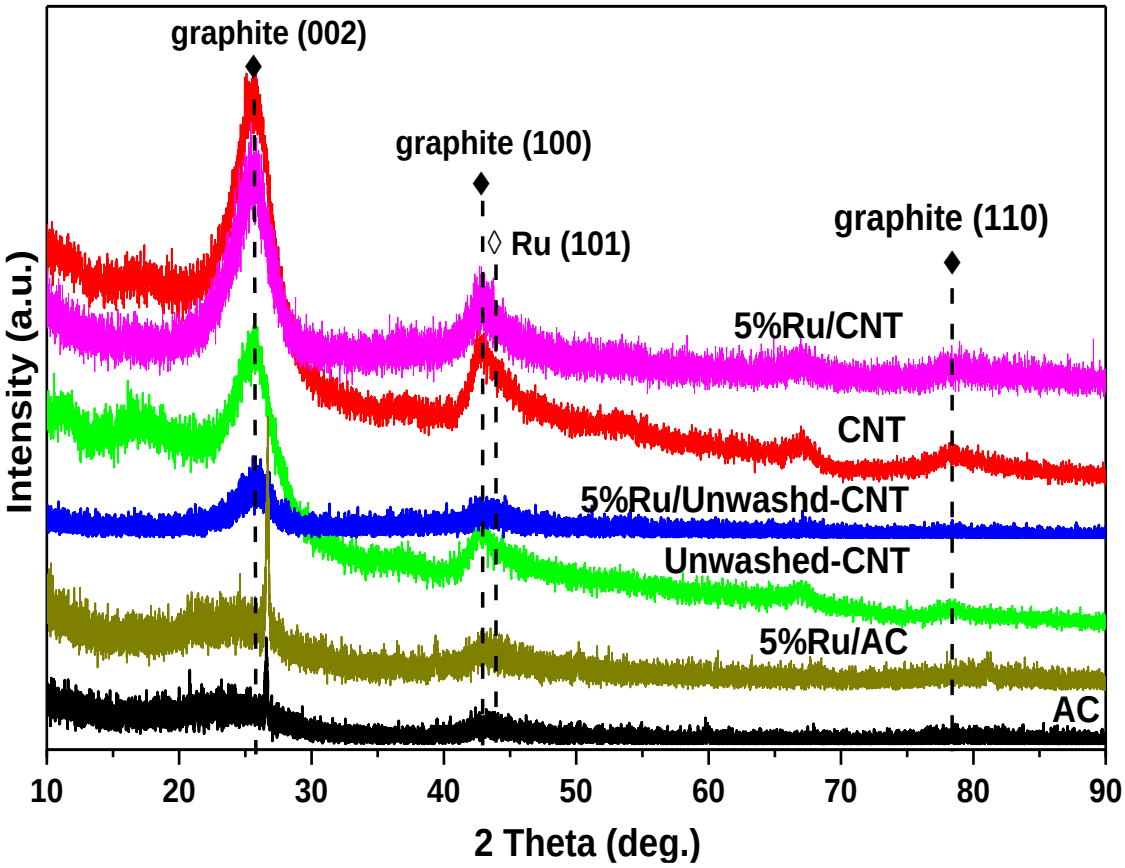

Figure 3.1. XRD patterns of carbon nanotubes, reduced Ru catalysts with different supports.

There are no diffraction peaks of metallic Ru, in Ru prepared catalysts supported on CNT, which indicates that the Ru particles are highly dispersed, even at 10 wt. % of Ru, the low intensity of the C (002) peak suggests an overall lack of graphitic ordering in the carbon,[225] which is observed in many Ru catalysts, such as 5% Ru(IN)CNT, 5% Ru/unwashed-CNT and 10% Ru/CNT catalyst (Figure 3.2).

5% Ru(IN)CNT sample also does not show any other diffraction peaks apart from the characteristic diffraction peaks of CNT.

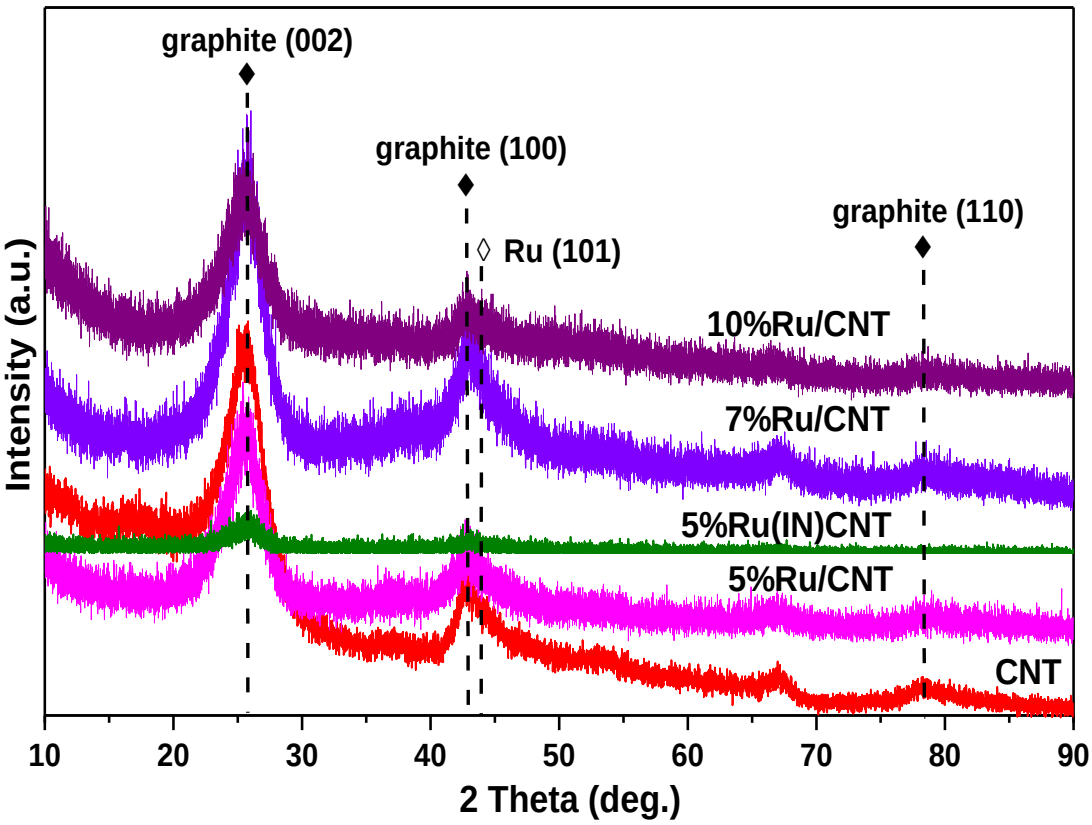

Figure 3.2. XRD patterns of carbon nanotubes, reduced Ru catalysts with different Ru's loading.

The XRD patterns of 5% Pd/CNT and 5% Pt/CNT are compared together with 5% Ru/CNT in Figure 3.3. Peaks at 39.9°, 46.4° and 67.8° and 40°, 46.5° and 67.2° correspond to the (111), (200), and (220) planes of the face centered cubic phases of Pd,[226] and Pt,[227,228] respectively.

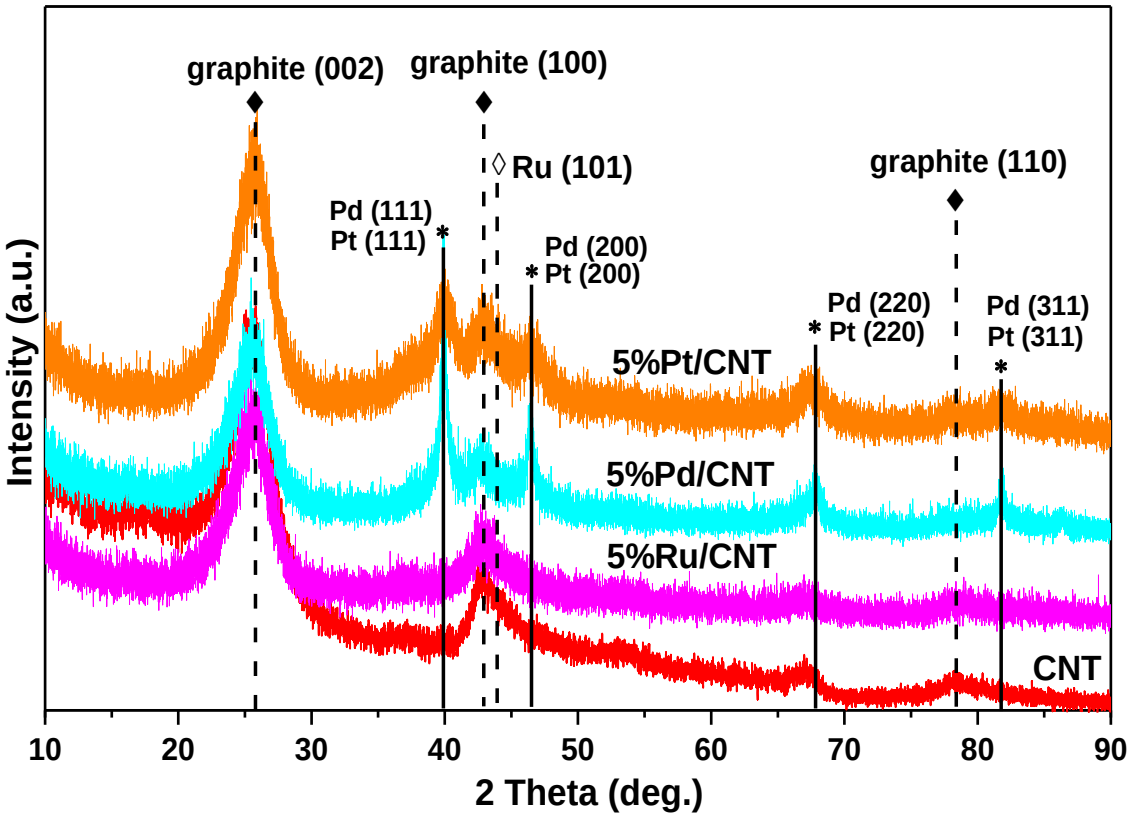

Figure 3.3.XRD patterns of carbon nanotubes, reduced Ru, Pd, and Pt catalysts

3.3.1.2. Dispersion of Metal Particles by CO Chemisorption

We investigated the dispersion of active metals on the surface of the catalyst using CO chemisorption. In **Table 3.1**, the capacity of the catalysts to chemisorb CO is reported along with the dispersion values obtained.

The Ru dispersion differs from one catalyst to other, for example, 5% Ru/unwashed-CNT show a lower Ru dispersion which might be due to the presence of those impurities, whilst the opposite was observed with the washed-CNT catalyst (5% Ru/CNT). The 5% Ru(IN)CNT showed lower dispersion compared to 5% Ru/CNT which might indicate that the Ru particles are located inside the CNTs.

Table 3-1 List of educed catalysts, results of CO chemisorption and average particle size for reduced catalysts. Metal dispersion was calculated from CO chemisorption.

Catalyst	CO uptake, µmol/g	Metal Dispersion, %	Average Particle Size (TEM), nm
5% Ru/AC	66.2	13.3	1.3±0.2
1% Ru/CNT	13	13.4	-
3% Ru/CNT	20	6.6	-
5% Ru/CNT	40.0	8.0	1.4±0.4
5% Ru/unwashed-CNT	24.5	4.9	-
5% Ru(IN)CNT	28.3	5.7	-
7% Ru/CNT	57.9	11.7	1.4±0.4
10% Ru/CNT	83.6	16.9	1.6±0.3
5% Pd/CNT	19.6	2.1	2±0.7; 10±2.2
5% Pt/CNT	60.0	12.8	2±0.5

A direct method to confirm whether the Ru particles are located inside or outside of the tubes and also the size of those particles is TEM.[157] However, because of an absence of TEM images of 5% Ru(IN)CNT, it has not been confirmed where the particles are placed. A selection of Ru catalysts supported on CNT with different loading were prepared.

Table 3.1, showed also that the quantity of CO uptake increases as increasing the Ru loading from 1 to 10 wt. %., and apart from 1% Ru/CNT the Ru dispersion increased from 6.6, 8.0, 11.7, to 16.9 % for 3, 5, 7, and 10 wt. % of Ru respectively. It should be noted here that for an unknown reason the metal particle size from TEM measurement does not match with the metal dispersion obtained from CO-chemisorption analyses. However, an obtained metal particle size from TEM studies would be more accurate than the estimation from CO-chemisorption analyses since the latter method is considered to be an indirect method to obtained metal practical size compared to TEM measurements.

3.3.1.3. Particle Size Distributions by Transmission Electron Microscopy (TEM)

Representative TEM images with respective particle size distributions are shown below. In all ruthenium-based catalysts, most of Ru particles were finely dispersed on the support with a narrow size distribution in the range of 0.7–3.0 nm.

The loading of Ru on CNTs does not affect much the distribution of the active phase since it can be seen from the images that as the Ru content is increased the average size of Ru particles increases slightly.

The Ru particle size is 1.4±0.4, 1.4±0.4, and 1.6±0.3 nm for 5% Ru/CNT, 7% Ru/CNT, and 10% Ru/CNT, respectively as shown in **Figure 3.4**, **Figure 3.5**, and **Figure 3.6**. Moreover, Ru particles are located outside and inside of the tubes in all TEM images for the samples (5, 7, and 10 wt. %).

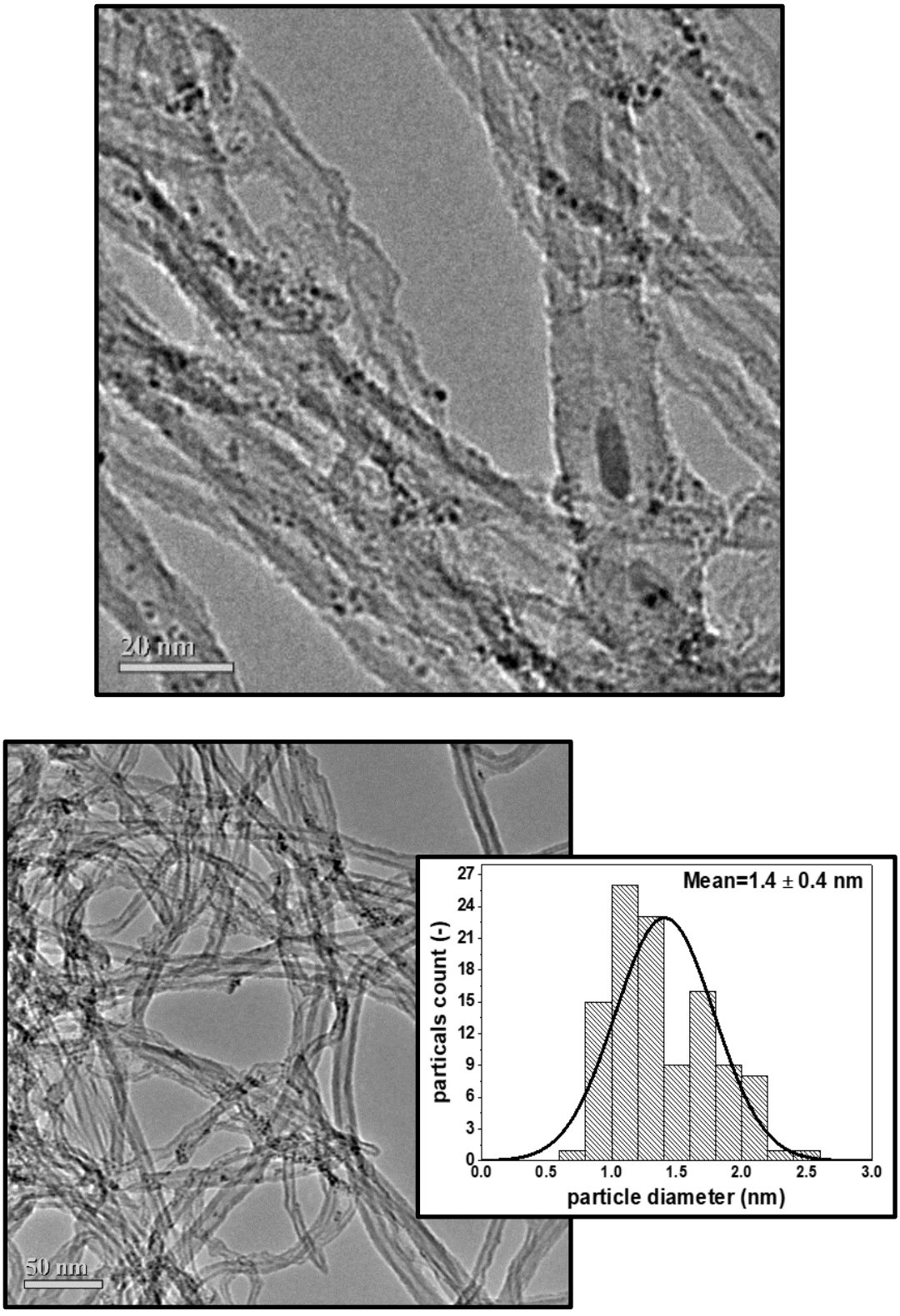

*Figure 3.4.*TEM images of reduced 5% Ru/CNT and particle size distribution.

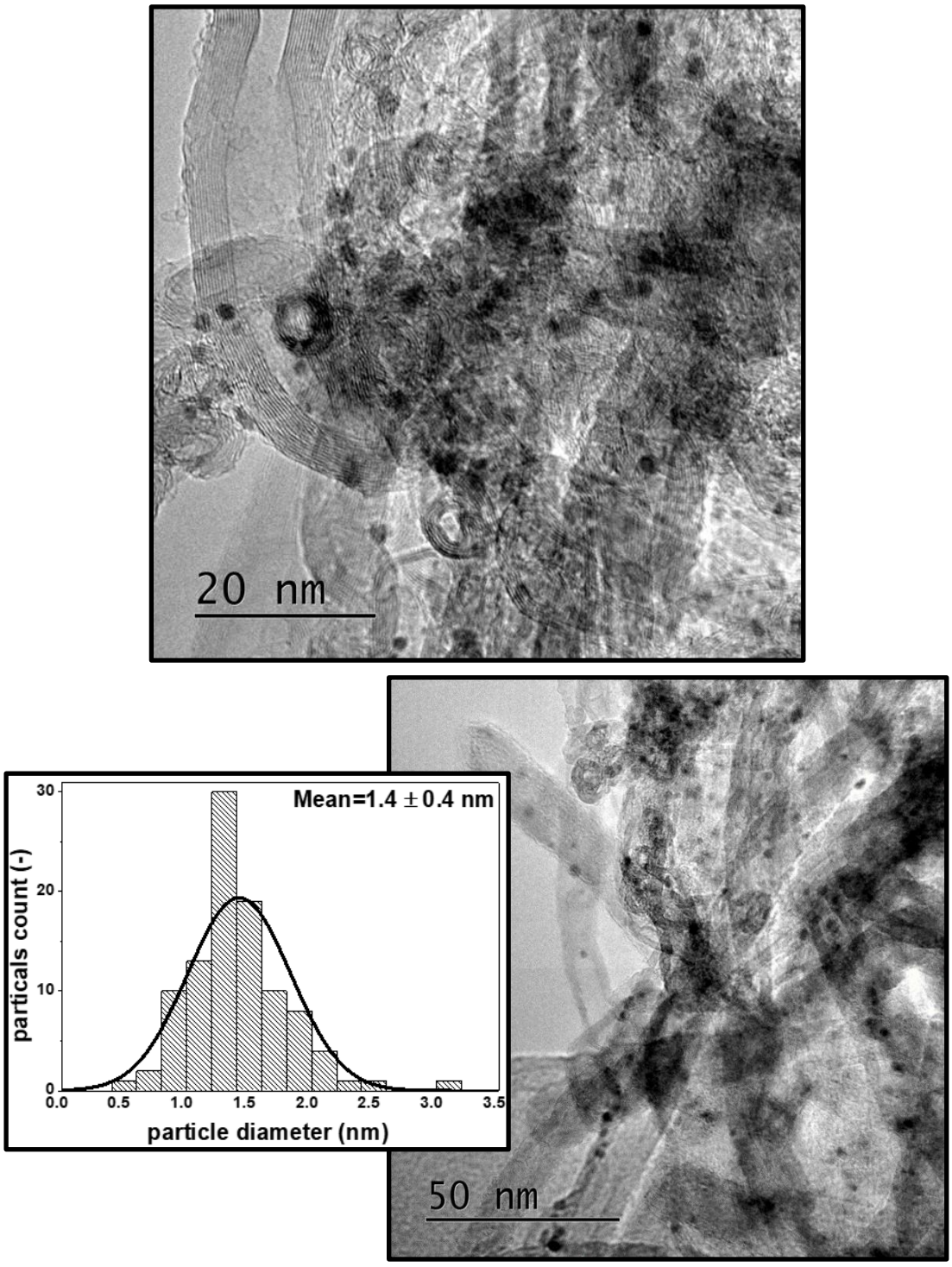

Figure 3.5. TEM images of reduced 7% Ru/CNT catalyst and particle size distribution.

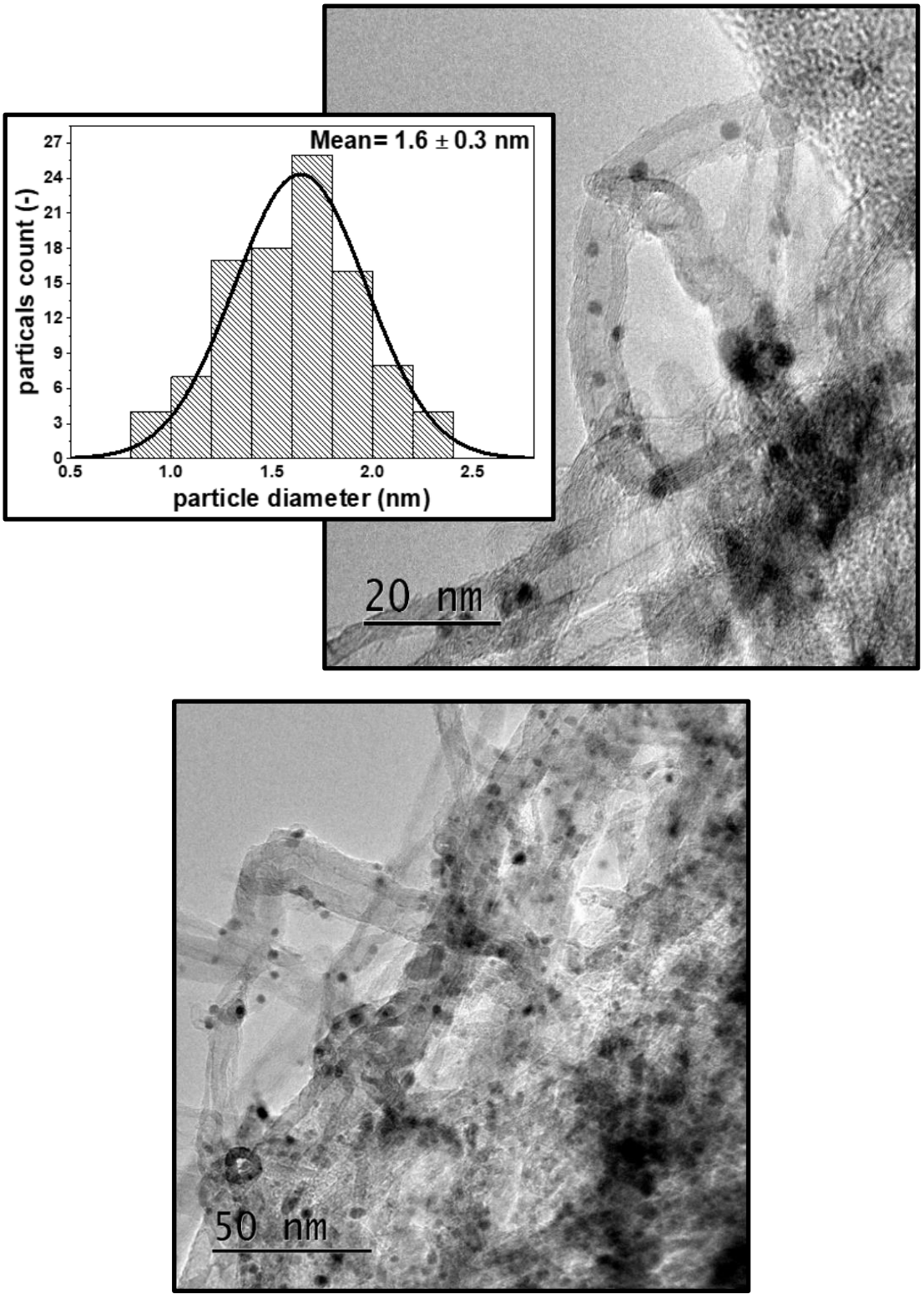

Figure 3.6. TEM images of reduced 10 % Ru/CNT catalyst and particle size distribution.

The CO-uptake results obtained from 5% Pd/CNT and 5% Pt/CNT are compared to 5% Ru/CNT. Pd shows low dispersion on the CNTs compared to Ru and Pt which might attributed to the formation of bigger Pd particles on the CNTs. This finding agreed with the results acquired from TEM where this catalyst exhibited a bimodal distribution showing agglomeration to large particles between 6 and 13 nm apart from the small (2±0.7 nm) nanoparticles (**Figure 3.7**). This distribution with big particles would decrease the CO-uptake and the overall activity of Pd catalyst.[229]

Moreover, Pt particles showed better dispersion (12.8 %) on CNT compared to dispersion of Ru particles on CNT (8 %). A further investigation by TEM showed that Pt particles on CNT are well dispersed, and the average size of the metal was 2 nm which is slightly higher than the Ru average particle size in 5% Ru/CNT. TEM images with particle size distribution are presented in **Figure 3.8** and show Pt particles inside the tube in some of images.

There is a difference between the results obtained from 5% Ru/AC and 5% Ru/CNT which could affect the overall activity of a given catalyst. The dispersion of Ru in 5% Ru/CNT (8 %) was lower than in 5% Ru/AC (13.4 %). However, TEM results showed that Ru average particle size on AC was smaller (1.3±0.2 nm) than on CNT (1.4±0.4 nm) however, considering the standard deviation they are similar. TEM images with particle size distribution of 5% Ru supported on AC are presented in **Figure 3.9.**

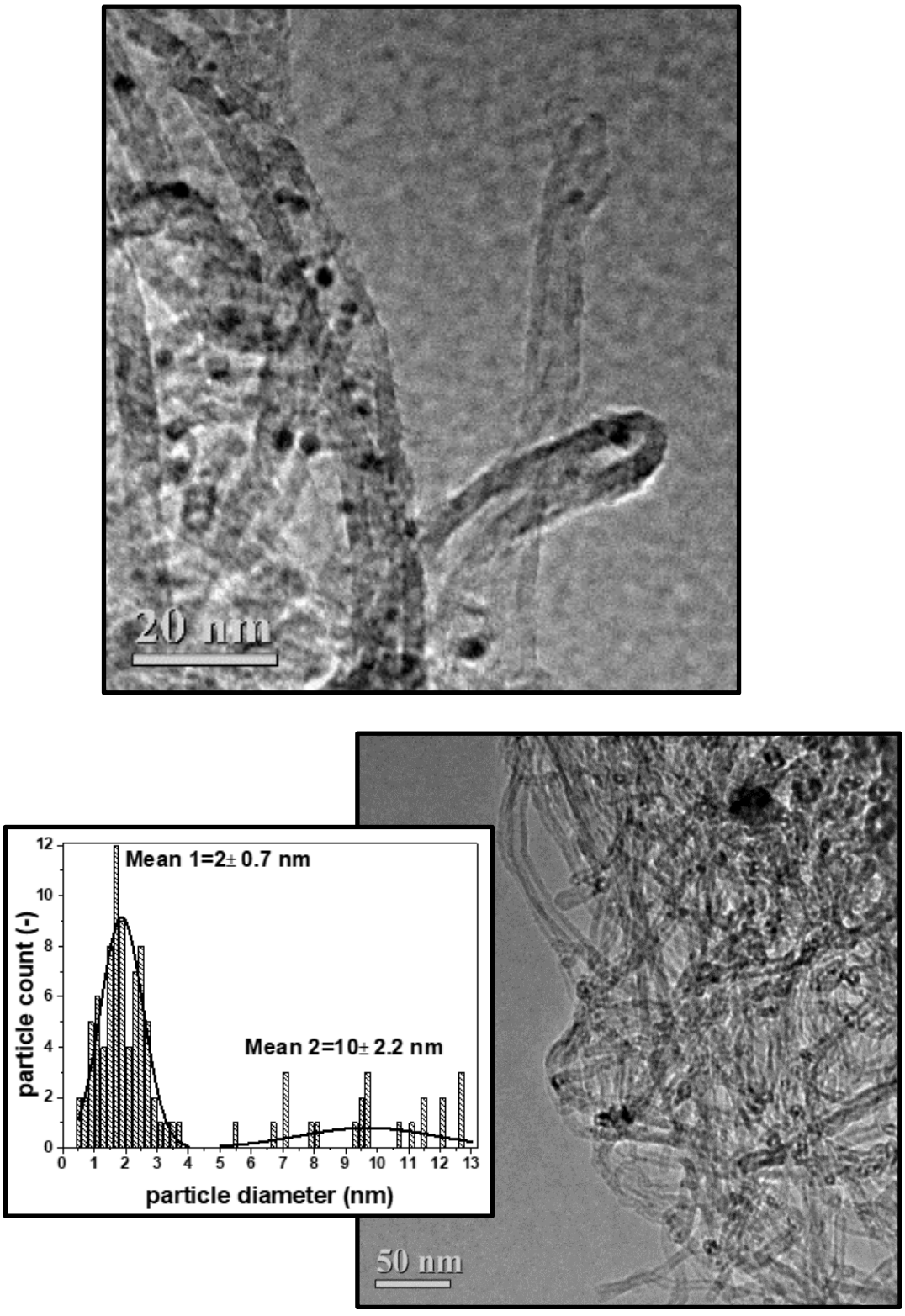

Figure 3.7. TEM images of reduced 5% Pd/AC catalyst and particle size distribution.

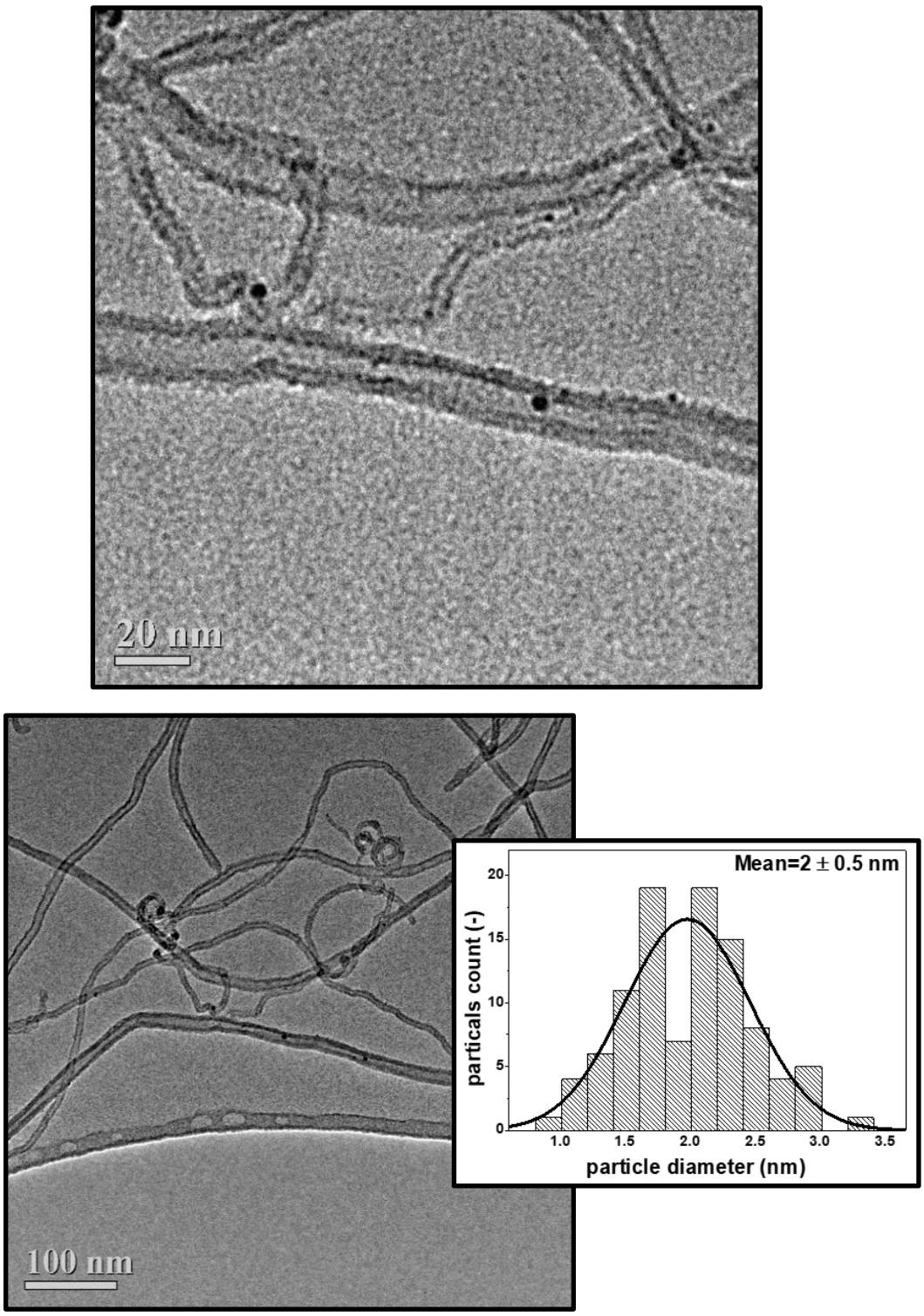

Figure 3.8 TEM images of reduced 5% Pt/CNT catalyst and particle size distribution.

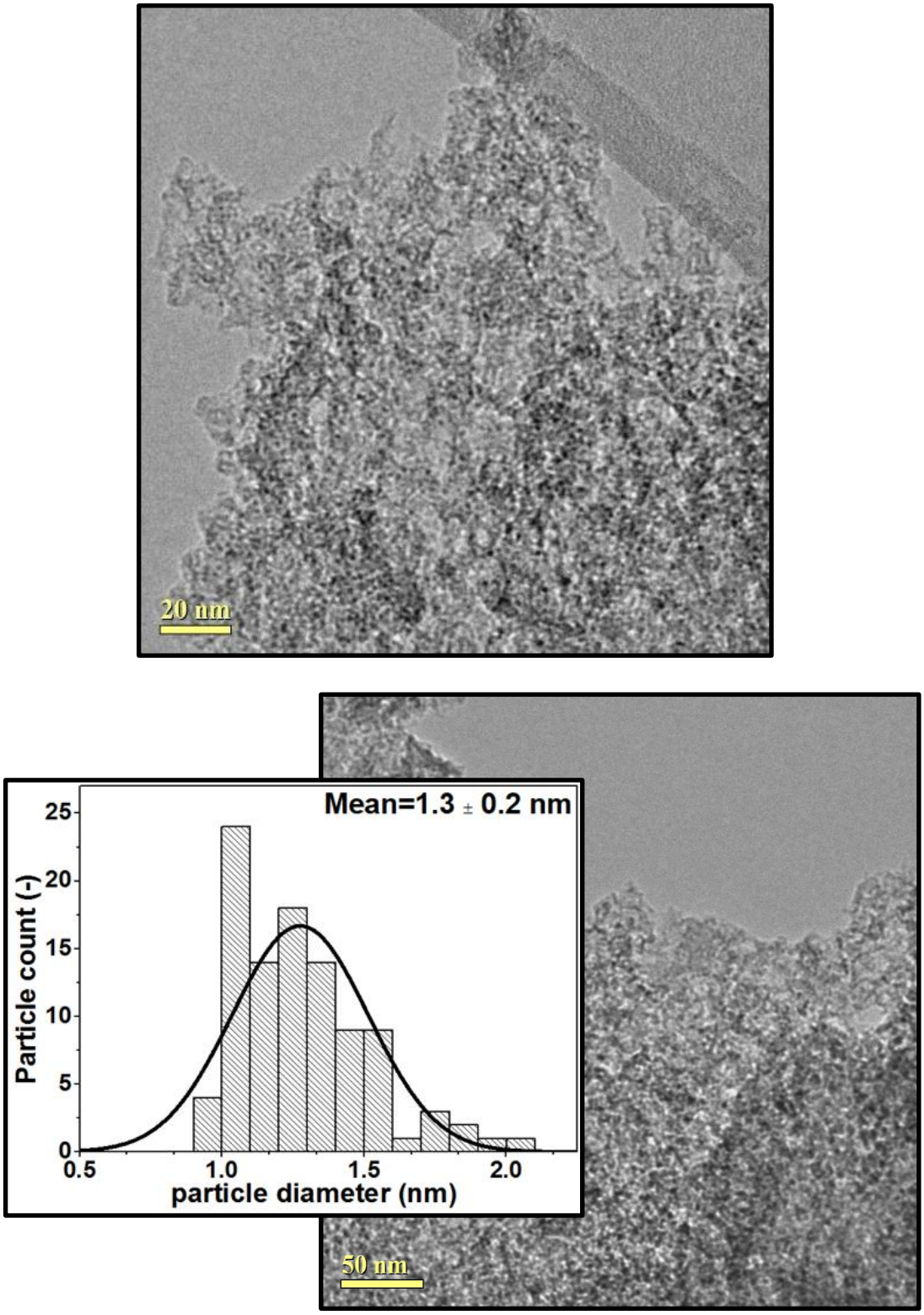

Figure 3.9. TEM images of reduced 5% Ru/AC catalyst and particle size distribution

3.3.1.4. Reducibility of the Pd, Pt, and Ru Based Catalysts by H_2-TPR

Temperature programmed reduction (H_2-TPR) was used to investigate the reducibility of the as-synthesized catalysts and to understand their redox properties and interaction between Ru, Pd, Pt, and supports.[208,230-233] Furthermore, TPR experiments determined the appropriate reduction temperature for the catalyst before activity assessment. The profiles for Ru based catalysts are present in **Figure 3.10.**

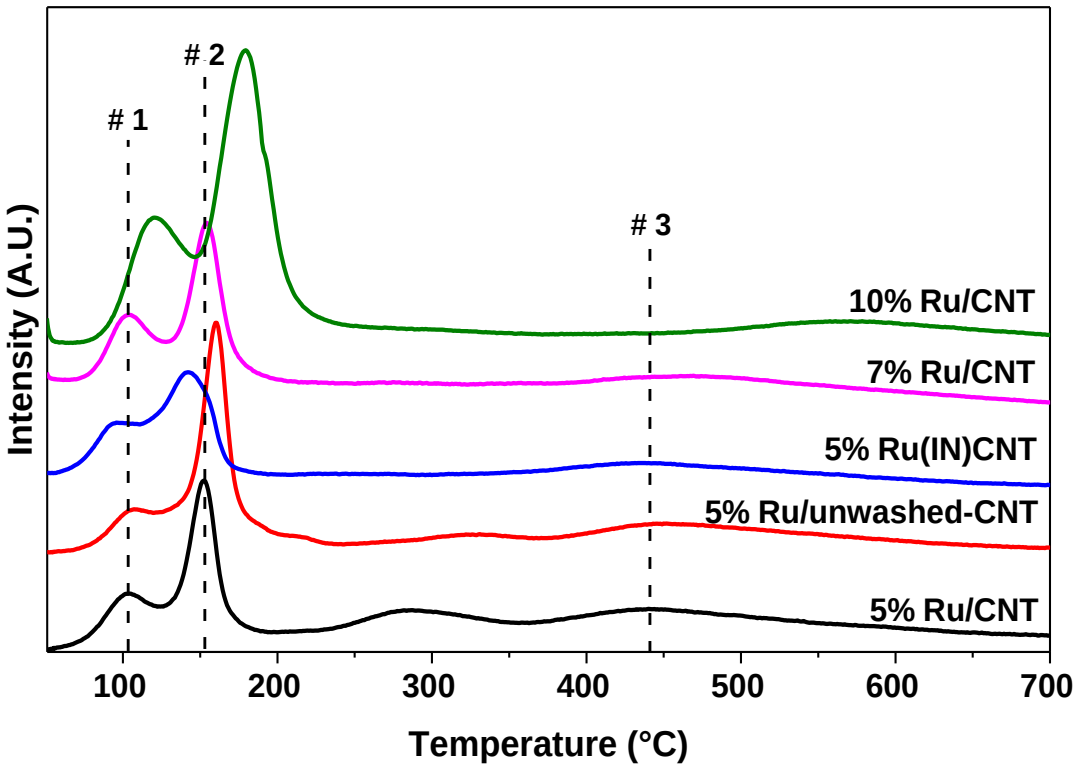

Figure 3.10. H_2-TPR profiles for different Ru catalysts (Unreduced).

Two temperature ranges are apparent in the TPR profiles, above and below 250 °C. At temperatures below 250 °C, it shows the decomposition of the precursor chlorides and reduction of the metal precursor to a metallic state. For Ru catalysts prepared from $RuCl_3$, three reduction peaks were observed. The first peak at about 104 °C (#1) could be assigned to a reduction of Ru^{3+} species to metallic Ru.[230]

The second peak with a maximum at approximately 153 °C (#2) is similar to the reduction temperature of unsupported $RuCl_3$.[232,234] The third broad peak between ca. 400-500 °C corresponds to a reduction of carbon species or carbon-related functional groups[233] or due to carbon methanation by the presence of supported metals,[85,230,232] which could be followed by catalyst deactivation.[233] The last peak is less evident in Pt, Pd, and Ru(IN) catalysts supported on CNT whereas this peak shifted to a higher temperature with increasing the wt. % of Ru in the catalysts supported on CNT.

5% Ru(IN)CNT spectra displayed two broad H_2 consumption peaks at temperature of 95 °C, and 144 °C, which are lower than the results obtained from 5% Ru/CNT. Ru species inside the CNTs channels are easier to reduce,[212] perhaps due to an interaction between the anionic chlorine in $RuCl_3$ and the electron-deficient carbon nanotubes concave surface which may weaken the bonding strength of $RuCl_3$ which makes ruthenium species easy to be reduced.[235]

Regarding different Ru catalysts loading, a small shift occurs towards higher temperature in 7% Ru/CNT compared to 5% Ru/CNT, although 10% Ru/CNT shows a further shift. The group of J.A. Lopez-Sanchez,[236] have used different loading of ruthenium catalysts supported on CNT to hydrogenation of 2,5-hydroxymethylfurfural to 2,5-dimethylfuran. The study reported that based on the catalyst preparation (Current study used the same procedure to prepared the catalyst) the metal particles started to fill inside the of carbon nanotube and as increasing the metal percentage the partials started to form outside of the tube. They characterised these different percentage of Ru catalysts loading using temperature programmed reduction.

They found that increasing metal loading shifts the reduction peak to higher temperatures as we have seen here in current study. They referred this observation to the presence of those particle inside the tube. As stated early (while we characterised 5%Ru(IN)CNT) that the partials inside the tube are easy to reduce due to the electron-deficient carbon nanotubes concave surface.[212]

For these reasons, TPR results of the current study showed the reduction peak at lower temperature for 5% Ru/CNT compared to 7% Ru/CNT and 10% Ru/CNT since the latter two catalysts might have a lot of the particles outside the tube which difficult their reduction and consequences of that the catalysts (7% Ru/CNT and 10% Ru/CNT) reduced at higher temperature.

The 5% Ru/unwashed-CNT reduction peak shows a shift to a higher temperature also indicating that there is a strong interaction between metal salt ($RuCl_3$) and unwashed-CNT[237] or might be due to the presence of impurities that in CNT which would influence catalytic rates. We also compared the reducibility of Ru/CNT with different metals and support as shown in **Figure 3.11.**

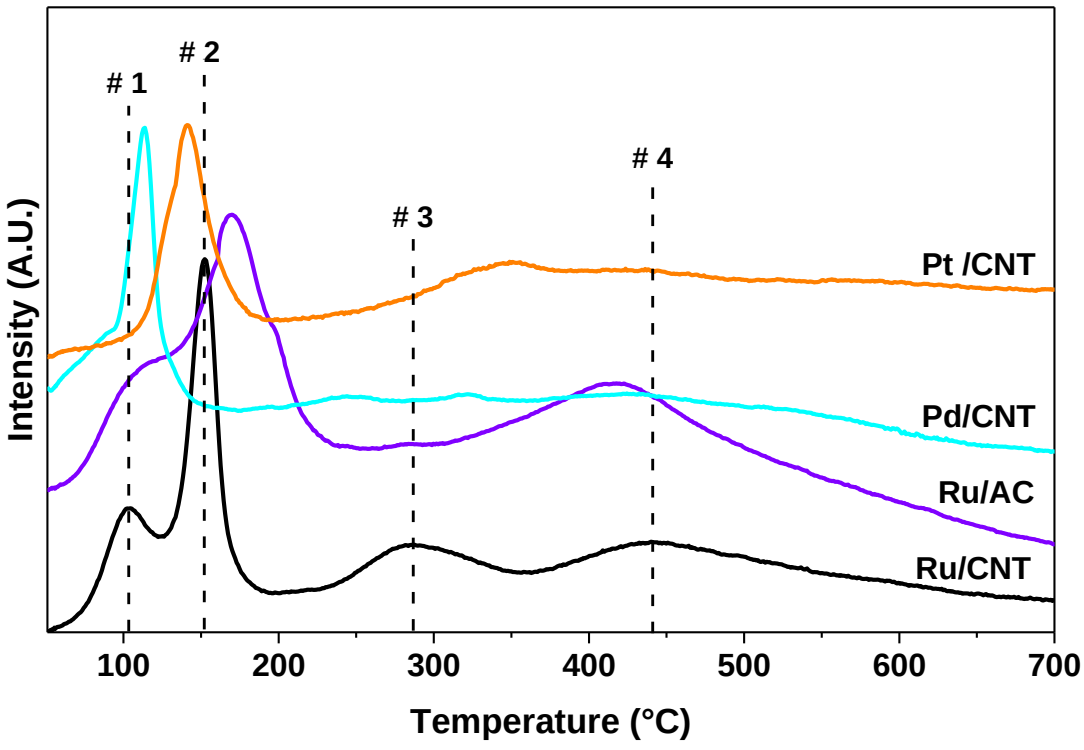

Figure 3.11.H_2-TPR profiles for 5%Ru, 5%Pd, and 5%Pt catalysts *(Unreduced)* supported on CNT.

Ru supported on AC exhibited a different trend. Ru/AC reduction peaks shifted to higher temperatures compared to 5% Ru/CNT which indicates a stronger interaction between Ru and AC. This observation suggests that the support significantly affects the reducibility of the Ru particles.[211]

On the other hand, 5% Pt/CNT showed a peak at higher temperature (139.6 °C) compared to 5% Pd/CNT which indicated the hard reducibility of Pt species compared to the Pd sample, and this peak is associated with the continuous multi-step single-electron reduction of Pt^{n+} species.[238,239]

It is worth noting that there is another peak at about 290 °C which is perhaps related to a reduction of oxygen-containing functional groups on the surface of the carbon.[232] This peak can be seen in 5% Ru/CNT and, 5% Ru/unwashed-CNT (**Figure 3.10**), whereas this peak is shifted slightly to a higher temperature in Pt and Pd catalysts.

3.3.1.5. Surface Analysis by X-Ray Photoelectron Spectroscopy

X-ray photoelectron spectra for Ru $3p_3$ core levels of reduced 5 % Ru on AC and CNT is shown in **Figure 3.12.**

A difference between the binding energies of 5% Ru/AC 463.6 eV) and 5% Ru/CNT (462.1 eV) was observed. The differences are -1.5 eV in Ru $3p_3$ core level. The binding energies for 5% Ru/CNT are lower which could be a contributing factor to the change in the catalysts reactivity. These downwards shift in binding energy in the latter catalyst compared to 5% Ru/C could be an indicator of the existence of an electronic effect of CNT over ruthenium as will be discussed in detail in Chapter 4 later (page 146 in Table 4.2).

We deconvoluted the XPS spectra of Ru $3p_3$ core level to find out the oxidation state of Ru in the samples. Ru $3p_3$ core level energies for 5% Ru/AC and 5%Ru/CNT are a little higher than those reported for Ru in the literature (i.e. 461.7 eV for Ru^0, 463.2 eV for RuO_2, 463.5 eV for RuO_3 and 463.8 eV for $RuCl_3$).[240,241]

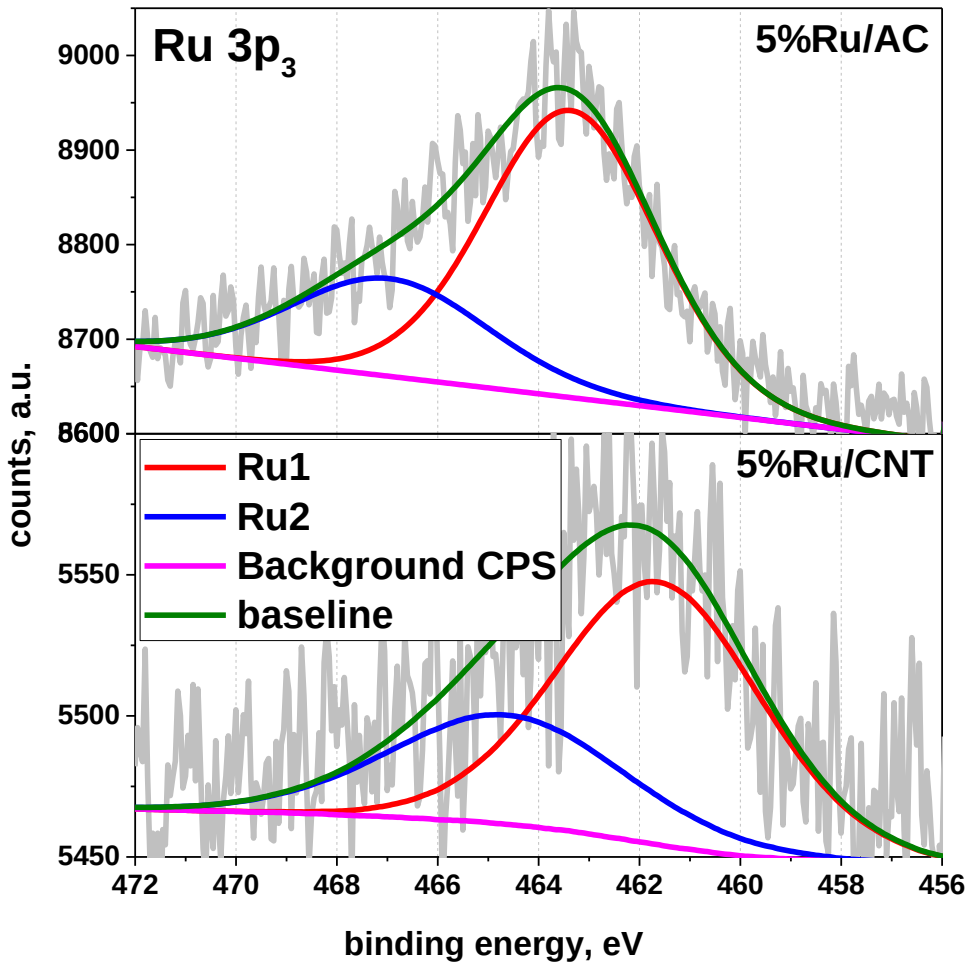

Figure 3.12. XPS profiles of reduced 5% Ru/AC and 5% Ru/CNT for $Ru3p_3$ core level showing the binding energies for the maxima of each curve.

3.3.2. Catalytic Hydrogenation of Succinic Acid

Ru was selected to perform a full time online reaction to be able to understand the reaction and its products distribution. **Figure 3.13**, shows a typical reaction time profile over a Ru supported catalyst at 150 °C and 50 bar hydrogen pressure for 23 h reaction time.

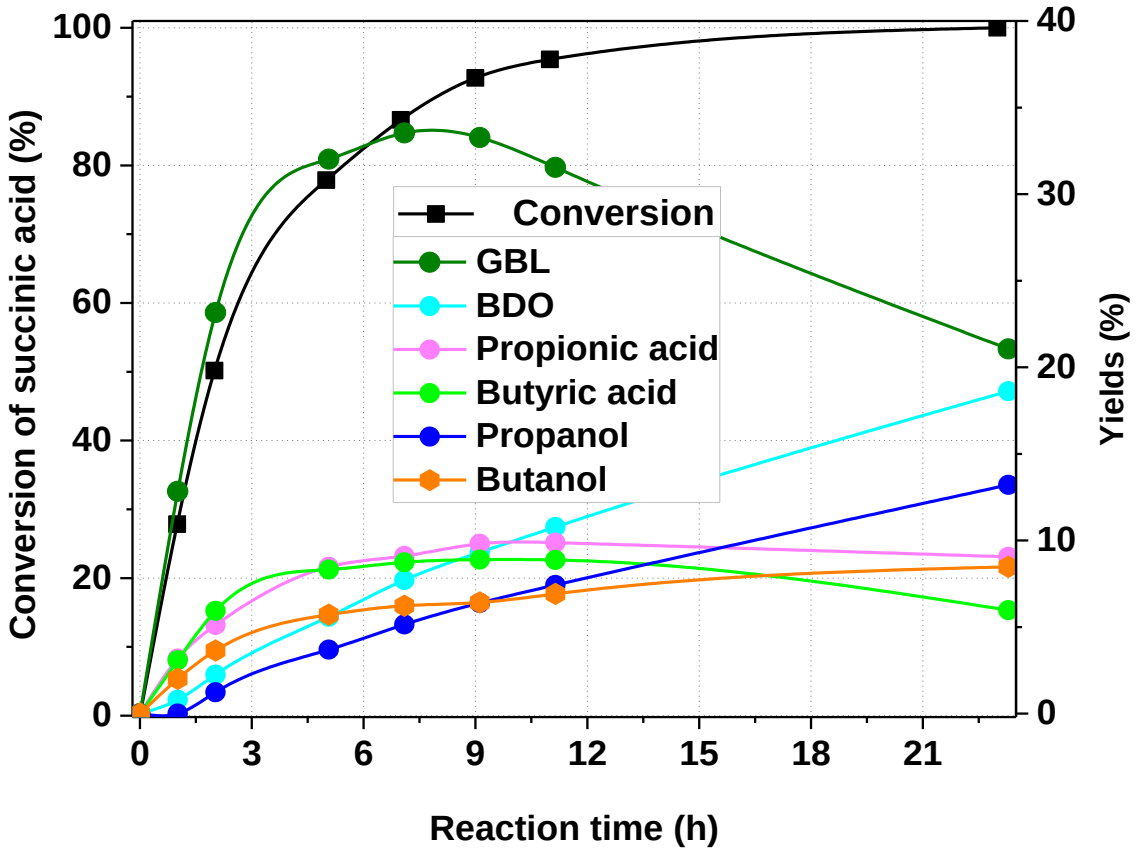

Figure 3.13. Conversion of succinic acid and yields of the reaction products time profile for hydrogenation of SA using 5% Ru/CNT catalyst. Reaction conditions: T: 150˚C; H_2 pressure: 50 bar; succinic acid: 0.1 g; catalyst: 0.05 g; solvent: 25 mL H_2O.

SA is converted into a mixture of products, mainly GBL and after 11 hours, 95.4 % conversion of succinic acid was reached with the highest selectivity towards the lactone (GBL), which at later stages converted to alcohols such as BDO, propanol or butanol.

At the end of the reaction (23h), the total yield of propanol, butanol, and BDO close to 40 % where the yield to BDO was ~19 %. Using Ru/CNT, all alcohol products were produced due to the same process (C-C cleavage) however, increasing the selectivity to single alcohol (BDO) is more desired. Furthermore, carbon mass balance gradually decreases to 76 % due to the formation of gaseous products formed by unselective C-C cleavage and over-hydrogenation of the products as reported previously.[119]

One of the objective of the study is to find the most active catalyst and reaction conditions for this reaction and then produce BDO in high yield. We decided to investigate different parameters, i.e., the effect of reaction pressure, temperature, time and other parameters to optimize this hydrogenation process.

3.3.2.1. The Stirring Rate Effect on Hydrogenation of Succinic Acid

To understand the effect of the gas-liquid mass transfer resistance on the conversion and selectivity of hydrogenation of succinic acid, the stirring rate was varied from 600, 1000, to 1200 revolutions per minute (rpm) using 5% Ru/CNT.

Figure 3.14 shows the effect of the stirring speed on the conversion of succinic acid. The conversion of SA was almost constant at all stirring speeds, which indicates that the chemical reaction is not influenced by liquid-solid or gas-liquid mass-transfer limitations. All further experiments henceforth were carried out at 1000 rpm to deliver the optimum speed for the gas entrainment stirrer as advised by the manufacturer.

The carbon mass balance and the selectivity toward the reaction products remained the same between three different stirring speeds. The reaction outcome showed formation of all products, but the selectivity was higher for GBL.

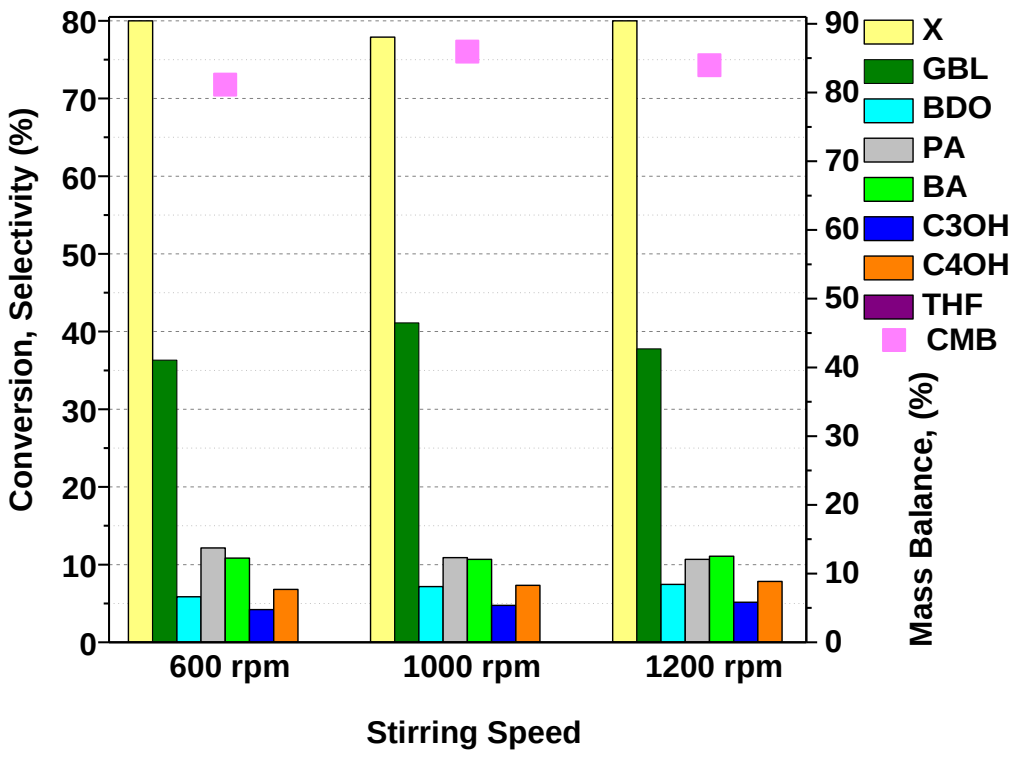

Figure 3.14 Effect of using a different agitation speed on the catalytic activity and selectivity in the hydrogenation of SA using 5% Ru/CNT. Reaction conditions: Temperature: 150 °C; reaction pressure: 50 bar; succinic acid: 0.1 g; catalyst: 0.05 g; reaction time: 5h; solvent: 25 mL H_2O. Legends, Conversion (X); gamma-butyrolactone (GBL); 1,4-butanediol (BDO); propionic acid (PA); butyric acid (BA); propanol (C_3OH); butanol (C_4OH); carbon mass balance(CMB).

3.3.2.2. Effect of Temperature on Hydrogenation of Succinic Acid

- Activity

The reaction temperature is crucial in obtaining high yields and selectivity to the desired product.[242] Ru is one of the most efficient active metal for hydrogenolysis[23] so, when the temperature increased, the hydrogenolysis of SA to form propionic acid can occur along with the desired product GBL. The effect of reaction temperature on the hydrogenation of SA is shown in **Figure 3.15**. The highest conversion occurs at higher temperatures whereas to increase the conversion to the same level at lower temperature requires a longer reaction time.

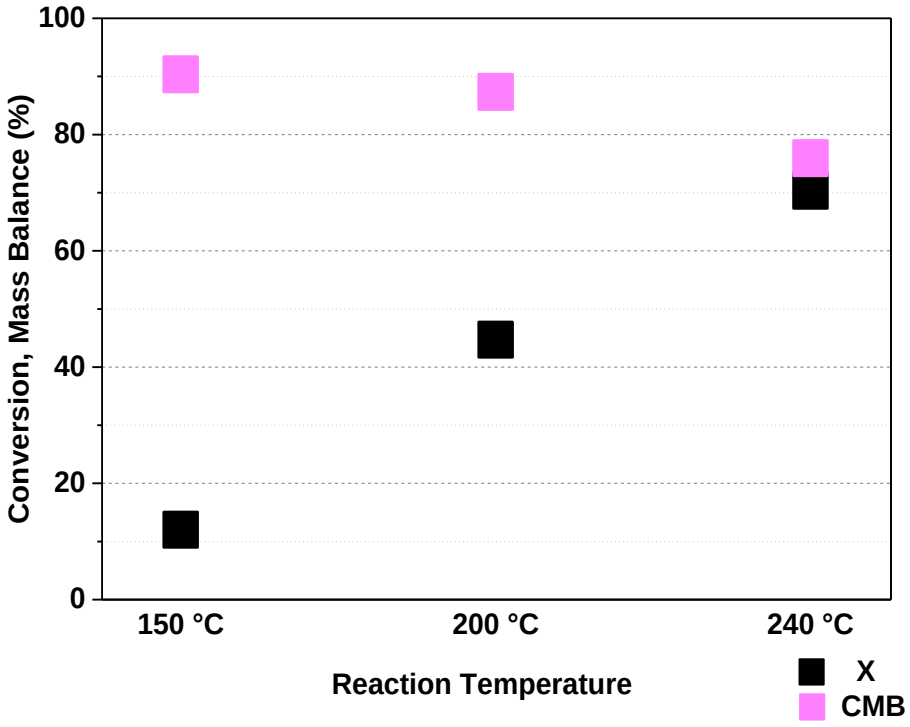

Figure 3.15. Comparison of the activity with respect of temperature in hydrogenation of succinic acid using 5% Ru/CNT. Reaction conditions: H_2 pressure: 10 bar reaction time: 1h; succinic acid: 0.1 g; catalyst: 0.05 g; solvent: 25 mL H_2O.

It was expected that higher conversion could be achieved at higher temperatures, but at such high temperatures, precautions must be taken to ensure safe operation and to lower costs of the heating, although the higher reactivity comes at the price of losing selectivity as C-C cleavage is favoured.

- Selectivity

Figure 3.16 shows the product distribution at iso-conversion compared at around 45 % conversion for 150 °C (23h) and 200 °C (1h). BDO is formed from further hydrogenation of GBL, thus the more GBL produced, the more BDO we could obtain. **Figure 3.16** shows that the selectivity to GBL decreased from 40.4 % at 150 °C to 23.17 % at 200 °C, whereas selectivity for propionic acid increased from 15.9 % at 150 °C to 31.3 % at the expense of GBL with increasing temperature.

These results demonstrate that hydrogenolysis of SA (formation of propionic acid) reduced the formation of GBL over CNT supported Ru catalysts when high temperatures were applied. It is worthwhile mentioning that the initial hydrogenolysis by-products were propionic and butyric acids, which were later reduced to propanol and butanol, respectively. As increasing the temperature, the solubility of H_2 decreased[243] in which it might affect the formation of BDO. Therefore, taking these results into account, 150 °C was selected instead of a higher temperature in the hydrogenation of succinic acid in this study to prevent C-C cleavage and enhance the formation of desired products.

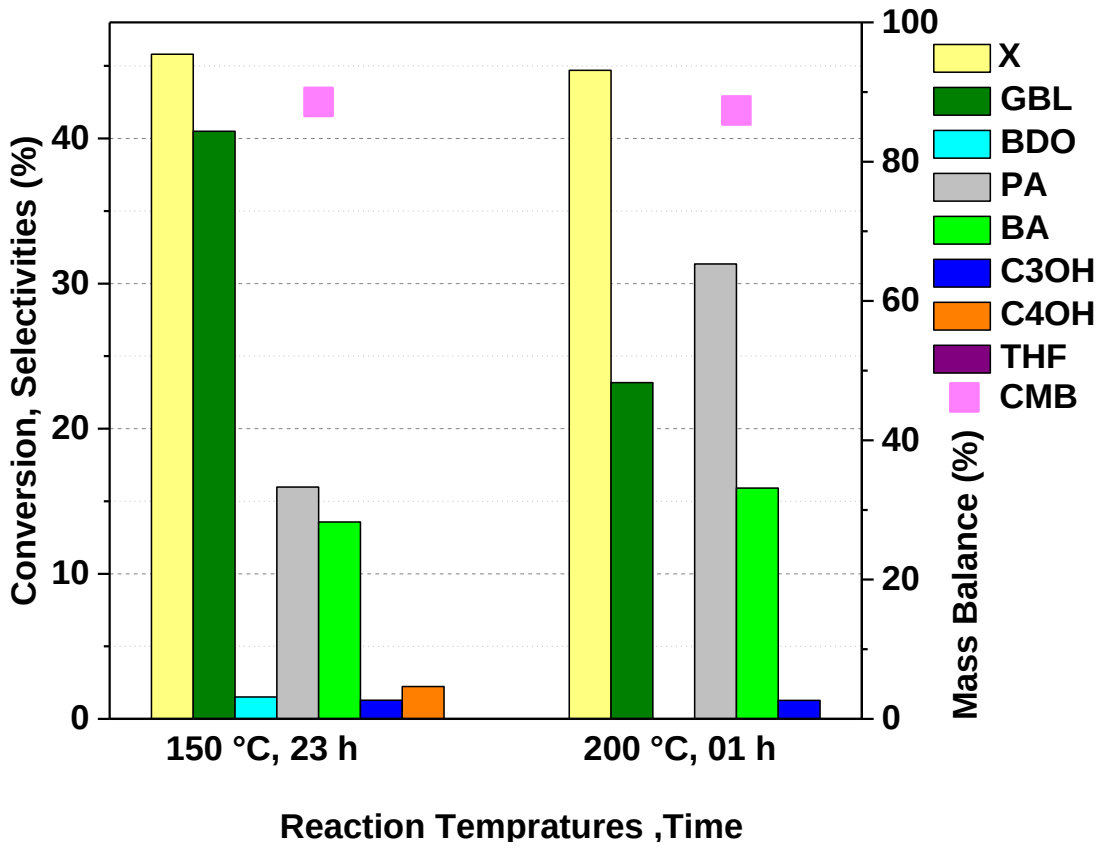

Figure 3.16. Comparison of the selectivity at iso-conversion of succinic acid at different reaction temperature. Reaction conditions: H_2 pressure: 10 bar; succinic acid: 0.1 g; catalyst: 0.05 g; solvent: 25 mL H_2O. Legends, Conversion (X); gamma-butyrolactone (GBL); 1,4-butanediol (BDO); propionic acid (PA); butyric acid (BA); propanol (C_3OH); butanol (C_4OH); carbon mass balance(CMB).

3.3.2.3. Effect of Reaction Pressure on Hydrogenation of Succinic Acid

- Activity

Hydrogen pressure displayed a significant effect on a catalytic performance in liquid phase hydrogenation of succinic acid which might be because of the solubility of the gas in the high pressure. Based on Henry's law, the amount of dissolved gas is proportional to its partial pressure in the gas phase. Therefore, the succinic acid conversion increased from 27 to 41 to 78 % when the hydrogen pressure was raised from 10 to 25 to 50 bar, respectively (**Figure 3.17**). Thus 78 % conversion of SA was achieved at 50 bar within 5-hours reaction time using Ru catalyst at 150 °C. Murahashi *et al.*[244] suggested that Ru needs high hydrogen pressure for efficient hydrogenation. Therefore 50 bar was suitable to increase the reaction rate.

The hydrogen solubility in water is limited when compared to organic solvents such as 1,4-dioxane.[245,246] Thus, increasing hydrogen pressure was required to increase the solubility of hydrogen.[247] Many of the previous studies[90,87] used 1,4-dioxane as a solvent because of the high solubility of hydrogen and substrate compared to those in the water.[248]

Regardless, both 1,4-dioxane and aqueous systems share the need for high temperature (>200 °C), high hydrogen pressure (>60 and more typically >100 bar) and hours of reaction times, so the use of an organic solvent is not ideal. Therefore, all reactions were performed in water which also meets the high need of greener systems, non-toxicity, and low cost.

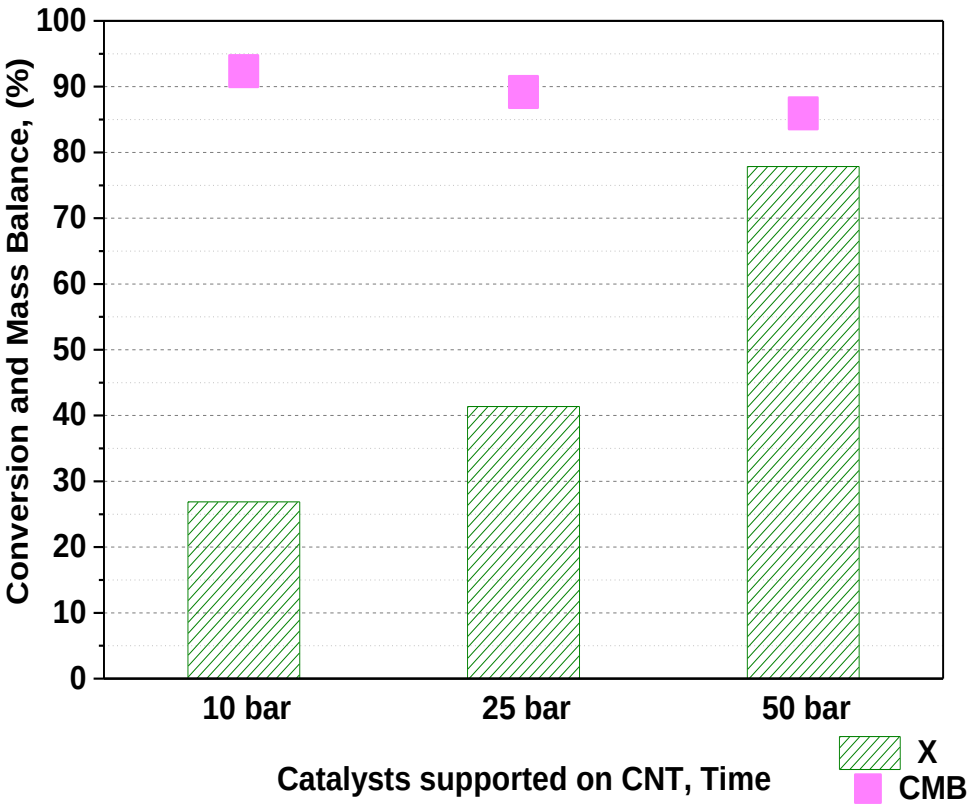

Figure 3.17. Comparison of the activity with respect of pressure in hydrogenation of succinic acid using 5% Ru/CNT. Reaction conditions: T: 150 ˚C; reaction time: 5h; succinic acid: 0.1 g; catalyst: 0.05 g; solvent: 25 mL H_2O.

- Selectivity

Regarding the selectivity, **Figure 3.18** compares the product selectivity at iso-conversion. As the H_2 pressure increased from 10 to 50 bar, the selectivity of propanol, butanol, and BDO increased from 1.2, 2.2, 1.5 % to 2.4, 7.2 and 4.4 %, respectively, due to the higher hydrogen availability. It seems that the hydrogenolysis products (propionic acid and butyric acid) decreases with increasing the H_2 pressure. Butyric acid formed from GBL or SA *via* a hydrogenolysis reaction and this product could affect the formation of BDO. Increasing the H_2 pressure led to increased BDO formation so, 50 bar hydrogen pressure was fixed for further investigations of hydrogenation of succinic acid at 150 °C.

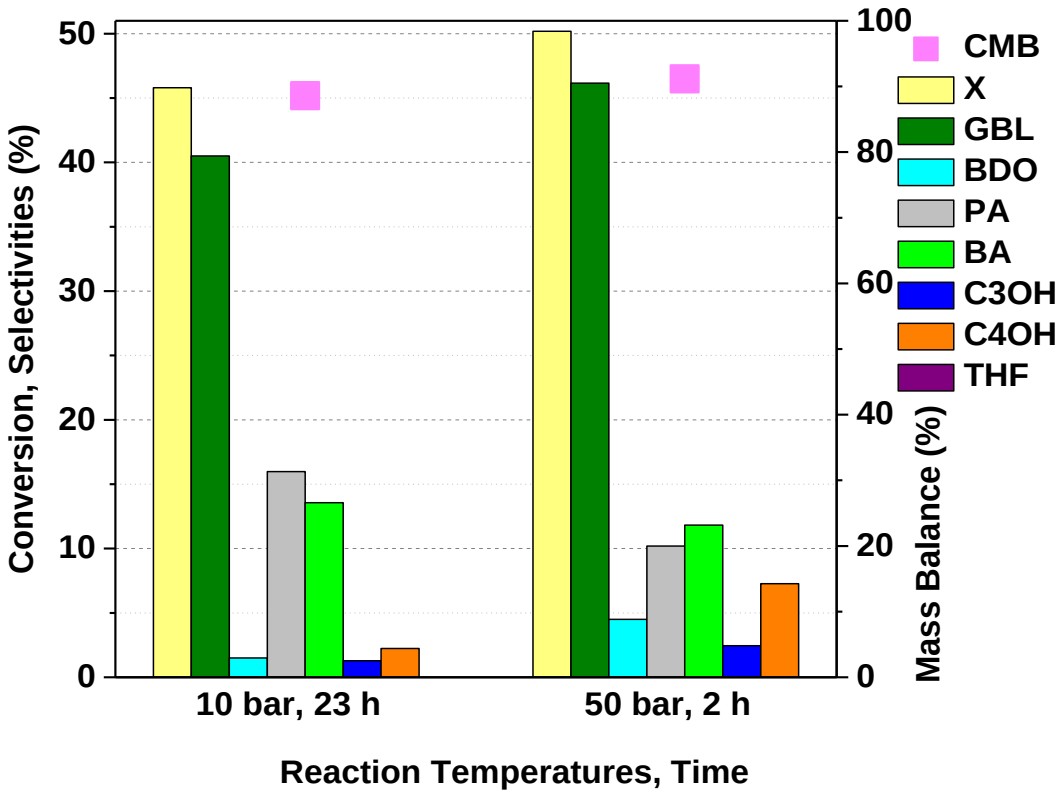

Figure 3.18.Comparison of the selectivities at iso-conversion of succinic acid at different hydrogen pressure. Reaction conditions: T: 150 ˚C; succinic acid: 0.1 g; catalyst: 0.05 g; solvent: 25 mL H_2O. Legends: Conversion (X); gamma-butyrolactone (GBL); 1,4-butanediol (BDO); propionic acid (PA); butyric acid (BA); propanol (C_3OH); butanol (C_4OH); carbon mass balance(CMB).

3.3.2.4. Effect of Washing of CNTs on Hydrogenation of Succinic Acid

- Activity

To evaluate if the washing of CNTs was required, 5 wt. % of Ru catalyst supported on CNTs as received without washing were prepared using the procedure as described in the experimental Chapter (2). This step was intended to wash away loosely bound impurities such as iron and cobalt which are present in the nanotubes.

It was found that even after the mild washing step the carbon nanotubes contain ca. 0.6 % Co and 0.3 % Fe, mostly as particles grown within the tube pore. **Figure 3.19** exhibited that 5% Ru/CNT (washed-CNT) has higher catalytic activity than 5% Ru/unwashed-CNT under same reaction conditions with around 26 % more conversion.

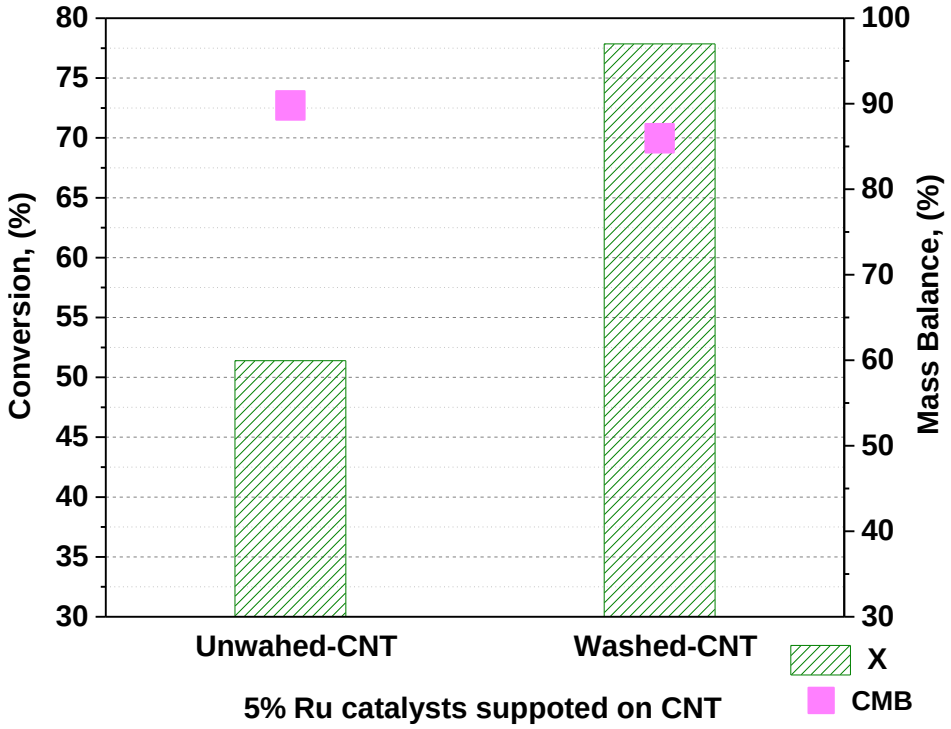

Figure 3.19. Effect of washing step on the catalytic activity of 5% Ru/CNT in the hydrogenation of succinic acid. Reaction conditions: T: 150 ˚C; H_2 pressure: 50 bar; reaction time, 5h; succinic acid: 0.1 g; catalyst: 0.05 g; solvent: 25 mL H_2O. Legends: Conversion (X); carbon mass balance (CMB).

This result was not surprising since **Table 1.3** previously showed that the Ru dispersion in 5% Ru/unwashed-CNT was less than 50 % compared to a distribution of Ru on washed-CNT (5% Ru/CNT). According to the literature, better dispersed catalysts are generally more active.[249] Lower dispersion of the 5% Ru/unwashed-CNT might be due to the presence of the impurities such as Fe and Co which hinder the adsorption Ru.

- Selectivity

The effect of washed CNT sample on product selectivity at the same conversion was also evaluated. **Figure 3.21** showed that there is no significant difference between the two catalysts regarding product distribution at the same level of conversion. This means that the washing step just helps to increase the reactivity of the catalyst without changing the product distribution.

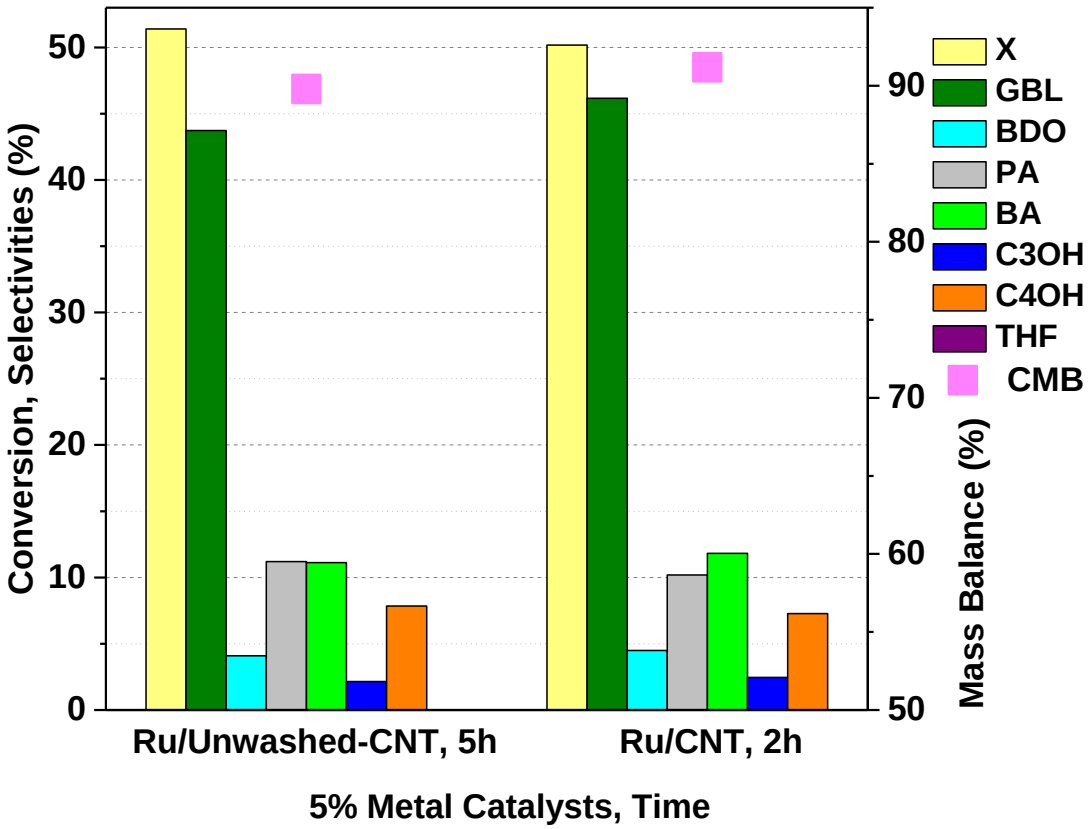

Figure 3.20. Comparison of the selectivities at iso-conversion of succinic acid,5% Ru/unwashed-CNT vs 5% Ru/CNT (washed CNTs). Reaction conditions: T: 150˚C; H_2 pressure: 50 bar; succinic acid: 0.1 g; catalyst: 0.05 g; solvent: 25 mL H_2O. Legends, Conversion (X); gamma-butyrolactone (GBL); 1,4-butanediol (BDO); propionic acid (PA); butyric acid (BA); propanol (C_3OH); butanol (C_4OH); carbon mass balance (CMB).

3.3.2.5. Effect of Ru Loading in the Hydrogenation of Succinic Acid

- Activity

Initially, the evaluation of three different loading of Ru catalysts supported on CNT (1, 3, and 5 wt. %) and the bare CNT support was carried out at 150 °C and 50 bar total pressure. The blank run in the absence of catalyst gave virtually no conversion of succinic acid. **Figure 3.22** shows that the succinic acid conversion increased with increasing loading of Ru as follows, 1% Ru (11 %), 3% Ru (52 %), and 5% Ru (78 %).

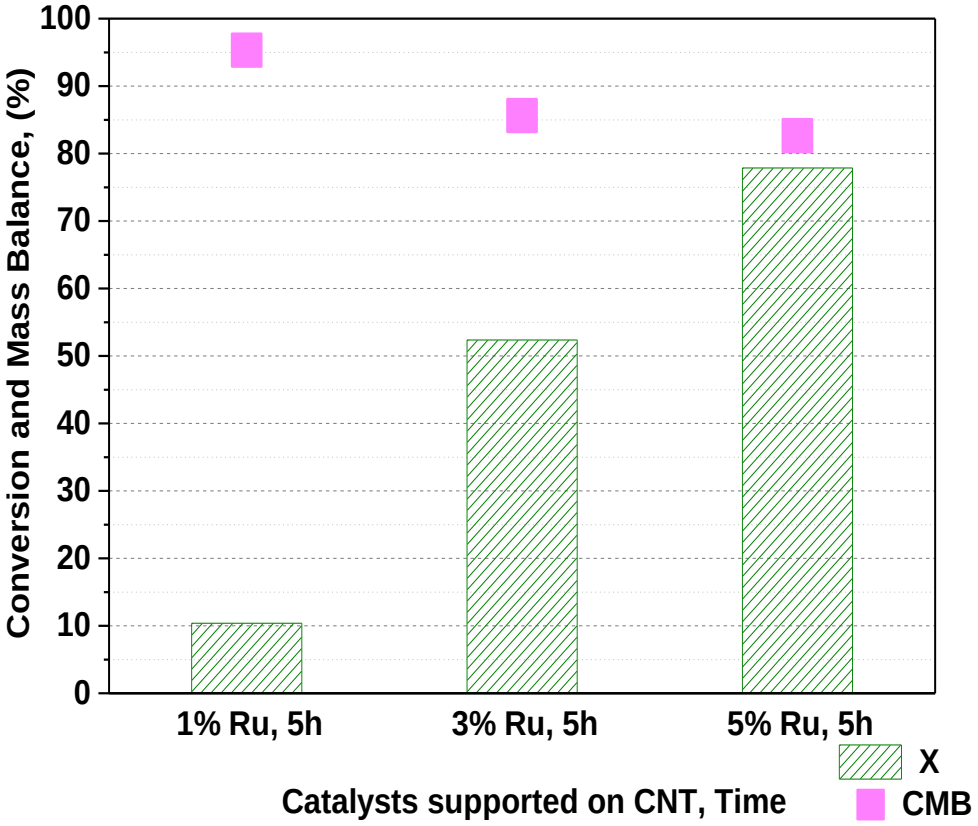

Figure 3.21. Comparison of the activity using different Ru wt. % (1, 3, and 5 %) on of succinic acid. Reaction conditions: T: 150 ˚C; H_2 pressure: 50 bar; reaction time: 5h; succinic acid: 0.1 g; catalyst: 0.05 g; solvent: 25 mL H_2O. Legends: Conversion (X), carbon mass balance (CMB).

Other catalysts were prepared with 7 and 10 wt. % to evaluate if increasing the loading could still raise the activity of the Ru catalyst. The results were compared at a shorter reaction (1 h) because of the high reactivity of the catalysts limit their comparison at 5h. The results in **Figure 3.23** showed that the conversion of succinic acid still increases as the loading of a catalyst is increased from 5% to 7 wt. % and 10 wt. %. The conversion increased from 27.8 % (5% Ru), 34.35% (7% Ru), to 45.26 % (10% Ru) supported on CNTs.

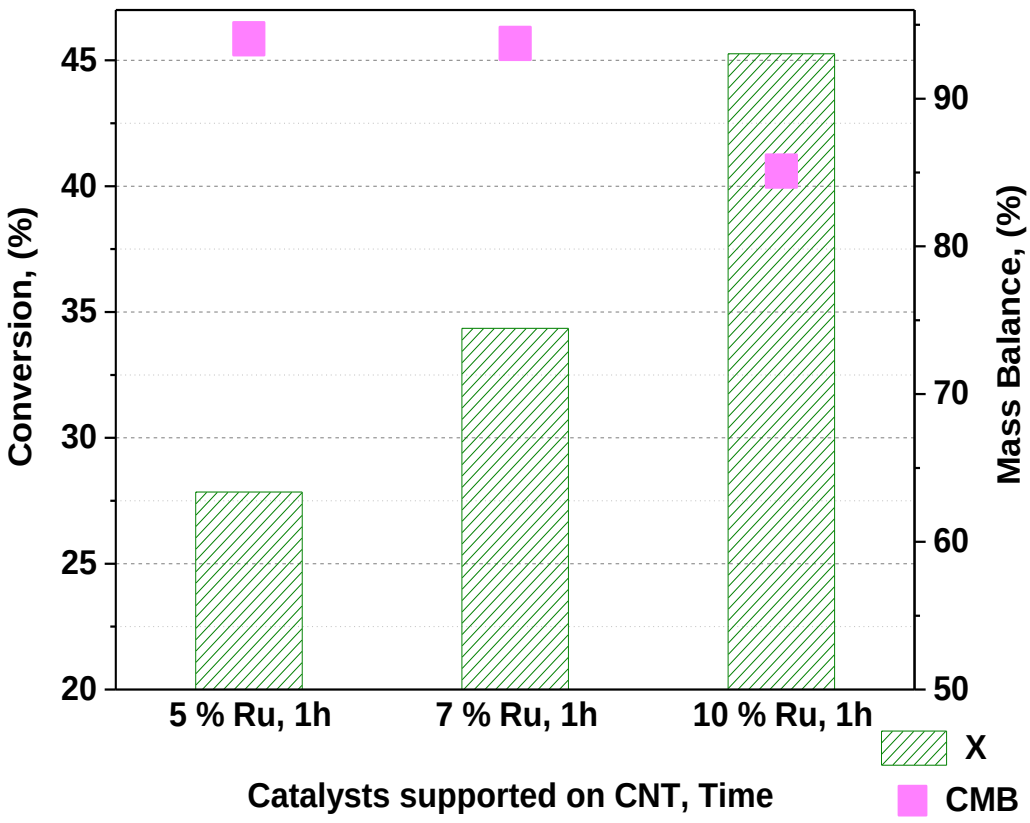

Figure 3.22. Comparison of the activity using different Ru wt. % (5, 7, and 10 %) on of succinic acid. Reaction conditions: Temperature: 150˚C; H_2 pressure: 50 bar; reaction time (1h); succinic acid: 0.1 g; catalyst: 0.05 g; solvent: 25 mL H_2O. Legends: Conversion (X), carbon mass balance (CMB).

This finding is not in agreement with previous studies on Ru catalyst supported on Starbon®, a novel porous polysaccharide derived material, where it was observed that increasing Ru loading above 5 wt. % showed reduced activity in the hydrogenation of succinic acid in aqueous solution.[104] Therefore, the CNTs in this study proved to be a better support since 10 wt. % of Ru was smoothly dispersed on CNT surface without losing the activity of a catalyst. The CO-chemisorption results in **Table 3.1** showed that the metal (Ru) dispersion is increased with increasing the loading (5% Ru < 7% Ru < 10% Ru) supported on CNTs.

The TEM measurements confirmed that the size of Ru particles increases slightly from 1.4, 1.4, to 1.6 nm for 5% Ru, 7% Ru and 10% Ru respectively supported on CNT and TPR results (**Section 3.3.1.4**) supported this observation. Apart from 1% Ru/CNT, it seems the activity of the catalyst is correlated to the dispersion as CO-chemisorption showed that an increased dispersion of Ru led to an increased conversion of succinic acid. The results indicate that the activity of Ru catalyst does not depend simply on the size of Ru particle or the dispersion but also on the availability of them.

- Selectivity

Regarding the products distribution, 5% and 10% Ru loadings supported on CNT were compared at iso-conversion to see if increasing the loading would reduce the problem of C-C cleavage and the results are shown in **Figure 3.24**. GBL was the primary product observed. However, the initial formation of GBL decreases rapidly to other products using 10% Ru/CNT whereas the creation of hydrogenolysis products such as propionic acid is increased. Furthermore, a drop-in carbon mass balance was seen over 10% Ru/CNT indicating that the formation of gaseous products is potentially enhanced at this loading.

On the other hand, the SA decarboxylation products (e.g. propionic acid) decreased using 5% Ru/CNT, whilst production of alcohols (butanol, 1,4-butanediol, and propanol) products via hydrogenation increased.

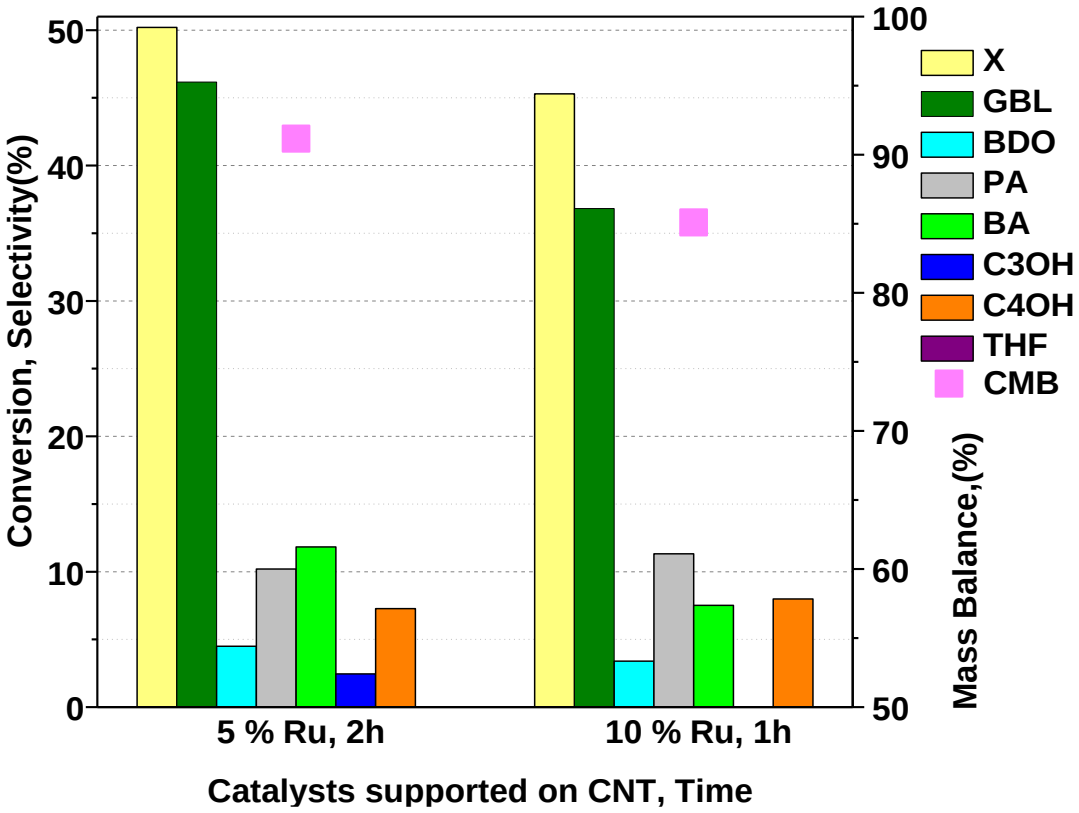

Figure 3.23. Comparison of the selectivities at iso-conversion of succinic acid at different Ru wt. % loading. Reaction conditions: T: 150˚C; succinic acid: 0.1 g; catalyst: 0.05 g; solvent: 25 mL H_2O. Legends, Conversion (X); gamma-butyrolactone (GBL); 1,4-butanediol (BDO); propionic acid (PA); butyric acid (BA); propanol (C_3OH); butanol (C_4OH); carbon mass balance(CMB).

In the aqueous phase hydrogenation of succinic acid, catalysts with higher metal loadings are preferable, to convert SA in a reasonable time. 10% Ru/CNT showed better activity compared to all other Ru loadings because of the high dispersion and the availability as we observed in **Table 3.1**, however the lower mass balance and a high cost

of this catalyst led us to pick 5% Ru based catalyst instead for further investigations. The effect of support on similarly loaded Ru was then investigated to probe the potential of CNT supported Ru catalysts.

3.3.2.6. Effect of using Ru (IN)/CNT Catalysts in Hydrogenation of Succinic Acid

- Activity

With the intention of dispersing Ru particles inside the nanotube, a catalyst was prepared using a procedure adapted from Wang et al.[157] This is different to any other prepared catalysts in this thesis. A known amount of Ru, acetone, and CNT was mixed homogeneously with the help of ultrasound and under continuous stirring at room temperature for 0.5 h. The mixture was heated in air at 1 °C/min up to 110 °C, held at 110 °C for 11 h to be able to evaporate the acetone. The extended stirring was necessary to drive Ru salt solution into the CNT channels, due to the concentration difference, followed by the slow evaporation. **Figure 3.25** displays the catalytic performances of Ru(IN)CNT for hydrogenation of SA reaction in comparison to 5% Ru(MIX)CNT.

The 5% Ru(IN)CNT exhibits a low catalytic activity which agrees with the CO-chemisorption results. The results in **Table 3.1** showed that 5% Ru(IN)CNT has a low dispersion compared to the 5% Ru(MIX)CNT. Another explanation might be that the Ru particles are inside the channels of the CNT and are not exposed to the reactant.

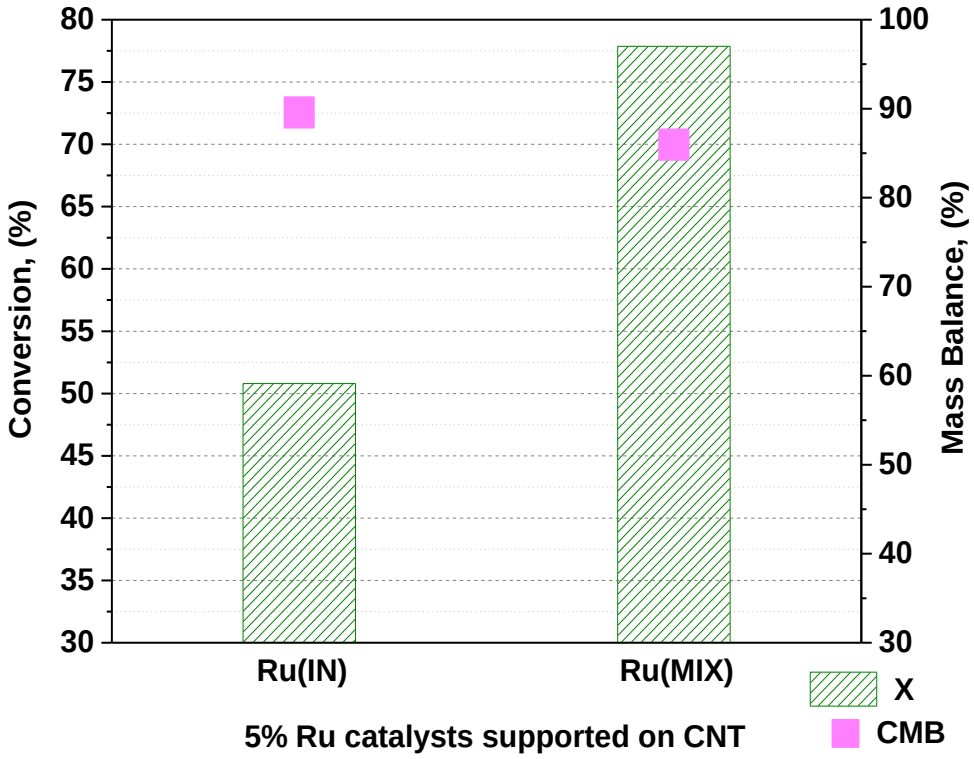

Figure 3.24. Effect of presenting the Ru particles inside the CNT on the catalytic activity of 5% Ru/CNT in the hydrogenation of SA. Reaction conditions: T: 150 ˚C; succinic acid: 0.1 g; catalyst: 0.05 g; reaction time: 5h; solvent: 25 mL H_2O. Note: Ru(MIX)/CNT is referred to Ru/CNT. Legends: Conversion (X), carbon mass balance (CMB).

- Selectivity

5% Ru(MIX)CNT and 5% Ru(IN)CNT were compared at close to iso-conversion to see if better selectivity to BDO and less formation of C-C cleavage products obtained. **Figure 3.26** showed that there was no improvement in the selectivity of all products (look similar). Until now CNTs proved to be a satisfactory support to Ru catalysts because we showed that by increasing the metal loading, the reactivity of the catalyst is enhanced, which translates into no agglomeration when increasing the percentage of Ru. However, no improvement regarding selectivity to BDO using different protocols and parameters was achieved as C-C cleavage was still a problem. Therefore, we decided to investigate the effect of support on catalytic activity.

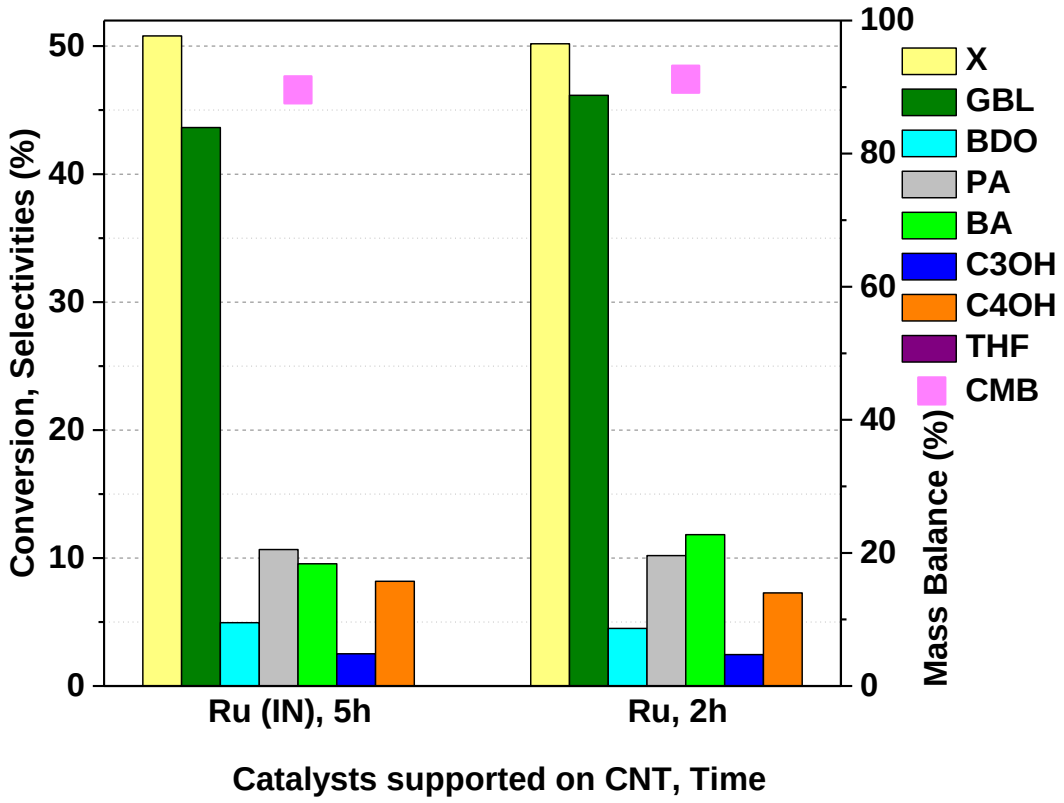

Figure 3.25 Comparison of the selectivities at iso-conversion of SA using 5 % Ru catalyst where the particles are supposed to be inside of the CNT. Reaction conditions: T: 150 ˚C; H_2 pressure: 50 bar; SA: 0.1 g; catalyst: 0.05 g; solvent: 25 mL H_2O. Legends, Conversion (X); gamma-butyrolactone (GBL); 1,4-butanediol (BDO); propionic acid (PA); butyric acid (BA); propanol (C_3OH); butanol (C_4OH); carbon mass balance (CMB).

3.3.2.7. Effect of the Supports for the Ru Catalysts in Hydrogenation of Succinic Acid

- Activity

CNTs are different when compared to AC since the latter has meso- and a vast quantity of micropores, which could reduce the activity of a catalyst[250] where CNTs have mesoporous[225] structure with well-defined tubular morphology.[251] It was suggested[48,250] that most of the mesopores in CNT are aggregated pores formed by the interaction of isolated nanotubes and could be important in decreasing mass-transfer limitations in liquid-phase reactions.

Figure 3.27, shows a comparison between the results obtained from two different supports in a hydrogenation of SA at 150 °C and 50 bar of hydrogen pressure. The results show that 5% Ru/CNT exhibits higher activity than 5% Ru/AC in the liquid phase hydrogenation of succinic acid. 5% Ru/AC gave 49.4 % conversion whereas using 5% Ru/CNT gave 77.8 % conversion.

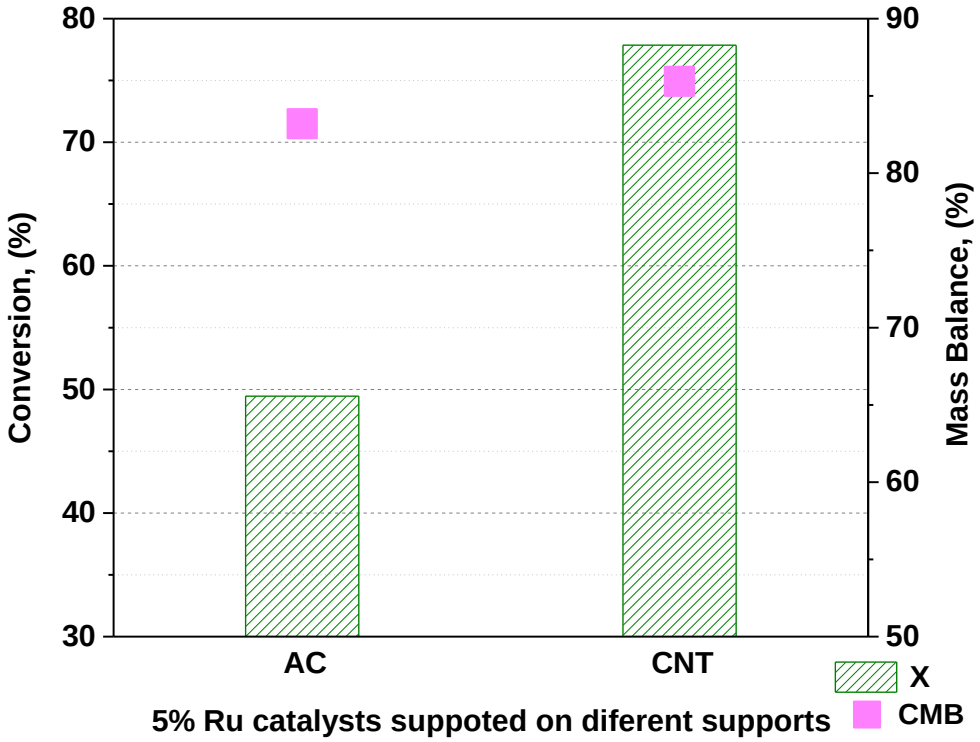

Figure 3.26 Effect of using different supports on catalytic activity of 5% Ru catalyst in the hydrogenation of succinic acid. Reaction conditions: T: 150 ˚C; H_2 pressure: 50 bar; reaction time: 5h; succinic acid: 0.1 g; catalyst: 0.05 g; solvent (H_2O): 25 mL. Legends: Conversion (X), carbon mass balance (CMB).

The reactivity of the catalyst can be supposed from TPR results. The lower the reduction temperature, the better reduction capability of the catalyst.[252] This fact was in line with the results obtained from TPR of Ru catalysts, specifically for 5% Ru/CNT since the H_2 consumption peak for the later catalyst appeared at low temperature compared to 5% Ru/AC.

Electronic effects have been declared as responsible for the revised activity of CNT-supported catalysts but never for hydrogenation of succinic acid or another acid to alcohol. The group of J.A. Lopez-Sanchez[236] have reported the activity of using Ru nanoparticles supported on CNT towards 2,5-hydroxymethylfurfural conversion to 2,5-dimethylfuran.

The study found that CNT supported Ru catalyst produced 83.5 % yield of 2,5-dimethylfuran in under 1 h whereas Ru supported on activated carbon required more than 3 h to give 80.3 % yield of the same compound. They explained that the increment on the performance of ruthenium on CNTs was due to the electronic promotion of the carbon nanotubes.

The electronic properties of CNT decreased the binding energy of Ru in comparison with AC. A −1.5 eV shift is appreciated in in Ru($3p_3$) core level (Figure 3.12). Therefore, the higher catalytic activity of CNT based catalyst in succinic acid hydrogenation could be due to the promoting effect of the electron transfer between CNTs and Ru as it was demonstrated multiple times in the literature.[253-258]

TPR results exhibited differences in the redox properties between two catalysts (5% Ru/AC and 5% Ru/CNT) which may support an electronic promotional effects.[236]

TEM measurement showed that the Ru average particle size is slightly different between the two catalysts which were prepared using AC (1.3±0.2 nm) and CNT (1.4±0.4 nm). This observation was made as well in another study reported by Nieto et al.[259] which could be due to a low surface area of CNT in comparison with AC. 5% Ru/AC has smaller Ru particles size compared to the CNT based catalyst but 5% Ru/CNT shows better activity.

- Selectivity

We hoped selectivity to a specific product could be improved by varying metal particle size, the electronic effect of the support, and morphology.[207,260]

Figure 3.28 shows the product distribution at iso-conversion for the tests carried out over 5% Ru/AC and 5% Ru/CNT.

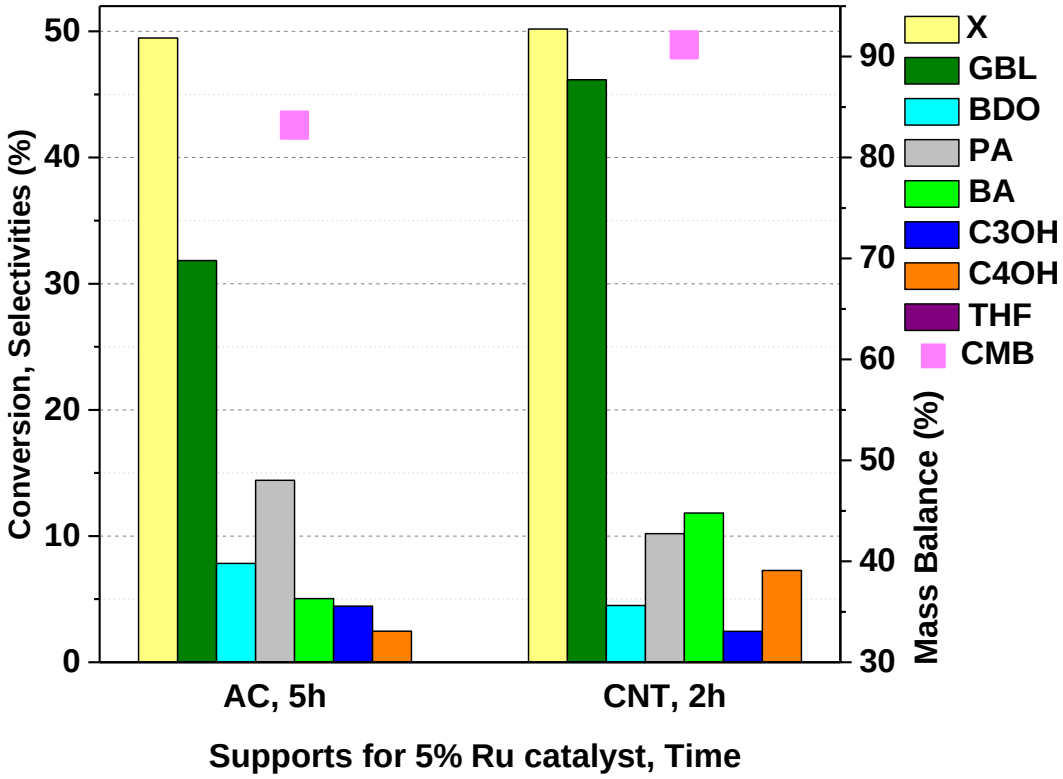

Figure 3.27 Comparison of the selectivities at iso-conversion of succinic acid, 5%Ru/AC vs. 5%Ru/CNT. Reaction conditions: T: 150˚C; H_2 pressure: 50 bar; succinic acid: 0.1 g; catalyst: 0.05 g; solvent (H_2O): 25 mL. Legends: Conversion (X), carbon mass balance (CMB).

At iso-conversion, the selectivity to the C-C cleavage product (propionic acid) increased when using 5% Ru/AC whereas the main hydrogenation product (GBL) was maximised using CNT. This is another significant advantage of using CNT instead of AC. The formation of undesired C-C cleavage products, i.e., propionic acid was lower using 5% Ru/CNT. Moreover, the formation of gaseous products was higher using 5% Ru/AC since the carbon mass balance decreased. This result indicates that the use of CNTs as support not only increase the activity of the catalyst but also reduces unwanted hydrogenolysis by-products.

Using Ru catalyst to hydrogenate succinic acid was recommended in the literature as showed in the introduction, however, other metals might be interesting for the hydrogenation of succinic acid since each metal has a unique set of characteristics. Vu *et al*.[207] claimed that Pt/CNT was more active than Ru/CNT, and Pt supported on AC in the hydrogenation of cinnamaldehyde. Therefore, to fully explore if the benefits of CNT as a support for Ru catalyst could be extended to other metals, Pt and Pd catalysts supported on AC and CNT were prepared.

3.3.2.8. Effect of Noble Metals on Hydrogenation of Succinic Acid

- **Activity**

Initially, 5% Pd and 5% Pt catalysts supported on activated carbon were screened and compared to 5% Ru/AC. **Figure 3.29, A** shows that 5% Pd/AC and 5% Pt/AC were less active than 5% Ru/AC since the conversion of succinic acid was 2 % (5% Pd/AC), 5 % (5% Pt/AC), and 49 % (5% Ru/AC) under the same reaction conditions.

Pd and Pt catalysts supported on CNT displayed a remarkable increase in conversion of succinic acid compared to the catalysts supported on activated carbon (**Figure 3.29, B**). The conversion using Pt and Pd catalysts supported on CNT was much lower than the conversion obtained from using 5% Ru/CNT. The succinic acid conversion increased from 49 % (5% Ru/AC) to 78 % (5% Ru/CNT), from 2 % (5% Pd/AC) to 6 % (5% Pd/CNT), and from 5 % (5% Pt/AC) to 10 % (5 % Pt/CNT) therefore, the effect of using CNTs in hydrogenation of succinic acid as a support for different metals might considered to be a universal. One of the reasons regarding this increment in activity when using CNTs as a support for different noble metals is the electronic promotion of the carbon nanotubes.

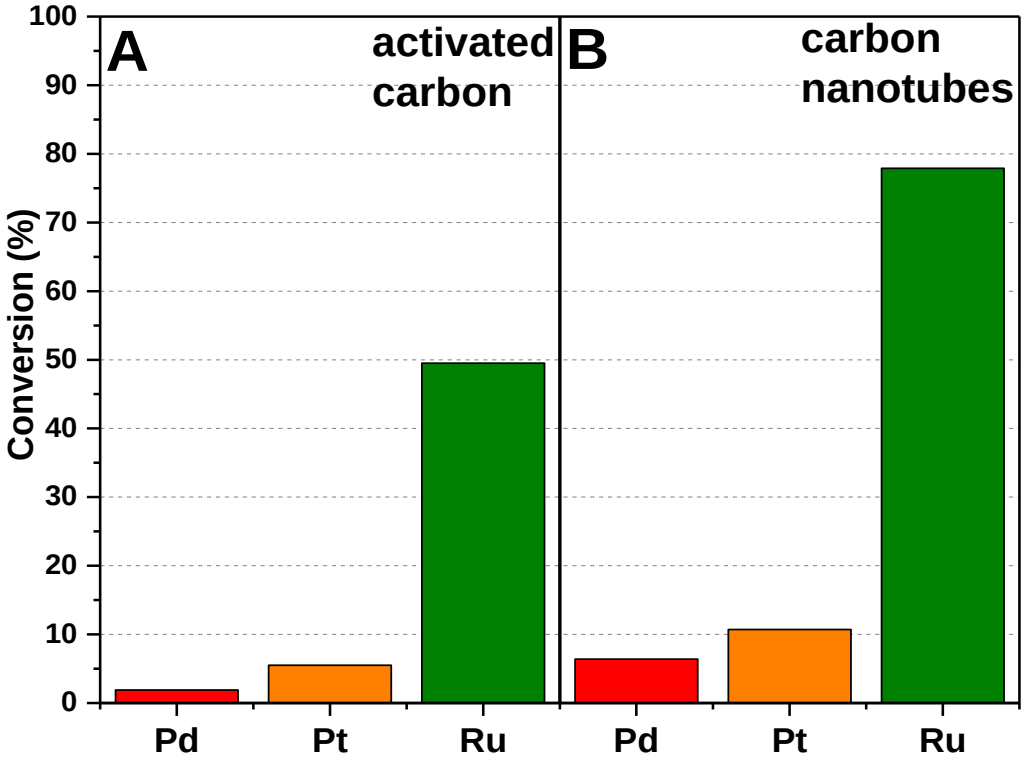

Figure 3.28. A and B. Conversion of succinic acid in its hydrogenation using 5 % metal catalysts supported on (A) activated carbon and (B) carbon nanotubes. Reaction condition: T: 150 ˚C; H_2 pressure: 50 bar; reaction time: 5h; succinic acid: 0.1 g; catalyst: 0.05 g; solvent (H_2O): 25 mL.

In this Chapter, we have demonstrated that Ru displays an order of magnitude superior activity to Pd and Pt catalysts. Pd based catalyst showed low activity amongst them. The catalytic activity of 5% Pd/CNT agreed with the results obtained from characterisation since CO-chemisorption showed that the 5% Pd/CNT has a lower dispersion (2.1 %) compared to Ru (8 %) and Pt (12.8 %) catalysts. Also, TEM images, 5% Pd/CNT exhibited a bimodal distribution, indicative of agglomeration to larger particles between 6 and 13 nm apart from the small 2±0.7 nm nanoparticles. The presence of those agglomerates might be the reason for the lower reactivity of this catalyst.

Zhu *et al.*[261] reported that the performance of Pd catalysts is influenced by three main parameters; interaction with the support, nature of the Pd precursor and Pd particle size. Therefore, to improve the activity of Pd catalyst, a catalyst with low Pd loading (1 wt. %) was prepared to get better dispersion and avoid the presence of large Pd particles which might decrease the reactivity of the catalyst.

Zhang *et al*.[262] noticed that as Pd loading decreased, the resulting average particle size decreased correspondingly and the activity of the catalyst increased in the hydrogenation of succinic acid. However, this approach did not help to produce a better catalyst in this study as shown in Table 3.2, entries 1 and 2. Since no improvement in the conversion was found possibly due to agglomeration.

It has been reported that larger Pd particles can be made from $PdCl_2$ due to the presence of chlorine, which promotes sintering.[263] However, it can be seen in Table 3.2, entry 3, that using Pd $(NO_3)_2$ salt did not improve the activity of the catalyst since the conversion of SA remained constant. Hydrogenations that proceed sluggishly at a low temperature can be driven to hydrogenated products by merely raising the temperature and/or pressure, as is commonly done in the hydrogenation of itaconic acid to methyl-γ-butyrolactone over Pd/C catalysts.[226]

Therefore, the effects of temperature and pressure were investigated further using 5% Pd/CNT. Table 3.2, entries 4-8 shows that 200 °C and 70 bar hydrogen pressure increased the conversion of succinic acid with 5-fold, with 100 % selectivity to GBL.

Furthermore, 5% Pt/CNT has also been tested under the same reaction conditions (200 °C, 70 bar), Table 3.2, entries 9 and 10 showed that the conversion increased 3-fold compared to other reaction conditions (150 °C and 50 bar) with improved selectivity to GBL and BDO. The high selectivity (100 %) towards GBL using the Pd based catalyst and decent selectivity to BDO using Pt catalyst could be a new platform where the need for another metal as a promoter to increase the activity of those catalysts is required.

Table 3-2. Tested catalysts (Reduced) at 5 h reaction time in the hydrogenation of succinic acid. Reaction conditions: 50 mg catalyst, 0.1 g SA in 25 mL water. Legend: succinic acid (SA); gamma-butyrolactone (GBL); 1,4butanediol (BDO); butyric acid (BA); propanol (C_3OH); butanol (C_4OH); carbon mass balance(CMB); propionic acid (PA); p, pressure; t, time; T, temperature; X, conversion; Y, yield; NA, not available; #, entry. All catalysts supported on CNT.

#	Cata.	T, °C	p, bar	X,SA %	Y,GBL %	Y,BDO %	Y,PA %	Y,BA %	Y,C_3OH %	Y,C_4OH %	CMB %
1	1%Pd	150	50	3.04	0.81	0	0	0	0	0	97.7
2	5%Pd ($PdCl_2$)	150	50	6.38	3.66	0	0	0	0	0	97.2
3	5%Pd ($PdNO_3)_2$	150	50	5.25	3.58	0	0	0	0	0	98.3
4	5%Pd	150	25	0.33	0	0	0	0	0	0	99.6
5	5%Pd	200	25	8.40	7.35	0	0	0	0	0	98.9
6	5%Pd	240	25	26.1	20.68	0	3.94	0	0	0	98.2
7	5%Pd	200	40	20.4	14.51	0	0	0	0	0	94.5
8	5%Pd	200	70	32.0	25.67	0	0	0	0	0	93.8
9	5%Pt	150	50	10.6	5.20	0	0	0	0	0	94.5
10	5%Pt	200	70	32.3	26.59	1.73	1.99	1.38	0	0	99.3

But for now, ruthenium is a superior catalyst as compared to Pd and Pt under mild reaction conditions (150 °C, 50 bar) in the hydrogenation of succinic acid.

3.3.2.9. Reproducibility and Recyclability Test

Reproducibility and recycling the best catalyst so far (5% Ru/CNT) was investigated. In terms of reproducibility, Table 3.3 shows that under the same reaction condition, we have achieved almost the same conversion and selectivity.

Table 3-3. Reproducibility test using 5% Ru/CNT (Reduced) at 5 h reaction time in the hydrogenation of succinic acid. Reaction conditions: 50 mg catalyst, 0.1 g SA in 25 mL water. Legend: succinic acid (SA); gamma-butyrolactone (GBL); 1,4-butanediol (BDO); butyric acid (BA); propanol (C_3OH); butanol (C_4OH); carbon mass balance(CMB); propionic acid (PA); p, pressure; t, time; T, temperature; X, conversion; S, Selectivity.

Run	T, °C	p, bar	X,SA %	S,GBL %	S,BDO %	S,PA %	S,BA %	S,C_3OH %	S,C_4OH %	CMB %
1	150	50	77.8	41	7.2	11	10.7	4.7	0	85.9
2	150	50	75.8	38	5	12	10	3.8	0	81.4

Regarding the recyclability test, after each reaction test, the spent catalyst (5% Ru/CNT) was separated from the mixture by filtration, washed with deionized water, and dried it in a vacuum oven at 80 °C. As it can be seen from **Figure 3.30**, the activity decreased rapidly after the each run from 75.8 to 34 to 21 % (conversion). No leaching of Ru was observed in the aqueous solution after the reaction. As the catalyst was exposed to the air between the runs during the washing and drying, the change of Ru oxidation state as the probable reason for this decrease in activity.

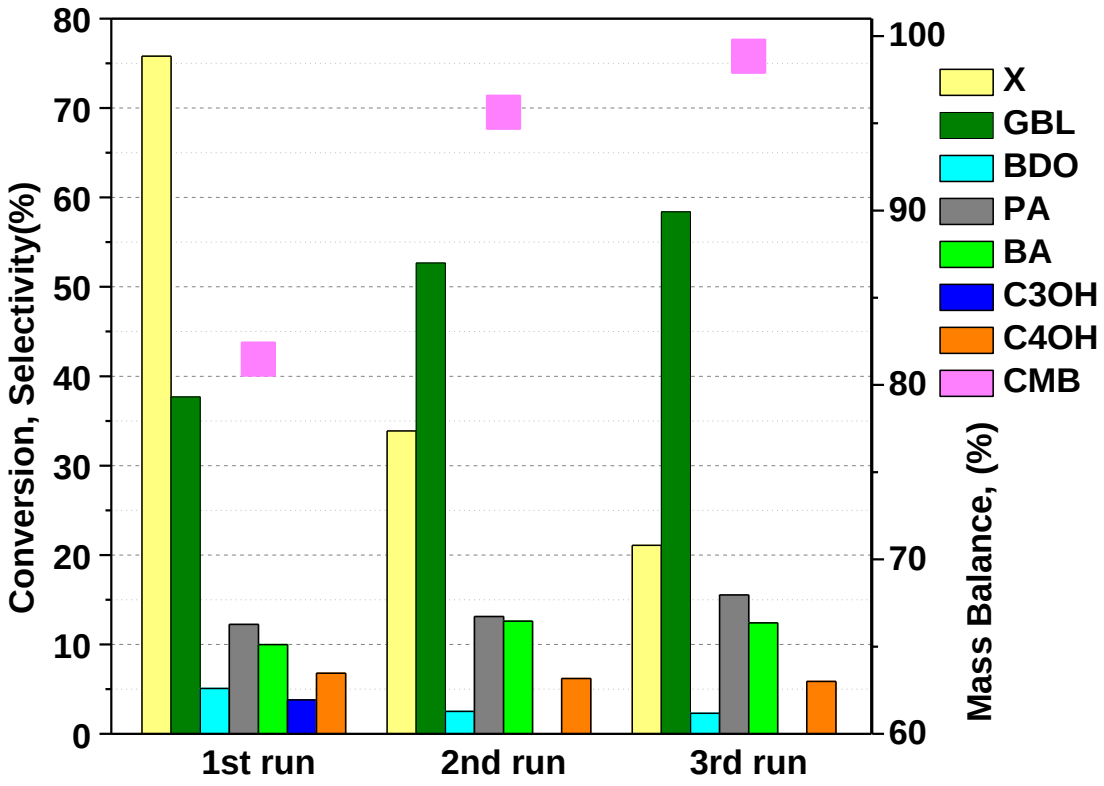

Figure 3.29. Recycling tests of reduced 5%Ru/CNT (just wash and dried between the runs). Reaction condition: T: 150 ˚C; H_2 pressure: 50 bar; reaction time:5h; succinic acid: 0.1 g; catalyst: 0.05 g; reaction time: 5 h, solvent (H_2O): 25 mL. Legends: Conversion (X), carbon mass balance (CMB).

Su and co-workers[264] studied Ru nanoparticle-based catalysts and found that air sensitivity of metallic ruthenium can be connected to its morphology and metal-support interaction. Furthermore, TEM images, taken after the second run are presented in **Figure 3.31** along with the particle size distributions.

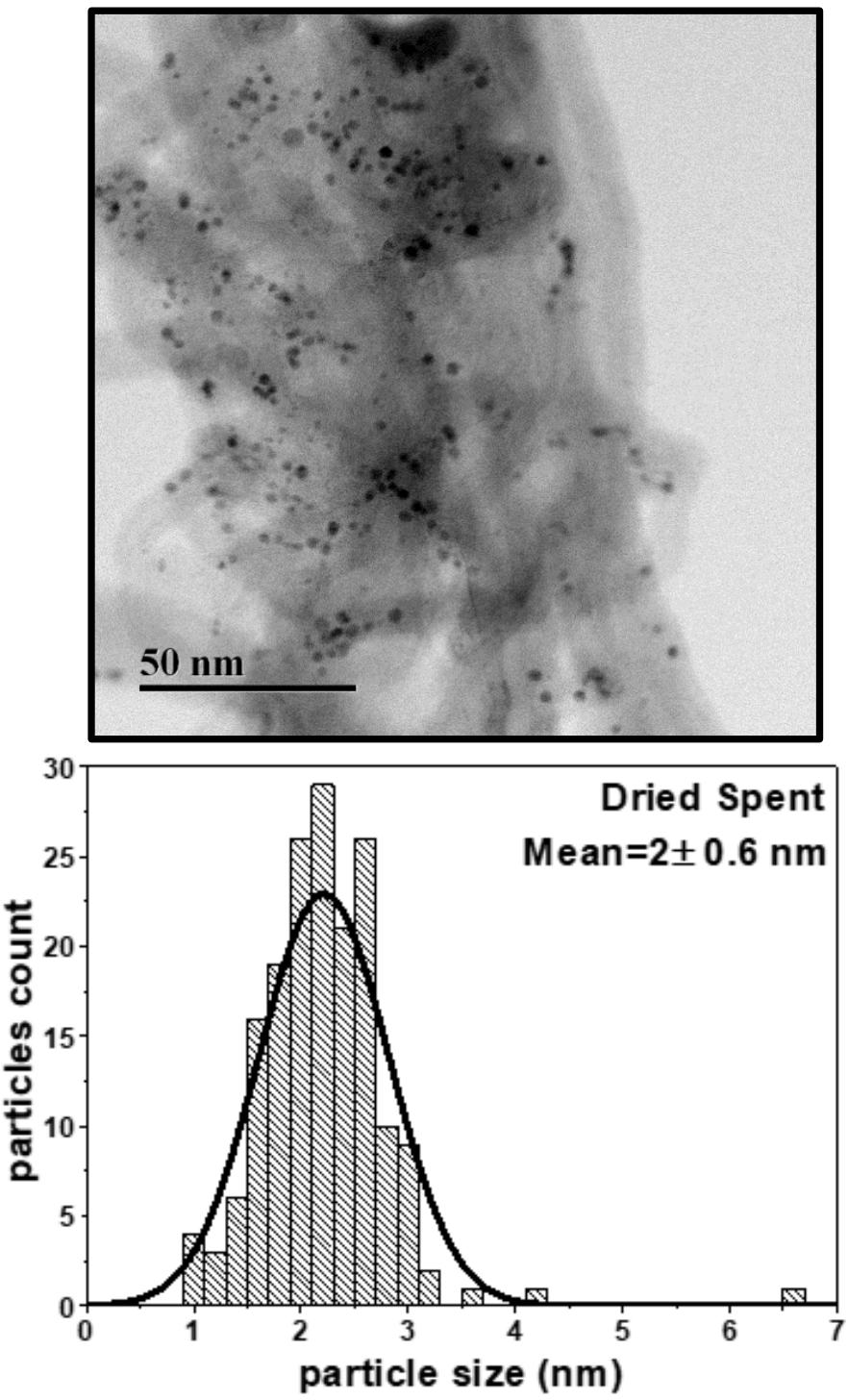

Figure 3.30. TEM images and particle size distributions of spent 5 %Ru/CNT after second catalytic run (washed and dried between the cycles).

The results show that the Ru particle size increased from 1.4 nm (freshly reduced 5% Ru/CNT) to 2 nm (after a second catalytic run). This may be responsible for the low reactivity of 5 %Ru/CNT. Another recycling test was performed using the same catalyst (5% Ru/CNT) with a reduction step (treating a catalyst in flowing of H_2 to regenerate it) between the applied, and the results are displayed in **Figure 3.32**.

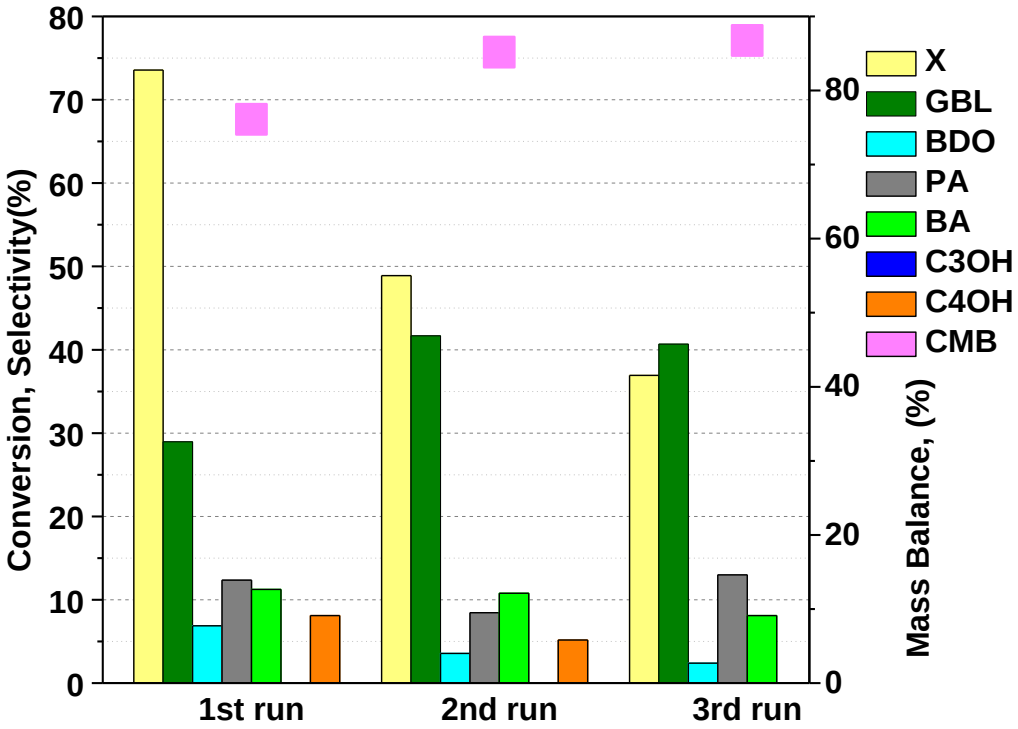

Figure 3.31. Recycling tests of 5%Ru/CNT re-reduced at 400 °C and 1 h between the runs. Reaction condition: T: 150˚C; H_2 pressure: 50 bar; succinic acid: 0.1 g; catalyst: 0.05 g; reaction time: 5 h, solvent (H_2O): 25 mL. Legends: Conversion (X), carbon mass balance (CMB).

It seems the reduction step slows down the deactivation issue since the conversion of succinic acid decreased from 73.5 to 49 to 40 % instead of 76 to 34 to 21 % when washing and drying alone was used.

The reduction step could regenerate Ru, and in a typical industrial fixed-bed reactor the catalyst would not be exposed to air. Hydrogenation of succinic acid leads to a reaction sequence and the increased selectivity to GBL in successive runs as conversion decreases also indicates the reaction is simply being slowed down and even in this case the activity could be compensated by increasing the reaction time. From these observations, it appears that the case for deactivation is a combined effect of agglomerations, but also re-oxidation when the catalyst is exposed to air.

3.4. Conclusions

Liquid-phase hydrogenation of succinic acid to 1,4-butanediol is a demanding reaction. Several parameters have been investigated such as temperature, pressure, and metal percentage as well as metal-support interactions. The conversion increase as temperature and pressure increases. Elevated temperatures up to 240 °C significantly increased the reaction rate, but also negatively impacted the selectivity to desired alcohol products. The reaction was carried out in aqueous solution without the assistance of any additives and performed under mild conditions (150 °C, and 50 bar) compared to those previously reported where more severe conditions along with the organic solvent, i.e., 1,4-dioxane was used, thus meeting the criteria of green chemistry. Moreover, mild conditions also diminish the hydrogenolysis side reactions enhancing the prospects of BDO production *via* GBL.

Washing CNT (with water) produced more active Ru based catalyst for the hydrogenation of succinic acid. Furthermore, a mixture of particles (inside and outside) of the CNT, 5% Ru/(MIX)CNT, showed better activity than the sample (5% Ru(IN)CNT) where we assumed (based on the preparation procedure) that the particles are inside the channels. This might be due to the fact the Ru particles are inside the channels of the CNTs and are not exposed to the reactant.

CO-chemisorption showed that 5% Ru(IN)CNT has a lower dispersion compared to the 5% Ru(MIX)CNT. Moreover, the succinic acid conversion increased with Ru loading. The most active catalyst had 10 wt. % Ru loading giving 100 % conversion of SA within two hours under same reaction conditions (150 °C and 50 bar). However, 5% Ru/CNT showed better selectivity towards alcohol products.

The reaction proceeded faster using a Ru catalyst supported on CNT compared to AC, we found that the hydrogenation activity in the transformation of succinic acid increases over 5 times in terms of turnover frequency using carbon nanotubes as support for ruthenium nanoparticles. In addition, 5% Ru/AC and 5% Ru/CNT were also characterised by XPS, suggesting that the binding energy of ruthenium decreased due to the electronic properties of CNT in comparison with AC, which could in turn enhance the catalytic activity of Ru/CNT. The benefits of using CNT as support on activity extended to Pd and Pt beside Ru. The Pd catalyst was an inactive catalyst in the hydrogenation of SA which may be due to a lack of proper dispersion. However, regardless the metals used, the superior activity of the catalysts supported on CNT might be due to the electronic promotional effect of the carbon nanotubes which is supported by previous literature (more characterisation might be needed to explain this high activity, and it will be discussed in Chapter 4).

In recycling tests, the activity of the catalyst decreased rapidly after the first run perhaps due to the Ru particle size or change in Ru oxidation state since the catalysts were exposed to the air. However, introducing a reduction step in between the runs slowed the deactivation that it is due to particle agglomeration.

In this chapter, 5% Ru/CNT efficiently converted aqueous succinic acid under mild conditions, (150 °C and 50 bar) i.e. 95.4 % succinic acid conversion in 11 hours. The total alcohols (1,4-butanediol, propanol, and butanol) yield using 5% Ru/CNT after 23 h reaction time was 40 % but the selectivity to a single alcohol remains as an issue. The Ru catalyst might benefit from a promoter to fulfil this goal.

CHAPTER 4

Ru Catalysts Modified with Sn for Liquid-Phase Hydrogenation of Succinic Acid to 1,4-Butanediol

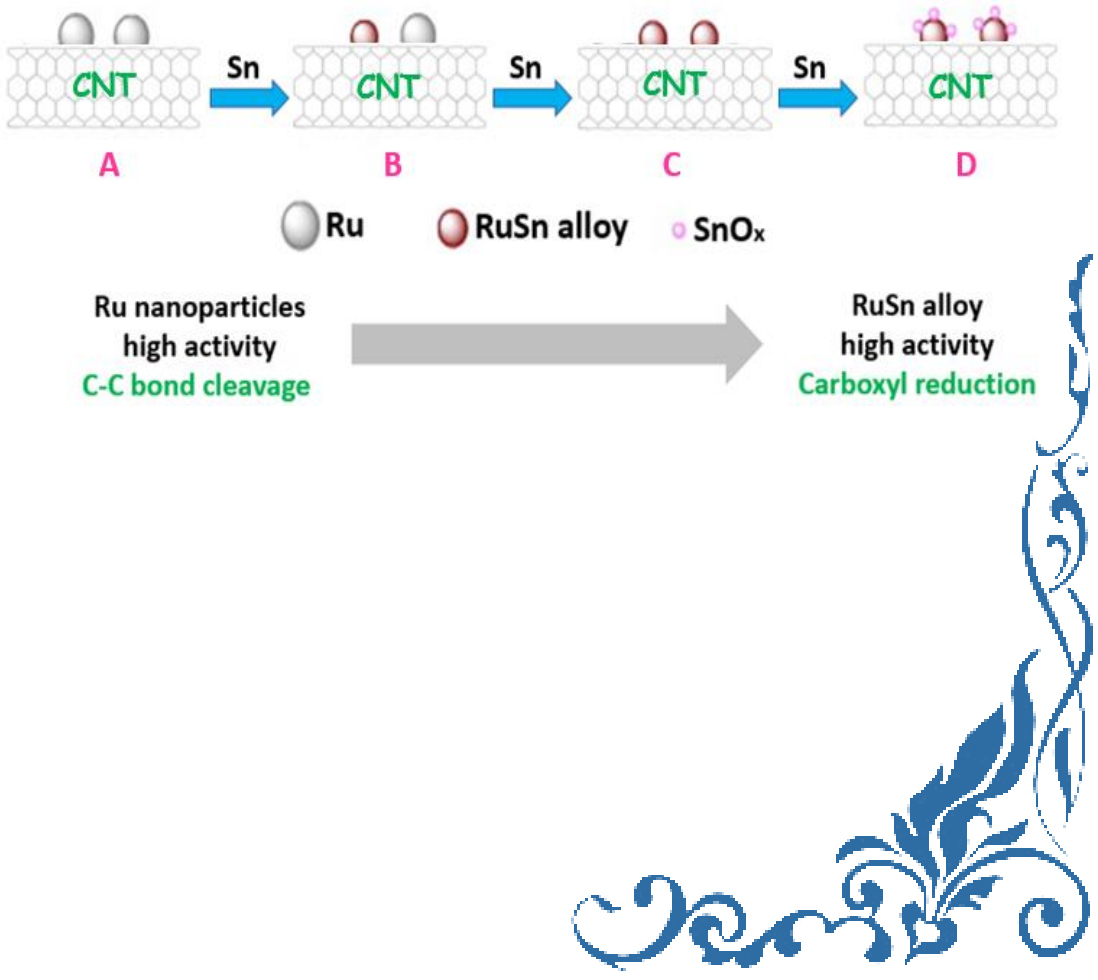

Chapter 4: Ru Catalysts Modified with Sn for Liquid-Phase Hydrogenation of Succinic Acid to 1,4-Butanediol

4.1. Introduction

Bio-based succinic acid (SA) is a promising platform chemical from the bio-refinery, mainly produced by a fermentative process using renewable biomass,[64] which has the potential to become a full replacement of the traditional fossil-based routes.[79] The fermentation processes along with the catalytic processes driven by hydrogen could bring an economical and clean competitive pathway for the manufacture of BDO from renewable carbohydrate feedstock (fermentation of glucose/saccharose)[265,266] instead of petroleum.

The universal demand for BDO is expected to grow as the consumption of these polymers is rapidly increasing across the automobile and electronics industries. BDO could also be converted to gamma-butyrolactone (GBL), which is a very well-known intermediate in the preparation of various pharmaceuticals, *via* dehydrogenation processes.[267] BDO could be transformed to tetrahydrofuran (THF) by dehydration processes, and is mainly used to produce poly-tetra-methylene glycol (PTMEG) and polyvinyl chloride (PVC).[268]

BDO is entirely manufactured from petroleum-based feedstock through numerous routes such as acetylene, propylene, maleic anhydride, and butadiene.[269,270] These processes, conversely, have some inherent disadvantages due to their oil-derived nature. For example, during the maleic anhydride process, the release of CO_2 is unavoidable because it is produced by oxidation of benzene or *n*-butane.[270] From an economic perspective, the price of BDO is influenced by the price of crude oil.[108] Therefore, finding another resource such as biomass to produce it, is highly demanded since it could accomplish economic and environmental perspectives.

One of the early reports on the hydrogenation of succinic acid was published in 1955 by Carnahan *et al.*[271] Under high H_2 pressure (720–950 bar) and 152–192 °C, the study showed 59 % total yield of BDO, *n*-propanol, and *n*-butanol over RuO_2 catalyst. The synthesis of a single alcohol, however, would have been preferred. In 2002, Deshpande and co-workers studied the hydrogenation of succinic acid in 1,4-dioxane extensively using Ru-Co catalyst.[272]

Using harsh reaction conditions (250 °C, 103 bar), the study achieved 50 % and 60 % selectivity for BDO and THF respectively. It should be noted that producing a single product, particularly BDO from the hydrogenation of succinic acis is challenging task due to the formation of another by-products, which diminishing the selectivity towards 1,4-butanediol.

Previous research, has concluded that the monometallic catalysts were unselective to BDO. This series of monometallic Pd,[273,274] Ru,[23] and Re,[105] catalysts supported on different carbon materials have been reported for the hydrogenation of succinic acis to THF and GBL. However, bimetallic catalysts have displayed selectively to BDO, suggesting a direct effect on the catalytic activity of a system.[275] Comparatively, monometallic catalysts tend to have lower catalytic performance in specific reactions compared to bimetallic catalysts.[276]

The size and morphology of active particles could improve along with catalyst selectivity after adding metal (s) to the given catalyst; this effect is not yet well understood.[27,276] Throughout literature reports Pd–FeO_x/C,[122] Pd–Re/TiO_2,[106] and Re–Ru/C.[86] Re and Fe were successfully used as promoters to increase the production of BDO. Liu *et al*.[122] used Pd-Fe/C to hydrogenate succinic acid. The study reported that the good dispersion, catalyst high acidity and the synergy between Fe and Pd species, improved the yield of BDO.

Re alone was not sufficient to attain a high yield for BDO.[81,115,130,277] The role of Re as a promoter to enhance the selectivity for BDO was not adequately clarified in these reports. The combination of a noble metal and rhenium made the chemical and structural analyses difficult.[86] For instance, noble metals such as Ru, Pt, and Pd can be miscible since all these metals have quite similar atomic size making probing the characterization complicated.[86,121] Due to the high cost of Re the need to explore an alternative metal is recommended.

Tin (Sn) has been successfully used as a promoter for Pt-based catalysts in hydrogenation reactions.[278-280] Most of the studies considered the addition of Sn to Pt catalysts to enhance the selectivity for alcohol products due to the performance of Sn^{n+} species.[52] The presence of Lewis acid sites (provided as Sn^{2+}) near the metal particles may interact with the lone electron pairs of the carbonyl oxygen, which then lead to this activity.[281]

Researchers examined the effects of Sn on Pt/CNT system in the hydrogenation of acetic acid to ethanol.[282] Sn inhibits the C-C bond activity of Pt catalyst, which resulted in the increased selectivity of ethanol. Carbon nanotubes proved to be a better support for the Pt-Sn catalytic system than TiO_2, ZrO_2 or SiO_2 in the hydrogenation of acetic acid to ethanol. The study explained this phenomenon by the formation of a well-dispersed Pt-Sn alloy on CNT surface.[282]

Several researchers have successfully used Ru-Sn systems supported on Al_2O_3, SiO_2, and AC to hydrogenate the C=O bond in different reactions such as croton-aldehyde, fatty acids, and their esters to the corresponding alcohols.[148,283,284]

The Coq *at el.*[285] performed hydrogenation of cinnamaldehyde using different promoters (Sn, Ge, Zn, Fe, and Au) to Ru catalyst, however, tin proved to be the better option. The reaction has performed at 109 °C, 45 bar, and the mean size of the particles was 2.1 nm.[285]

Ru-Sn catalyst increased both the activity (conversion) and selectivity to cinnamyl alcohol due to two reasons: (i) the electron transfer from Sn to Ru which increase the electron density at the active Ru site; (ii) presence of Ru-Sn sites which contain Sn cations. These are play an important role to co-ordinate the oxygen atom in the carbonyl group and activate them.[285]

Pouilloux et al.[286] hydrogenated methyl oleate into oleyl alcohol over Ru-Sn/alumina catalysts. In their proposed reaction mechanism, Sn^{2+}/Sn^{4+} Lewis acid sites polarize the carbonyl group of methyl oleate while metallic Ru sites promote the H_2 dissociation (**Figure 4.1**).

Lewis acid Sn sites have the potential to activate the carbonyl group and this property has been used for reduction of the aldehydes/acids to alcohols.[287] The polarization of the carbonyl group of the ester/carboxylic acid can be accomplished *via* the interaction with Lewis acids typically by tin ions.[23]

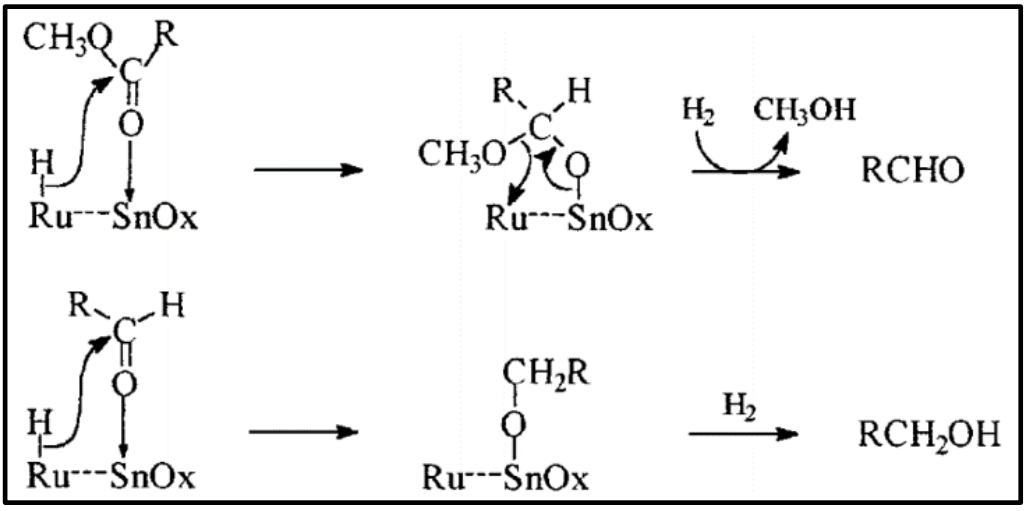

Figure 4.1.Mechanism of the hydrogenation of methyl oleate into oleyl alcohol via the formation of aldehyde. Adopted from Pouilloux et al.[286]

It was demonstrated in the literature that the alcohols formation is strongly depends on the Sn/metal ratio. Musci *et al*.[288] reported that the best Sn/Ru ratio is 0.4, where 85 % selectivity for furfuryl alcohol was achieved in the hydrogenation in furfural at 90 °C and 12.5 bar. On the other hand, Galvagno reported that as increasing the Sn/Ru ratio, the catalytic activity decreases in hydrogenation of cinnamaldehyde due to a poisoning effect of Sn.[289] The presence of tin can block the Ru metal sites on the catalyst and depress the catalytic acidity (geometric effect).[289]

Recently, several studies are referring this high selectivity strongly to a formation of metal-tin alloy.[290] Ru-Sn alloy showed better selectivity to alcohol product for some of hydrogenation reactions.[291,292] The achievement of these previous reports have encouraged us to develop Ru-Sn based catalysts for the hydrogenation of succinic acid and levulinic acid to produce the diols.

A series of Ru-Sn catalysts was prepared using CNTs and AC as supports to compare their intrinsic activities and selectivity's in SA hydrogenation to produce BDO. The supported catalysts characterized by X-ray powder diffraction (XRD), temperature-programmed reduction (TPR), transmission electron microscopy (TEM), X-ray photoelectron spectroscopy (XPS), and CO chemisorption. These techniques have been used to be able to find out the critical role of the tin in Ru-Sn catalyst in which the use of this promoter did increases the selectivity for BDO.

4.2. Experimental

All catalysts in the current chapter were prepared using incipient wetness impregnation method. We performed the catalytic reactions in stainless steel Parr 4590 series reactor equipped with an overhead gas entrainment stirrer. The procedure along with the catalysts preparation method are described in detail in Chapter 2.

4.3. Results and Discussion

4.3.1. Catalysts Characterization

4.3.1.1. X-Ray Diffraction Analysis (XRD)

The XRD patterns of Ru catalysts with different Sn loading after the reduction at 400 °C is presented in **Figure 4.2**. In all diffractograms, the strongest diffraction peak appears at around 25.7°, peaks with medium intensity at 42.5° and weak peak, at 78.1° and can be indexed as (002), (100), and (110) reflections of graphite structure, respectively.[223,224] (JCPDS 001-0640, 003-0401) There was only a possible indication of a broad maximum of Ru (101) at 44° and Ru (110) at 68° (JCPDS 001-1253) in 5% Ru/AC and **2% Sn**-5% Ru/**AC**. No sign of crystalline phases of metallic Ru in the other Ru catalysts supported on CNT was found, suggesting that the Ru nanoparticles are too small to be analyzed by XRD.

Regarding, 2% Sn/CNT, no clear diffraction peaks were assignable to Sn particles, suggesting well-dispersed particles on CNT's as all the diffractions were below the XRD detection limit. **Figure 4.2** shows the x-ray diffraction of Ru-Sn catalysts with database diffraction pattern of the intermetallic compound (Ru-Sn). We could not detect any diffraction peaks related to the alloys. The species of ruthenium-tin alloys might be too small to be distinguished by X-ray apparatus or might be because of their low content in the catalyst.

Based on many reports on the hydrogenation of fatty acid derivatives, the formation of Ru-Sn alloys and Ru_3Sn_7 crystalline phase (**Figure 4.1**) were an active component of the catalysts.[23,293] We should note here that due to the inability to detect the Ru-Sn alloy, we could not have concluded. However, it has been reported that it could be Ru_3Sn_7.[23,293]

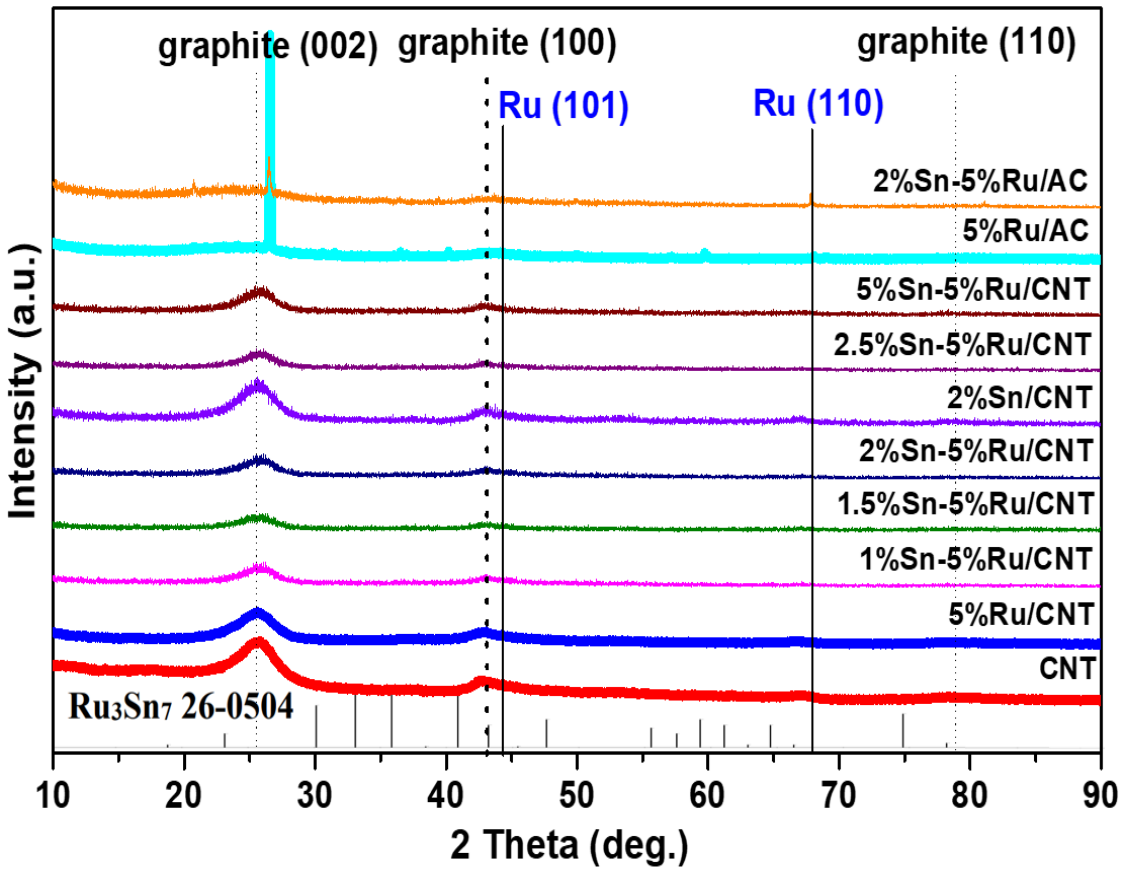

Figure 4.2. XRD patterns of activated carbon, carbon nanotube, reduced Ru-Sn catalysts. The database diffraction pattern of Ru_3Sn_7 alloy, adopted from Lee et al.[23]

4.3.1.2. Transmission Electron Microscopy (TEM)

TEM analysis confirmed that Ru nanoparticles were highly dispersed on both supports and no agglomerations were observed. TEM images of (**2% Sn**-5% Ru/CNT and **2% Sn**-5% Ru/AC) were acquired together with the profile analyses of the surface compositions by EDX. The result showed that Sn is approximately located at the identical places as Ru. This could be a significant indication for a formation of Ru-Sn alloy. **Figure 4.3** and **4.4** show TEM images of bimetallic catalysts (**2% Sn**-5% Ru/CNT and **2% Sn**-5% Ru/**AC**) along with the particle size distribution histogram.

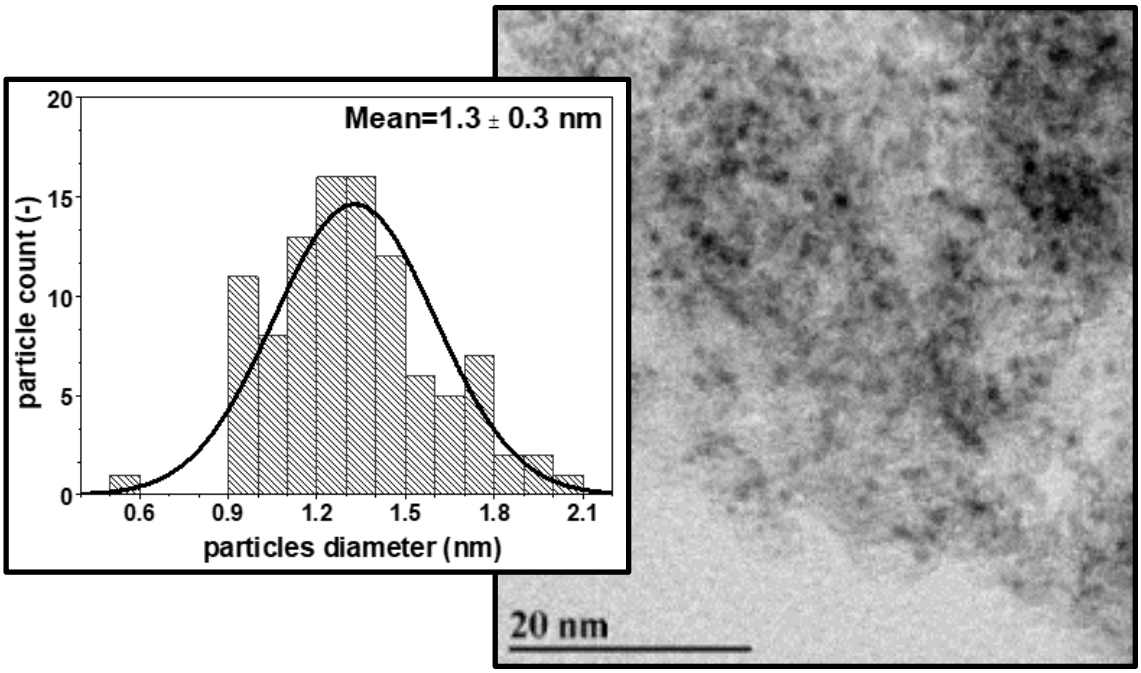

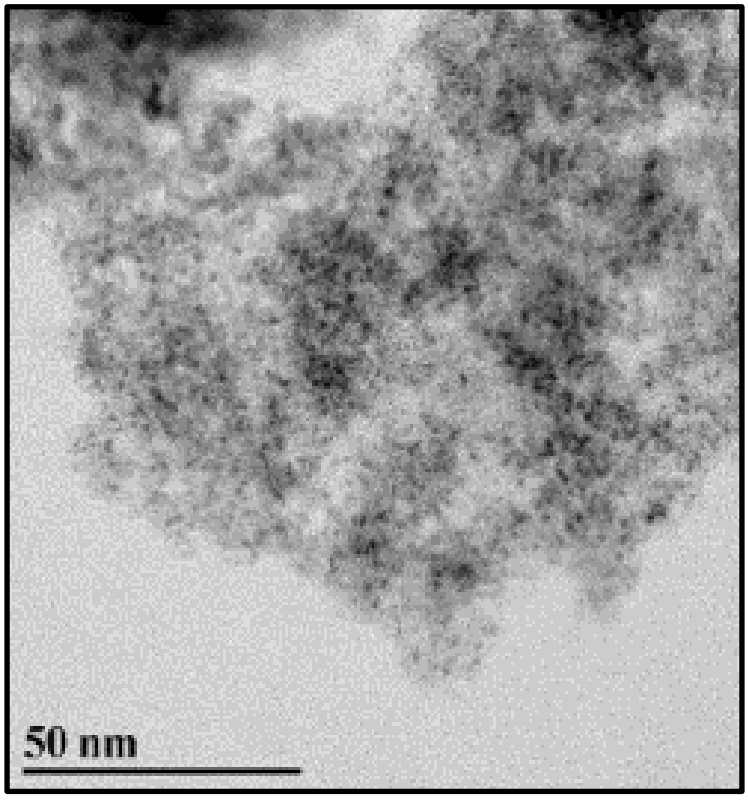

*Figure 4.3.TEM images of reduced **2% Sn**-5% Ru/**AC** (scale bars of 20 and 50 nm) and the corresponding histograms with particle size distributions.*

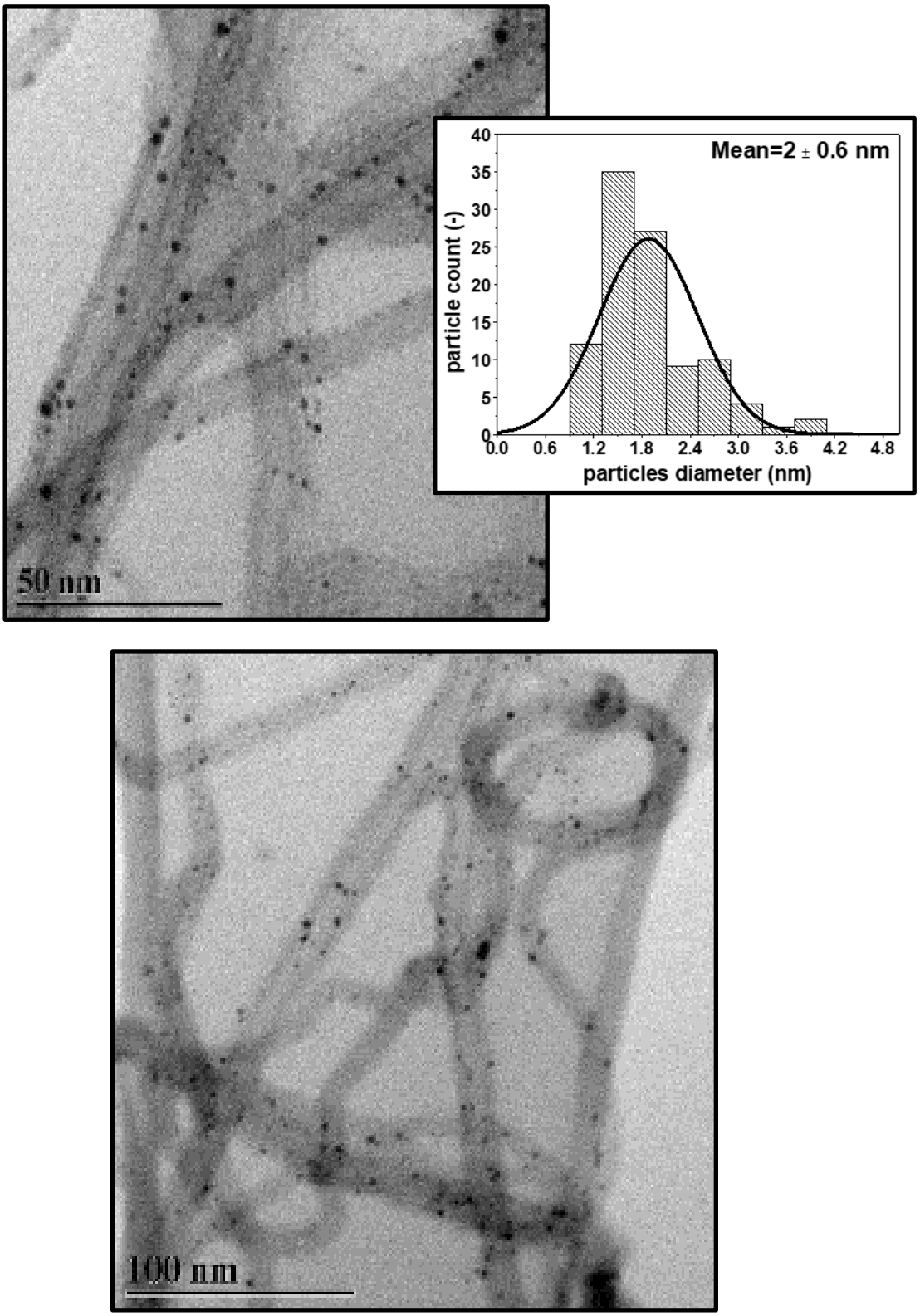

*Figure 4.4. Images of reduced **2% Sn**-5% Ru/CNT (scale bars of 50 and 100 nm) and the corresponding histograms with particle size distributions.*

The surface properties of the carbon support could significantly affect the metal particle size,[294] which was observed in monometallic Ru catalysts supported on AC and CNT. In Chapter 3, a fair distribution of the Ru particles was detected in monometallic samples. The average particle size was 1.3±0.2 nm and 1.4±0.3 nm for 5% Ru/AC and 5% Ru/CNT respectively. The same trend was also observed here in bimetallic Ru catalysts since **2% Sn**-5% Ru/**AC** and **2% Sn**-5% Ru/CNT showed size of 1.3±0.3 nm and 2±0.6 nm respectively.

4.3.1.3. Metal Dispersion by CO-Chemisorption

Bimetallic catalysts showed an increased particle size on both supports (AC and CNT) after the introduction of Sn, which was supported by the CO-chemisorption results. According to the literature, this increasing in particle size could suggests the formation of a deposit of Sn in Ru.[288] The CO chemisorption and calculated metal dispersions are presented in **Table 4.1**.

CO does not adsorb irreversibly on ionic Sn, metallic Sn, or noble metal particles decorated or coated by Sn.[295-297] Thus, in the Ru-Sn bimetallic system, it is considered that CO is only chemisorbed on the Ru surface. The addition of Sn, according to **Table 4.1**, decreases the CO uptake, which strongly suggested that Sn is binding to Ru sits and blocking adsorption.[289] It can be seen that a monometallic 5% Ru/CNT had highest CO uptake than bimetallic catalysts (Table 4.1, entries 2-4).

Table 4-1. List of redudced catalysts, results of CO chemisorption, nitrogen physisorption, and TEM for reduced catalysts. Metal dispersion was calculated from CO chemisorption.

Entry	Catalyst	CO uptake, µmol/g	metal dispersion %	average particle size (TEM) nm	S_{BET}, m^2/g	Total pore volume cm^3/g	Average pore diameter nm
1	5%Ru/AC	66.2	13.3	1.3±0.2	636	0.7	4.9
2	5% Ru/CNT	40.0	8.0	1.4±0.4	317	1.2	15.7
3	1%Sn-5% Ru/CNT	36.8	7.4	-	284	1.5	22.2
4	2%Sn-5% Ru/CNT	34.9	7.0	2±0.6	239	1.8	30.2
5	2%Sn-5% Ru/AC	56.1	11.3	1.3±0.3	584	0.7	5.0
6	AC				664	0.8	4.7
7	CNT				283	1.2	17.3

In Table 4.1, entries 2-4, the Ru dispersion on CNT decreased as the Sn loading increased which might be due to the strong interaction between Ru and Sn. In addition, the same trend was noticed for Ru catalysts supported on AC (Table 4.1, entries 1 and 5). These results suggest that the synthesis method resulted in a strong interaction of Ru with Sn rather than isolated Ru and Sn species.

4.3.1.4. Nitrogen-Physisorption Analyses

We analysed the surface area and the pore size of the catalysts, the results were shown in **Table 4.1.** The monometallic ruthenium catalysts supported on AC and CNT displayed high surface areas, but low total pore volume compared to bimetallic catalysts. Regarding the Ru/AC, the total pore volume and the surface area decreased after introducing Sn whereas the average pore diameter increased (Table 4.1, entries 1 and 5).

The surface area for Ru-Sn catalysts supported on CNT decreased as introducing Sn to the catalyst and as increasing, the Sn loading the surface area decreased further. The surface area decreased from 317 m^2/g for (5% Ru/CNT) to 284 m^2/g and 239 m^2/g for **1% Sn**-5% Ru and **2% Sn**-5% Ru respectively (Table 4.1, entries 2-4).

The total pore volume for Ru-Sn catalysts supported on CNT augmented as increasing the Sn loading. **2% Sn**-5% Ru/CNT had the lowest catalyst surface 239 m^2/g and high pore diameter 30 nm compared to all monometallic and bimetallic Ru catalysts (Table 4.1, entry 4).

4.3.1.5. X-Ray Photoelectron Spectroscopy (XPS)

XPS was used to explore the oxidation state of Ru and Sn on the prepared catalysts. It should be noted that Ru catalyst systems are difficult to study by XPS due to the overlap of two core levels (C 1s and Ru 3d). However, some information was obtained using Ru 3p core level spectra.[298] As shown in Table 4.2, the binding energy (BE) is shifted after introducing tin depending on the support. Monometallic Ru catalyst supported on AC a displayed highest binging energy (463.60 eV) however; it showed shifting toward lower BE values after the addition of Sn (462.70 eV) (Table 4.2, entries 1 and 4).

Table 4-2. The binding energy (eV) of ruthenium species in the different analysts.

Entry	core level/species	5%Ru/AC		5%Ru/CNT	
		B.E., eV	rel. composition, %	B.E., eV	rel. composition, %
1	**Ru 3p$_3$**	463.6		462.10	
2	Ru(0)	463.3	71.8	461.61	67.6
3	RuO_x	466.9	28.1	464.61	32.3
Entry	**core level/species**	**2%Sn-5%Ru/AC**		**2%Sn-5%Ru/CNT**	
		B.E., eV	**rel. composition, %**	**B.E., eV**	**rel. composition, %**
4	**Ru 3p$_3$**	462.7		462.5	
5	Ru(0)	462.2	74.0	462.0	89.5
6	RuO_x	465.2	25.9	465.0	10.4
7	**Sn 3d$_3$**	483.2		483.2	
8	Sn(0)	483.3	11.3	482.0	15.8
9	SnO_x	486.1	88.7	486.1	84.2

Note: B.E. stands for binding energy.

5% Ru/CNT presented the lowest BE value amongst all tested catalyst (462.10 eV). Here also, Ru supported on CNT showed shifting but to higher BE values after introducing tin (462.50 eV). This shifting in BE might confirm the electronic effect of tin over Ru.[288] Furthermore, the BE shifts indicated a strong interaction between Ru and Sn which it would be sign of a formation of alloy.[12,299]

We deconvoluted the XPS spectra of Ru 3p$_3$ (Figure 4.5) and Sn 3d$_3$ (Figure 4.6) core level to find out the oxidation state of Ru and Sn in the samples.

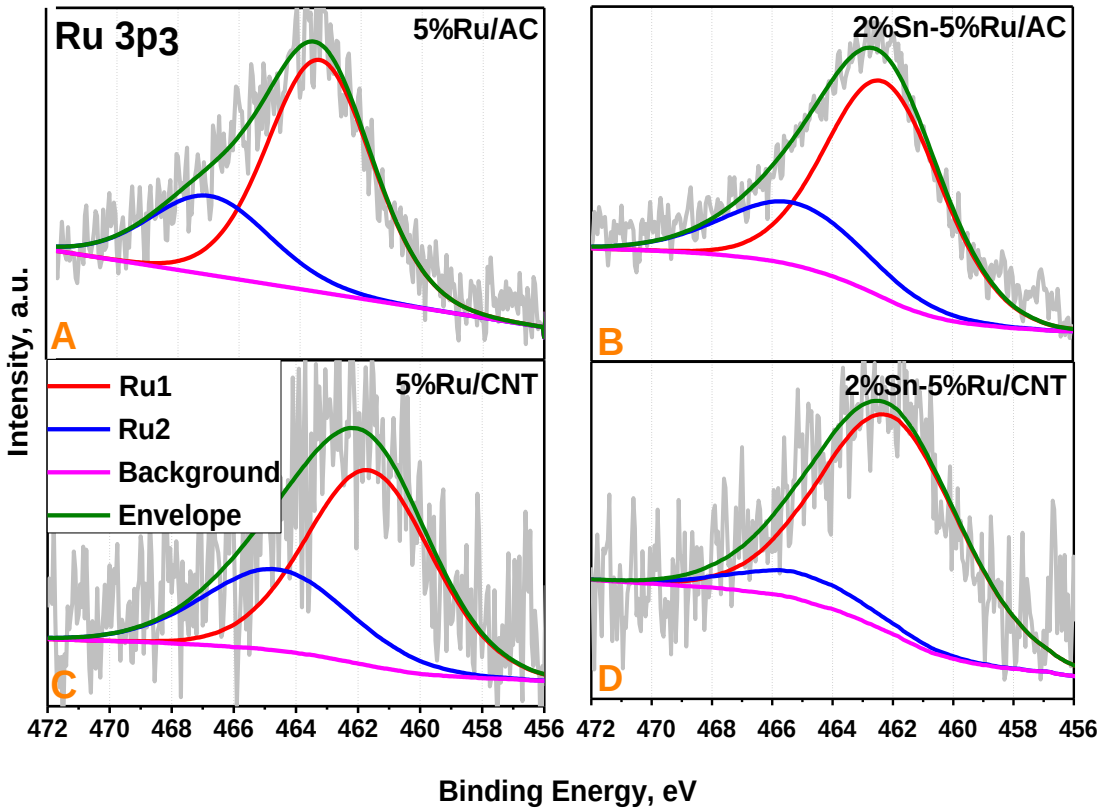

Figure 4.5. Ru $3p_3$ core-level spectra for different Ru catalysts showing the fitted spectra.

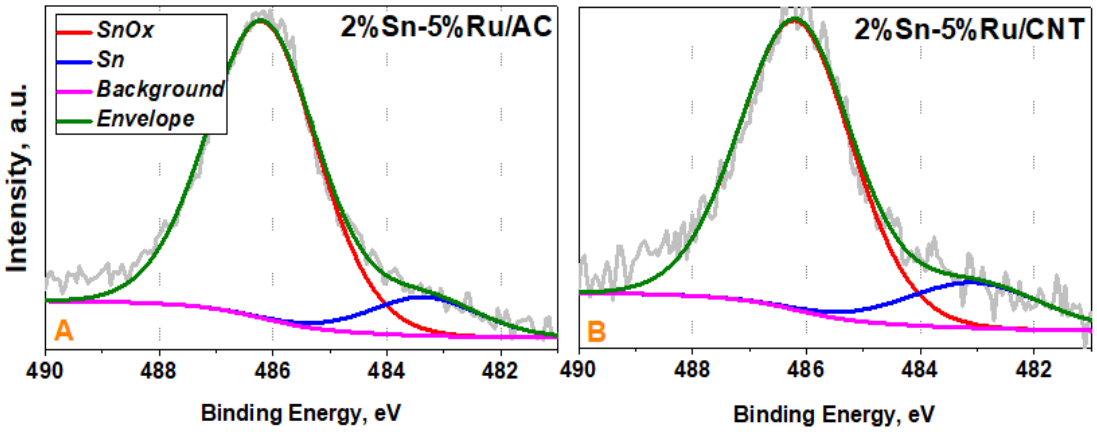

Figure 4.6. Sn $3d_3$ core-level spectra of different Ru catalysts showing the fitted spectra.

Ru $3p_3$ core level energies for 5% Ru/AC, 5%Ru/CNT, 2%Sn-5%Ru/AC, and 2%Sn-5%Ru/CNT are a little higher than those reported for Ru in the literature (i.e. 461.7 eV for Ru^0, 463.2 eV for RuO_2, 463.5 eV for RuO_3 and 463.8 eV for $RuCl_3$).[240,241] H_2-TPR results later (Figure 4.7) confirmed the reduction of Ru occurred well below the pre-treatment temperature therefore it is anticipated that majority of ruthinum is in oxidation state 0.

The surface composition of Ru determined by XPS is very similar in 5% Ru/AC, 2%Sn-5% Ru/AC, 5% Ru/CNT ca. 67-74 % and 25-32 %, whereas 2% Sn-5% Ru/CNT showed the highest percentage for Ru^0 (89.6 %) and the lowest percentage for RuO_x (10.4 %) (Table 4.2, entries 1-4).

In the Sn 3d core level energies, the BE for 2%Sn-5%Ru/AC and 2%Sn-5%Ru/CNT are different than what was reported in the literature (i.e. 285.5 eV for Sn^0 and 287 eV for SnO_x).[288] The results in Table 4.2 showed that the binding energies in 2%Sn-5%Ru/AC are 483.33 eV (Sn^0) and 486.18 eV (SnO_x) whereas in 2%Sn-5%Ru/CNT, the BE were 483.05 eV (Sn^0) and 486.18 eV (SnO_x).

The surface composition of Sn in (2% Sn-5% Ru/AC and 2% Sn-5% Ru/CNT) samples are quite similar and the percentage of SnO_x is higher than Sn^0 in both samples (Table 4.2, entries 8 and 9).

4.3.1.6. Reducibility of the Ru Based Catalysts by H_2-TPR

The reducibility of the as-synthesized samples using temperature programmed reduction with hydrogen (H_2-TPR) was investigated to understand the redox properties and interaction between Ru and supports.[232,233] The analysis indicated the interaction between the support and the active component, as well as determined the appropriate reduction temperature for activating the catalyst prior to the activity assessment.[173,300] **Figure 4.7** displays the reduction profiles for various **X% Sn**-5% Ru/CNT catalysts, including **2% Sn**-5% Ru/**AC** and 2% Sn/CNT for comparison.

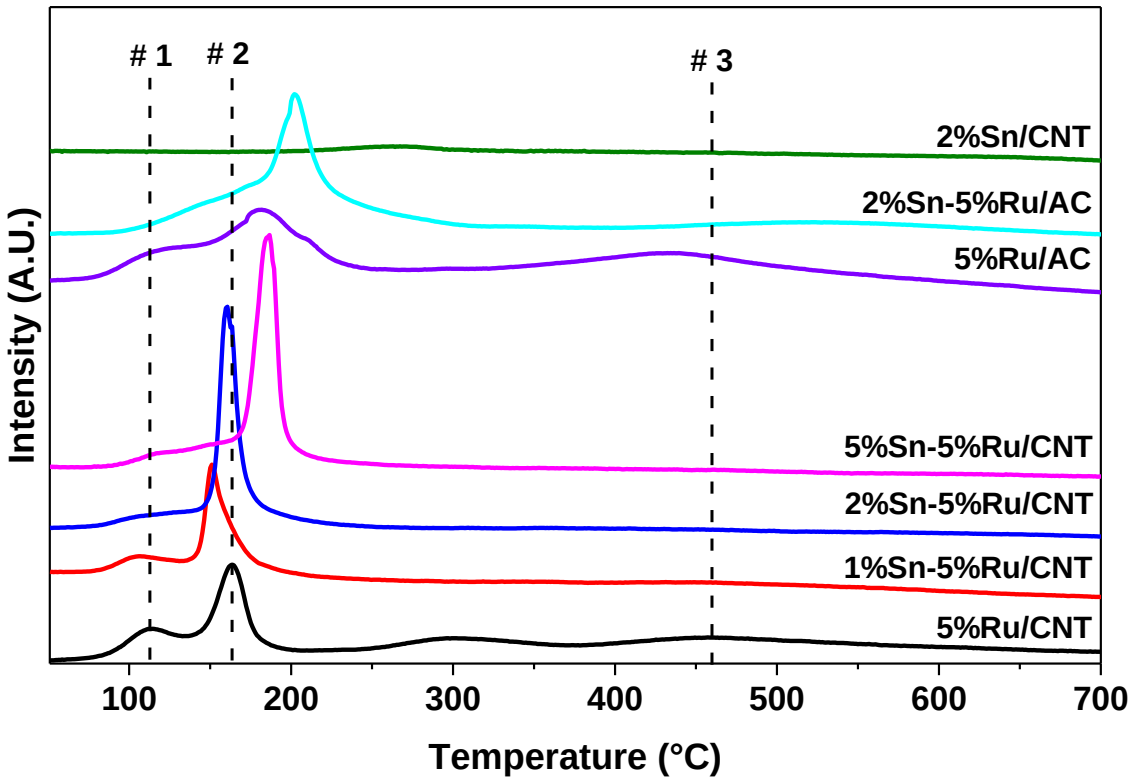

Figure 4.7. H_2-TPR profiles for different catalysts (reduced) supported on CNTs and AC.

The H_2 consumption patterns are different from all the tested catalysts which might reflect in their catalytic performance. The high-temperature intake of H_2 over 5% Ru/CNT (0% Sn) at 420-580 °C was due to the methane formation through reduction of functionalized carbon in the presence of supported metals.[85] Methane formation was less evident for samples containing 2 % and 5 % Sn than samples with 1 % Sn, monometallic Ru (5 %), and **2% Sn**-5% Ru/**AC**. As the loading of Sn increased in the catalyst, the reduction peak (#1) disappeared compared to 5% Ru/CNT which might be due to the decrease of the surface of Ru catalyst as being addressed in the literature.[292] It is possible that the disappearance peak might relate to undetected free Ru, suggesting the formation of a Ru-Sn alloy,[297] or potentially due to the strong interaction between Ru-Sn, preventing the Ru reduction.[286]

The second reduction peak (#2) shifted towards higher temperature in samples containing, Sn and the intensity of this peak was enlarged as the Sn content increased in Ru-Sn catalysts supported on CNT. This peak was shifted further in the case of **2% Sn**-5% Ru/**AC** compared to 5% Ru/AC.

On the other hand, 2% Sn/CNT showed peak at 260 °C which perhaps correlates to the reduction of Sn (II).[301] This peak was absent in all bimetallic Ru-Sn catalysts. Under reduced conditions (400 °C), all metals salts used in the current chapter could be completely converted into metallic form without loss of the carbon support.

4.3.1.7. Acidity and Basicity Results by Temperature Programmed Desorption

Ammonia (NH_3) and carbon dioxide (CO_2) TPD were employed to investigate the total acidity and basicity of different catalysts supported on AC and CNT. The results of deconvoluted temperature programmed desorption profiles of NH_3 and CO_2 are presented in **Figure 4.8.** The full profiles can be found in appendix (**Figures 8.18 and 8.19**).

AC displays virtually no acidity compared to CNT which gives 123.43 and 100.35 µmol/g, respectively. Furthermore, both 5% Ru/CNT and 5% Ru/AC, do not show any significant basicity compared to bare supports. However, 5% Ru/AC displays a high amount of acid sites as compared to untreated AC while an increase in the acidity is less noticeable in 5% Ru/CNT.

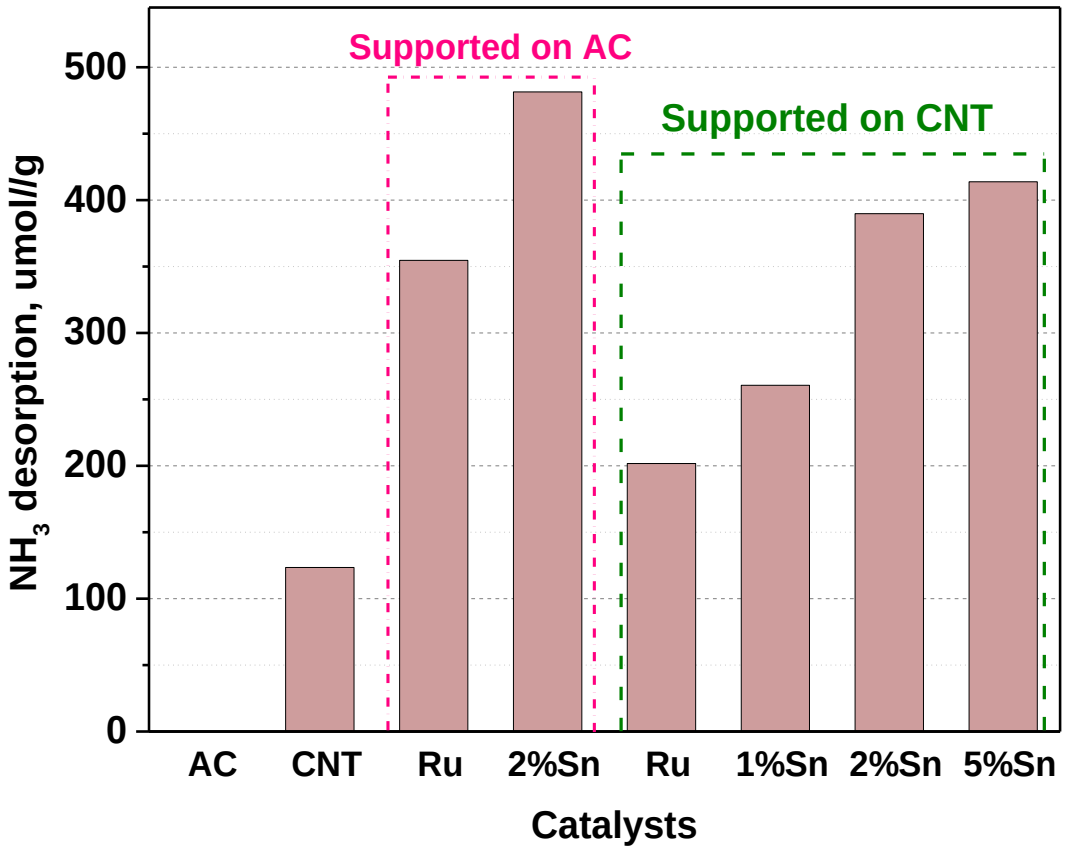

Figure 4.8. Acid properties represented by amounts of NH_3 desorbed from respective temperature programmed desorptions [µmol/g]. Note (All catalysts are reduced before the test).

On the other hand, after introducing Sn to the monometallic Ru catalysts supported on AC and CNT, the acidity and the basicity of the catalysts increased. Regarding the Ru catalysts supported on CNT, as the Sn wt. % increased from 1 to 5 %Sn the acidity of the catalyst increased indicating the increasing surface acidity of Ru-Sn catalysts.

It should be noted here, that the acidic peak at around 220 °C (**Figure 8.19, Appendix**) on monometallic Ru catalysts supported on CNT disappeared after introducing Sn to the catalyst. This site might be the active site which is responsible for 5%Ru/CNT C-C bond cleavage activity, as it will be shown later.

Comparing the basicity of bimetallic catalysts, the basicity of the catalyst increased in **1% Sn**-5% Ru/CNT and **2% Sn**-5% Ru/CNT compared to 5% Ru/CNT however, **5% Sn**-5% Ru/CNT showed lowest basicity (35.7 µmol/g) when compared to all tested catalysts (**Figure 4.9**).

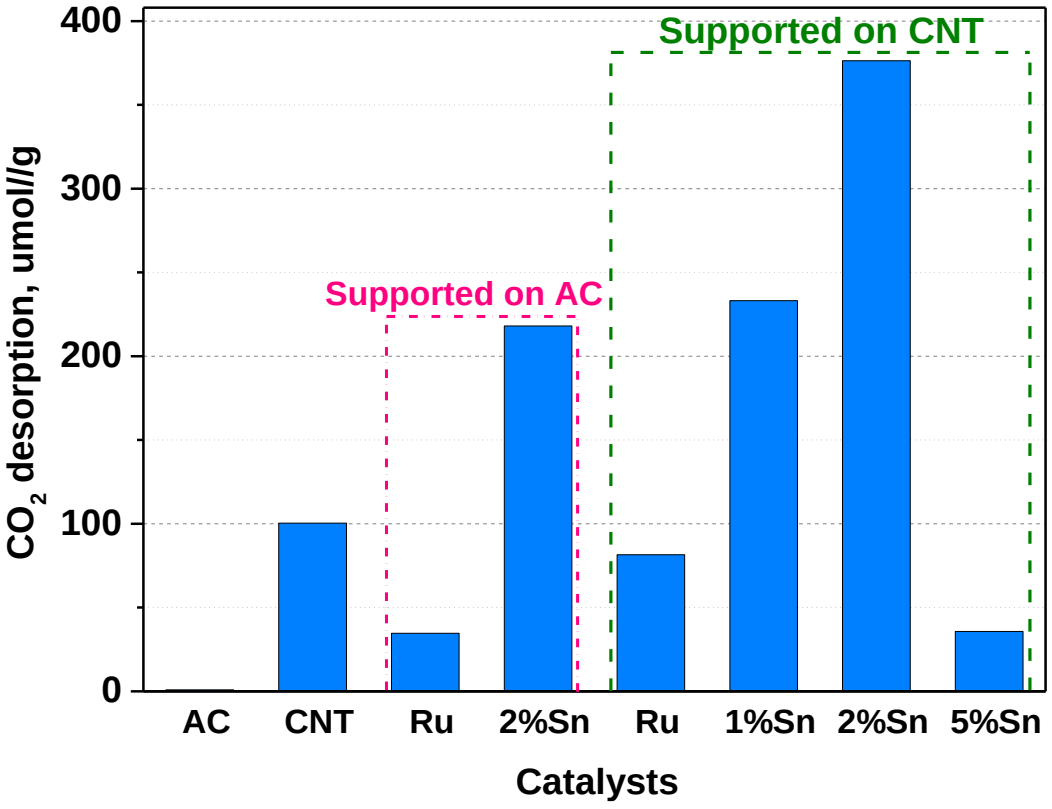

Figure 4.9. Basic properties represented by amounts of CO_2 desorbed from respective temperature programmed desorptions [µmol/g]. Note (All catalysts are reduced before the test).

2% Sn-5% Ru/CNT showed low acidity and high basicity whereas **2% Sn**-5% Ru/**AC** showed the opposite trend. **2% Sn**-5% Ru/CNT showed highest basicity, 376.3 µmol/g and in **Figure 8.20, Appendix,** the peak appear at lower temperature (96° C) compared to 5% Ru/CNT (101 °C), **1% Sn**-5% Ru/CNT (101 °C) and **5% Sn**-5% Ru/CNT (102.9 °C).

4.3.2. Hydrogenation of Succinic Acid over Ru-Sn/CNT Catalysts

Through SA hydrogenolysis and hydrogenation, useful C4 alcohols, such as BDO and 1-butanol, can be derived using a monometallic catalyst. We showed in Chapter 3 that monometallic Ru catalysts are not selective for BDO production due to a high cracking ability of Ru catalysts, as also reported in the literature.[81]

5% Ru/CNT showed ~40 % yield of alcohols (BDO, *n*-propanol, and *n*-butanol) at 150 °C, 50 bar. However, selectivity towards a single alcohol is desired. BDO is the most significant chemical from the hydrogenation of succinic acid due to its huge global use in the polymer industry.[302] Therefore, the development of Ru based catalyst using a promoter is essential to decrease the Ru catalysts cracking ability, which will then increase the selectivity for BDO.

Initially, we doped 5 wt. % Sn with 5% Ru/CNT and the prepared catalyst (**5% Sn**-5% Ru/CNT) was tested at (150 °C and 50 bar) in the pressure autoclave reactor. The results showed excellent selectivity (100 %) to GBL and no formation of any other products including C-C cleavage bond products. However, the activity was diminished since the conversion decreased from 78 % to 15 % after 5 h reaction time as shown in **Table 4.3**, entries 1 and 2.

The carbonyl group of carboxylic acid is less reactive than that of aldehydes and ketones due to the intrinsic steric hindrance, and a weak polarisability of the C=O bond. Therefore, to increase the rate of the reaction, we must have performed the reaction in severe reaction conditions.[290]

The results in **Table 4.3**, entries 2 and 3 showed that the conversion increased from 15 % to 66 % at 240 °C and 25 bar. Likewise, when the hydrogen pressure was kept at 25 bar (limited by the reactor), and the temperature was increased to 240 °C, the GBL selectivity remained at 95 %, which was useful achievement at a first glance.

Table 4-3.Tested reduced catalysts at 5 h reaction time in the hydrogenation of succinic acid. Reaction conditions: 50 mg catalyst, 0.1 g SA in 25 mL water. Legend: succinic acid (SA); gamma-butyrolactone (GBL); 1,4-butanediol (BDO); butyric acid (BA); propanol (C_3OH); butanol (C_4OH); carbon mass balance(CMB); propionic acid (PA); p, pressure; t, time; T, temperature; X, conversion; Y, yield; NA, not available. All catalysts supported on CNT.

#	Cata.	T, °C	p, bar	X,SA %	Y,GBL %	Y,BDO %	Y,PA %	Y,BA %	Y,C_3OH %	Y,C_4OH %	CMB %
1	5%Ru	150	50	77.8	32.01	5.59	8.48	8.31	3.69	5.72	85.9
2	5%Sn-5%Ru	150	50	15.4	10.29	0	0	0	0	0	94.8
3	5%Sn-5%Ru	240	25	66.4	53.04	0	0	1.36	0	0	87.9
4	2%Sn	240	25	1.1	0	0	0	1.08	0	0	99.9

We know that the BDO formation is a result of the further hydrogenation of GBL and based on some tests (not shown here), increasing the H_2 pressure was the critical step to push the reaction further to BDO. To do so, we had to change the reactor and use the Parr reactor where more hydrogen pressure could be introduced. Reaction conditions of 200 °C and 70 bar were chosen for further investigation.

We used **5% Sn**-5% Ru/CNT again but in Parr reactor rather than pressure autoclave reactor at 200 °C and 70 bar. The result showed less conversion compared to 5% Ru/CNT which was perhaps because of the excess of Sn which was might cover a high range of Ru particles as described in the literature.[303] By Serrano-Ruiz *et al*.[303] who proposed that the high percentage of Sn decreases the activity of Pt-Sn catalyst in the hydrogenation of citral.

Therefore, we prepared another Ru-Sn catalyst with loading of Sn=1 %. The results of hydrogenation of succinic acid using **1% Sn**-5% Ru/CNT compared with 5% Ru/CNT at 200 °C and 70 bar are displayed in **Figure 4.10**. The reaction was faster using the monometallic Ru catalyst as compared to **1% Sn**-5% Ru/CNT. The latter catalyst converted SA in 8 h reaction time where the monometallic Ru catalyst showed the same conversion at 45 min.

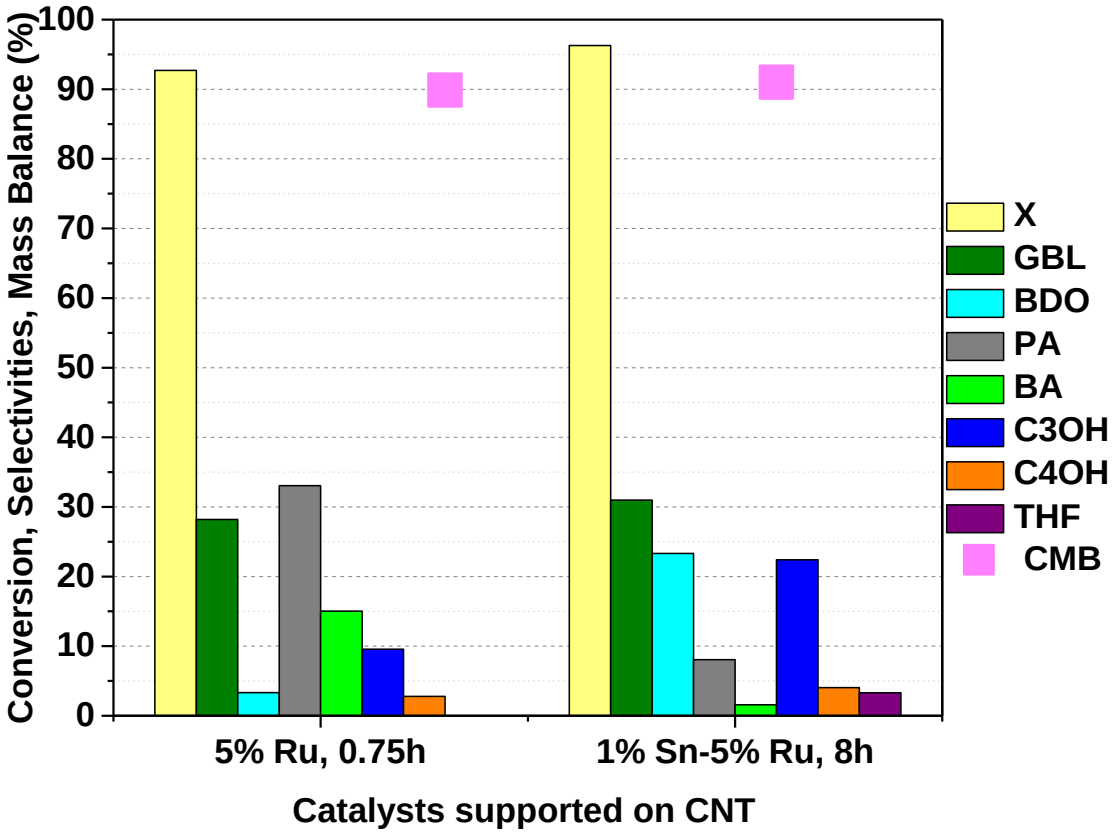

*Figure 4.10. Comparison of the selectivities at iso-conversion of succinic acid supported of CNT, 5% Ru/CNT vs **1% Sn**-5% Ru/CNT at 200 °C, 70 bar hydrogen pressure using 50 mg catalyst, 100 mg succinic acid in 25 mL H_2O.*

The proper selectivity comparison should be made at iso-conversion. However, we could not get any iso-conversion point due to the fast of the reaction using 5% Ru/CNT.

Nevertheless, the selectivity for GBL/BDO was better after introducing 1 wt. % of Sn to 5% Ru/CNT since the selectivity for BDO increased 6-fold and the competitive products to GBL that comes from the C-C cleavage (propionic acid/butyric acid) are less prevalent. The reaction mixture also displayed the formation of *n*-propanol, *n*-butanol, and THF.

The formation of those undesired by-products could result from the further hydrogenation and dehydration of BDO, respectively. *n*-Propanol and *n*-butanol possibly will be formed from the hydrogenation of propionic acid and butyric acid, respectively. Due to by-products formation, producing high yield of BDO could be low. The presence of Sn drastically changed the product distribution leading to the formation of BDO. However, 1% Sn was not enough to prevent C-C bond cleavage of Ru catalyst. Therefore, we prepared different ratios for Ru/Sn catalysts to achieve higher selectivity for BDO.

4.3.2.1. Effect of Ru to Sn Atomic Ratio on the Formation of BDO

The influence of different wt. % of Sn on the catalytic performance over the 5% Ru/CNT was investigated, and the results are presented in **Figure 4.11**. At 98 % conversion of SA, 200 °C, 70 bar, and 1 h, 5% Ru/CNT with 0% Sn displayed only 4.3 % selectivity to BDO. The formation of undesired products took place which are resulted of the C-C bond cleavage.

The maximum selectivity to BDO depended on the loading of Sn present on the catalyst. The yield of BDO augmented after introducing 1 % Sn and as increasing the loading of Sn in 5% Ru/CNT from 1 %, 1.5 %, and 2 % Sn the yield increased further. However, the selectivity decreased again using 2.5 % and 5% Sn based Ru catalyst. BDO selectivity displayed a volcano trend, where the optimal Sn loading was 2 wt. % and the formation of undesired products decreased. The selectivity to BDO increased up to 83 %.

The C (1s)/Ru(3d) core-level spectra showed that the BE increased in the following order: **2% Sn**-5% Ru/CNT < **5% Sn**-5% Ru/CNT < **1% Sn**-5% Ru/CNT. It seems that the BE value correlated with selectivity trend in the reaction. The BDO selectivity increased as the BE value decreased which was observed in **2% Sn**-5% Ru/CNT.

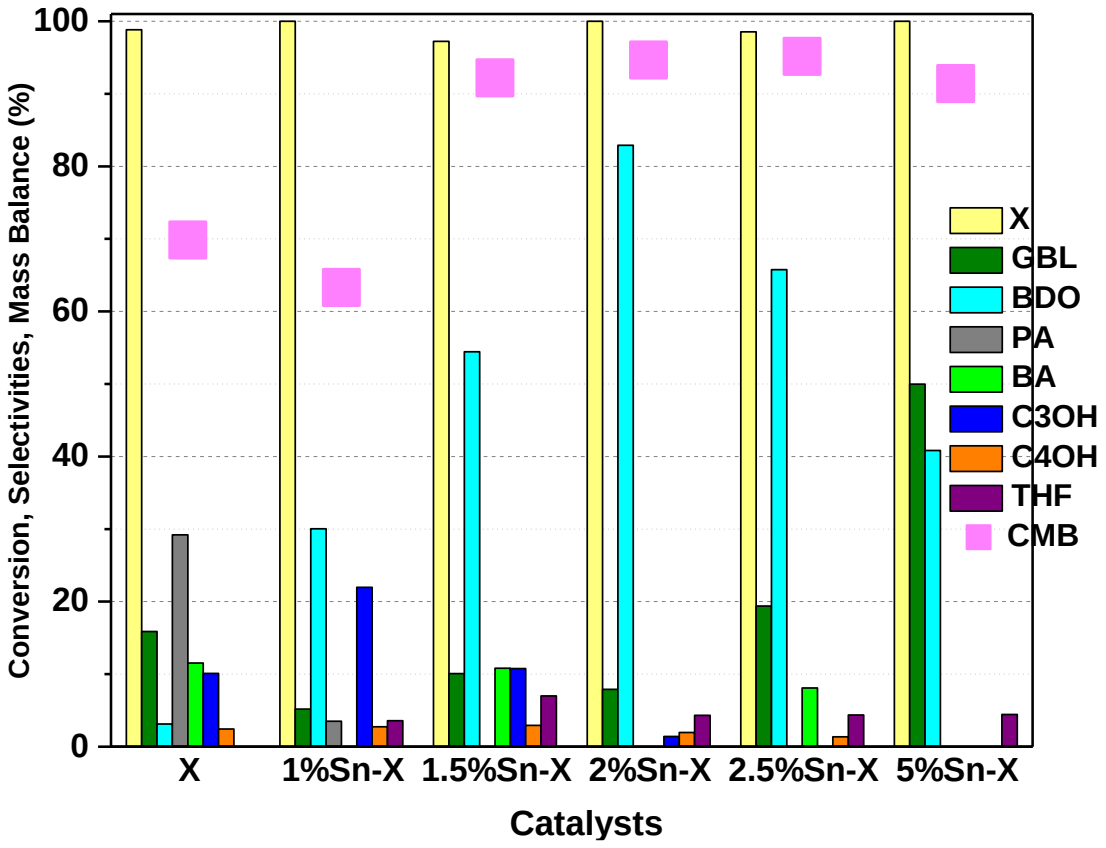

Figure 4.11. Comparison of the selectivities in succinic acid hydrogenation supported of CNT, 5% Ru/CNT Vs X% Sn-5% Ru/CNT at 200 °C, 70 bar hydrogen pressure using 50 mg catalyst, 100 mg succinic acid in 25 mL H_2O at 23h reaction time. Note, 5%Ru/CNT result at 1 h reaction time whereas the rest at 23 h reaction time. X: referred to 5%Ru/CNT. Legends: Conversion (yellow), selectivity to propionic acid (Grey), GBL (green), 1,4-butanediol-(Cyan), butyric acid (light green), propanol (blue), butanol (orange), THF (purpul), and carbon mass balance (pink).

Using **5% Sn**-5% Ru/**CNT**, the yield of BDO decreased but for GBL increased (**Figure 4.11**). We believed that this was due to the excess of Sn content, which blocks the active sites and suppresses the catalytic activity, affecting the further reactions. Same observation reported in the literature using Ru-Sn catalyst but on different reactions.[289]

TPR results showed that the hydrogen consumption of **5% Sn**-5% Ru/CNT appeared at the higher temperature compared to other bimetallic catalysts, which might be due to the strong interaction between Sn and Ru which complicates the activity of the catalyst.

NH_3-TPD results in **Figure 8.19 (Appendix)** showed that 5% Ru/CNT has two different strengths of acidic sites. One site was observed at a low-temperature region around (196 °C) and another was at 221 °C. It was observed that after introducing Sn to the 5% Ru/CNT the acidic sites at high temperature disappear. The acidic sites at 221 °C might be the responsible for the C-C activity in 5% Ru/CNT which affected the formation of BDO, since C-C cleavage products were observed in the reaction mixture using 5% Ru/CNT. However, after introducing Sn to the catalyst, those by-products formations start to decrease and the formation of BDO increased.

Another explanation would be that after the addition of Sn, the acidic sites which appeared at low (196 °C) and high temperature (220 °C) are merged and migrated to 206 °C. This result might have indicated the formation of Ru-Sn alloy which resulted in new acid sites. These new acid sites are more selective for BDO.

2% Sn-5% Ru/CNT showed high basicity compared to other bimetallic catalysts. Also, this catalyst showed high selectivity to BDO. Therefore, it seems that these basic sites served as critical active sites for the selective formation of BDO from hydrogenation of SA

The actual role of Sn in the Ru based catalysts unclear yet in this study however **Figure 4.12** depicts how the excess of Sn makes the catalyst (Ru-Sn/CNT) less active (Hypothesize). In the beginning, Ru particles were solely on CNTs surface (5% Ru/CNT), and they showed better activity for the hydrogenation of SA to GBL, propionic acid, and another by-product due to C-C bond cleavage (**Figure 4.12, A**).

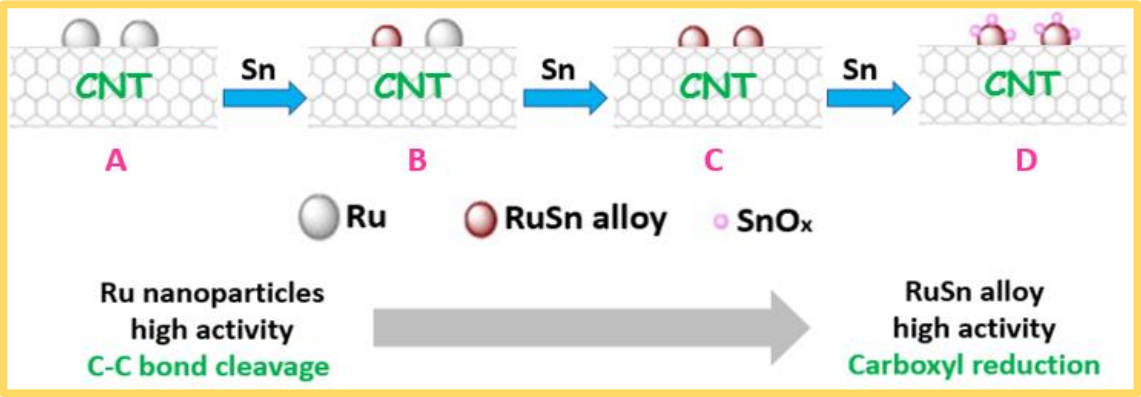

Figure 4.12. Effect of the Sn content on the activity of the catalyst and its promoting reactions. Adopted from Zhang *et al.*[282]

When 1% Sn was added to the catalyst (5% Ru/CNT), Ru-Sn alloys start to form (**Figure 4.12, B**) but there is free Ru or Sn was not enough to alloy with Ru. Therefore, C-C bond cleavage happened to a lower extent beside the improvement to BDO selectivity. In (**Figure 4.11**), 1.5 % Sn-based catalyst showed further improvement in BDO selectivity (56.8%) compared to 1% Sn (45.6 %).

In **Figure 4.12,** the selectivity to BDO increased to 83 % using 2% Sn-based Ru catalyst. This due to the prevention of the C-C bond cleavage activity which implies that all Ru particles where alloyed with Sn and might be no Ru particles remain as showed in (**Figure 4.12, C**). However, increasing loading of the Sn to 2.5 and 5 %, could partly block and poison the Ru-Sn alloy active sites and diminish the catalytic activity as presented in **Figure 4.12, D**. One of the accepted explanations for the action of Sn in Ru/CNT catalyst is the formation of Ru-Sn alloys, which have better activity and selectivity in the hydrogenation of succinic acid to BDO *via* GBL.

The previous reports,[292,304] suggested that Ru and Sn form alloys, however, based on the techniques that we used to characterize the catalysts in the current study, we have not confirmed it yet. The high dispersion of Ru and Sn on the support are preventing the display of their signals in XRD analysis.

However, the TPR reduction peak shift to higher temperature, different binding energies values, and reducing CO-uptakes after introducing Sn to the monometallic Ru catalyst suggested the formation of the alloys as discussed in the characterization section. Based of theses evidences, we might conclude here that there are bimetallic nanoparticles probably alloyed.

4.3.2.2. Effect of Supports on 2% Sn-5% Ru Catalyst to Hydrogenation of Succinic Acid

At 8-hours reaction time, the conversion was high using **2% Sn**-5% Ru/CNT 98.6 % compared to 63.9 % using **2% Sn**-5% Ru/**AC. 2% Sn**-5% Ru/CNT showed bigger particle size than on **2% Sn**-5% Ru/AC. However, the earlier catalyst displayed better activity. **Figures 4.3** and **4.4** displayed that the Ru-Sn particles are well dispersed, small, and un-agglomerated on both supports. The average particle size of about 2±0.6 nm and 1.3±0.3 nm for **2% Sn**-5% Ru/CNT and **2% Sn**-5% Ru/AC respectively. Therefore, the support has a substantial role in the catalytic performance of the catalyst in the hydrogenation of SA is the support.

N_2-physisorption results (**Table 4.1**) showed that **2% Sn**-5% Ru/CNT has a high pore size (30.21 nm) whereas **2% Sn**-5% Ru/**AC** showed low pore size (5.05 nm). According to those results, the activity of the catalysts might depend on the porosity. **2% Sn**-5% Ru/CNT showed high activity which might be due to its high porosity compared to Ru-Sn catalyst supported on AC. Also, another reason regarding this increment in activity is the electronic promotion of the carbon nanotubes as we addressed in Chapter 3. On the other hand, introducing **2% Sn** into 5% Ru/AC was not sufficient to improve the selectivity of the catalysts compared to **2% Sn**-5% Ru/CNT, owing to C-C bond cleavage.

The binding energy of $Ru3p_3$ in **2% Sn**-5% Ru/CNT was 462.50 eV which is higher than on Ru/CNT, 462.10 eV, (Table 4.2, entry 4). Mitsui *et al*.[305] addressed that when the binding energy of Ru is higher, the electron deficient ruthenium species (Ru^{n+}) on the catalyst would be higher. Chen *et al*.[211] reported that more electron deficient Ru species (Ru^{n+}) would lead to a low degree of C–C bond cleavage. According to these two previous studies, **2% Sn**-5% Ru/CNT showed lower C-C bond cleavage activity. On the other hand, the binding energy of Ru in **2% Sn**-5%Ru/**AC** was lower (462.70 eV) compared to the 5%Ru/AC (463.60 eV) sample. This fact was correlated with results obtained. **2% Sn**-5%Ru/CNT displayed high selectivity for BDO due to minimizing the production of undesired products by reducing C-C bond cleavage (**Figure 4.13**).

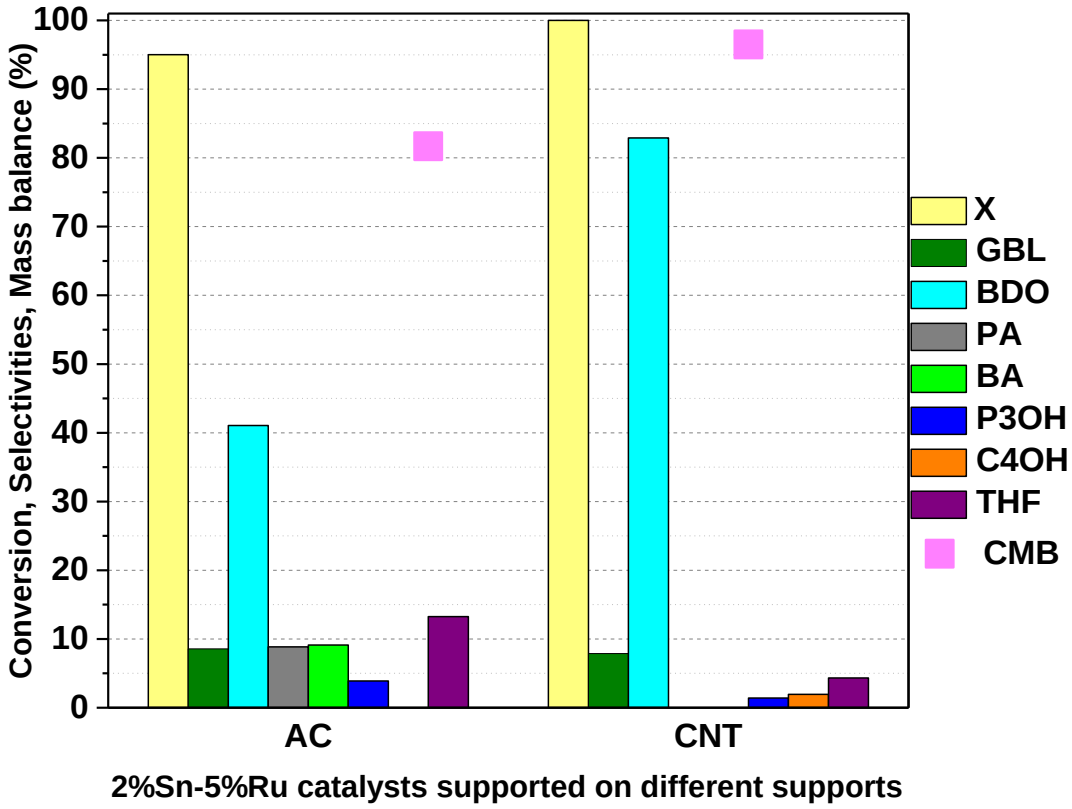

*Figure 4.13. Comparison of the selectivities of all products, **2% Sn**-5% Ru/**AC** vs **2% Sn**-5% Ru/CNT at 200 °C, 70 bar hydrogen pressure, and 23h reaction time using 50 mg catalyst, 100 mg succinic acid in 25 mL H_2O.*

The selectivity for BDO increased from 40 % using **2% Sn**-5%Ru/**AC** to 83 % using **2% Sn**-5% Ru supported on CNT. The low formation of BDO using **2% Sn**-5% Ru/AC was because the latter catalyst could not stop the formation of undesired products. The formation of the Ru-Sn alloy on AC was not successful as reported in the literature.[291] Lee *at el*.[291] suggested that the strong interactions between metal–support in supported Ru-Sn catalysts might hinder the formation of Ru-Sn alloy. This fact agrees with the TPR results shown in **Figure 4.8**. The reduction peak of **2% Sn**-5% Ru/**AC** appeared at a higher temperature compared to all prepared bimetallic Ru catalysts due to a strong interaction between the Ru-Sn and activated carbon. Methanation related peak also observed in this catalyst along with **1% Sn**-5% Ru/CNT and monometallic Ru catalysts supported on AC and CNT. However, this peak is missing on **2% Sn**-5% Ru/CNT and **2% Sn**-5% Ru/CNT and those catalysts showed better selectivity to BDO. It seems to be that methanation peak as well is linked to the selectivity somehow. The formation of active bimetallic Ru-Sn particles may be controlled by support. In this regard, CNT proved to be more efficient than AC for the hydrogenation of succinic acid to BDO.

On the other hand, the previous results on hydrogenation of SA to BDO raised a question if increased selectivity would also be observed with other carboxylic acids, such as levulinic acid to get 1,4-pentanediol (PDO). PDO, is another useful compound that could be used as a monomer for the manufacture of polyesters or as biofuel.[65,135]

Using the best catalyst (**2% Sn**-5% Ru/CNT), the reaction was performed under the same reaction conditions. LA was completely hydrogenated to the corresponding lactone (γ-valerolactone), and as the time increased, the formation of diols was observed. The results showed selectivity 56.1 % and 40.1 % to PDO and GVL respectively.

Figure 4.14 shows the yield of different diols using **2% Sn**-5% Ru/CNT at 100 % acids conversion. After 23h, 55.3 and 83 % yields were obtained for PDO and BDO from hydrogenation of levulinic acid and succinic acid respectively.

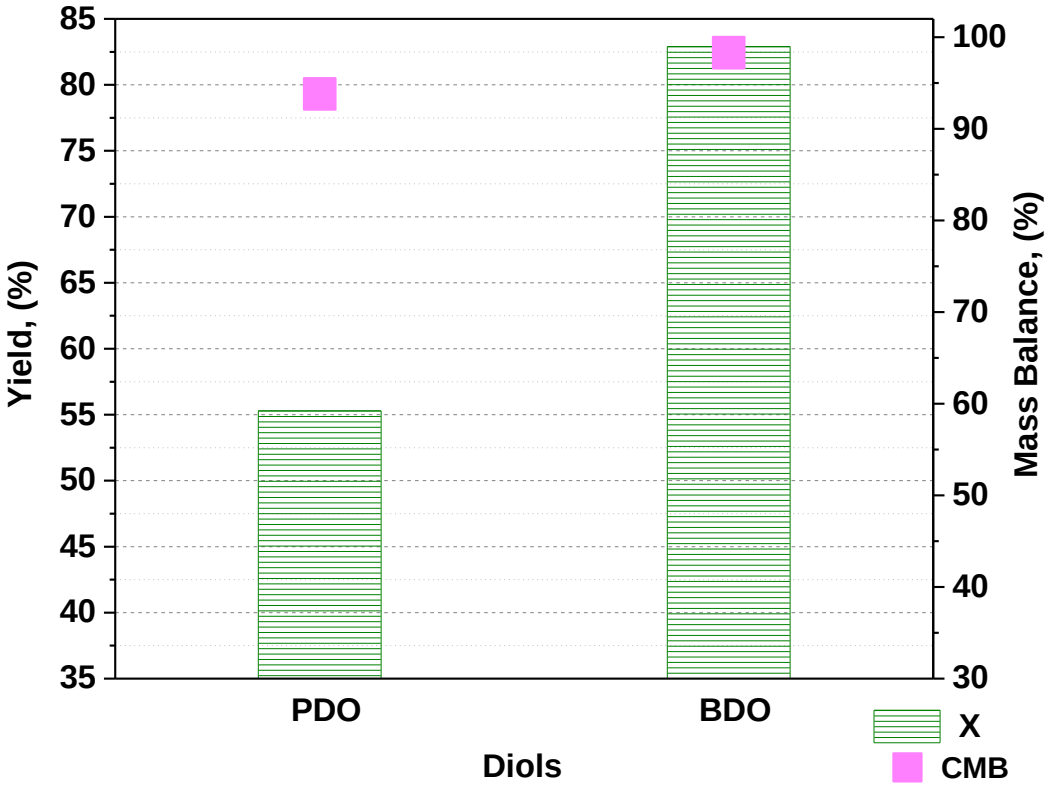

*Figure 4.14 Hydrogenation of different acids (succinic acid and levulinic acid) to BDO and PDO respectively, **2% Sn**-5% Ru/CNT at 200 °C, 70 bar hydrogen pressure, and 23h reaction time using 50 mg catalyst, 100 mg succinic acid in 25 mL H_2O.*

Hydrogenation of LA to PDO needs further optimization to obtain PDO in high yield. The synthesis of PDO from LA is difficult; as a result, there is plenty of works in the hydrogenation of LA to γ-valerolactone which can be used as a fuel additive,[65] whereas there is little reports on the hydrogenation of LA to PDO.[130-132] Nevertheless, this reaction needs further investigation to improve the yield of PDO.

4.4. Conclusions

It has been demonstrated that the biomass-derived acids could be efficiently reduced to alcohols in high yield using a Ru-based catalyst. The high activity of **2% Sn**-5% Ru/CNT in the hydrogenation of SA to BDO compared to **2% Sn**-5% Ru/**AC** might be due to higher porosity and the electronic properties of CNT as mentioned in XPS results section. N_2-physisorption results showed that **2% Sn**-5% Ru/CNT has a higher pore size whereas the **2% Sn**-5% Ru/**AC** showed low porosity. The porosity of the catalyst has a positive impact on the activity of **2% Sn**-5% Ru/CNT in hydrogenation of succinic acid.

The formation of a Ru-Sn alloy might be the result of a unique interaction between CNT, Sn, and Ru and this is the main reason for the better selectivity to BDO. Ru-Sn alloy is suggested based on XPS and TPR results of the all Ru-Sn catalysts. The alloy may be not formed successfully in Ru-Sn catalyst supported on AC which might need to find a precise ratio between Ru and Sn. Result of that the selectivity for BDO was lower along with the formation of undesired by-products compared to **2% Sn**-5% Ru/CNT.

The results showed that the selective catalyst for the production of BDO in hydrogenation succinic acid is Sn(2%)-Ru(5%)/CNT. At lower Sn loading for example, 1 and 1.5 %, less BDO formation of BDO is detected since the C-C bond cleavage products reduce the formation of BDO. Conversely, when the Sn loading increased, for example, to 2.5 and 5%, the catalytic activity of the catalyst slows down. However, if the reaction run longer, we would eventually get more BDO from further GBL hydrogenation.

Amongst all bimetallic catalysts used in this chapter, **2% Sn**-5% Ru/CNT proved to be an effective catalyst to produce diols from hydrogenation of succinic acid and levulinic acid with the yield of 83 % and 55 % for BDO and PDO, respectively.

CHAPTER 5

Selective Hydrogenation of cis, cis-Muconic Acid using Selected Catalysts

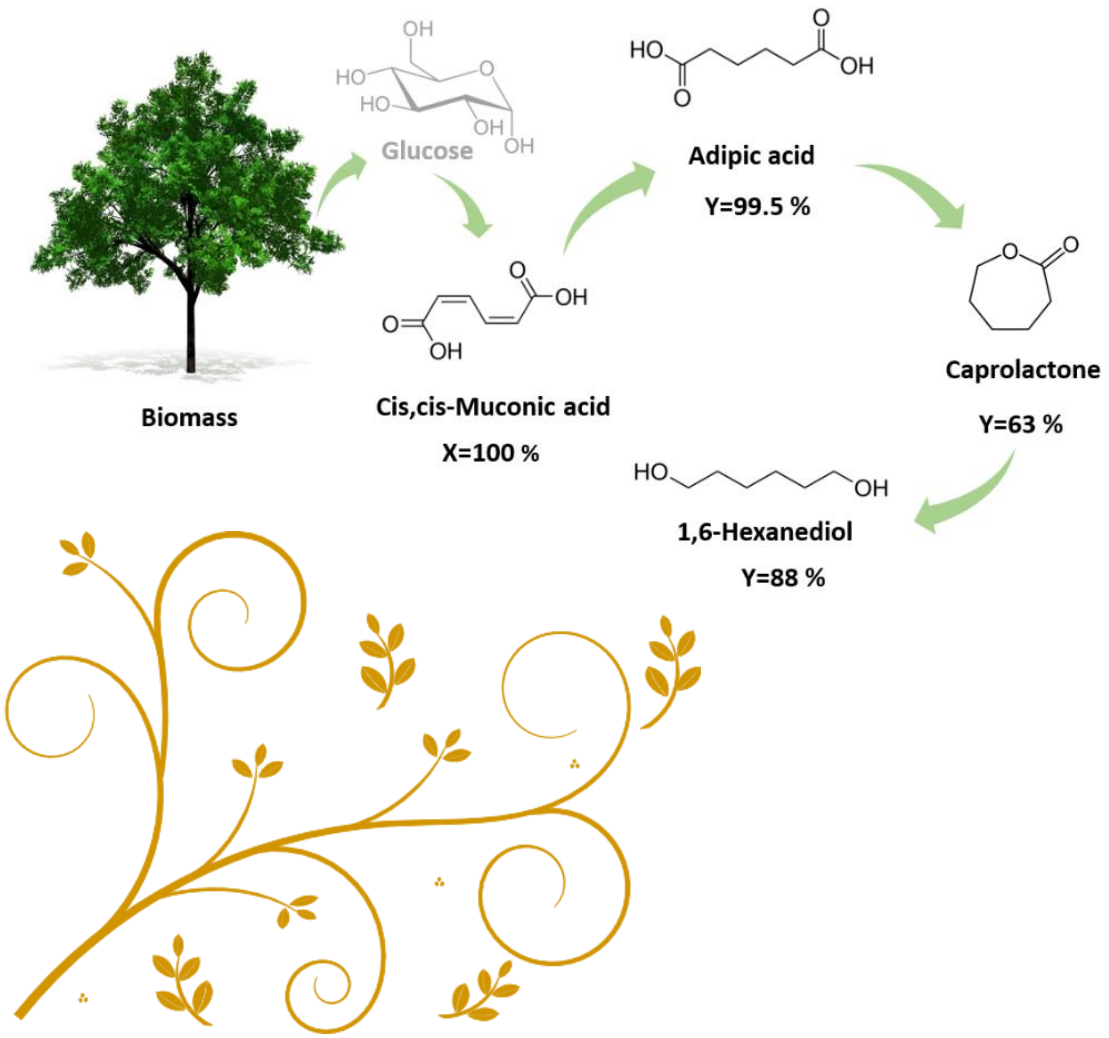

Chapter 5. Selective Hydrogenation of cis, cis-Muconic Acid using Selected Catalysts

5.1. Introduction

In this chapter, the liquid-phase hydrogenation of cis, cis-muconic acid (ccMA) has been studied using selective catalysis to synthesise three valuable products, adipic acid (AA), ε-caprolactone (ECL), and 1,6-hexanediol (HDO). **Scheme 5.1** shows the reaction pathway for the hydrogenation of ccMA to different valuable products through hexenedioic acid (HAD).[143]

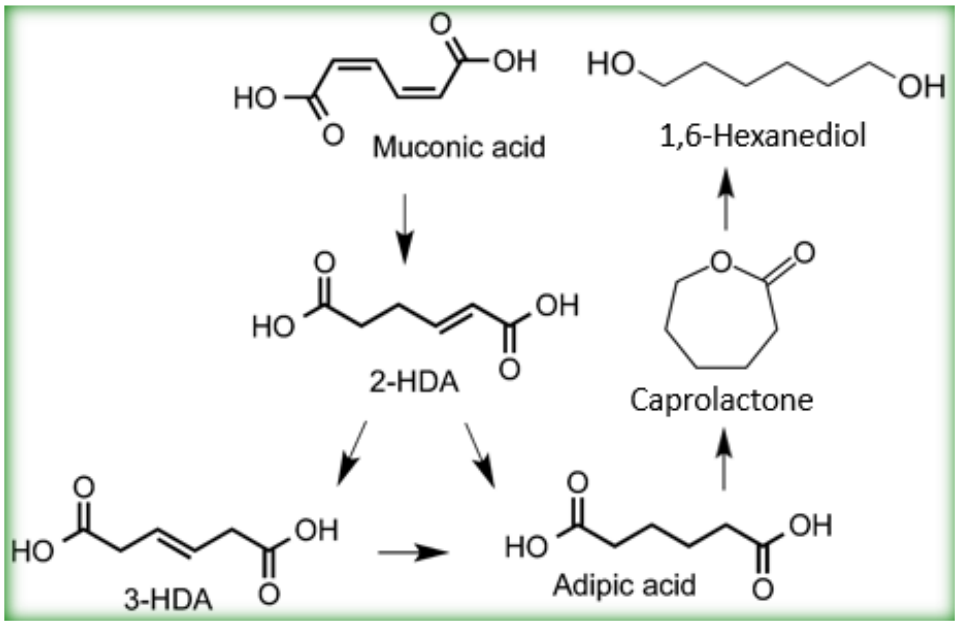

Scheme 0.1. Suggested scheme for the hydrogenation of cis,cis-muconic acid. Adopted from Vardon et al. [143] and Matthiesen et al.[135] Note: HDA, hexenedioic acid

AA is traditionally produced *via* petrochemical routes, unsustainable reagents such as benzene and nitric acid.[140] Alternatively, AA can be synthesised from glucose through ccMA, or glucaric acid as described in Chapter 1. The formation of AA from ccMA will be discussed further in this chapter.

The hydrogenation of cis, cis-muconic acid can be catalysed by transition metals in both aqueous and organic solvents. At room temperature and 35 bar of H_2, 10% Pt/C delivered 97 % yield of AA after 150 minutes in aqueous solution.[142] However, in organic solution, the reaction was considerably faster. 1% Rh supported on carbon could transform 100 % of ccMA in 35 minutes with a 99.8 % yield of adipic acid under mild conditions; 24 °C with 24 bar H_2 pressure and using ethanol as a solvent.[143] However, 5% Pd/C was by far the most active catalyst since less than 5 minutes was required for 100 % conversion and 97 % selectivity towards AA. The reaction was conducted under 4 bar H_2 pressure at room temperature.[134]

Non-noble metals have also been successfully used in aqueous solution to synthesise AA. Full conversion of ccMA with 99.8 % yield of AA has been achieved using a 14.2% Ni/Al_2O_3 catalyst under 10 bar H_2 pressure, 60 °C and 5 h reaction time.[141]

Another valuable product from ccMA is HDO which is produced mostly *via* petrochemical routes through multiple reactions, including cyclohexane oxidation or the hydrogenation of AA.[151,306,307] However, a recent study shows the manufacture of HDO *via* HMF is possible.[145] The third important compound from ccMA is ECL which has a high potential in the polymer industry. Nowadays, ECL is manufactured at large scale through cyclohexanone oxidation reaction in presence of hydrogen peroxide.[308] The catalytic hydrogenation of ccMA to ECL, AA, and HDO is an alternative to the traditional process.

The aim of this chapter is to determine if CNTs based catalyst can be a suitable for the hydrogenation of bio-based ccMA into three valuable products. Since Pd on activated carbon was the best catalyst in hydrogenation of ccMA to AA[134] and throughout the literature, Pd catalysts proved to be a highly active and selective towards hydrogenation of ethylenic bonds,[309,92] this catalyst supported on CNT was selected to be a candidate to hydrogenation of ccMA to AA. So, we could assess whether CNTs can also promote the activity of this hydrogenation process.

Finally, different percentages of Ru-Sn catalysts were synthesised by incipient wetness impregnation studied for the hydrogenation of succinic acid and levulinic acid to the corresponding diols (Chapter 4). Therefore, this longer carbon chain carboxylic acid (ccMA) will be used as a substrate again to produce HDO by Ru-Sn catalyst to see if this catalyst would be a universal to hydrogenate a wide range of carboxylic acids.

5.2. Experimental

All catalysts (monometallic and bimetallic) used in this chapter were prepared as described in Chapter (2) and the catalytic experiments were carried out in a pressure autoclave reactor, however; one reaction using 2% Sn-5% Ru/CNT was performed in a Parr reactor at reaction conditions (200 °C and 70 bar) and the results appear in the effect of pressure section.

5.3. Results and Discussion

The activity and selectivity have been studied using monometallic Pd, Pt, Ru with different metal loading and bimetallic Ru-Sn catalyst. The characterisation of 1% metal catalyst and activity results of all catalysts are discussed below.

5.3.1. Catalyst Characterizations

5.3.1.1. X-Ray Diffraction Analysis (XRD)

Figure 5.1, shows the XRD patterns of different catalysts supported on CNT and AC. No discernible Ru reflections are detected for 1% Ru/CNT and 1% Ru/AC, indicating the high dispersion of Ru or that the Ru nanoparticles are too small to be characterised by XRD.

On the other hand, Pd catalysts showed diffractions of the respective metallic phases. Peaks at 40.3° and 46.5° correspond to (111), and (200) planes of the face-centered cubic phases of Pd (JCPDS 001-1201). In all CNT-based diffractograms, peaks at 25.7°, 42.5°, and 78.5° were indexed as (002), (100) and (110) reflections of graphite structure, respectively[223,224] (JCPDS 001-0640, 003-0401).

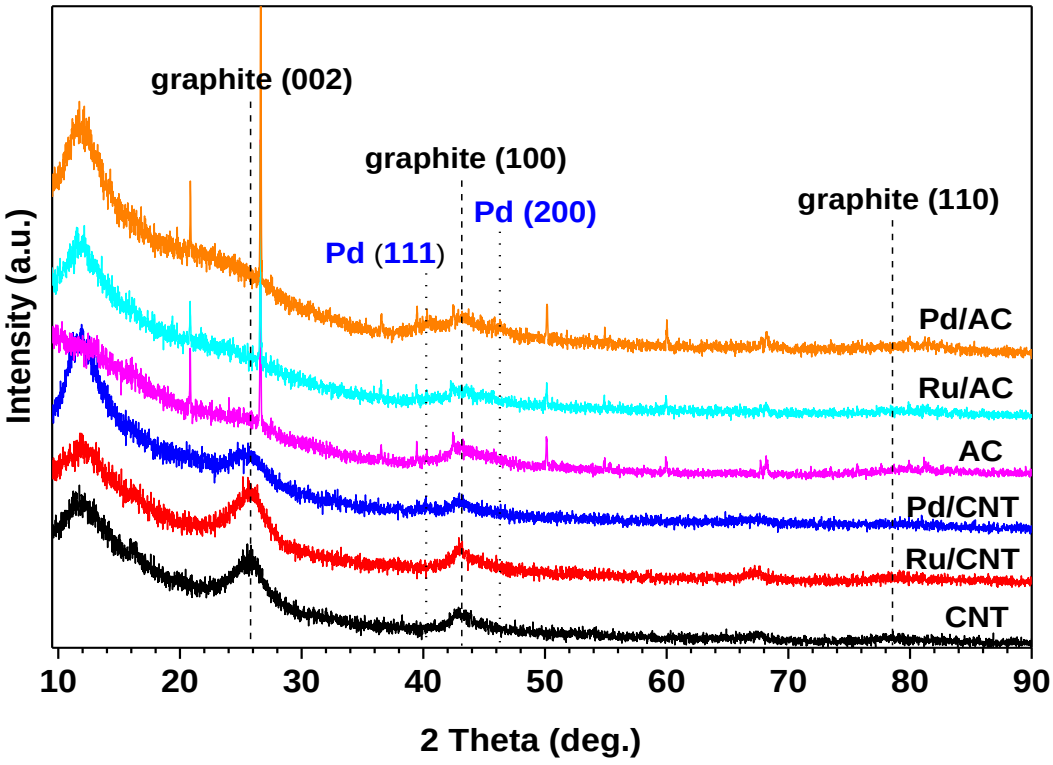

Figure 0.1. XRD patterns of activated carbon, carbon nanotubes, reduced catalysts: 1% Ru/CNT, 1% Pd/CNT, 1% Pd/AC, and 1% Pd/AC.

The pattern of 1% Pd/CNT showed very weak peaks compared to a pattern of Pd supported on AC, which might be an indication of a well-dispersed Pd particles on CNTs. Moreover, XRD peaks of Pd in the Pd/CNT are more flattened than those in Pd/C, which indicates that the Pd average particle size on CNT is smaller than on AC.[310] This finding is in agreement with the results of XRD patterns obtained from Liao *et al*.[310] when Pd supported on AC and CNT were compared.

5.3.1.2. Metal Dispersion by CO-Chemisorption

To estimate the dispersion of metal species, CO-chemisorption experiments were carried out. **Table 5.1** shows the CO-chemisorption measurements of different catalysts.

Table 0-1. List of reduced catalysts, results of CO chemisorption..

Catalyst	CO uptake, µmol/g	Metal dispersion, %
1% Ru/AC	14	14.5
1% Ru/CNT	13	13.5
1% Pd/AC	4.6	2.4
1% Pd/CNT	5.4	2.9
2% Sn-5% Ru/CNT	34.9	7.0

1% Ru/AC and 1% Ru/CNT show almost the same dispersion. The dispersion of the 1% Pd catalysts is quite similar in both supports but slightly better on CNT. However, it is still lower than Ru uptake which might be due to an agglomeration of Pd particles in Pd based catalysts. Overall, Ru particles have better dispersion on both supports than Pd. CO does not adsorb irreversibly on Sn thus, in the Ru-Sn catalyst, it is considered that CO chemisorbed only on the Ru surface.[295] Ru-Sn showed better dispersion than Pd based catalyst but not as good as Ru (alone) catalyst.

5.3.1.3. Reducibility of the 1% of Pd and Ru Based Catalysts by H_2-TPR

The reducibility of the as-synthesised samples using temperature programmed reduction with hydrogen (H_2 TPR) is presented in **Figure 5.2**. Two temperature ranges are visible in the TPR profiles, lower and higher than 250 °C. <250 °C shows the reduction of the metal (Ru and Pd) precursors to a metallic state.

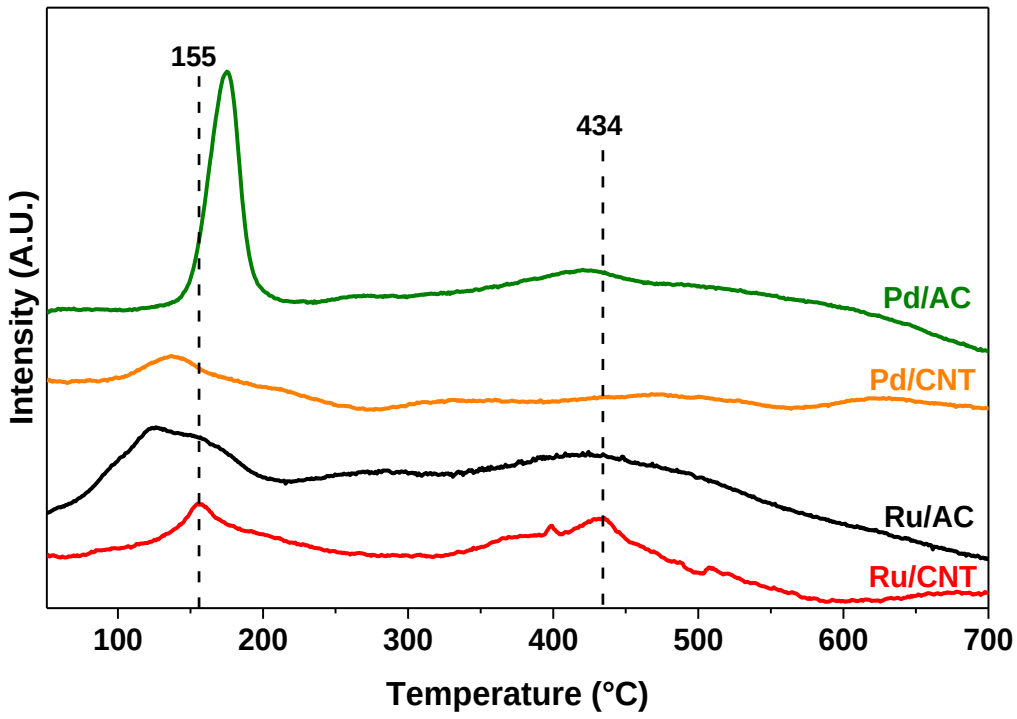

Figure 0.2. H_2-TPR profiles for 1 wt. % of different noble metals catalyst (Unreduced) supported on CNT and AC

The reduction peak of 1% Pd/AC is sharper compared to all other catalysts which demonstrates the formation of a narrower Pd particle size, however, this finding is not in line with the CO-chemisorption since the dispersion was 2.45 % which is low compared to all tested 1 % metal based catalysts in this chapter.

Moreover, this peak is shifted to a higher temperature which indicates a strong interaction between Pd precursor and support (AC) this result agrees with the findings of He *et al, report.*[311] H_2 TPR results also show different redox properties between two metals supported on CNT which might be attributed to the electronic promotional effect. Pd supported on CNT seem to be easier to reduce (reduction peak appears at a lower temperature) compared with Pd/AC whereas the opposite trend observed regarding Ru based catalysts. Small Ru particles could be reduced at a lower temperature than larger particles due to a high interaction between those large particles and the support,[312] and this fact is clearly shown in the H_2 TPR results. The Ru/AC reduction peak appears at a lower temperature compared to Ru supported on CNT which might be an indication of the formation of small particles. A broad peak around 400-500 °C corresponds to the reduction of carbon species or carbon-related functional groups,[233] or due to the carbon methanation which was shown to occur in the presence of supported metals.[85,230,232] This can be seen clearly in all catalysts and this could be followed by subsequent catalyst deactivation.[233]

5.4. Activity Measurement

5.4.1. Hydrogenation of cis, cis-Muconic acid to Adipic Acid

AA was successfully produced from ccMA using 4-different catalysts at 80 °C and 10 bar of H_2 pressure, as seen in **Figure 5.3**. Ru/CNT catalyst showed less activity than both Pd catalysts supported on AC and CNT in the hydrogenation of ccMA to AA, and the yield followed the sequence Pd/AC > Pd/CNT > Ru/AC > Ru/CNT. Comparing activity, 1% Ru/AC, was better than 1% Ru/CNT and on the other hand 1% Pd/AC was better than 1% Pd/CNT.

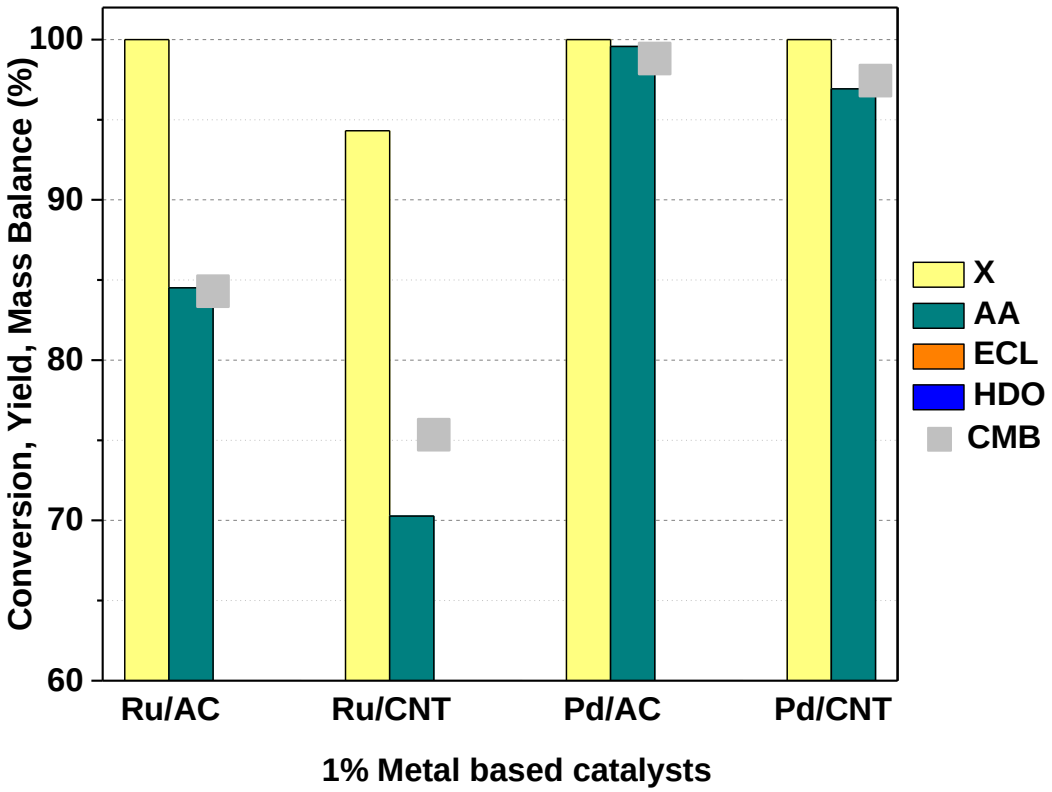

Figure 0.3. Hydrogenation of muconic acid (MA) to adipic acid for 15 min. Reaction conditions: 1% of metal in all catalysts (0.017g), MA (0.068g) solvent (30 mL), Temperature (80 ˚C), H_2 pressure (10 bar), and reaction time (15 min). Legends: Conversion (yellow)-(X), yield to adipic acid (AA)-(green), epsilon-caprolactone (ECL)-(orange), 1,6-hexanediol (HDO)-(blue), carbon mass balance (CMB)-(gray).

The electronic effect of the CNT as a support enhanced some reported reactions such as hydrogenation of 2,5-hydroxymethylfurfural to 2,5-dimethylfuran[236] and hydrogenation of acetic acid to ethanol.[282] However, this effect might be the reason for low activity in the hydrogenation of ccMA (contained C=C double bond) to AA. The electron density at the active metal sites increased by the electrons transfer from CNT to them in which it decreases the chance of hydrogenation of the C=C bond via dropping the interaction between the metal and the π bonds of C-C.[285] It seems that the activity enhancement using CNT is not universal but reaction dependent.

Do to the higher activity of metals supported on AC, they were compared again at a shorter reaction time, 5 min. **Figure 5.4**, shows that 1% Pd/AC was the best catalyst for hydrogenation ccMA to AA since full conversion was achieved in less than 5 min with 98.1 % yield of AA. However, 1% Ru/AC was less active and show 81 % conversion of ccMA with 29 % yield of AA.

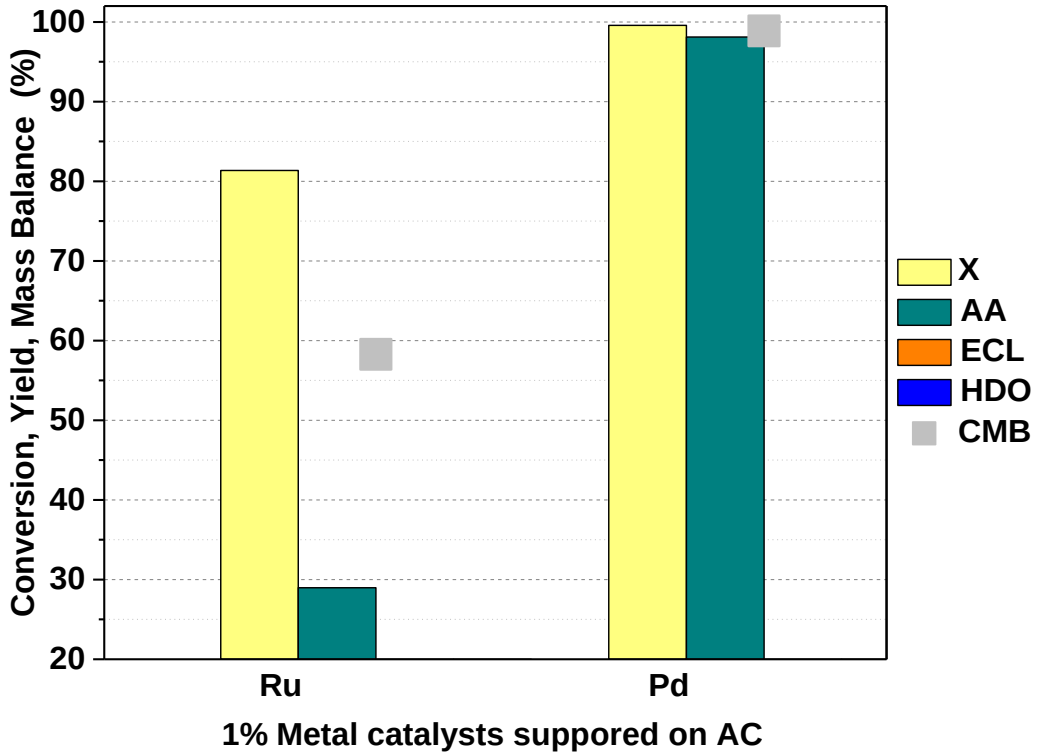

Figure 0.4.Hydrogenation of muconic acid (MA) to adipic acid for 5 min. Reaction conditions: 1% metal catalysts (0.017g), MA (0.068g) solvent (30 mL), T (80˚C), H_2 pressure (10bar), and reaction time (5min). Legends: Conversion (yellow)-(X), yield to adipic acid (AA)-(green), epsilon-caprolactone (ECL)-(orange), 1,6-hexanediol (HDO)-(blue), carbon mass balance (CMB)-(gray).

The low carbon mass balance in Ru based catalysts was not because the C-C cleavage since the formation of AA was improved as increasing the reaction time and so forth the carbon mass balance (**Figure 8.21. Appendix**).

This is might due to the formation of intermediate (HAD) as showed in **Scheme 5.1** previously. The yield of AA increased to 84.5 % at 100 % conversion in 15 min. The yield increased further to 95.4 % after 1 h reaction time. Therefore, using 1% Ru/AC at 5-minute reaction time was insufficient to produce AA in high yield as compared to Pd catalysts.

The impressive activity of 1% Pd/AC motivated the study to perform another reaction but at a room temperature. **Figure 5.5**, shows the result of hydrogenation of ccMA using 1% Pd/AC at different temperatures. The reaction rate at 25 °C, was slow and complete conversion was achieved at 80 °C in 15 min compared to 5 h at 25 °C.

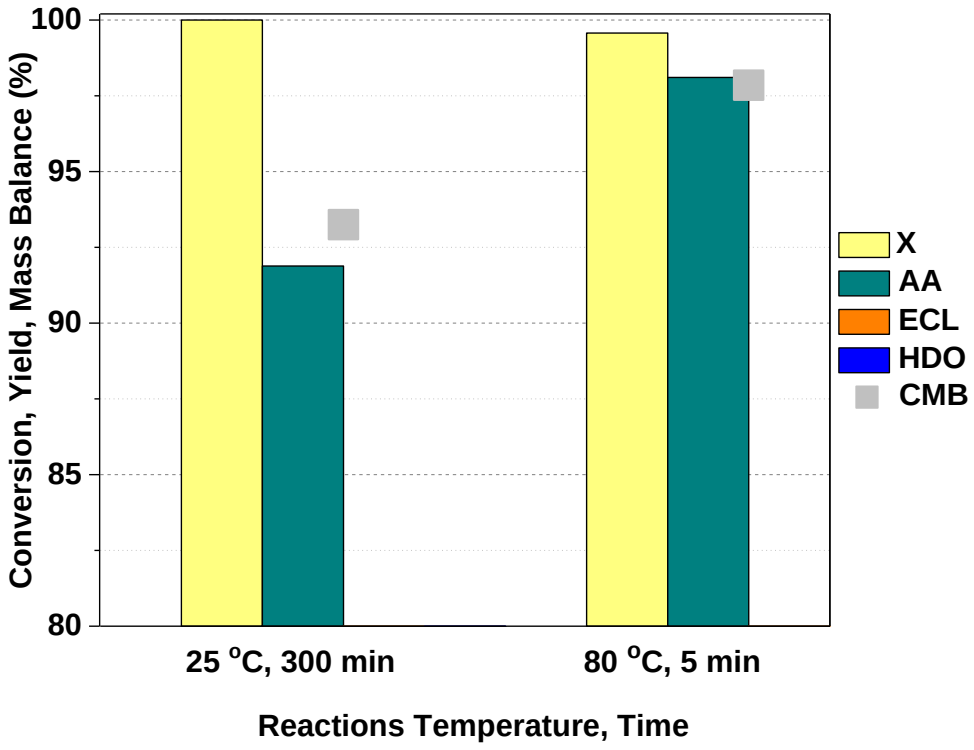

Figure 0.5. Hydrogenation of muconic acid (MA) to adipic acid at different time. Reaction conditions: 1% Pd/AC (0.017g), MA (0.068g) solvent (30 mL), H_2 pressure (10 bar). Legends: Conversion (X)-(yellow), yield to adipic acid (AA)-(green), epsilon-caprolactone (ECL)-(orange), 1,6-hexanediol (HDO)-(blue), carbon mass balance (CMB)-(gray).

Nevertheless, 1% Pd/AC proves to be the best catalyst amongst others to hydrogenate the double bonds (ccMA to AA). C=C hydrogenation is thermodynamically favoured compared to C=O by ca. 35 kJ/mol^{-1}.[12] Pd catalysts throughout the literature are also highly active and selective towards hydrogenation of ethylenic bonds.[309,92]

5.3.2. Hydrogenation of cis, cis-Muconic Acid to Caprolactone and 1,6-Hexanediol

5.3.2.1. Catalyst Screening

Initial screening for the hydrogenation of ccMA to ECL and HDO involved a series of catalysts; 5% Pd/CNT, 5% Pt/CNT and Ru-Sn/CNT. **Table 5.2**, shows the results for the screening of those catalysts in the hydrogenation of ccMA carried out at 200 °C and 10 bar hydrogen pressure for 1 h and 23 h. It should be noted here that, 5 % Ru/CNT was not tested due to its high C-C cracking which has been discussed in the literature.[81] Also, the same problem was observed during the hydrogenation of succinic acid in the current study (Chapter 1).

ccMA was successfully converted to AA using all catalysts apart from Ru-Sn/CNT. No other catalyst showed any formation of ECL after 1h reaction time (Table 17.5, entries 1, 3, 5). However, 5 % Pt/CNT catalyst produced some ECL after 23 h reaction time but the yield was just 9.4 % (Table 5.2, entry 3). 5 % Pd/CNT failed to produce any yield of ECL even after 23 h reaction time. This low reactivity might be due to the lack of Pd dispersion on CNT as shown in **Table 5.2**.

Ru-Sn catalyst displayed admirable selectivity to ECL (Table 5.2, entry 5) where close to 9 % yield was attained in just 1 hour reaction time, so this catalyst was chosen for further investigation.

Table 0-2. Selective hydrogenation of ccMA over different catalysts systems supported on CNT. Reaction conditions: T (200 °C); hydrogen pressure (10 bar); substrate (ccMA), 0.05g; catalyst, 0.025g; solvent (H_2O), 25 mL. AA (adipic acid), caprolactone (ECL), and 1,6-hexanediol (HDO).

Entry	Catalysts	Conv. %	Time (h)	Yield (%)			Carbon mass Balance (%)
				AA	ECL	HDO	
1	5%Pd/CNT	100	1	99.9	0	0	99.9
2	5%Pd/CNT	100	23	98.6	0	0	98.6
3	5%Pt/CNT	100	1	99.1	0	0	99.1
4	5%Pt/CNT	100	23	88.4	9.3	0	97.80
5	5%Ru-2%Sn/CNT	100	1	90.7	8.7	0	99.31

5.3.2.2. Ru-Sn/CNT Catalyst

The catalytic performance of Ru-Sn/CNT for ccMA hydrogenation was studied. The influence of temperature (150 °C, 200 °C, and 240 °C), pressure (2, 5, 10, and 70 bar), and reaction time were studied to tune the reaction to produce a high yield of either ECL or HDO.

5.3.2.2.1. Effect of Temperature

Figure 5.6, shows product (AA, ECL, and HDO) yields vs. reaction temperature at 10 bar H_2 pressure. It should be noted that all ccMA was converted to AA during the heating-up stage. However, transforming AA further is the critical step. As shown in the **Figure**

5.6, 150 °C was not sufficient to reduce AA significantly to ECL since only a 7.5 % yield of ECL was observed after 23 h reaction time.

Furthermore, a reaction at 240 °C delivered 53 % yield of ECL but the carbon mass balance was low perhaps due to chain scission (C-C cleavage), also observed in Chapter 3. The reaction carried out at 200 °C provided the highest yield of ECL with a good carbon mass balance. Ru-Sn catalyst is preeminent by higher yield, therefore, the optimum conversion of ccMA to ECL and HDO through adipic acid was studied at 200 °C for further investigation of yield optimization.

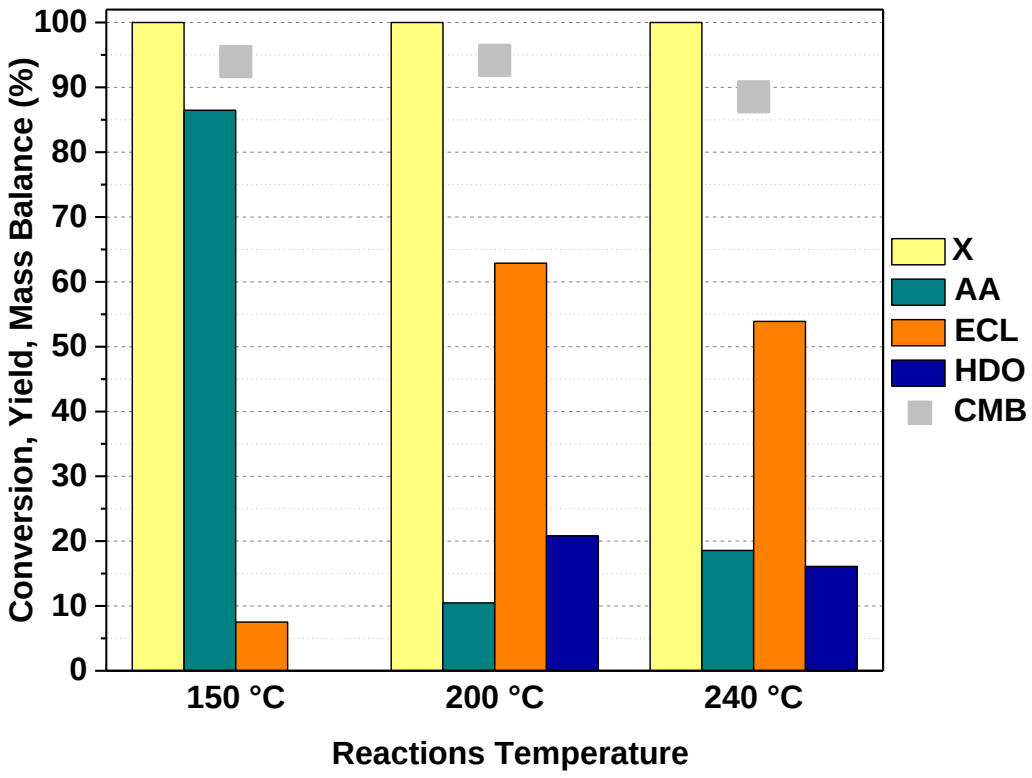

Figure 0.6. Effect of Temperature on hydrogenation of cis, cis-muconic acid (ccMA). Reaction conditions: catalyst 5% Ru-2% Sn/CNT (0.025 g), ccMA (0.05 g) solvent (25 mL), H_2 pressure (10 bar), reaction time (23h). Legends: Conversion (X)-(yellow), yield to adipic acid (AA)-(green), epsilon-caprolactone (ECL)-(orange), 1,6-hexanediol (HDO)-(blue), carbon mass balance (CMB)-(gray).

5.3.2.2.2. Effect of Time

The overall activity and product distribution of bimetallic Ru–Sn catalyst were compared with reaction time to determine the optimum time to achieve maximum ECL yield and the results are presented in **Figure 5.7**. ccMA was converted during the heating step as mentioned before with high selectivity to AA however, to obtain high yield of ECL, AA needs to be converted and sequential reduction to HDO should be suppressed, as well as C-C bond cleavage. Having selected water as a solvent, temperature (200 °C) and mild pressure (10 bar H_2), the reaction required a long time to completely convert all AA, since at end of the reaction (23 h) there is still 11 % of AA remaining. Furthermore, the formation of HDO had already started and the yield was 21 %.

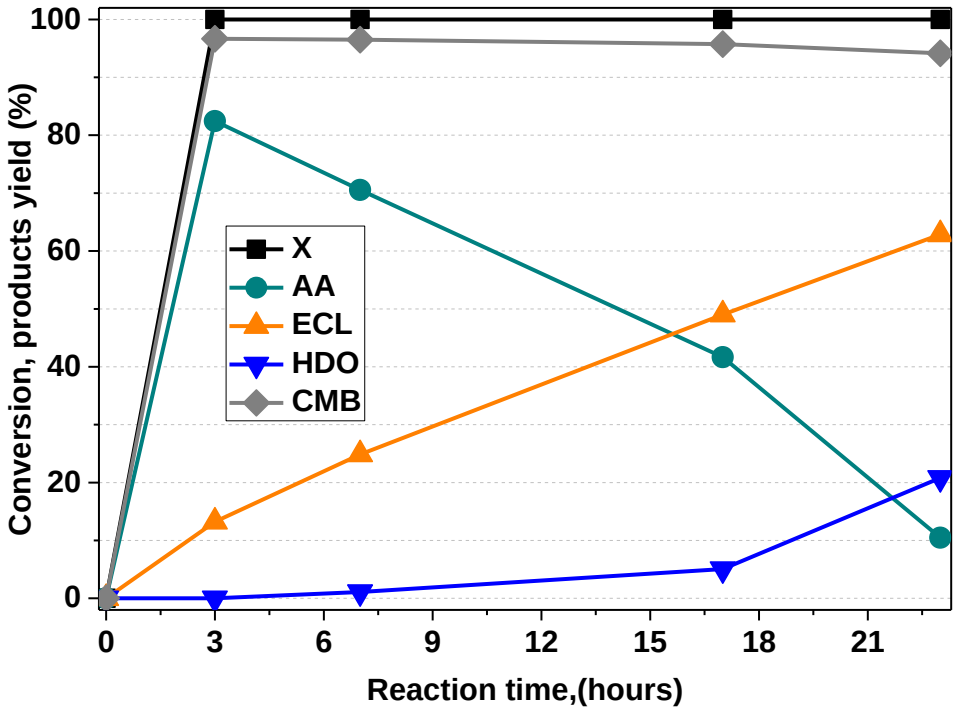

Figure 0.7. Time online reaction of ccMA hydrogenation with 2 % Sn-5 % Ru/CNT. Reaction conditions: catalyst (0.025 g), ccMA (0.05 g) solvent (25 mL), H_2 pressure (10 bar). Legends: Conversion (X)-(black), yield to adipic acid (AA)-(green), epsilon-caprolactone (ECL)-(orange), 1,6-hexanediol (HDO)-(blue), carbon mass balance (CMB)-(gray).

Therefore, based on these promising results with an excellent carbon mass balance value (94 %), we decided to perform other reactions with different H_2 pressure values to determine the effect of H_2 pressure on the final yield of HDO and ECL.

5.3.2.2.3. Effect of Pressure

Reactions were carried out over Ru-Sn/CNT at a constant temperature of 200 °C and different H_2 pressures (2, 5, 10, and 70 bar) to determine the effect of H_2 pressure on the product distribution (**Figure 5.8**).

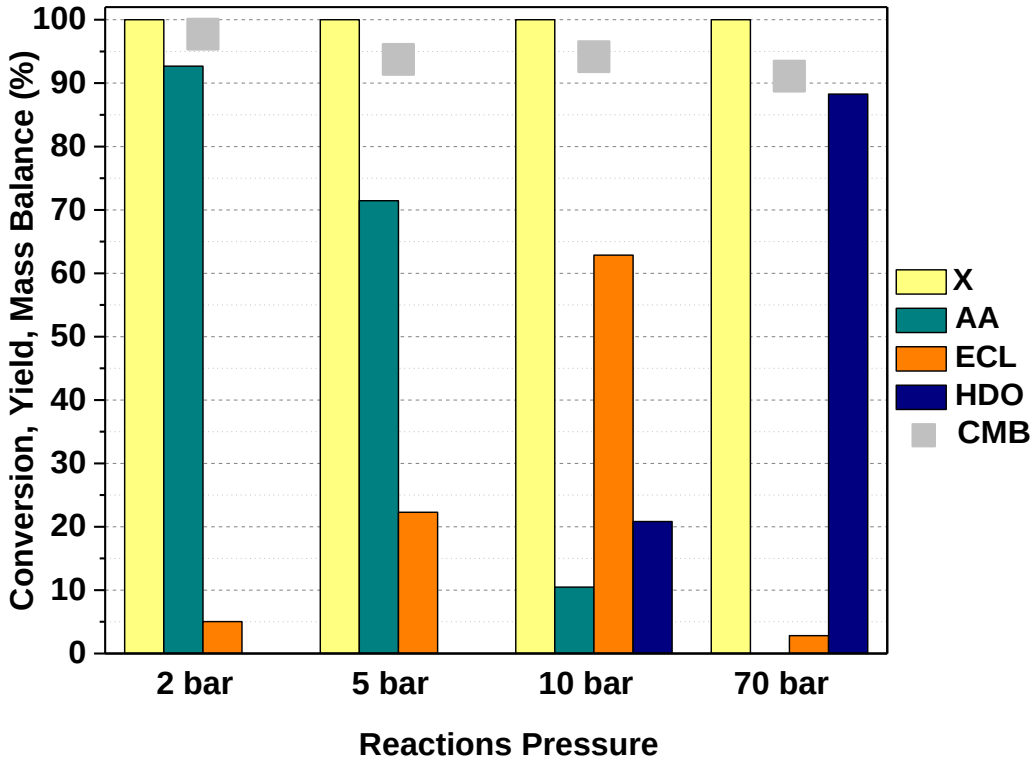

Figure 0.8. Effect of pressure on hydrogenation of cis, cis-muconic acid (ccMA) to caprolactone. Reaction conditions: catalyst 5% Ru-2% Sn/CNT (0.025 g), ccMA (0.05 g) solvent (25 mL), Temperature (200 ˚C), reaction time (23h). Legends: Conversion (X)-(yellow), yield to adipic acid (AA)-(green), epsilon-caprolactone (ECL)-(orange), 1,6-hexanediol (HDO)-(blue), carbon mass balance (CMB)-(gray).

With increasing reaction pressure, the yield of AA decreased rapidly with the concurrent increase of ECL formation and then HDO. Enhancement in ECL yield was observed from 5 % to 63 % with increases in hydrogen pressure from 2 to 10 bar. However, 21 % HDO was also produced at this hydrogen pressure whereas at 5 bar no HDO was observed.

On the other hand, since the HDO was formed with a yield of (21 %) in just 10 bar of hydrogen using 5% Ru-2% Sn/CNT at 200 °C and 10 bar, the H_2 pressure was increased to 70 bar which resulted in increased yield of HDO from 20.8 % to 88 % after 23 h, as shown in **Figure 5.8.** This result was expected, since from the performance of this exact catalyst in Chapter 4 where BDO and PDO were successfully produced in high yield from hydrogenation of succinic acid and levulinic acid respectively.

5.4. Conclusions

In this chapter, the direct catalytic hydrogenation of ccMA was efficiently achieved with many different catalysts and different product distributions were achieved. The high ccMA hydrogenation activity and AA selectivity makes 1% Pd supported on AC a better catalyst than Pd supported on CNT. It seems that the activity enhancement using CNT is not universal but reaction dependent. AA could be produced at almost 100 % yield under 80 °C, and 10 bar H_2 in 5-minutes.

Bio-based ECL and HDO were synthesised from ccMA hydrogenation using bimetallic catalysts (Ru-Sn). At 200 °C and 10 bar hydrogen pressure, formation of ECL was achieved with 63 % yield whereas increasing the pressure to 70 bar was enough to transform the majority of ECL and remaining AA to HDO in an 88 % yield. It seems that 2% Sn-5 %Ru/CNT is a universal for hydrogenation, since different carboxylic acids have been successfully hydrogenated to the correspond diols.

CHAPTER 6

Hydrogenation of Acids using High-Pressure Microwave Reactor

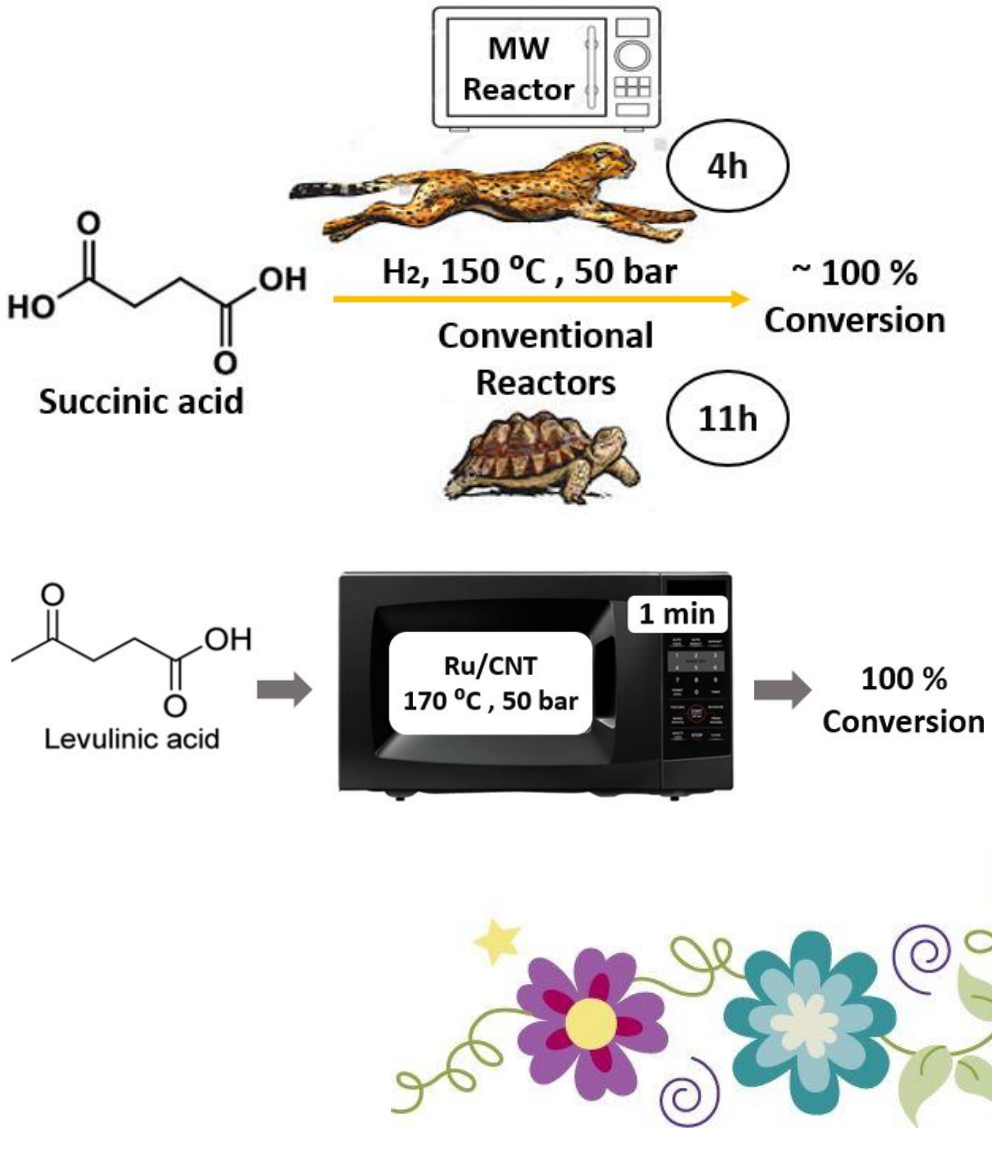

Chapter 6: Hydrogenation of Acids using High-Pressure Microwave Reactor

6.1. Introduction

Hydrogenation of succinic acid (SA) requires considerably long reaction times (generally days) due to the low activity of the carbonyl groups.[313] In order to overcome this limitation, microwave irradiation has been used as an alternative energy source in chemical syntheses due to its ability to increase the reaction rates.

The capability of some compounds such as water could be used to convert electromagnetic energy into heat.[281] The electromagnetic waves produced by the equipment have both magnetic and electric field components, which prompt microwaves to offer fast heating compared to conventional heating reactors, thereby, reducing the overall time of reaction.[88] Moreover, a number of authors have spotted the existence of ‘‘hot spots’’ in samples irradiated with microwaves, which are thought to be responsible for the high reactivity.[281, 314]

The hot spots might be produced due to in-homogeneity of distribution of electromagnetic field. These in-homogeneities of temperature during the heating of microwave are generally due to the use of a monomode cavity. The temperature in the hot spots has been estimated to be about 100–200 °C higher than the bulk temperature, and their size was estimated to be 100 µm.[281] Chemat et al.[315] referred the reaction rate increases under microwave heating to the hot spots that were formed by selective heating on the catalyst particle.

In Chapter 3, 5% Ru/CNT was shown as the most active catalyst in the hydrogenation of SA in a pressure autoclave reactor, although it required long reaction time, about 11 h, to fully convert the SA with a low selectivity to 1,4-butanediol (BDO), which was later overcome by the addition of Sn as showed in Chapter 4. The selectivity to BDO was increased after introducing 2% of Sn to 5% Ru/CNT.

Therefore, in this chapter, the use of microwaves in the hydrogenation of SA is discussed, and compared with the results obtained from reactions done under conventional heating (pressure autoclave reactor). Specifically, using 5% Ru/CNT with the aim of improving the rate of reaction and selectivity to BDO.

The effect of using different supported metal catalysts i.e., Ru, Pd, Pt, and Re on different supports under microwave irradiation has also been investigated. Alternative supports, such as SiO_2 and Al_2O_3 or metal like Re, were explore in which to be a comparable to the high activity of 5% Ru/CNT or at least could reduce C-C bond cleavage issue, therefore new catalysts were synthesised and tested in succinic acid hydrogenation.

Different ratios of Ru-Sn/CNT were assessed in a microwave reactor as well to find if the highest yield of BDO would be achieved faster since 2% Sn-5% Ru/CNT gave ~80 % yield of BDO in 23 h in a conventional heating reactor.

Levulinic acid (LA) is one of the most important biomass derived molecules and has attracted attention due to its huge potential as a platform chemical in synthesis of useful products.[316] Gamma-Valerolactone (GVL) is an important example of a valued product derived from LA and has found useful applications in the synthesis of various fine chemicals and as a promising biofuel.[317] Numerous reports have focused on the catalytic hydrogenation of LA using conventional heating media [318,319,320] however, Bermudez *et al*,[321] recently have used MW irradiation for hydrogenation of LA at 150 °C and formic acid as a hydrogen-donor solvent. No microwave-induced study has been found using H_2 as a source of hydrogen for the hydrogenation of LA. Thus, hydrogenation of LA to GVL was performed using a MW reactor due to the importance of this substrate as a potential "green fuel".

Most of the catalysts were characterized using N_2 isotherms, XRD, TEM, CO-chemisorption, and TPR to study their chemical and physical properties. The results generated, as well as the relationships between the performance and characteristics of used catalysts, are presented and discussed in following sections.

6.2. Experimental

Two different reactors, high pressure microwave reactor (MW) and conventional reactor, pressure autoclave (PA) have been used to perform the reactions in this chapter. The procedure is described in detail in Chapter 2. It is worth mentioning that all monometallic catalysts reported in this chapter have 5 wt. % metal, unless otherwise mentioned.

6.3. Results and Discussion

6.3.1. Catalysts Characterization Results

X-ray diffraction (XRD), temperature programmed reduction (TPR), CO-chemisorption, and transmission electron microscopy (TEM) were used to analyse the size, dispersion, and reducibility of metals nanoparticles. The following section solely focuses on the characterisation of new catalysts, such as metals catalysts supported on Al_2O_3 and SiO_2, since the characterization results of Ru catalysts supported on AC and CNT have been extensively discussed in Chapter 3. Additionally, Pd and Pt catalysts supported on AC, CNT, and Al_2O_3 are discussed here in detail.

6.3.1.1. X-Rays Diffraction Analyses (XRD)

6.3.1.1.1. Ru Catalysts

All diffraction patterns of catalysts were obtained after reduction and before catalytic testing. **Figure 6.1** shows the XRD patterns of various Ru catalysts supported on different supports, i.e., Ru/SiO_2 and Ru/Al_2O_3, Ru/AC, and Ru/CNT, in the range of 10 to 90°.

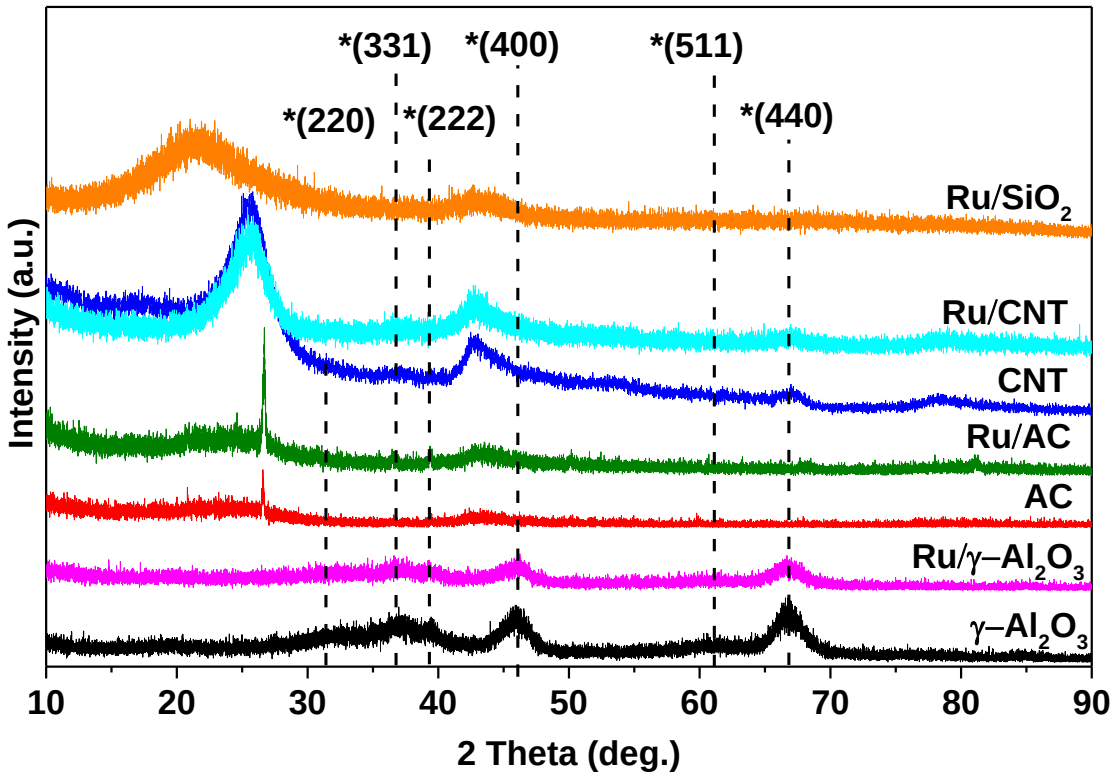

Figure 0.1. XRD patterns of γ-Al_2O_3, activated carbon, carbon nanotubes, and reduced 5% metals catalysts. (*): The diffraction lines of γ-Al_2O_3.

The diffraction peaks of γ-Al_2O_3 support as shown in **Figure 5.1** are 32.0°, 36.8°, 45.7°, 61.4° and 66.7° were indexed as (220), (331), (222), (400), (511), and (440) respectively, those diffraction peaks agree with the literature findings.[322,323] Moreover, when 5% Ru was loaded on γ-Al_2O_3 the intensity of the Al_2O_3 peaks decreased, indicating that the Ru particles on this support are finely dispersed.[226]

In addition, no diffraction peak was detected for Ru, suggesting that the Ru particles size is under the detection limit. Regarding the Ru/SiO_2 catalyst, there were no observed diffraction peaks, probably indicating that the Ru particles were small (<4 nm)[235] as previously observed in Ru supported on AC and CNT. This conclusion agrees with the TEM and TPR results shown below.

6.3.1.1.2. Pd and Pt Catalysts

The powder XRD patterns of Pd and Pt catalysts supported on different supports are shown in **Figure 6.2** which also includes XRD patterns of activated carbon, and carbon nanotube supports for comparison.

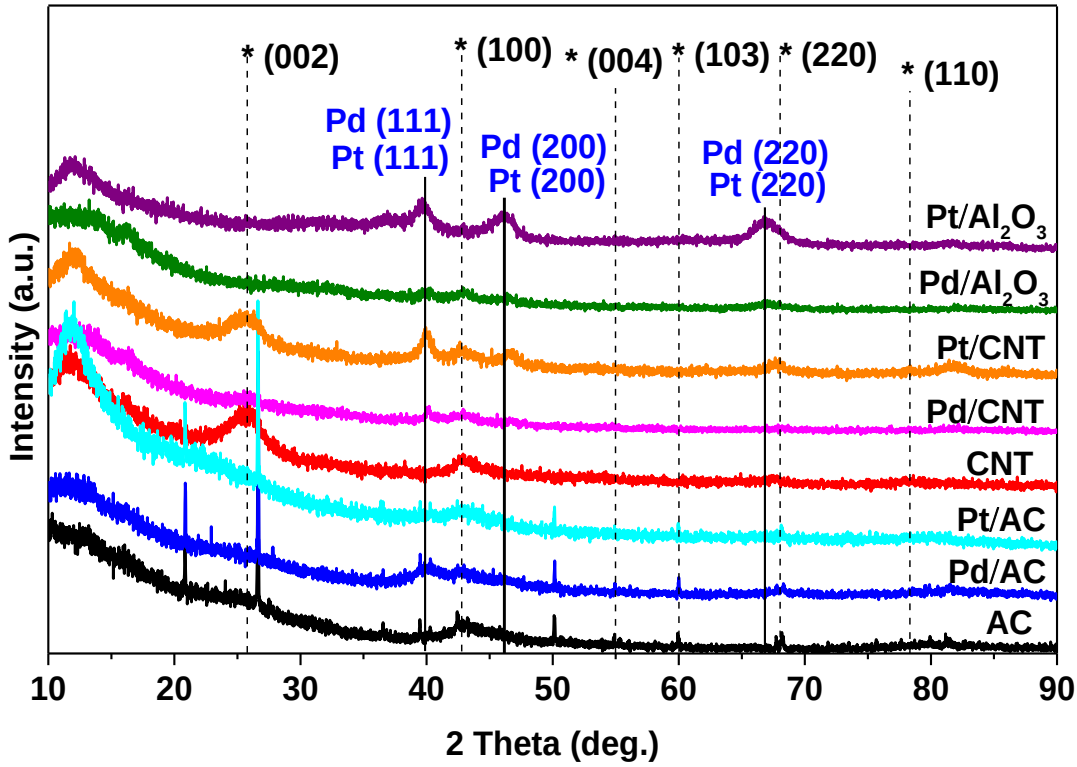

Figure 0.2. XRD patterns of activated carbon, carbon nanotubes, and reduced 5 % metals catalysts. (*): The diffraction lines of graphite.

The diffraction peaks of 25.7°, 42.9°, 54.8°, 59.8°, 68.1°, and 78.1° correspond to crystalline carbon planes (002), (100), (004), (103), (220), and (110) respectively of the graphitic structure[223,324] (JCPDS 001-0640, 003-0401). The XRD pattern of Pd nanoparticles have three identifiable diffraction peaks at 39.9°, 46.5°, and 67.9° which correspond to the (111), (200), and (220) diffraction patterns assignable to a face-centred cubic phase of Pd (JCPDS 001-1201).

The central peaks associated with Pd nanoparticles namely, 39.9° (111) and 46.5° (200) are less intense in samples Pd/CNT and Pd/Al_2O_3 indicating that the majority of Pd particles were finely dispersed on those samples.[226] On the other hand, Pd/AC shows relatively broad diffraction peak which suggests the formation of large Pd particles in the catalyst as reported in the leterature.[237] This finding aligns with results of TPR, as show later, where the Pd reduction peak of Pd/AC sample appeared at a higher temperature compared to CNT and Al_2O_3 supported Pd catalysts. This is another indication of the presence of large Pd particles.

Figure 6.2 also showed the diffraction peaks at 2θ of 39.8°, 46.6° and 68.1° which are attributed to cubic metallic Pt (JCPDS 001-1190) and those diffraction patterns are consistent with the literature.[325] Pt catalysts supported on CNT and Al_2O_3 showed diffraction peaks associated to Pt, whereas AC supported Pt exhibited less intense XRD peaks, indicating the Pt particles are highly dispersed on AC compared to CNT and Al_2O_3 samples.[226] The weak peaks (low intensity) of Pt indicates that Pt particles were finely dispersed on Pt/AC, which would be expected to improve activity, however, was not found to be consistent with the performance (activity) of this catalyst in the hydrogenation of SA compared to the performance of other Pt catalysts supported on CNT or Al_2O_3.

6.3.1.2. Metal dispersion by CO-Chemisorption

A CO chemisorption technique was used to estimate the metal dispersion on different supports. The results are displayed in **Table 6.1**. 5% Ru supported on Al_2O_3 gave highest metal dispersion while SiO_2 supported Ru catalyst showed similar dispersion as in 5% Ru/CNT (Table 6.1, entries 1-4). However, the noticeably low reactivity of this catalyst might be due to the presence of large Ru particles on SiO_2 compared to other Ru catalysts.

Table 0-1. List of reduced catalysts, results of CO chemisorption and average particle size. Metal dispersion and average particle size were calculated from CO chemisorption and TEM results respectively. All catalysts have 5 wt. % of a metal.

Entry	Catalysts	CO uptake, µmol/g	Metal dispersion, %	Average particle size (TEM), nm
1	Ru/AC	66.2	13.3	1.3±0.2
2	Ru/CNT	40.0	8.0	1.4±0.4
3	Ru/SiO_2	39.5	8.0	3±0.9
4	Ru/Al_2O_3	76.2	15.4	-
5	Pd/AC	51.3	5.4	-
6	Pd/CNT	19.6	2.1	2±0.7; 10±2.2
7	Pd/Al_2O_3	74.2	7.8	-
8	Pt/AC	64.9	13.9	-
9	Pt/CNT	60.0	7.04	2±0.5
10	Pt/Al_2O_3	60.0	12.9	-

The Pd catalysts have lower dispersion than all other catalysts, whereas Pt and Ru catalysts showed the opposite trend. The dispersion of Pd particles follows the trend CNT< AC < Al_2O_3, (Table 6.1, entries 5-7) which mean that Pd/Al_2O_3 have more active sites and smaller particles size.

This is supported with the results obtained from TPR and XRD data where Pd/Al_2O_3 showed reduction peak at a lower temperature and low intensity diffraction pattern respectively which would be consistent with the formation of a smaller Pd particles.

Table 6.1, entry 8-10, revealed that the dispersion of Pt particles on CNT (7.04 %) is lower than on AC (13.9 %) and on Al_2O_3 (12.8 %). However, this finding is not in an agreement with TPR data where it has been shown that the reduction peak of Pt/CNT was at a lower temperature compared to other Pt supported catalysts. TEM images, in Chapter 3, showed a good distribution of Pt on CNTs and the average Pt particle size was 2±0.5 nm.

6.3.1.3. Particle Size Distributions by Transmission Electron Microscopy

TEM images in **Figure 6.3**, showed that the average particle size of Ru on SiO_2 is different from the one observed for CNT and AC, as shown in **Figure 3.4** and **3.9** in (Chapter 3). The mean size of Ru particle supported on CNT (1.4 nm) is slightly larger than that of Ru on AC (1.3 nm), but significantly smaller than Ru supported on SiO_2 (3 nm), which could be due to the different interactions between the metal and support.[326]

TPR results suggested that the Ru particles size on SiO_2 would be larger due to the presence of reduction peak at higher temperature. However, TEM images of Ru/SiO_2 including Ru/AC, Ru/CNT in the previous chapter does not show any aggregation into larger clusters and Ru particles were well-dispersed on all supports.

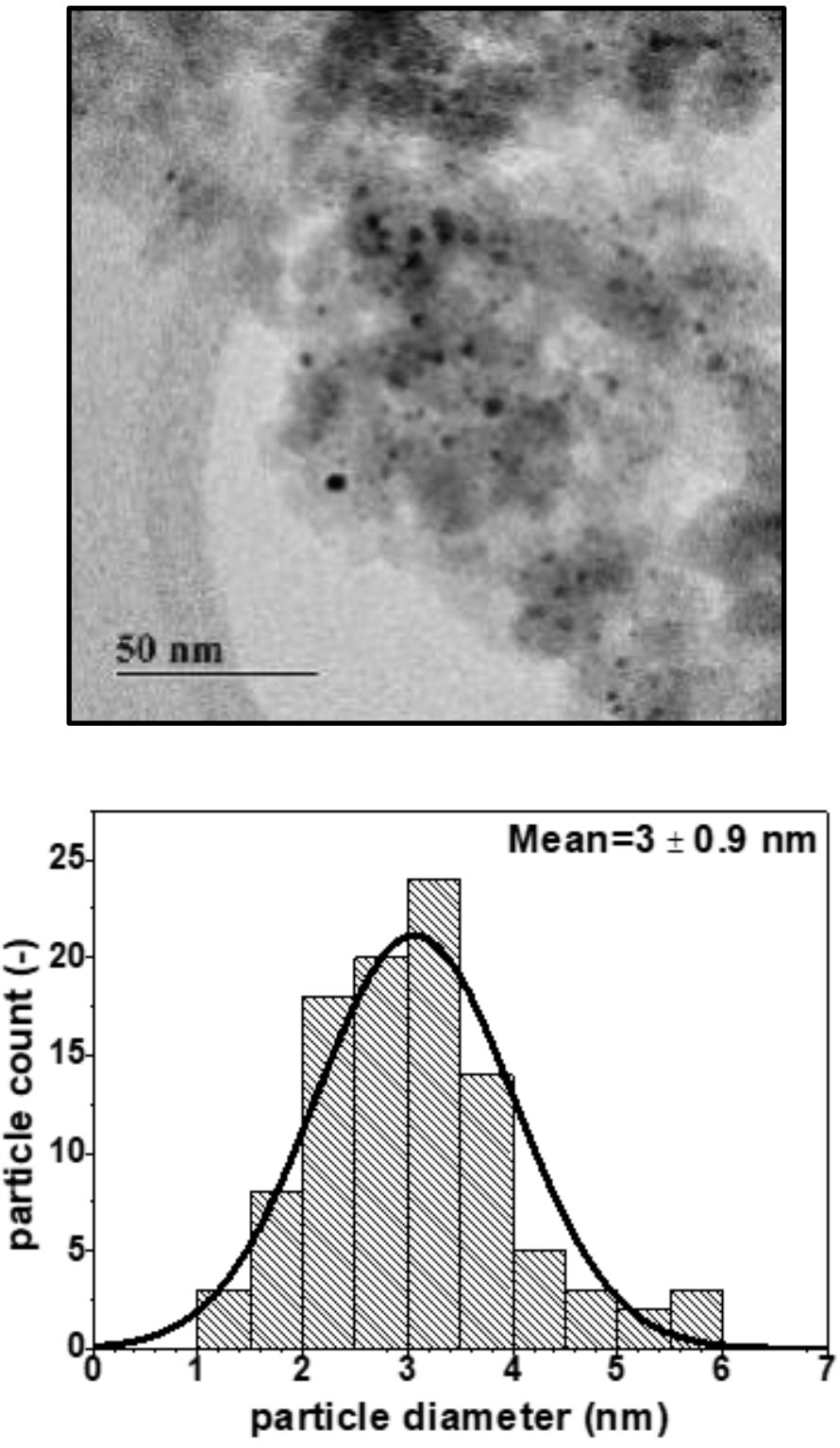

Figure 0.3. TEM images of Ru/SiO_2 with particle size distribution

6.3.1.4. Reducibility by Temperature Programmed Reduction (TPR)

H_2-TPR was used to study the reducibility and interactions between the metal and corresponding support. **Figure 6.4** and **Figure 6.5** show the H_2-TPR profiles of 12 catalysts, in which the reduction peaks of ruthenium, palladium, rhenium, and platinum species appear in the range of 50−350 °C. Two temperature ranges are noticeable in the TPR profiles: lower and higher than 350 °C. Below 350 °C, the decomposition of the precursor chlorides and reduction of the metal precursor from high oxidation state to metallic state is evident.

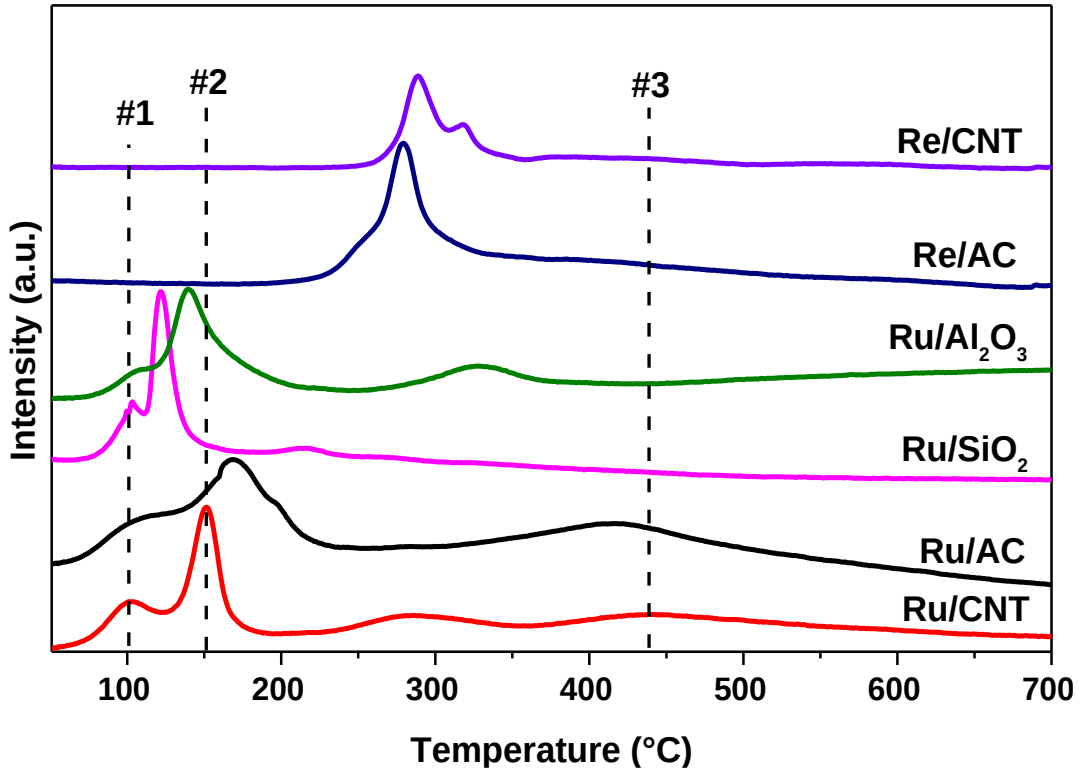

Figure 0.4. H_2-TPR profiles for (Unreduced) five wt. % of Ru and Re catalysts supported on different supports.

A broad peak was observed approximately at around 440 °C (#3) on all AC and CNT supported samples which could correspond either to the reduction of carbon species or carbon-related functional groups,[233] or as the consequence of a carbon methanation previously shown in literature to occur in the presence of supported metals.[85,232,327]

For the Ru catalysts, the TPR peaks of Ru dispersed on various supports appears at different temperatures. Ru catalysts supported on SiO_2 and Al_2O_3, show the same TPR profiles as those of Ru catalysts supported on AC and CNT; however, Ru catalysts supported on SiO_2 were reduced at lower temperature compared to the other Ru catalysts including Ru/Al_2O_3, indicating a weaker interaction between Ru species and their respective support (SiO_2).

The XRD results for Ru/SiO_2 does not show any diffraction peak related to Ru, this could be an indication of dispersion of small Ru particle on SiO_2.

Metallic elements have different reduction potential based on their physical and chemical properties. The reduction peak of Re appeared at a higher temperature when compared with results of the other metals. The reduction profile of Re catalysts supported on AC and CNT shows one sharp peak whereas another small peak was observed in Re/CNT. The peak at 280 °C was produced by the reduction of rhenium oxide as described in many reports.[277,328] Hong *et al*.[105] reported that the high-temperature peak of Re might indicate that there is a high interaction between Re salt and the support which might lead to the formation of large particles of Re. The latter study found that the average particle size of Re on AC was 4.9 nm.

TPR profiles of Pd catalysts (**Figure 6.5**) exhibit one reduction peak, and it should be noted that in all cases, a signal of H_2 consumption is linked to the complete reduction of Pd^{2+} to Pd^0, whereas a different peak location can correspond to different size of Pd species.[329] Lower temperature peaks could be attributed to a reduction of smaller Pd particles on the surface which could be linked to easily reducible species, while, the higher temperature peak is assigned to the reduction of bulk Pd particles.[330,329]

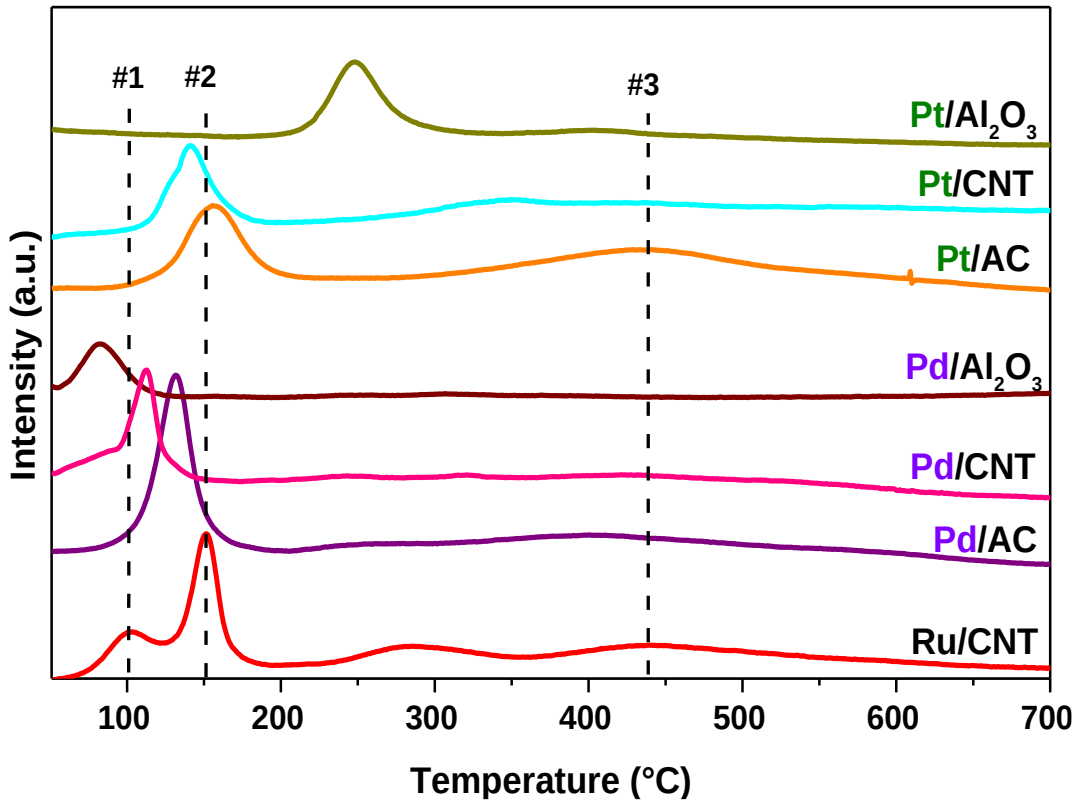

Figure 0.5. H_2-TPR profiles for (Unreduced) five wt. % of different noble metals catalysts supported on different supports.

A well-defined broad peak was found in AC supported Pd catalyst, and this peak shifted to a higher temperature (130 °C) compared to CNT (112 °C), and Al_2O_3 (81 °C) supported catalysts. This phenomenon is an indication of stronger interaction between $PdCl_2$ and AC, than that observed with CNT and Al_2O_3 supports.

Pt catalysts supported on AC and Al_2O_3 also showed one sharp peak at 157 °C and 248 °C, respectively. However, CNT supported Pt catalyst showed a peak at 140.5 °C. Those peaks could be attributed to the continuous multi-step reduction of a bulky portion of Pt^{n+} species.[238,239]

The Pt reduction peak is shifted to higher temperature in the Pt catalyst supported by AC compared to Ru/CNT, demonstrating that either; a strong interaction might have occurred between the Pt salt and AC or alternatively, relatively poor dispersion of Pt particles on AC has occurred compared to Pt catalyst supported on CNT.[238]

However, the H_2 reduction profiles for Al_2O_3-supported Pt catalysts are very different which agrees with the decrease in dispersion when using Al_2O_3 in Pt catalysts. The H_2 reduction peak was observed at higher temperature (248 °C) and this temperature is even higher than all Ru Pd, and Pt catalysts TPR profiles. This indicate, that the interaction between Pt precursor and Al_2O_3 is stronger than with other supports, e.g. AC or CNT. The XRD data where the diffraction peaks proposed that Pt/Al_2O_3 might have a larger Pt particles size when compared to other supported Pt catalysts.

6.3.1.5. Pore Size, Pore Volume, and Surface Area by N_2 Physisorption

The standard method used in measuring the porosity of given catalyst is N_2 physisorption (physical adsorption) where at low temperature, different features of porosity can be found from the isotherms.[331] Reactant and products transport (catalytic process) could be affected significantly by the pore size/structure of a given catalyst.[332] The highly active Ru catalysts in the current chapter (Ru/AC, Ru/CNT, and Ru/Al_2O_3) were investigated *via* N_2 physisorption and the N_2 isotherms are shown in **Figure 6.6**. N_2 adsorption isotherm for Ru/CNT appears to belong to the "Type IV" category, and "Type H1" hysteresis loop. This is for non-microporous materials as reported by Ribeiro *et al*.[333] and Ru/Al_2O_3 showed an isotherm like CNT based catalyst which indicates that this is also non-microporous materials.[334,335]

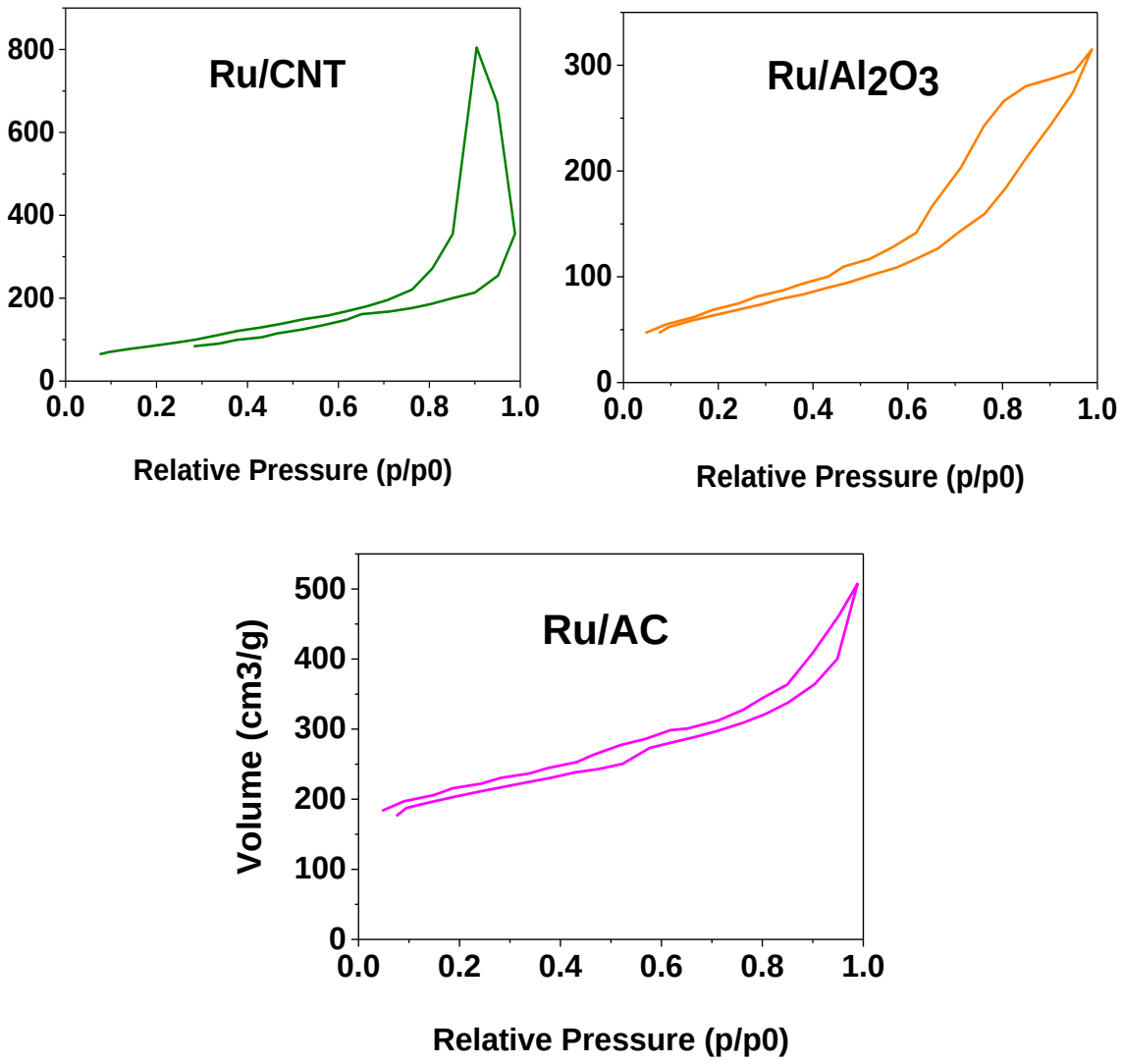

Figure 0.6. Nitrogen physisorption isotherms of reduced Ru catalysts in the range of relative pressures of 0.05-0.99.

On the other hand, Ru/AC showed "Type IV" isotherm and "Type H3" hysteresis loop based on the IUPAC classification of hysteresis loops indicating the existence of microspores in the catalyst.[23,335]

The total surface areas (S_{BET}) of those three catalysts was calculated by application of the BET method to the isotherms of N_2 adsorption at -196 °C and are given in Table 6.2.

Table 0-2. List of different Ru based catalysts, with the corresponding surface area.

Catalysts	Ru/AC	Ru/CNT	Ru/Al_2O_3
S_{BET}, m^2/g	636	317	236

Amongst these catalysts, AC support Ru catalyst showed the highest surface area (636 m^2/g) therefore the probability of formation of small metal particles would be high. This hypothesis was supported by the results obtained *via* TEM images as shown in Chapter 3 since the latter showed a narrower Ru particle size distribution on the surface of AC and an average size of the particle was 1.3 nm which was smaller than CNT sample.

On the other hand, the total surface areas found for Ru/CNT and Ru/Al_2O_3, were 317 m^2/g and 236 m^2/g respectively which are lower than Ru/AC. Liu *et al.*[336] reported that the surface areas cannot always be used as a determination for the activity of a given catalyst. Another study by García-García and co-workers[337] addressed that the effect of metal particle size on activity. However, Auer *et al.*[22] reported that the catalytic activity increased when using a highly porous material. Materials that offer easy access of the reactants to the catalytically active sites lead to higher activity. Based on those concepts, therefore, it is worthy to investigate the pore size of the most active Ru catalysts in this Chapter. The total pore volume and average pore diameter for different Ru catalysts supported on AC, CNT, and Al_2O_3 are given in **Figure 6.7**.

The results show that Ru/CNT has the higher total pore volume of 1.229 cm^3/g and average pore diameter of 17.36 nm in comparison to AC (0.785 cm^3/g, 4.94 nm) and Al_2O_3 (0.48 cm^3/g, 8.23 nm) respectively.

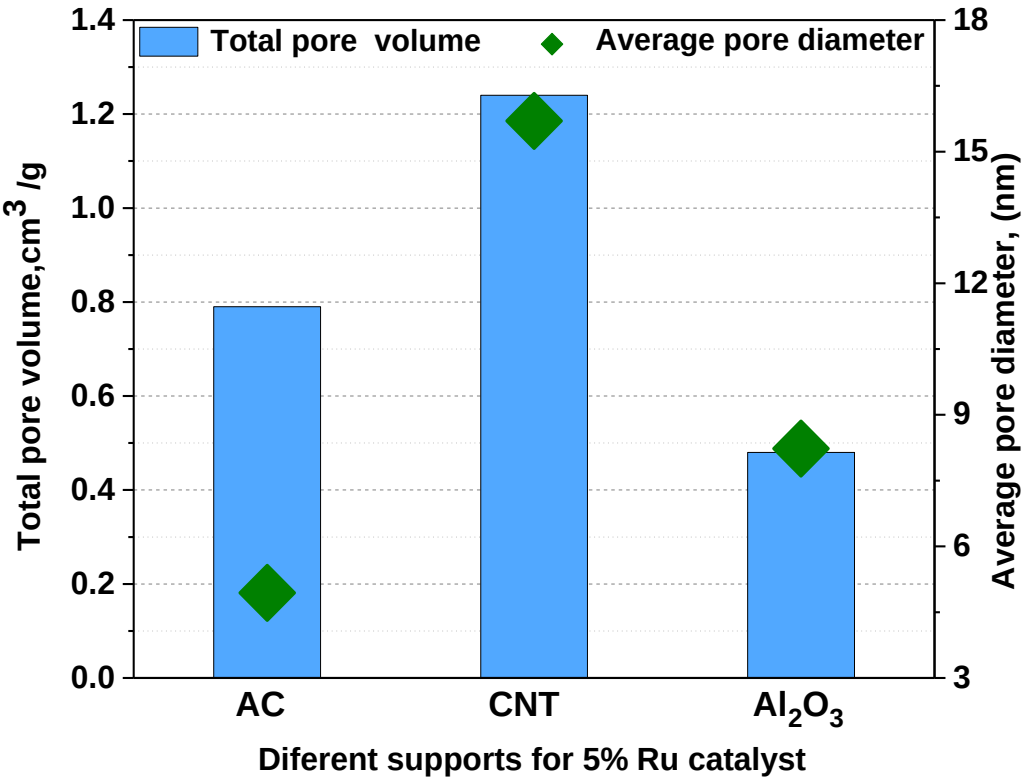

Figure 0.7. Total pore volume and average pore diameter for different reduced Ru catalysts supported on (AC, CNT, and Al_2O_3).

6.3.2. Activity Evaluation of the Catalysts

Hydrogenation of succinic acid using a microwave reactor was studied under several reactions parameters, i.e., reaction temperature, different metals and supports. However, it is important first to show the effect of the microwave on succinic acid hydrogenation. We examined the effect of microwave on succinic acid hydrogenation using of Ru/CNT. **Figure 6.8**, shows a comparison between the results obtained from two different reactors (PA and MW) in the hydrogenation of SA.

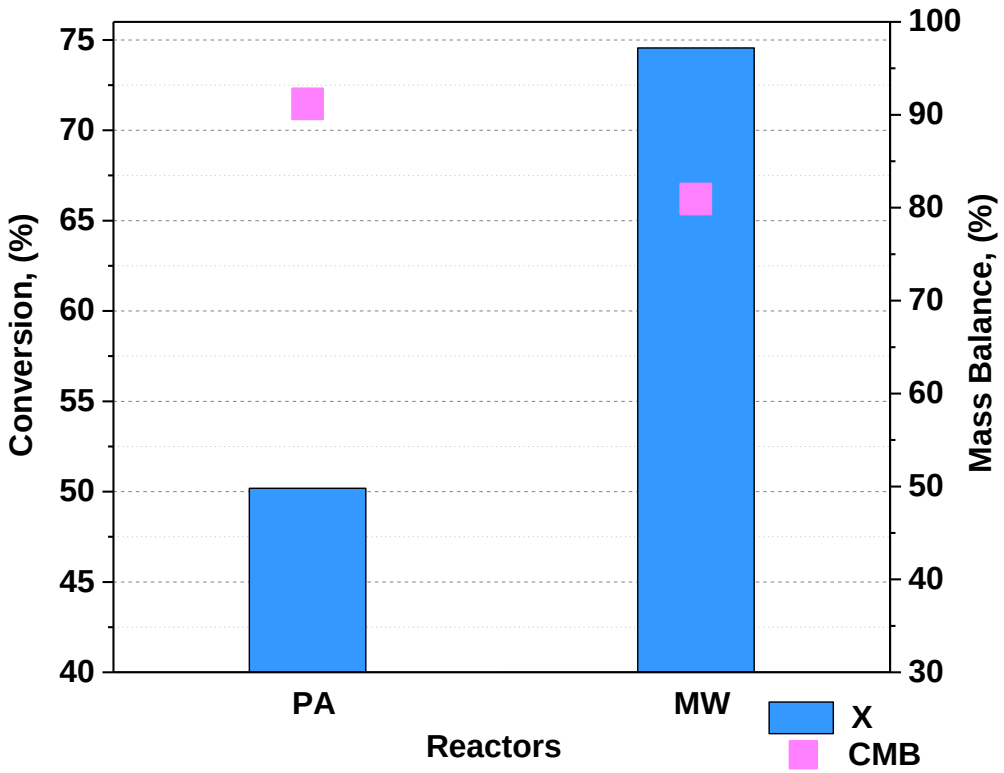

Figure 0.8. Effect of MW in hydrogenation of succinic acid using 5% Ru/CNT. Reaction conditions: T: 150 °C, P: 50 bar; reaction time: 2h. Note, conventional reactor: SA: 100 mg; catalyst: 50g; solvent (H_2O): 25 mL; microwave reactor: SA: 25 mg; catalyst: 12 mg; solvent (H_2O); PA, pressure reactor (conventional heating), MW. Microwave reactor.

The results displayed a large increase in the rate of the reaction using a microwave. The conversion using microwave was ~75 % whereas conventional heating reactor (pressure autoclave) converted 50 % of succinic acid. The reason behind this high activity using a microwave is the present of hotspots, certain areas in the reaction mixture with a higher temperature and energy, which led to an improvement of the conversion as has been claimed by number of authors.[314, 281] For the first time, the effect of microwave is shown for the hydrogenation of SA and it appeared to significantly increase the rate of the reaction.

6.3.2.1. Effect of Temperature at Hydrogenation of Succinic Acid using MW

- Activity

It has been discussed in Chapter 3, while using conventional heating reactor (pressure autoclave) that, one of the most promising ways to increase the catalytic activity of Ru catalyst is raising the temperature. However, this step resulted in a massive reduction in the carbon mass balance due to C-C bond cleavage. Therefore, the effect of different reaction temperatures on the hydrogenation of succinic acid in the MW reactor was studied, to improve the mass balance, which will have a positive impact on the formation of BDO. **Figure 6.9** shows the influence of the reaction temperatures (130, 150, and 170 °C) on the hydrogenation of SA over the Ru/CNT at 50 bar H_2 pressure.

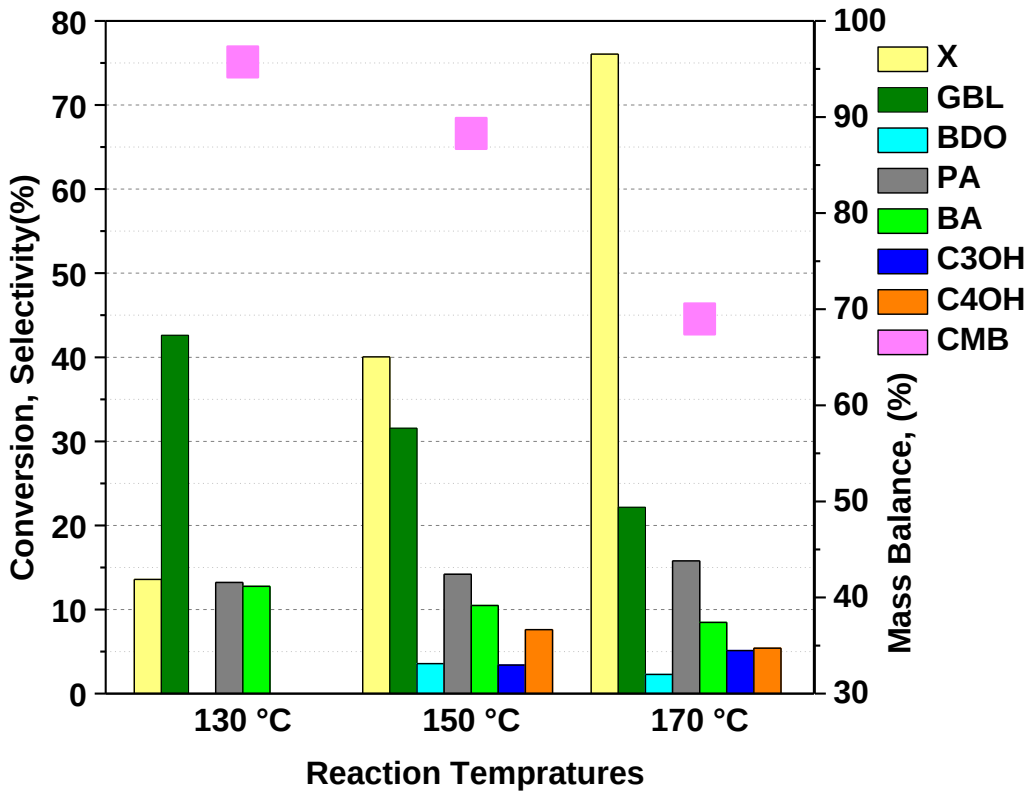

Figure 0.9. Comparison of the activity of Ru catalysts with respect to temperature in hydrogenation of succinic acid in MW. Reaction conditions: P: 50 bar; reaction time: 1 h; succinic acid: 25 mg; catalyst: 12 mg; solvent: 6 mL H_2O.

We have chosen Ru/CNT because it showed high catalytic activity and less formation of C-C cleavage products as discussed in Chapter 3. The catalytic activity, as expected, increases with increasing temperature from 130 °C to 170 °C. The conversion increased to 76 % at 170 °C compared to 13 % at 130 °C.

- Selectivity

Regarding the selectivity, the same problem (C-C bond cleavage) was observed using the MW reactor. The formation of the C-C cleavage products increased with increasing reaction temperature to 170 °C. 150 °C reaction temperature showed to be a reasonable result, but still poor selectivity to BDO. **Table 6.3** shows the influence of increasing temperatures (150 °C vs. 170 °C) on the selectivity using microwave reactor at iso-conversion. The result shows, no improvement in preventing the C-C cleavage products was achieved in MW reactor. The carbon mass balance and the selectivity to GBL decreased as the temperature of the reaction increased, prompting the formation of C-C cleavage products (decarboxylation of SA).

Table 0-3 Reaction conditions SA: 25 mg; catalyst (5% Ru/CNT): 12 mg; solvent (H_2O): 6 mL. T: 150 °C; P: 50 bar. Legend: PA, propionic acid; BDO, 1,4-butanediol; BA, butyric acid; C_3OH, propanol; GBL, γ-Butyrolactone; THF, tetrahydrofuran; C_4OH, Butanol; CMB, carbon mass balance; X, conversion; T, temperature; P, pressure; MW: microwave.

				Selectivity, %							
Catalysts	T, °C	t, h	X, %	**PA**	**BDO**	**BA**	**C_3OH**	**GBL**	**THF**	**C_4OH**	**CMB**
Ru/CNT	150	2	74.6	12	5.8	10	4.7	35	0	6.8	80.9
	170	1	76.1	15.8	2.3	8.5	5	22.2	0	5.4	68.9

Based on these preliminary experiments, the reaction temperature was selected to be 150 °C in the microwave reactor as previously when using a conventional reactor. This decision was made because C-C cleavage was higher at 170 °C. Accordingly (as mentioned earlier in this chapter), a new catalyst was developed using different metals than Ru to determine if better selectivity towards BDO or better activity than Ru/CNT could be achieved.

6.3.2.2. Effect of Noble Metals on Hydrogenation of Succinic Acid in MW

- Activity

Metals such as Ru, Pd, and Pt supported on AC were compared to Re/AC to determine if Re catalyst would be competitive regarding activity or selectivity. These catalysts were screened at 150 °C and 50 bar, as decided from the preliminary tests in the current chapter. The results for using several catalysts supported on AC to hydrogenation of succinic acid are presented in **Figure 6.10.** The results exhibited that Ru catalyst was still the most active catalyst in a microwave reactor. Pd, Pt, and even Re were not able to effectively convert SA. Pt and Re displayed approximately 6 % SA conversion after 1h reaction time, while the Pd and Ru catalysts converted <1 % and 17.6 %, respectively after the same reaction time.

By comparing the results from the microwave reactor vs. conventional reactor, the reaction time was reduced using MW. The same conversion has achieved at less reaction time using the MW reactor. **Table 6.4** shows that using microwave heating the reaction rate increased in all tested catalysts no matter which metal is present.

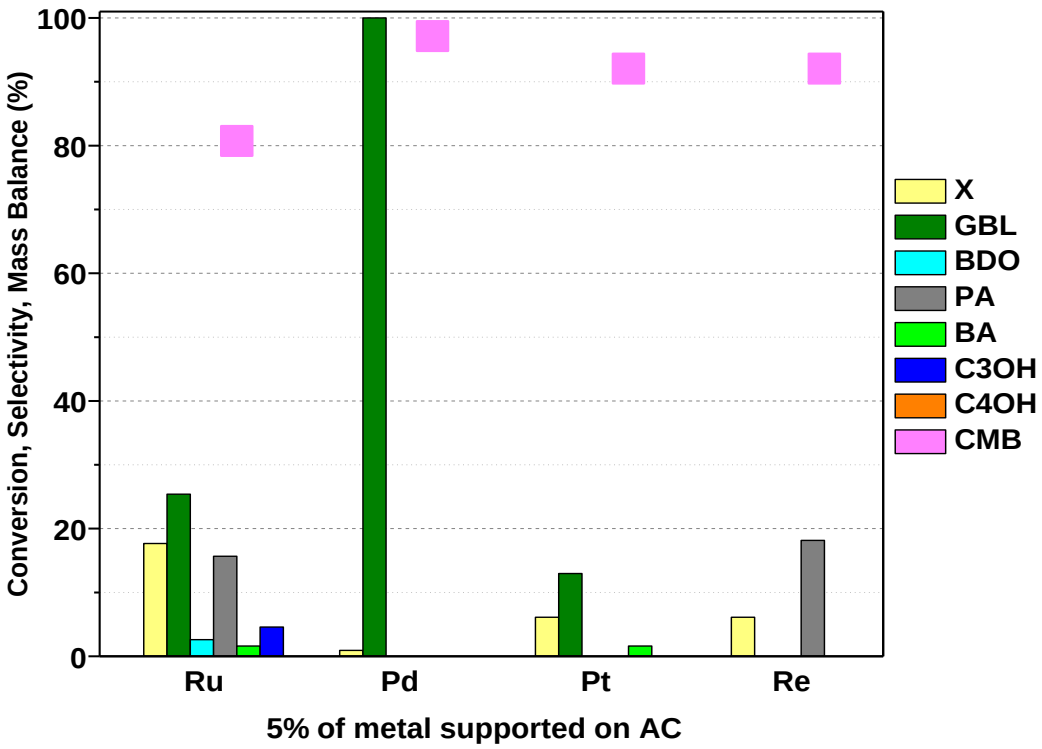

Figure 6.10. Comparison of the activity with respect to noble metals supported on AC in hydrogenation of succinic acid. Reaction conditions: T: 150 °C; P: 50 bar; reaction time: 1h; succinic acid: 25 mg; catalyst: 12 mg; solvent: 6 mL H_2O.

- Selectivity

To evaluate these catalysts regarding selectivity, **Table 6.4** shows the product distribution at iso-conversion for different noble metal catalysts supported on AC using both reactors. The results displayed that there is no much difference in performing the reaction in the microwave reactor since the products distribution and carbon mass balance values remain almost the same in both reactors.

Table 0-4 Reaction conditions (conventional reactor): SA: 100 mg; catalyst: 50g; solvent (H_2O): 25 mL; (microwave reactor): SA: 25 mg; catalyst: 12 mg; solvent (H_2O): 6 mL. T: 150 °C; P: 50 bar. Legend: PA, propionic acid; BDO, 1,4-butanediol; BA, butyric acid; C_3OH, propanol; GBL, γ-butyrolactone; THF, tetrahydrofuran; C_4OH, butanol; CMB, carbon mass balance; X, conversion; T, temperature; P, pressure; PAR: pressure autoclave conventional reactor; MW: microwave; Cat: catalysts; R:reactors.

Cat	R	t, h	X, (%)	Selectivity (%)							
				PA	BDO	BA	C_3OH	GBL	THF	C_4OH	CMB
Ru/AC	PAR	5	49.5	14.4	7.8	5	4.4	31.8	0	2.5	83.2
	MW	3	43.4	17.3	7.8	1.3	6.5	23.2	0	2.3	82.0
Pd/AC	PAR	23	5.6	0	0	0	0	0	0	0	94.4
	MW	3	7.5	0	0	0	0	50	0	0	96.3
Pt/AC	PAR	5	5.5	0	0	0	0	6.7	0	0	94.5
	MW	3	5.9	0	0	3	0	17.1	0	0	95.3
Re/AC	PAR	5	5.2	0	0	17.1	0	0	0	0	95.7
	MW	1	6.1	2.4	0	0	0	0	0	0	95.3

6.3.2.3. Effect of Support on Ru Catalyst to Hydrogenation of Succinic Acid in MW

- Activity

The primary purpose of a catalyst's support is to facilitate the effective dispersion of the active phase,[338] to decrease the amount of metal used and offer the surface for the reaction. The performance of a catalyst can be greatly influenced by the support.[339]

The metal dispersion and morphology might depend on the type of support.[340] In this section, the goal is to determine the best support for Ru catalyst, where high catalytic activity or low C-C bond cleavage activity would be obtained. **Figure 6.11** shows the effect of using different supports for Ru catalyst in the hydrogenation of SA in the microwave reactor.

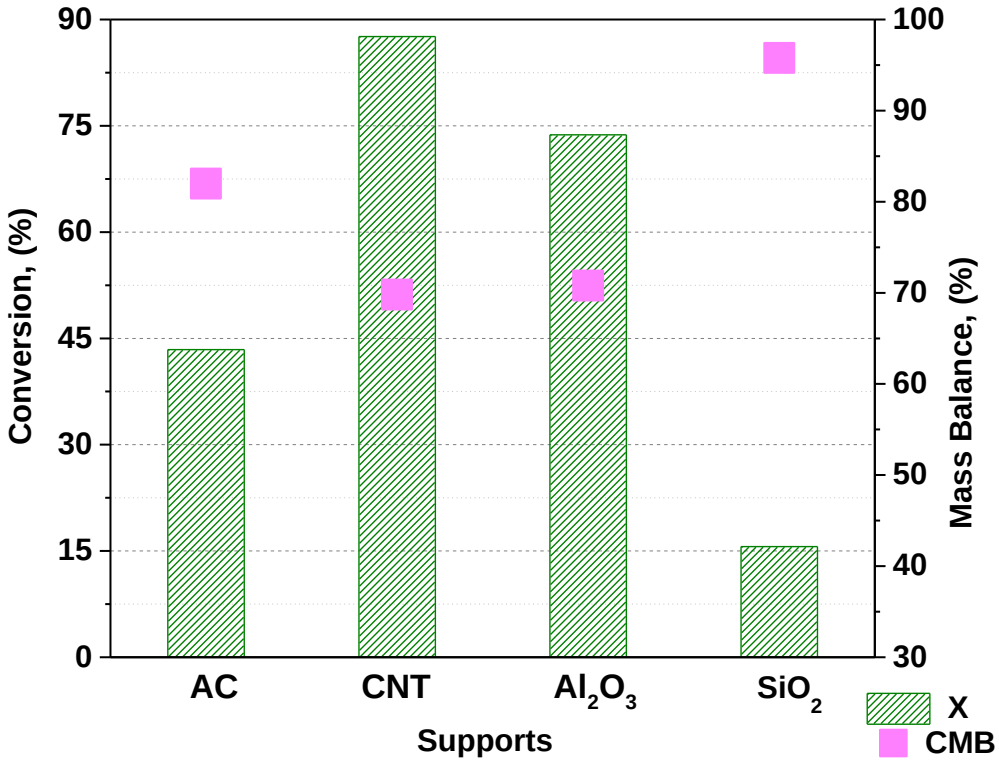

Figure 0.10. Comparison of the activity of Ru catalysts with respect of supports in hydrogenation of succinic acid. Reaction conditions: T: 150 °C; P: 50 bar; reaction time: 3h; succinic acid: 25 mg; catalyst: 12 mg; solvent: 6 mL H_2O.

Throughout Chapters 3 and 4, CNT was a better support for all noble metal-based catalysts (Pd, Ru, and Pt) and bimetallic catalyst in the conventional heating reactor. Ru/CNT proved to be the most active catalyst as well in the microwave reactor compared to other supported Ru catalysts. The conversion of SA increased using Ru/CNT to (86 %) from 43 % (Ru/AC), 74 % (Ru/Al_2O_3) and 16 % (Ru/SiO_2).

In catalysis, more exposure of the active surface would be provided by small metal nanoparticle which increases the availability to guest molecules. It can be seen from the TEM images (**Figure 3.4**) in Chapter 3 that fine metallic Ru particles are distributed on the surface of the CNT with small particles size (1.4 nm), which could contribute to the excellent catalytic activity of Ru/CNT. Whereas, the presence of larger particles of Ru in Ru/SiO_2 (3 nm) decreases the activity of the catalyst.

Ru/CNT showed better activity than Ru/Al_2O_3. This result was surprising because the CO chemisorption results showed that, Ru/Al_2O_3 has more active sites than Ru/CNT. The Ru dispersion was 15.8 % on Ru/Al_2O_3 and 8 % on Ru/CNT however, Ru/Al_2O_3 might have larger Ru particle size than in Ru/CNT.

The confirmation cannot be made whether the particles are large or small because of the absent TEM results for Ru/Al_2O_3. However, TPR data showed that the reduction peak presented at the higher temperature compared to Ru/CNT which might be a confirmation of the formation of larger Ru particles size in Ru/Al_2O_3, which caused the low catalytic reactivity.

CO-chemisorption displayed that Ru/AC has more active sites and Ru dispersion of the later catalyst was two-fold higher compared to Ru/CNT. TEM results showed that the Ru average particle size was smaller on Ru/AC compared to CNT. Based on these results, Ru/AC should be more active, but it is not. The higher activity of CNT based catalyst may depend on something else, and it could be pore size differences.

Previously, N_2-physisorption results (**Figure 6.7)** showed that Ru/CNT has the highest pore size 15.7 nm compared to 8.23 nm and 4.94 nm for Ru/Al_2O_3 and Ru/AC respectively. This could be the reason for the high activity of Ru/CNT since the molecules easily desorb and diffuse into the bulk solution to and from the Ru particles. The same observation has been addressed by Jiang et al.[341] where they claim that, Ru catalyst with much better porosity has better activity in benzoic acid hydrogenation. The microporosity of AC might be one the reason for the low reactivity of Ru/AC.

So far 2 possible explanations have been proposed for such activity; an enhancement of the porosity and particle size effects, however, the excellent electronic properties of CNTs could also play a significant role in the activity of the catalyst. The moving signals electron on the wall of CNTs and the semi-conductive features mean CNTs have a high ability to lose an electron.[342]

Jahjah *et al.*[343] and Pan et al.[326] found high catalytic activity of Ru catalyst supported on CNT compared to other supports (Al_2O_3 and SiO_2) in a hydrogenation of several unsaturated substrates and glucose hydrogenation to sorbitol respectively. Pan et al,[326] determined the high activity of Ru/CNTs to be due to a strong metal support interaction and a better particle size distribution.[326] However, the latter study also suggested that the ruthenium particles supported on CNT are electron-enriched nanoparticles.

Indeed, XPS results in Chapter 3 showed a shift in Ru binding energies which might induce a change in electron transfer on Ru nanoparticles and their interaction with carbon surface and this electron transfer might confer superior activity to Ru/CNT. Thus, CNTs has a positive effect when using as a support, Wang et al.[342] reported that CNTs are served not only support for the catalyst but also electronic catalyst-accelerator.

Regarding Pd and Pt catalysts supported on AC, CNT, and Al_2O_3, the results also showed that when those catalysts were supported on CNT, they were more active than Pt/Pd catalysts supported on other supports. The reason would be the same as suggested for Ru/CNT above. The results are shown in **Figures 6.12** and **6.13.**

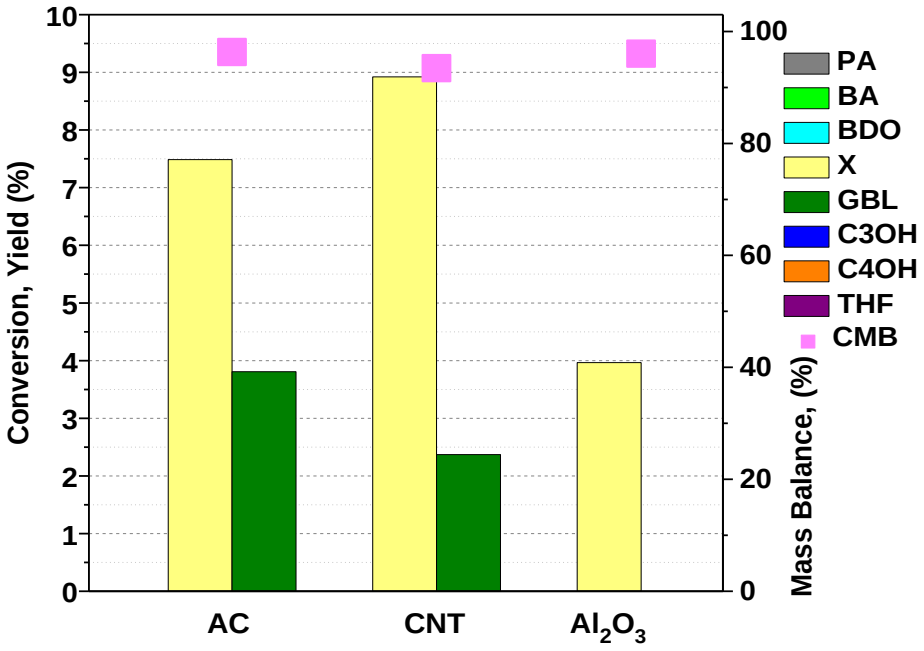

Figure 0.11. Comparison of the activity with respect of support for Pd catalysts in hydrogenation of succinic acid in MW. Reaction conditions: T: 150 °C; P: 50 bar; reaction time: 3h; succinic acid: 25 mg; catalyst: 12 mg; solvent: 6 mL H_2O.

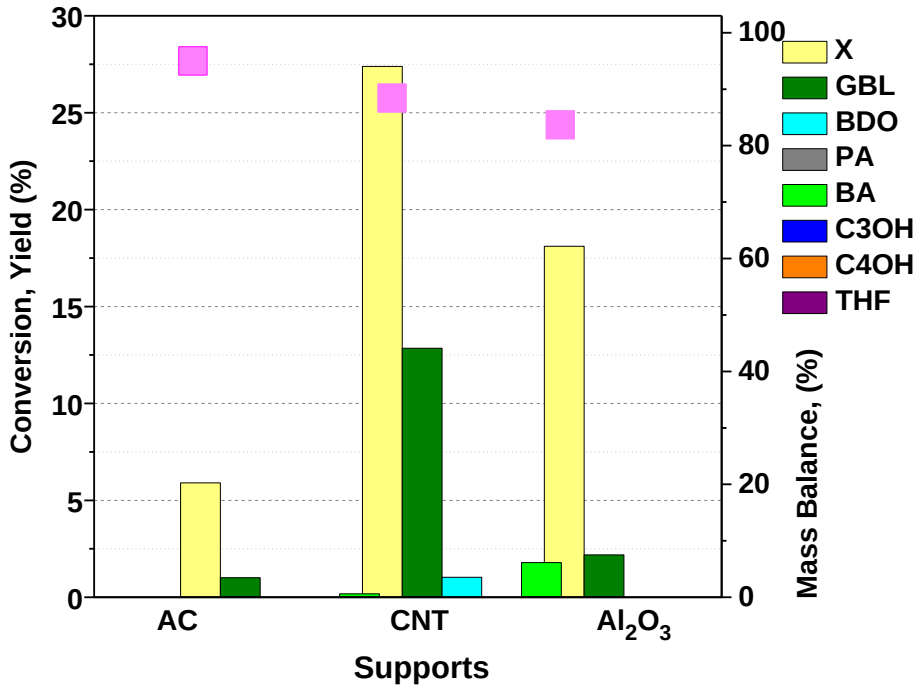

Figure 0.12. Comparison of the activity with respect of support for Pt catalysts in hydrogenation of succinic acid in MW. Reaction conditions: T: 150 °C; P: 50 bar; reaction time: 3h; succinic acid: 25 mg; catalyst: 12 mg; solvent: 6 mL H_2O.

The higher activity of Ru, Pd, and Pd supported on CNT for the hydrogenation of succinic acid might be due to the promoting effect of the electron transfer between the metal and CNT. Therefore, all results suggest that CNT is a more suitable support for aqueous phase hydrogenation of succinic acid regardless the metal.

- Selectivity

Regarding the selectivity, Ru/CNT and Ru/Al_2O_3 results where compared because of the high activity of those catalysts in the hydrogenation of succinic acid using microwave reactor. They have been compared at iso-conversion to investigate if different product distributions might occur. The results in **Table 6.5** showed that the selectivity did not change significantly.

Table 0-5 Reaction conditions: SA: 25 mg; catalyst: 12 mg; solvent (H_2O): 6 mL, T: 150 °C; P: 50 bar. Legend: PA, propionic acid; BDO, 1,4-butanediol; BA, butyric acid; C_3OH, propanol; GBL, γ-Butyrolactone; THF, tetrahydrofuran; C_4OH, Butanol; CMB, carbon mass balance; X, conversion; T, temperature; P, pressure; MW: microwave Cat: catalysts; R:reactors.

Cat	R	t, h	X, %	Selectivity, %							
				PA	BDO	BA	C_3OH	GBL	THF	C_4OH	CMB
Ru/CNT	MW	0.5	28.9	12.7	2.3	12.5	3.1	41.3	0	6	93.7
Ru/Al_2O_3	MW	1	26.3	16.9	1.4	9.1	0	32.5	0	3.5	90.4

For Ru catalysts, GBL, and propionic acid were the main products. However, the formation of propionic acid decreased, and the formation of GBL increased using CNT. Ru/CNT seems to be more efficient to drive the hydrogenation of SA to BDO throughout GBL as the C-C bond cleavage product (propionic acid) is less evident in Ru/CNT compared to other Ru catalysts.

6.3.2.4. Succinic Acid Products Distribution from Both Reactors using Ru/CNT

Ru/CNT was the most active catalyst for the hydrogenation of succinic acid and in MW, the rate of reaction increased compared to a conventional reactor (pressure autoclave). Regarding the selectivity, Ru/CNT showed better selectivity to alcohol products in Chapter 3 compared to other catalytic systems. The selectivity of Ru/CNT catalysts in the MW reactor was tested as well. Comparison at >50 % conversion was not found from both reactors due to the fast reaction in the MW thus the product distribution was compared at around 85 % conversion. The result at iso-conversion is plotted in **Figure 6.14**.

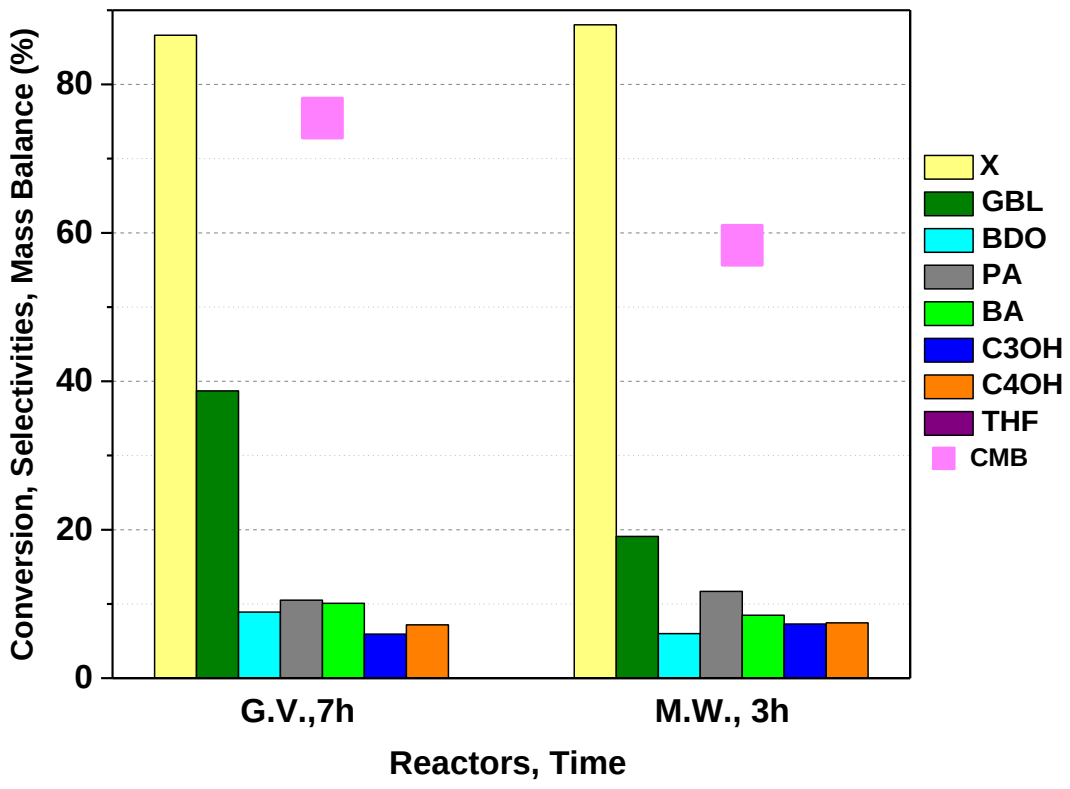

Figure 0.13. Comparison of the selectivity of Ru catalysts with respect of reactors in hydrogenation of succinic acid using 5%Ru/CNT. Reaction conditions: T: 150 °C; P: 50 bar; succinic acid: 25 mg; catalyst: 12 mg; solvent: 6 mL H_2O.

In MW reactor results, lower selectivity towards GBL and BDO was evident with increased production of propionic acid, propanol, butyric acid, and butanol compared to the conventional reactor. The selectivity to propionic acid increased from 12.9 % to 19.4 % with a concurrent decrease in selectivity to GBL from 47.6 % to 31.8 %. This indicates that the use of microwave reactor with any catalytic system, simultaneously increased unwanted hydrogenolysis products and decreased the carbon mass balance in which the decrease of GBL selectivity will lead to the lower BDO yield.

It must be mentioned here that using a microwave reactor increased the rate of the reaction tremendously compared to the conventional heating reactor (batch reactor). However, the C-C cleavage issue remains the same.

6.3.2.5. Effect of Ru-Sn Catalyst in Hydrogenation of Succinic Acid using MW

Due to the promising results that obtained in Chapter 4, after introducing tin to Ru/CNT, a series of Ru-Sn catalysts with different tin loading were tested again using MW reactor. As shown in **Figure 6.15**, the conversion of succinic acid decreased significantly from 100 % to 67.8 % and 24.5 % by increasing the Sn loading of the catalyst. Also, the carbon mass balance was greatly improved with increasing Sn loading, indicating that the formation of C-C cleavage products reduced.

Comparing the selectivity would be more valuable if we could do it at iso-conversion however, due to the speed of the reaction in a microwave reactor we could not. Nevertheless, 2 % Sn-based Ru catalysts showed the highest selectivity to GBL/BDO whereas Ru/CNT catalyst showed 0 % selectivity to GBL/BDO. 2% Sn-5% Ru/CNT showed high selectivity to GBL without much of C-C cleavage products, the possibility of producing BDO indeed would be high. However, the carbon mass balance is low in all bimetallic catalysts including 2% Sn-5% Ru/CNT for an unknown reason.

Therefore, at the end of the reaction, the yield of BDO may not be as high as being detected in Chapter 4 (~80 %), using the conventional heating reactor (Parr reactor).

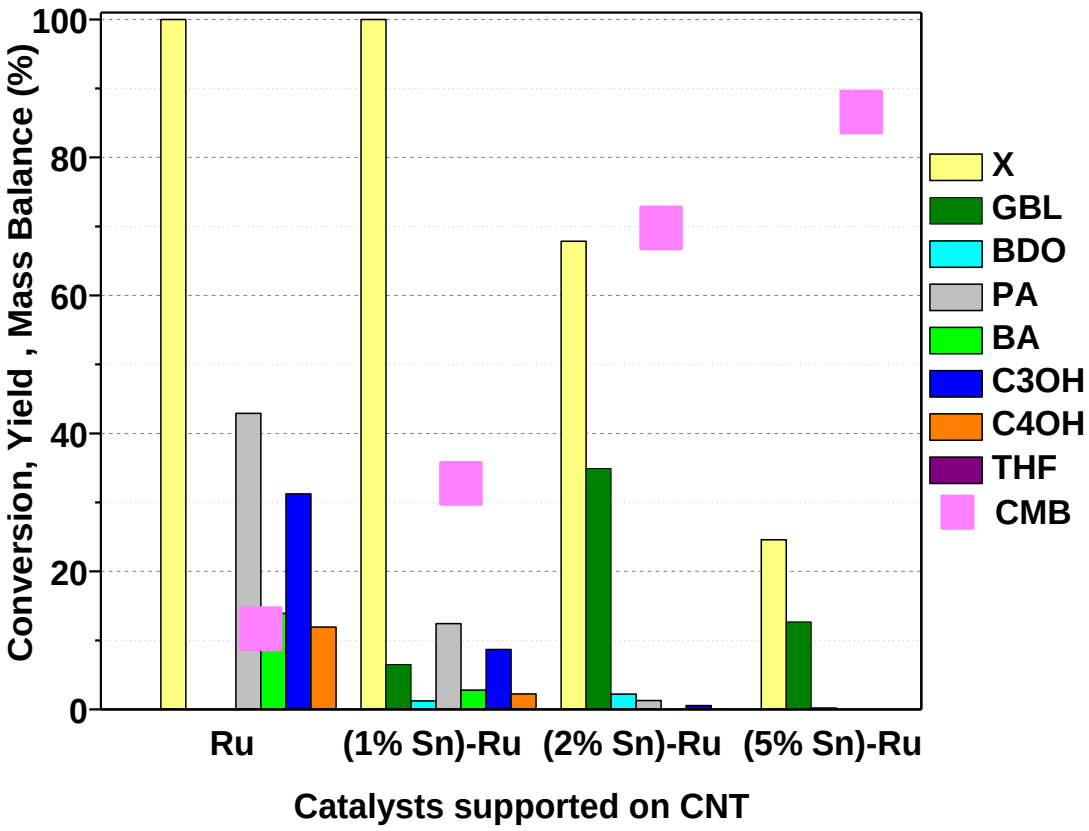

Figure 0.14. Comparison of the activity and selectivity with respect of Sn wt. in hydrogenation of succinic acid in MW. All catalysts have 5 wt. % of Ru. Reaction conditions: T: 170 °C; P: 50 bar; Time: 4h; succinic acid: 25 mg; catalyst: 12 mg; solvent: 6 mL H_2O.

In the microwave reactor, the reaction conditions were 170 °C and 50 bar whereas in the Parr reactor we used 200 °C and 70 bar. The lower hydrogen availability could also be one of the reasons for the low carbon mass balance since C-C bond cleavage activity decreased when the hydrogen pressure increased as shown in Chapter 3 (Section 3.3.2.3).

Another reason might be the differences in the operation of the two reactors such as the pressurizing step. In MW, the only way to pressurize the reactor first (at room temperature) and then start to heating which affects the final pressure. However, in the conventional heating reactor (Parr reactor), the hydrogen pressure was introduced after reaching the desired temperature.

Also, the cool down procedure was different between the two reactors. The microwave reactor includes a cool down unit which cools the reactor at the end of the reaction whereas a bowl of iced water was used to cool down the reaction in Parr reactor.

It should be noted that the results of using 5% Sn-5% Ru/CNT are promising too since C-C bond cleavage products might not appear at all and the selectivity to GBL should be high until the end of the reaction. Therefore, increasing the reaction time would be a solution to produce BDO latter from further hydrogenation of GBL using 5% Sn-5% Ru/CNT. However, the higher Sn loading (5 %) might also hinder the further hydrogenation of GBL to BDO as it has been shown in Chapter 4 using Parr reactor.

Once again 2% Sn-5% Ru/CNT proved to be the best catalyst to synthesise BDO, regardless of the reactor used.

6.3.2.6. Catalytic Hydrogenation of Levulinic Acid

To further validate the versatility of using the microwave reactor, a selective hydrogenation of levulinic acid was investigated. **Figure 6.16** summarises the catalytic hydrogenation results under 170 °C, 50 bar using three different monometallic catalysts supported on CNT. The highest activity was observed using Ru/CNT, as expected, where full conversion was reached within 1 minute of the reaction time, whereas by using Pt and Pd based catalysts the activity was lower, especially in the case of Pd/CNT.

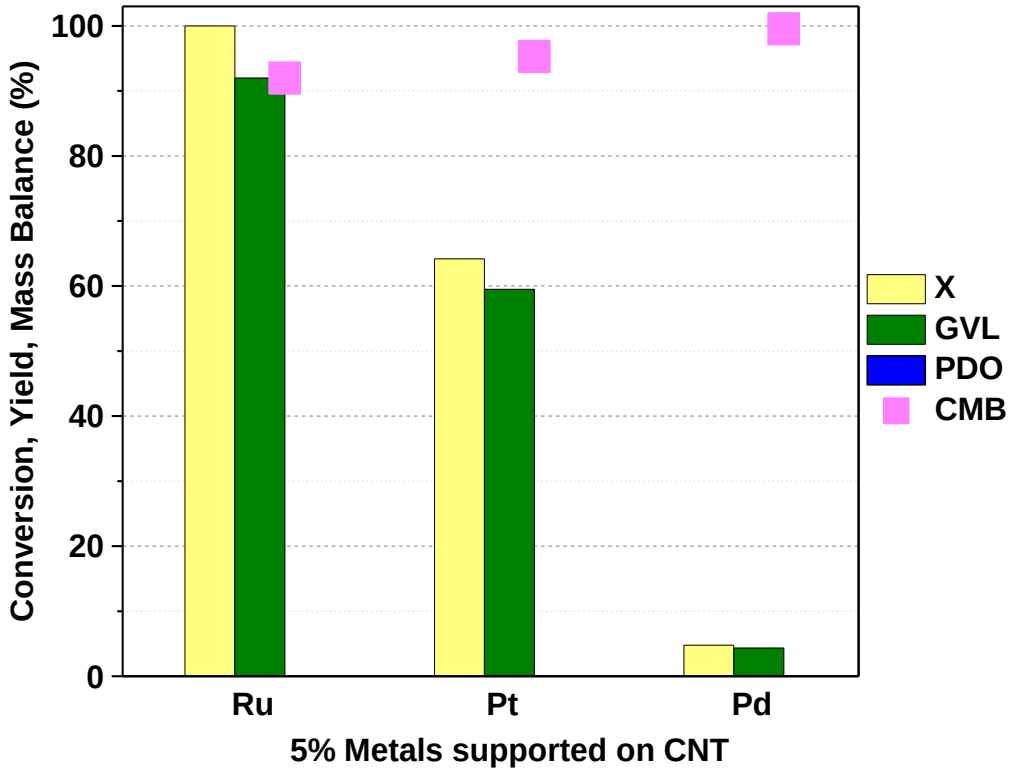

Figure 0.15. Comparison of the activity with respect of noble metals supported on CNT in hydrogenation of levulinic acid. Reaction conditions: T:170 °C; P: 50 bar; reaction time: 1 min; levulinic acid: 25 mg; catalyst: 12 mg; solvent: 6 mL H_2O.

6.4. Conclusions

A MW reactor was employed for several different catalysts to hydrogenate succinic acid and levulinic acid, giving promising results. The hydrogenation of succinic acid was performed over activated carbon, silica, alumina, and carbon nanotube supported Ru Pd, Pt, and Re catalysts in a microwave reactor.

Catalysts supported on carbon nanotubes gave high conversion compared to using other supports however, Ru/CNT provided full conversion at 150 °C and 50 bar hydrogen pressure in a very short reaction time <3.5 h, in comparison with any other catalyst in the microwave or conventional reactor (pressure autoclave). The same level of conversion was achieved in the half of reaction time, compared to the conventional reactor.

The reaction rate increased enormously at the same reaction temperature using a microwave compared to conventional reactor which might attributed to the presence of hotspots in the used catalyst. The high performance of Ru supported on CNTs may be explained by a combination of the superior porosity of CNTs and the electronic promotion.

There is no benefit to using a microwave in the hydrogenation of succinic acid regarding the decreasing the C-C cleavage. The product distribution was the same as observed using a conventional reactor; with no improvement in stopping the C-C bond cleavage activity.

2% Sn-5% Ru/CNT was also tested which was the best catalyst amongst the series of Ru-Sn/CNT towards the hydrogenation of succinic to BDO as shown in Chapter 4. However, the low yield of desired products, i.e., GBL/BDO using the microwave reactor compared to the conventional heating reactor (Parr reactor) might be because of the different reaction conditions along with different operation sequences such as the pressurising and a cooling down the process.

1 min reaction time at 170 ˚C and 50 bar H_2 pressure using 5% Ru/CNT in MW reactor was sufficient for the hydrogenation of levulinic acid to gamma-valerolactone. Further investigation is needed to show the advantages and exquisiteness of using an efficient, fast, safe, and easily-operated reactor especially for levulinic acid.

These results open a promising path for the enlargement of new MW catalytic reaction technologies to transform biomass components greenly and economically, which saves much more than time. The combination of microwave as a reactor and Ru supported on carbon nanotubes (excellent catalyst) has the potential to be an excellent option for the selective hydrogenation of succinic acid.

CHAPTER 7

Conclusions and Outlook

Chapter 7. Conclusions and Outlook

7.1. Conclusions

Hydrogenation of succinic acid is not an easy reaction to accomplish because of that most of the work in the literature had done at high reaction conditions and using an organic solvent instead of a green solvent such as a water. For that reason, the main objective of this study was to develop catalytic systems to improve reaction rates for the hydrogenation of succinic acid in water at mild reaction condition but also to find promoters to affect the catalyst activity so that selectivity to 1,4-butanediol can be achieved.

We focused on the hydrogenation of biomass-derived C4-C6 acids, performing all the catalytic reactions in an aqueous phase to meet the criteria of green chemistry. Initially, the results described in the current thesis contribute to a better understanding of the various factors persuading altering the catalyst performance in the hydrogenation of succinic acid. We investigated several factors that could influence the activity and selectivity, i.e., reaction temperatures, pressures, supports, type of metallic catalyst (mono-/bimetallic), different noble metals, the wt. % of the metal, metallic dispersion, the catalyst porosity, type of reactors (conventional, microwave).

Regarding the activity (conversion), the hydrogenation of succinic acid proceeded faster using Ru catalyst supported on CNT compared to AC in pressure autoclave (conventional heating reactor). 5% Ru/CNT efficiently converted 95.4 % succinic acid in 11 hours at 150 °C and 50 bar H_2 pressure.

It should be noted that when we tested the analogous catalysts supported on carbon nanotubes, we observed an increase in conversion for all three metals (Pd, Pt, Re) as compared to the use of activated carbon or Al_2O_3. This remarkable result emphasises the promotional effect that CNTs produce in hydrogenating catalysts for carboxylic acids.

Apart from the superior porosity of CNTs, the XPS results enable us to suggest that this enhanced performance of all noble metals supported on CNTs can be explained by the electronic promotion of carbon nanotubes.

We observed that as reaction temperature was raised the conversion of succinic acid increased. The rate of the reaction increased dramatically at 240 °C, however, we could not achieve high selectivity for a single product due to the C-C bond cleavage. On the other hand, increasing hydrogen pressure up to 50 bar has a positive impact on the reaction rate and selectivity for alcohol products. The optimal operating temperature and pressure were 150 °C, and 50 bar respectively; the catalysts function poorly below these parameters whereas increasing the reaction temperature reduces selectivity to the desired product.

We examined the effect of washing the carbon nanotube with water during the hydrogenation of succinic acid. Ru/unwashed-CNT showed a lower Ru dispersion and therefore lower catalytic activity. The washing step led to produce more active Ru based catalyst for the hydrogenation of succinic acid.

We prepared Ru/CNT and all other catalysts by an incipient wetness impregnation method. TEM results of Ru/CNT showed that the Ru particles are located inside and outside of the CNTs. One of the Ru catalysts was prepared to confine the Ru particles inside the CNT, Ru(IN)CNT, following a literature procedure. Ru(IN)CNT showed less catalytic activity compared to Ru/CNT. This result was expected since the dispersion of Ru/CNT is 2-fold higher compared to Ru(IN)/CNT. At the same level of conversion, no significant influence on the products distribution was observed for the two catalysts Ru(IN)/CNT and Ru/unwashed-CNT compared to Ru/CNT (washed CNT, Ru located inside/outside of the carbon nanotube).

The high dispersion and availability of the metal play a significant role to enhance the activity. Therefore, Ru/CNT activity increased as the loading of Ru on CNTs was increased 10 % Ru/CNT exhibited the highest active catalyst compared to 1, 3, 5, and 7 wt. %. 5% Ru /CNT nevertheless showed better selectivity towards alcohol products.

The hydrogenation of succinic acid was performed again in a microwave using Ru, Pd, Pt, and Re catalysts over other supports (silica, alumina) in addition to AC and CNTs. The rate of the reaction increased tremendously using the microwave reactor since the same level of conversion was achieved in half of the reaction time, compared to the conventional reactor, possibly due to the existence of ‘‘hot spots’’ in samples. The activation energy decreased using microwave reactor from 111 kJ mol^{-1} (conventional reactor) to 59.8 kJ mol^{-1}. The hydrogenation of SA is much easier in a microwave reactor than in a conventional reactor because of the lower activation energy.

Amongst all catalytic systems in the microwave chapter (Chapter 6), Ru based catalysts again showed better activity compared to the other noble metals Pt, Pd, and Re. We found the overall reactivity order to be Ru>>Pt>Pd, no matter which support was used. We showed the effect of using different support for Ru catalysts in the hydrogenation of succinic acid. CNT proved to be the best support for all noble metal including Ru catalysts. In the microwave chapter, the conversion of succinic acid increased using Ru/CNT to 86 % from 43 % with Ru/AC, 74 % with Ru/Al_2O_3 and 16 % with Ru/SiO_2.

The pore size of the catalyst has a huge influence on the catalytic activity. 5% Ru/CNT has a higher pore size than other catalysts which might be the reason for the high activity. N_2-physisorption results showed higher pore size of Ru/CNT (15.7 nm) in comparison to Ru/Al_2O_3 (8.23 nm) and Ru/AC (4.94 nm) which could contribute to the significant increase in activity between these catalysts.

Regarding the selectivity, Ru/CNT showed low selectivity for BDO in a conventional reactor due to its high C-C cracking ability as mentioned in the literature. Ru/CNT gives ~40 % combined yield of alcohols (1, 4-butanediol, n-propanol and n-butanol).

In the MW results, the C-C bond cleavage problem remained the same although the yield drops to 18.2 %. The use of a MW reactor simultaneously increased unwanted hydrogenolysis products and decreased the carbon mass balance. Increasing the yield for BDO is more desirable, and this issue has been tackled using tin a promoter in this thesis.

We developed Ru-Sn catalysts to attain high selectivity to the hydrogenation of carbonyl group and reduce C-C cleavage. Initially, 150 °C, 50 bar as reaction conditions were not sufficient for the hydrogenation of succinic acid. Therefore, we had to increase them to 200 °C and 70 bar.

The catalytic behavior of monometallic ruthenium catalysts supported on carbon nanotubes and active carbon changed after incorporation of tin. Based on the loading of Sn and Ru catalysts supported on the carbon nanotube, the catalytic activity decreased remarkably since the full conversion of succinic acid using 1% Sn-5% Ru/CNT required 8 h reaction time. Within an hour ~100 % conversion was achieved using 5% Ru/CNT and only 4 % selectivity for BDO was accomplished due to the high cracking ability of Ru catalyst. After introducing 1% Sn, the selectivity increased up to ~45 % (23 h reaction time). The selectivity for BDO increased as increasing the Sn wt. % (1 %, 1.5 %, and 2 %) and then decreased again using 2.5% and 5% Sn. 2% Sn-5%Ru/CNT was optimum to accomplish ~80 % selectivity for BDO whereas 5% Sn-5% Ru/CNT was selective to GBL. The selectivity to BDO could be accomplished using the 5% Sn-5% Ru/CNT. However, it might need longer reaction time.

We hypothesised that Ru-Sn alloy started forming on CNT where the Sn loading was <2. However, at low Sn loadings there are still Ru free particles which are active to C-C bond cleavage. Our results suggested that the Ru-Sn samples where the Sn loading is ≥2 the formation of Ru-Sn alloy is complete, and no Ru is free.

Alloyed particles are more selective for BDO, i.e. they are active for carbonyl reduction without performing C-C bond cleavage that resulted in increasing the selectivity to BDO.

5% Sn-5% Ru/CNT showed low selectivity for BDO not because of C-C cleavage, but because GBL was not hydrogenated further to BDO. This is perhaps due to the excess of Sn, which blocks the active sites and suppresses the catalytic activity, which affects the conversion to BDO. Thus, the optimal loading of Sn in Ru/CNT to maximize the selectivity for BDO is very significant.

Due to the high surface area of activated carbon, we prepared **2% Sn**-5% Rn catalysts supported on AC hoping that the reaction rate would increase. However, **2% Sn**-5% Rn/CNT showed better activity and selectivity for the hydrogenation of succinic acid to BDO compared to **2% Sn**-5% Rn/**AC**. The BDO selectivity decreased from 84 % to 50 % using **2% Sn**-5% Rn/ **AC**.

This unique selectivity to diols using **2% Sn**-5% Rn/CNT might be due to the successful formation of a new type of active site, most likely Ru-Sn alloy on CNT. Further investigations are however needed using other techniques which are currently underway to elucidate the exact role of tin in the bimetallic catalysts.

2% Sn-5% Ru/CNT proved to be a promising catalyst for the hydrogenation of other biomass-derived acids (levulinic acid, and cis,cis-muconic acid) besides succinic acid to their lactones and diols. We have achieved 83 %, 55 %, and 88 % yield for 1,4-butanediol, 1,4-pentanediol, and 1,6-hexanediol from hydrogenation of succinic acid, levulinic acid, and cis,cis-muconic acid respectively.

7.2. Future Work

Despite the strong evidence collected in this thesis, further characterization is needed to elucidate the precise structure and composition of the Ru-Sn alloys on CNT, which would be simultaneously beneficial to explain the precise role of tin in bimetallic ruthenium catalysts.

All the bimetallic catalysts in this current study were prepared by simple incipient wetness impregnation method, which is limited to control the structural parameters. Hence, other preparation methods should be applied for trying to make the catalyst more active.

Finding another type of carbon for Ru catalyst, which has high surface area and high pore size to be competitive with CNT, is highly attractive since the latter's pore size was one of the important features in the performance of the catalyst in hydrogenation of acids.

Doping of CNTs with some elements such as F and N has been investigated in the literature.[344] The electronic properties of the catalytic support could be enhanced by doping an electron-rich atom.[345] Nitrogen is the most common dopant used to modify the performance of CNT.[19] Nitrogen doping of the CNT support enhances the catalytic activity of Ru catalyst in the ammonia decomposition reaction by electronically modifying the ruthenium active sites. It has been observed as well during the cinnamaldehyde hydrogenation by enhancing Pd catalyst.[346] In this context, we could hydrogenate the succinic acid using the best catalysts (5% Ru/CNT) or (2% Sn-5% Ru/CNT) from this study, only after doping one of those elements with CNT to further enhance the activity of the catalyst, since there is no literature background.All the bimetallic catalysts in this current study were prepared by simple incipient wetness impregnation method, which is limited to control the structural parameters. Hence, other preparation methods should be applied to make the catalyst more active.

CHAPTER 8

Chapter 8. Appendix

Chapter 2

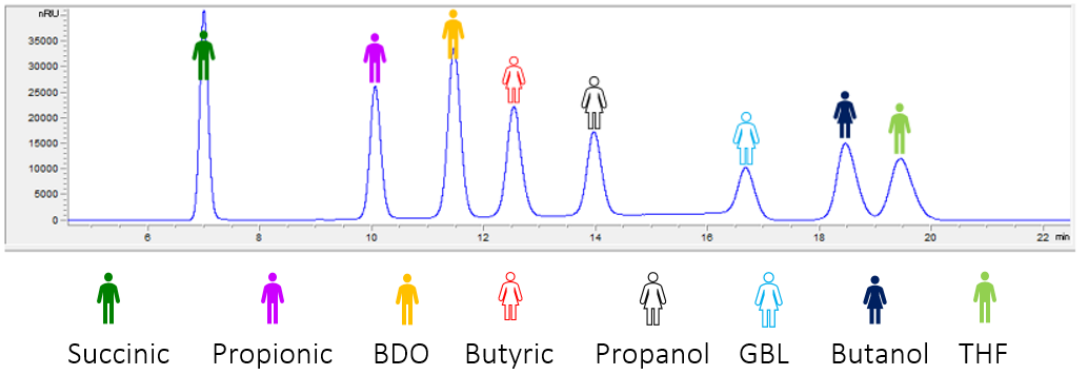

Figure 0.1. Typical HPLC chromatogram for succinic acid hydrogenation

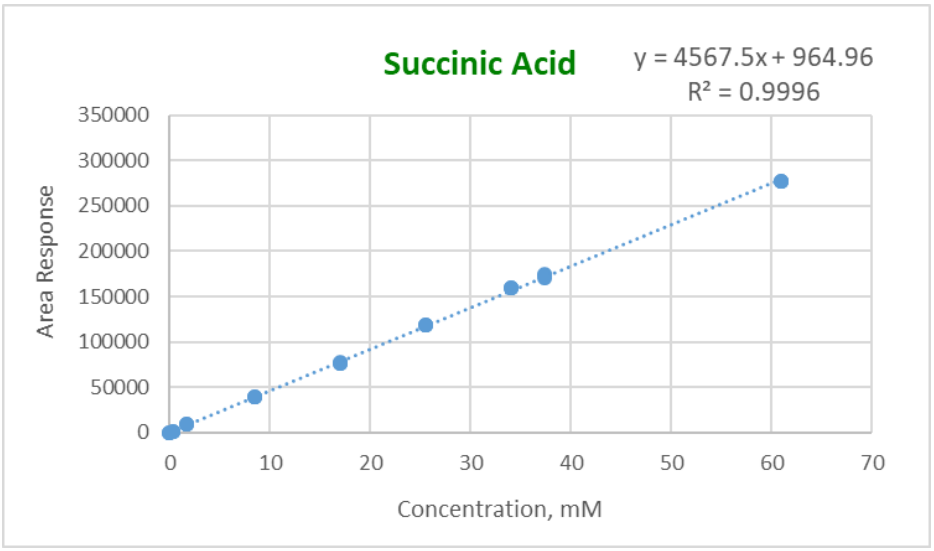

Figure 0.2. Calibration plot for succinic acid

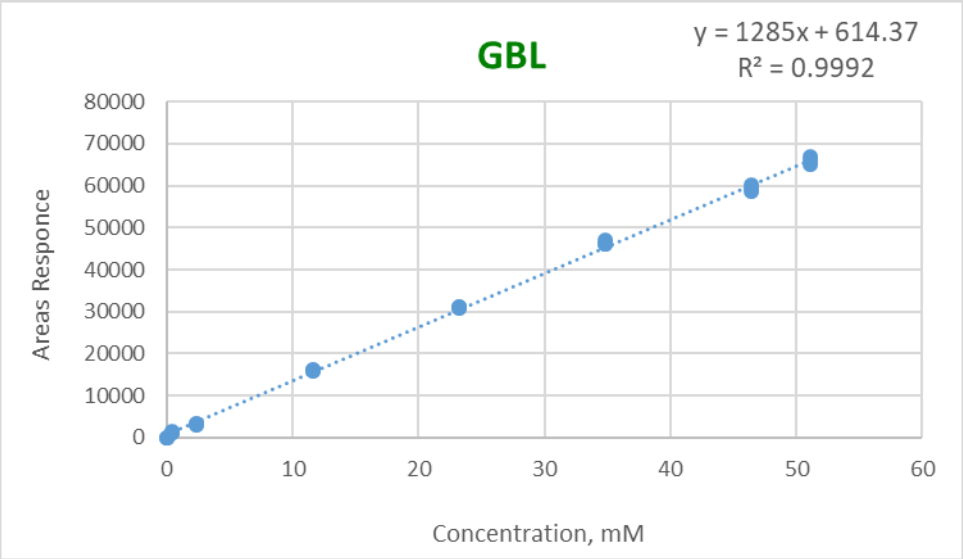

Figure 0.3. Calibration plot for gamma-butyrolactone (GBL)

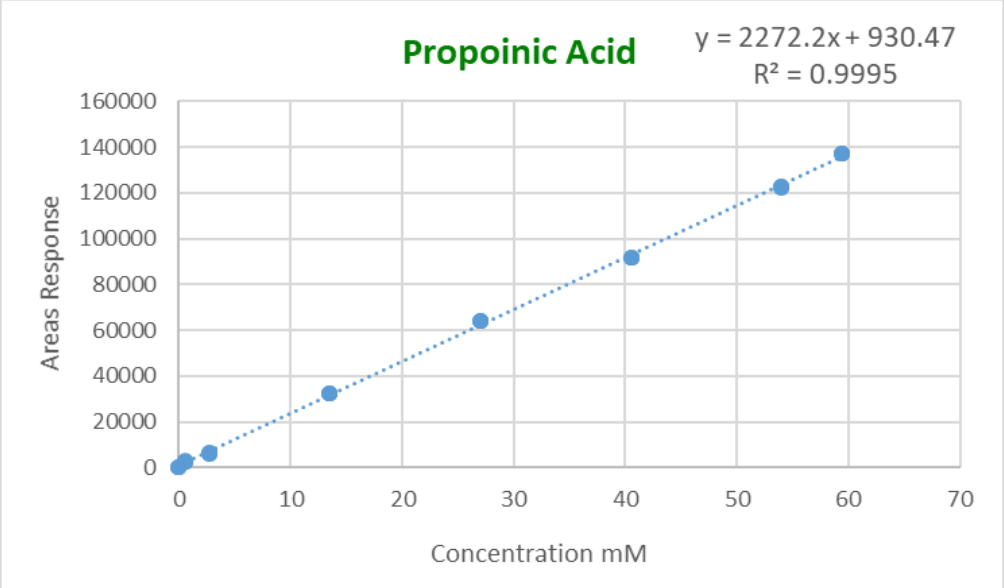

Figure 0.4. Calibration plot for *propionic acid.*

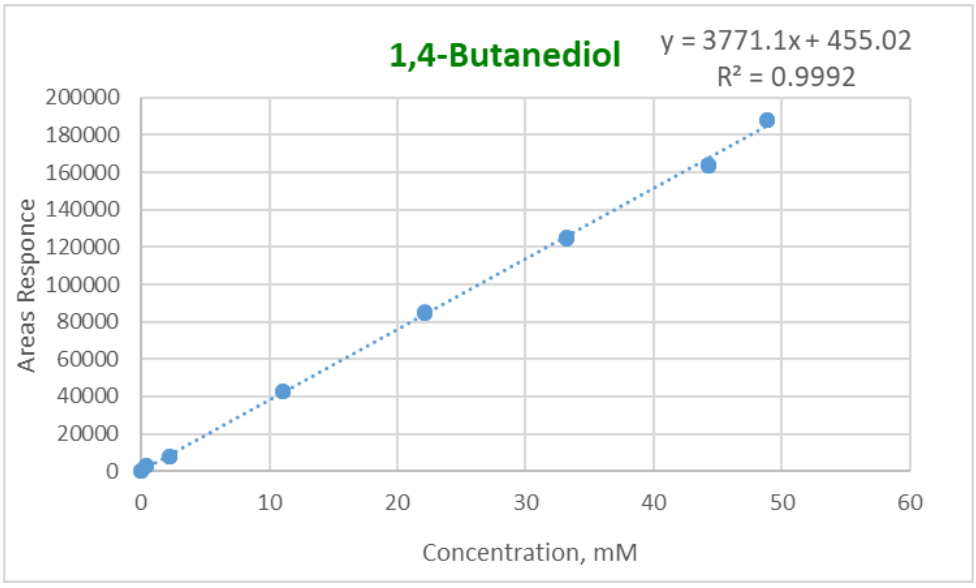

Figure 0.5. Calibration plot for *1,4-butanediol*

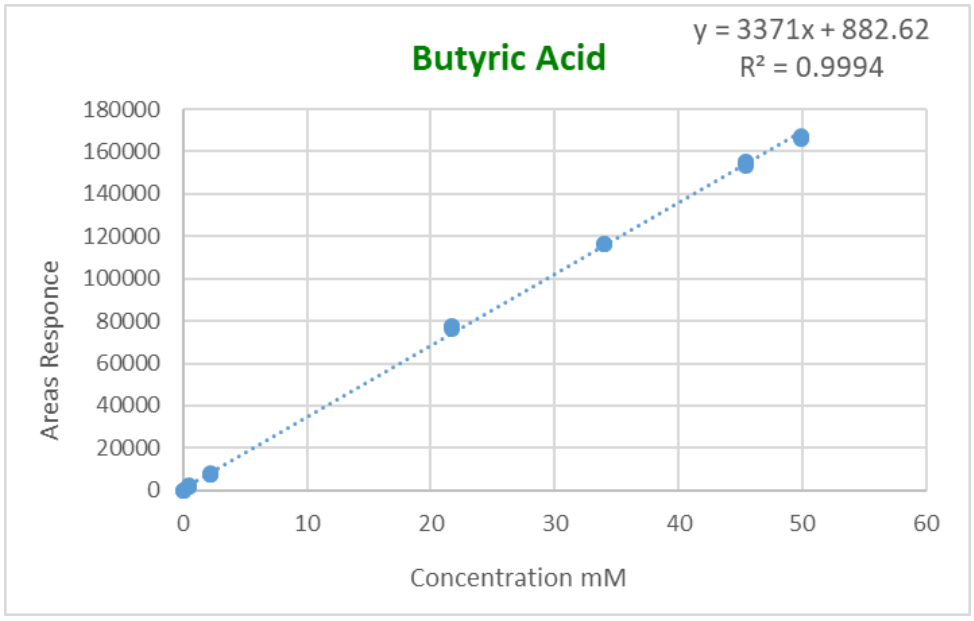

Figure 0.6. Calibration plot for butyric acid

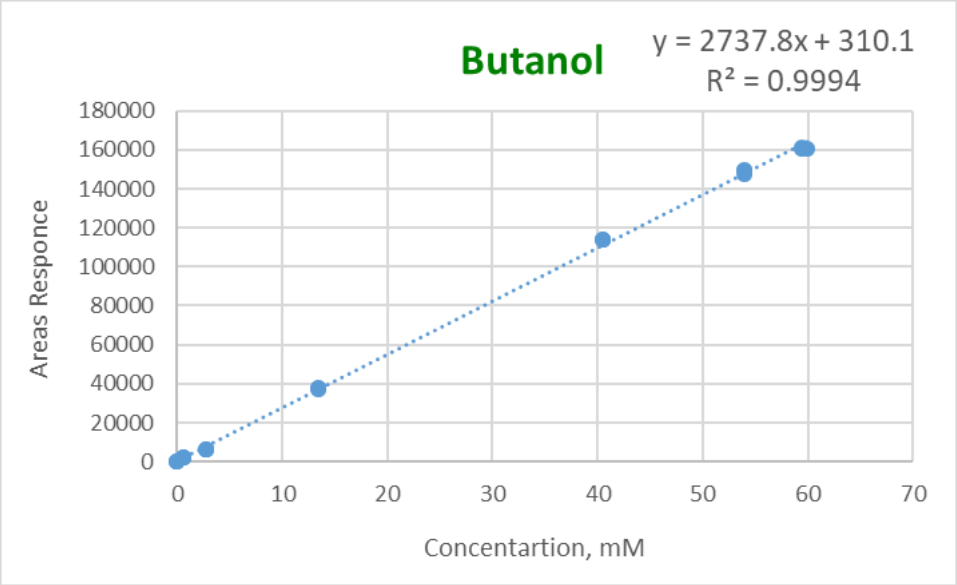

Figure 0.7. Calibration plot for butanol

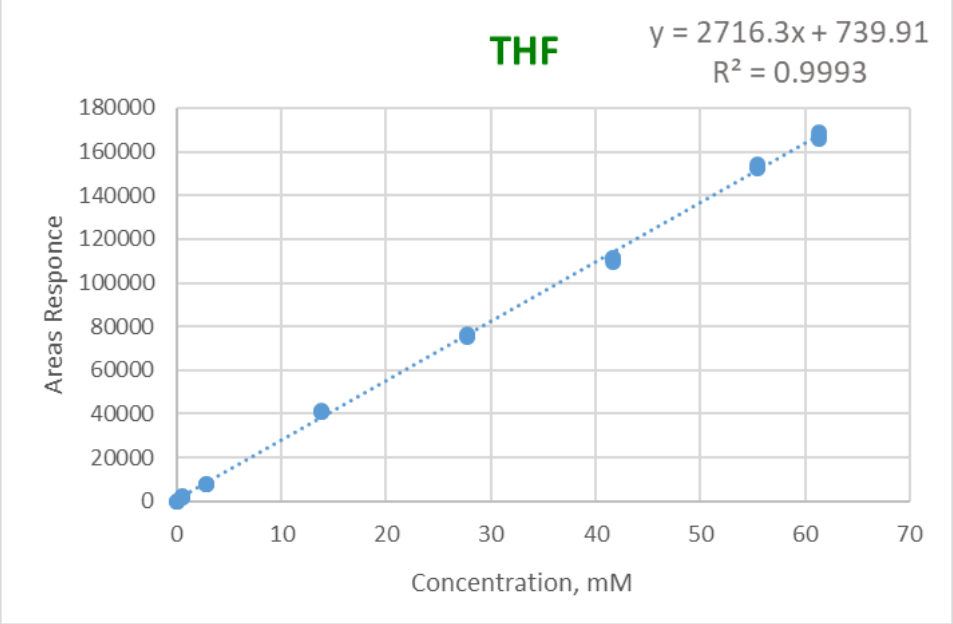

Figure 0.8. Calibration plot for butanol

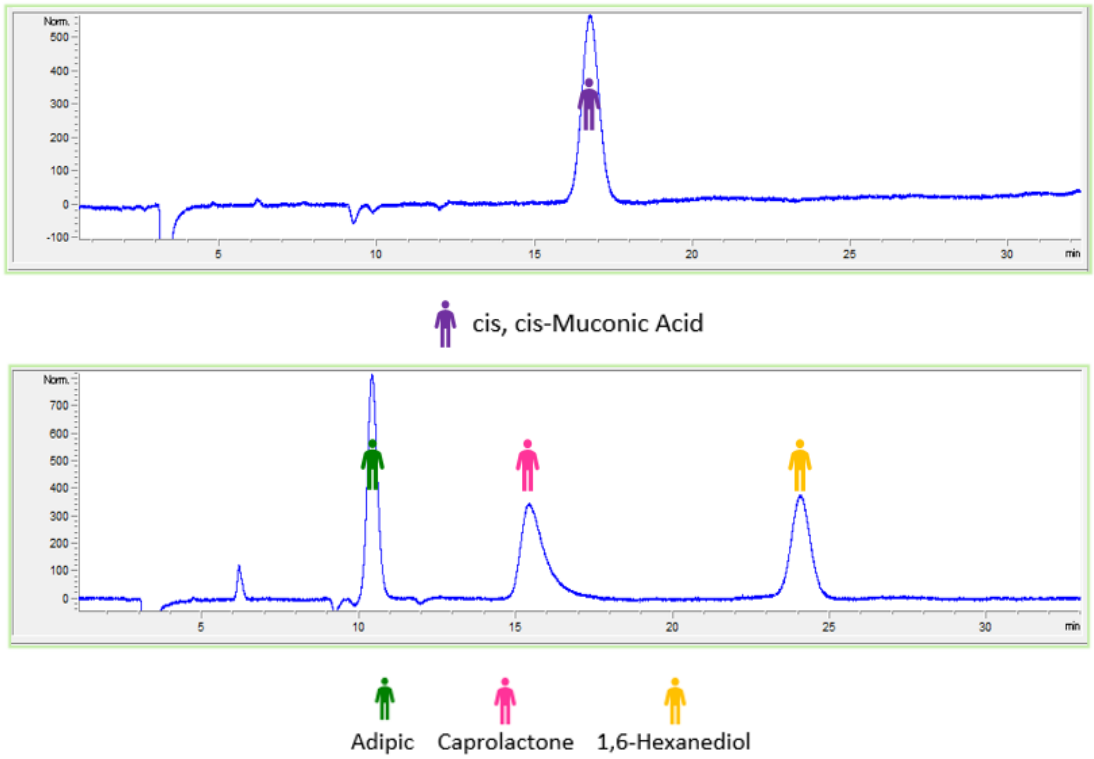

Figure 0.9. Typical HPLC chromatogram for cis,cis-muconic acid hydrogenation

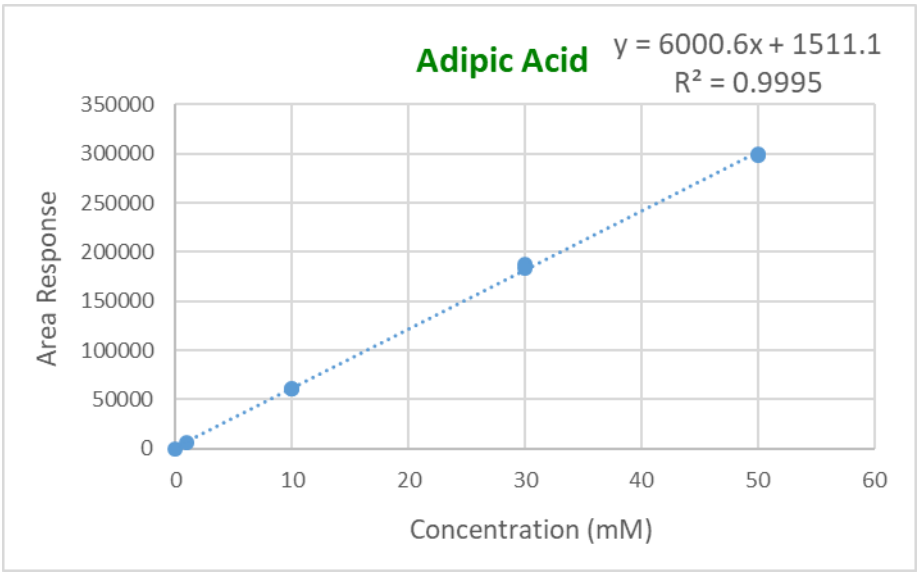

Figure 0.10. Calibration plot for adipic acid

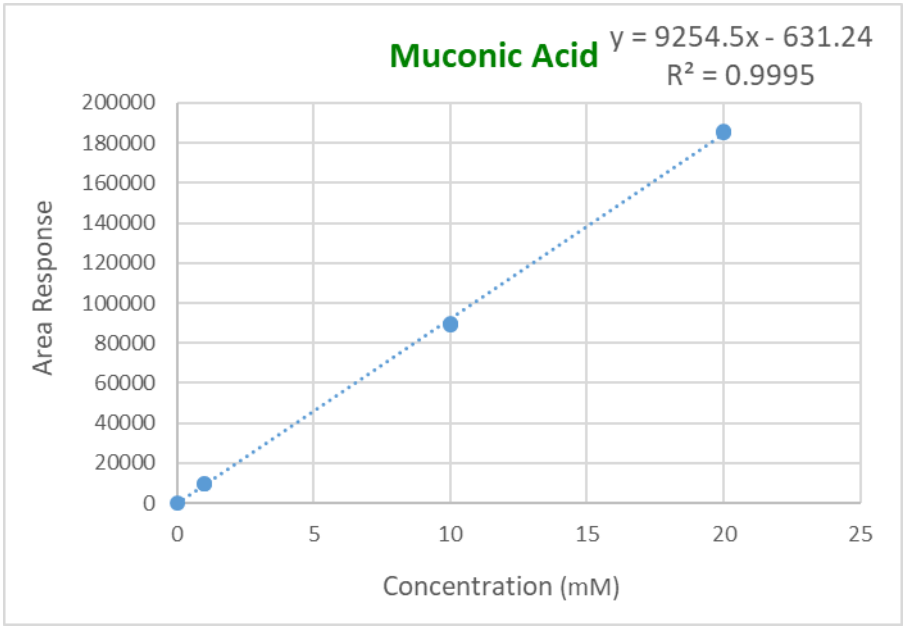

Figure 0.11. Calibration plot for cis,cis-muconic acid

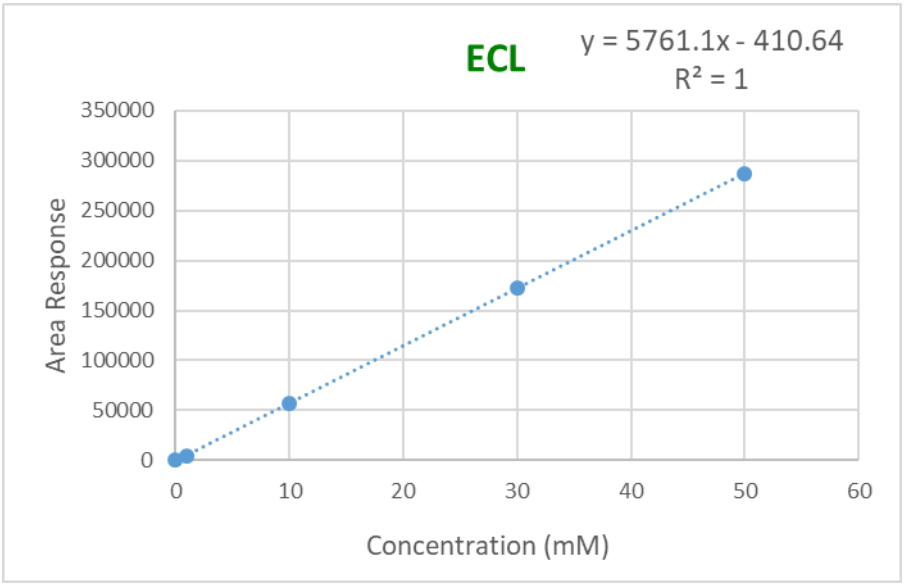

Figure 0.12. Calibration plot for caprolacton (ECL)

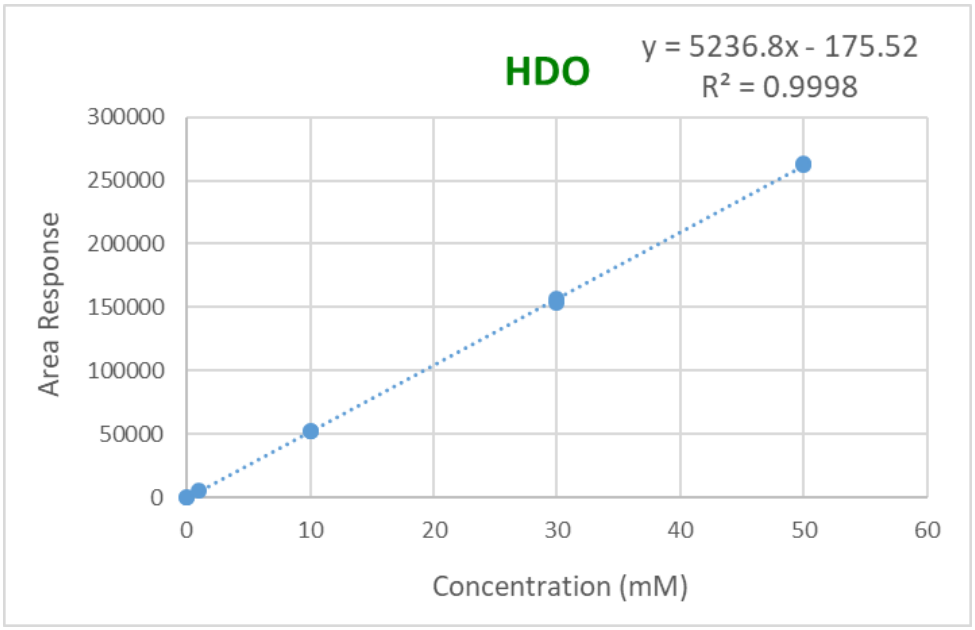

Figure 0.13. Calibration plot for 1,6-hexanediol (HDO)

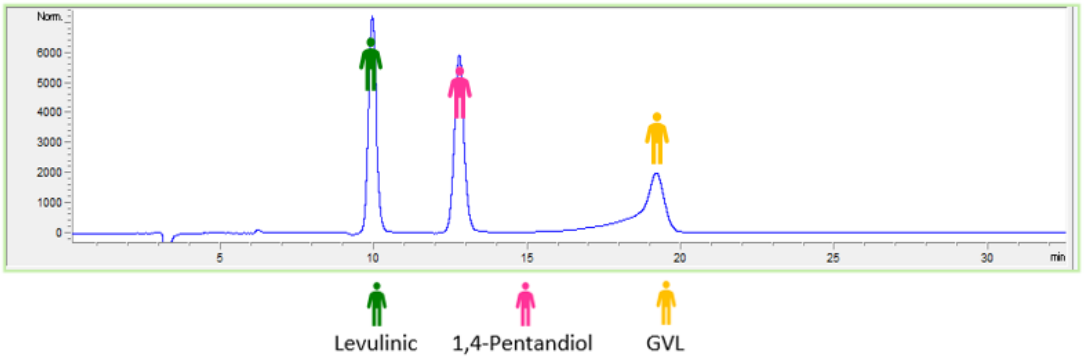

Figure 0.14. Typical HPLC chromatogram for levulinic acid hydrogenation

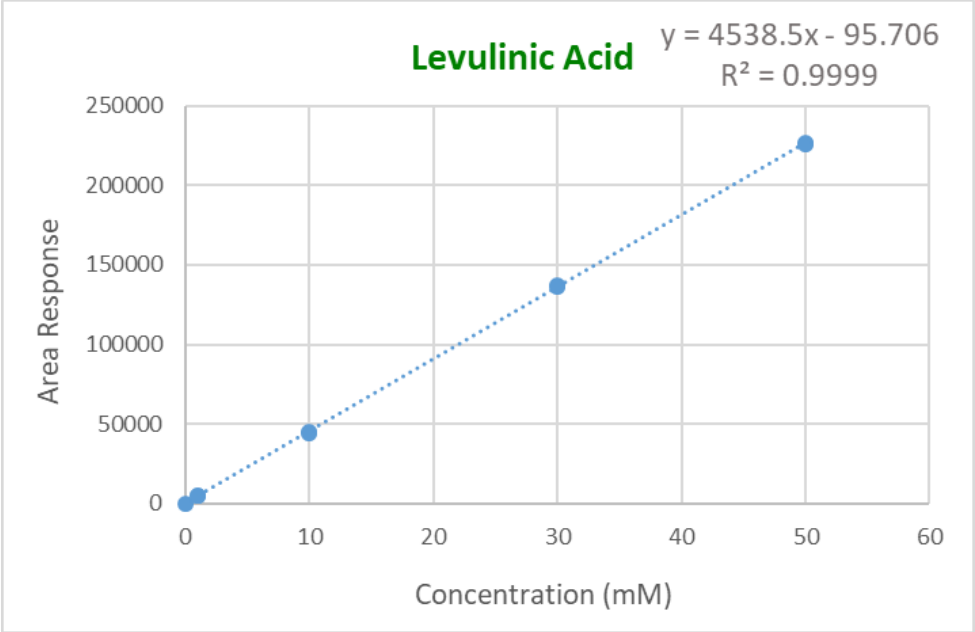

Figure 0.15. Calibration plot for levulinic acid

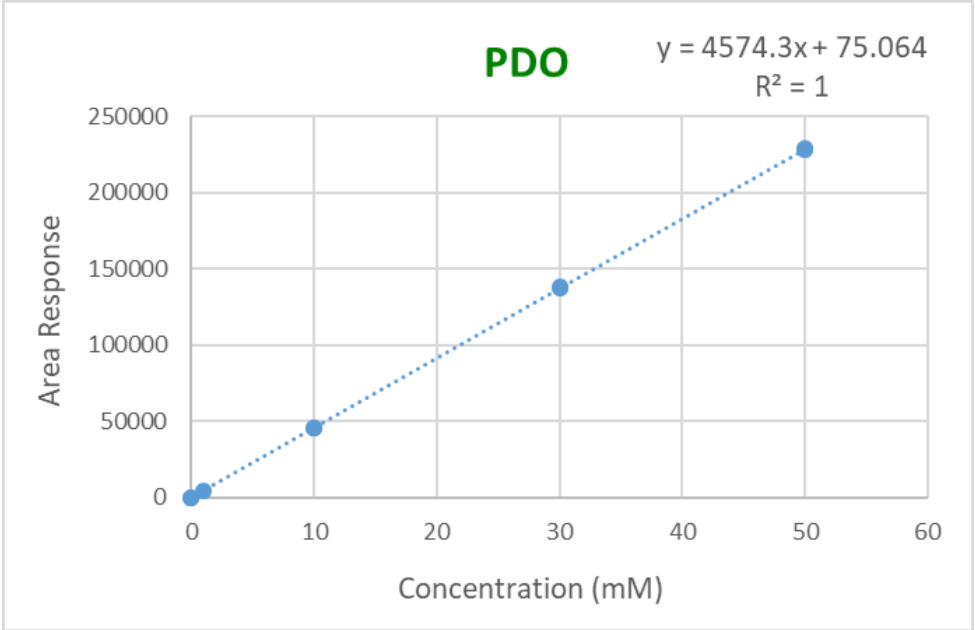

Figure 0.16. Calibration plot for 1,4-pentanediol (PDO)

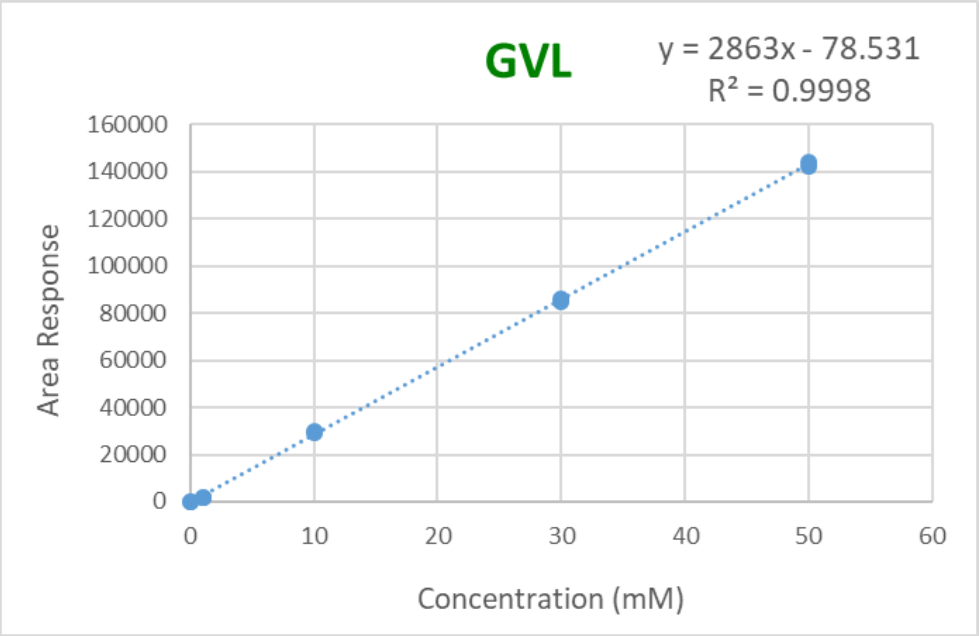

Figure 0.17. Calibration plot for gamma-valerolacton (GVL)

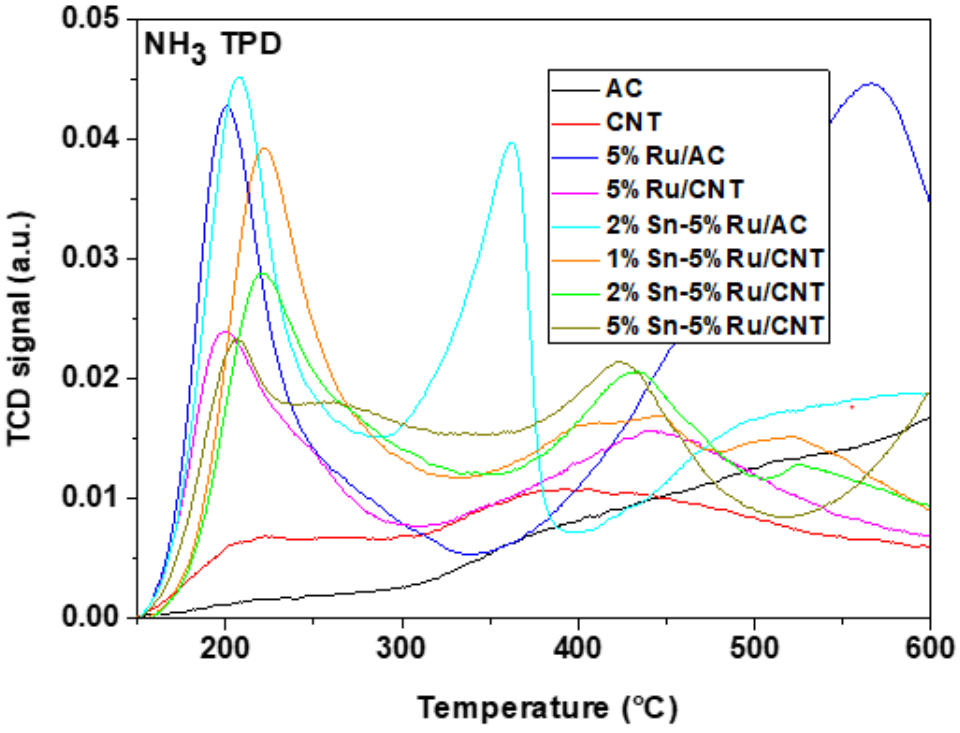

Figure 0.18.Profiles of the temperature programmed desorption of NH_3 for different Ru based catalysts.

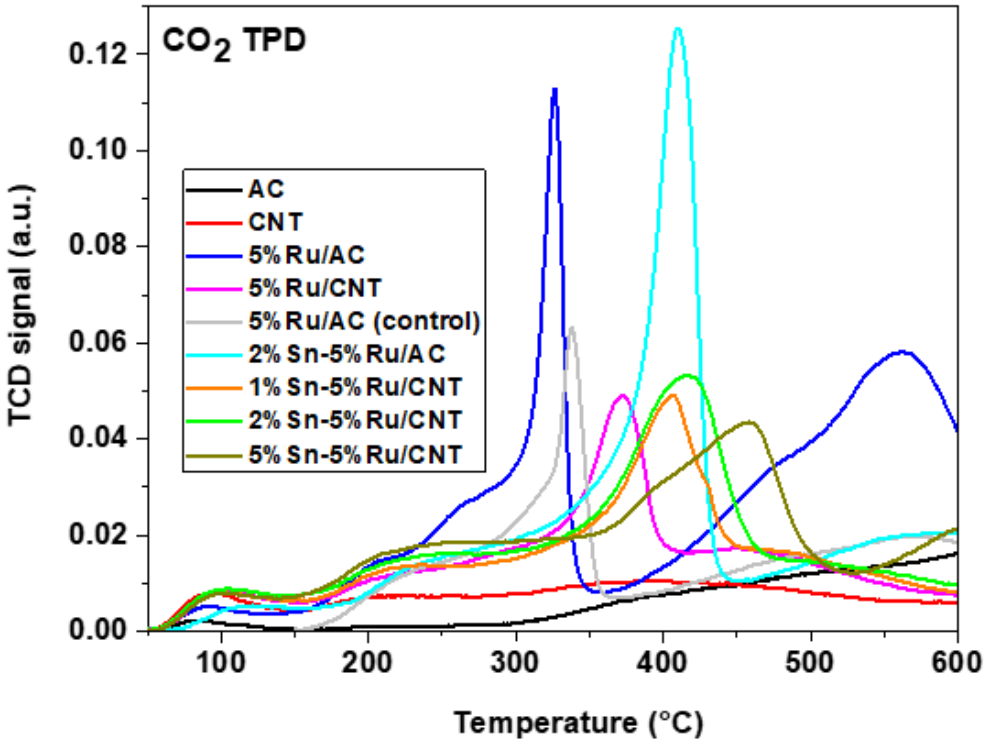

Figure 0.19. Profiles of the temperature programmed desorption of CO_2 for different Ru based catalysts. Control experiment in CO_2 desorption was carried out completely under He instead of CO_2.

Only peaks below 400 °C were considered due to the fact that catalysts were treated only at this temperature and at higher temperatures, other gaseous products apart from carbon dioxide or ammonia as described in the experimental section. Moreover, the intense peaks in CO_2 TPD between 250-420 °C for catalysts were excluded as the same peaks were found in control experiments where CO_2 adsorption was substituted with He.

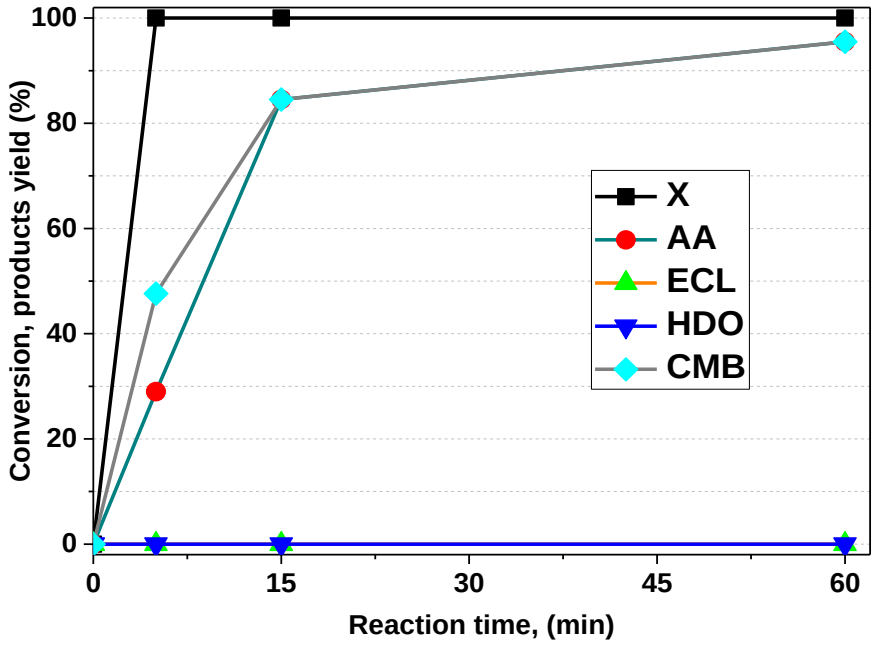

Figure 0.20. Time online reaction of ccMA hydrogenation with 1% Ru/AC. Reaction conditions: catalyst (0.025 g), ccMA (0.05 g) solvent (25 mL), H_2 pressure (10 bar), Temperature (80 °C). Legends: Conversion (X)-(black), yield to adipic acid (AA)-(green), epsilon-caprolactone (ECL)-(orange), 1,6-hexanediol (HDO)-(blue), carbon mass balance (CMB)-(gray).

Chapter 9. References

(1) Roberts, M. Birth of the catalytic concept (1800-1900). *Catalysis Letters* **2000**, *67*, 1-4.

(2) Deutschmann, O.; Knözinger, H.; Kochloefl, K.; Turek, T.: Heterogeneous Catalysis and Solid Catalysts. In *Ullmann's Encyclopedia of Industrial Chemistry*; Wiley-VCH Verlag GmbH & Co. KGaA, 2000.

(3) Hattori, H. Heterogeneous Basic Catalysis. *Chemical Reviews* **1995**, *95*, 537-558.

(4) Energy profile diagrams. http://emobiledesignwallh.gq/files/images/energy-profile-diagrams.html?page=5# (accessed 05 12 2017.

(5) Osorio-Vargas, P.; Flores-González, N. A.; Navarro, R. M.; Fierro, J. L. G.; Campos, C. H.; Reyes, P. Improved stability of Ni/Al2O3 catalysts by effect of promoters (La2O3, CeO2) for ethanol steam-reforming reaction. *Catalysis Today* **2016**, *259, Part 1*, 27-38.

(6) Garibyan, T.; Margolis, L. Y. Heterogeneous-Homogeneous Mechanism of Catalytic Oxidation. *Catalysis Reviews—Science and Engineering* **1989**, *31*, 355-384.

(7) Lin, Y.-C.; Huber, G. W. The critical role of heterogeneous catalysis in lignocellulosic biomass conversion. *Energy & Environmental Science* **2009**, *2*, 68-80.

(8) Pirkanniemi, K.; Sillanpää, M. Heterogeneous water phase catalysis as an environmental application: a review. *Chemosphere* **2002**, *48*, 1047-1060.

(9) Ross, J. R. H.: Chapter 6 - The Kinetics and Mechanisms of Catalytic Reactions. In *Heterogeneous Catalysis*; Ross, J. R. H., Ed.; Elsevier: Amsterdam, 2012; pp 123-142.

(10) Bartholomew, C. H.; Farrauto, R. J.: *Fundamentals of industrial catalytic processes*; John Wiley & Sons, 2011.

(11) Greeley, J. P. Active Site of an Industrial Catalyst. *Science* **2012**, *336*, 810-811.

(12) Mäki-Arvela, P.; Hájek, J.; Salmi, T.; Murzin, D. Y. Chemoselective hydrogenation of carbonyl compounds over heterogeneous catalysts. *Applied Catalysis A: General* **2005**, *292*, 1-49.

(13) Twigg, M. V.; Spencer, M. S. Deactivation of supported copper metal catalysts for hydrogenation reactions. *Applied Catalysis A: General* **2001**, *212*, 161-174.

(14) Yu, W.; Porosoff, M. D.; Chen, J. G. Review of Pt-based bimetallic catalysis: from model surfaces to supported catalysts. *Chemical reviews* **2012**, *112*, 5780-5817.

(15) Long, N. V.; Hien, T. D.; Asaka, T.; Ohtaki, M.; Nogami, M. Synthesis and characterization of Pt–Pd nanoparticles with core-shell morphology: Nucleation and overgrowth of the Pd shells on the as-prepared and defined Pt seeds. *Journal of Alloys and Compounds* **2011**, *509*, 7702-7709.

(16) Persson, K.; Jansson, K.; Järås, S. G. Characterisation and microstructure of Pd and bimetallic Pd–Pt catalysts during methane oxidation. *Journal of Catalysis* **2007**, *245*, 401-414.

(17) Narui, K.; Yata, H.; Furuta, K.; Nishida, A.; Kohtoku, Y.; Matsuzaki, T. Effects of addition of Pt to PdO/Al 2 O 3 catalyst on catalytic activity for methane combustion and TEM observations of supported particles. *Applied Catalysis A: General* **1999**, *179*, 165-173.

(18) Yang, Y.; Chiang, K.; Burke, N. Porous carbon-supported catalysts for energy and environmental applications: A short review. *Catalysis Today* **2011**, *178*, 197-205.

(19) Mabena, L. F.; Sinha Ray, S.; Mhlanga, S. D.; Coville, N. J. Nitrogen-doped carbon nanotubes as a metal catalyst support. *Applied Nanoscience* **2011**, *1*, 67-77.

(20) Matatov-Meytal, Y. I.; Sheintuch, M. Catalytic abatement of water pollutants. *Industrial & engineering chemistry research* **1998**, *37*, 309-326.

(21) Fuente, A. M.; Pulgar, G.; González, F.; Pesquera, C.; Blanco, C. Activated carbon supported Pt catalysts: effect of support texture and metal precursor on activity of acetone hydrogenation. *Applied Catalysis A: General* **2001**, *208*, 35-46.

(22) Auer, E.; Freund, A.; Pietsch, J.; Tacke, T. Carbons as supports for industrial precious metal catalysts. *Applied Catalysis A: General* **1998**, *173*, 259-271.

(23) Hong, U. G.; Kim, J. K.; Lee, J.; Lee, J. K.; Song, J. H.; Yi, J.; Song, I. K. Hydrogenation of succinic acid to tetrahydrofuran (THF) over ruthenium–carbon composite (Ru–C) catalyst. *Applied Catalysis A: General* **2014**, *469*, 466-471.

(24) Biniwale, R. B.; Kariya, N.; Ichikawa, M. Dehydrogenation of cyclohexane over Ni based catalysts supported on activated carbon using spray-pulsed reactor and enhancement in activity by addition of a small amount of Pt. *Catalysis Letters* **2005**, *105*, 83-87.

(25) CHAPTER 1 Carbon (Nano)materials for[space]Catalysis. In *Nanostructured Carbon Materials for Catalysis*; The Royal Society of Chemistry, 2015; pp 1-45.

(26) Ross, J. R.: *Heterogeneous catalysis: fundamentals and applications*; Elsevier, 2011.

(27) Oosthuizen, R.; Nyamori, V. Carbon nanotubes as supports for palladium and bimetallic catalysts for use in hydrogenation reactions. *Platinum Metals Review* **2011**, *55*, 154-169.

(28) Ismadji, S.; Bhatia, S. K. Characterization of activated carbons using liquid phase adsorption. *Carbon* **2001**, *39*, 1237-1250.

(29) Aksoylu, A. E.; Madalena, M.; Freitas, A.; Pereira, M. F. R.; Figueiredo, J. L. The effects of different activated carbon supports and support modifications on the properties of Pt/AC catalysts. *Carbon* **2001**, *39*, 175-185.

(30) Amenuvor, G.; Makhubela, B. C. E.; Darkwa, J. Efficient Solvent-Free Hydrogenation of Levulinic Acid to γ-Valerolactone by Pyrazolylphosphite and Pyrazolylphosphinite Ruthenium(II) Complexes. *ACS Sustainable Chemistry & Engineering* **2016**, *4*, 6010-6018.

(31) Furimsky, E.: *Carbons and carbon-supported catalysts in hydroprocessing*; Royal Society of Chemistry, 2008.

(32) Gao, L.; Nie, L.; Wang, T.; Qin, Y.; Guo, Z.; Yang, D.; Yan, X. Carbon nanotube delivery of the GFP gene into mammalian cells. *ChemBioChem* **2006**, *7*, 239-242.

(33) Melchionna, M.; Marchesan, S.; Prato, M.; Fornasiero, P. Carbon nanotubes and catalysis: the many facets of a successful marriage. *Catalysis Science & Technology* **2015**, *5*, 3859-3875.

(34) Raffaelle, R.; Landi, B.; Harris, J.; Bailey, S.; Hepp, A. Carbon nanotubes for power applications. *Materials Science and Engineering: B* **2005**, *116*, 233-243.

(35) Li, R.; Zhang, L.; Wang, P. Rational design of nanomaterials for water treatment. *Nanoscale* **2015**, *7*, 17167-17194.

(36) Eatemadi, A.; Daraee, H.; Karimkhanloo, H.; Kouhi, M.; Zarghami, N.; Akbarzadeh, A.; Abasi, M.; Hanifehpour, Y.; Joo, S. W. Carbon nanotubes: properties, synthesis, purification, and medical applications. *Nanoscale Res Lett* **2014**, *9*, 393.

(37) Davis, W. R.; Slawson, R. J.; Rigby, G. R. An Unusual Form of Carbon. *Nature* **1953**, *171*, 756-756.

(38) Castro Neto, A. H. The carbon new age. *Materials Today* **2010**, *13*, 12-17.

(39) Thostenson, E. T.; Ren, Z.; Chou, T.-W. Advances in the science and technology of carbon nanotubes and their composites: a review. *Composites Science and Technology* **2001**, *61*, 1899-1912.

(40) Niyogi, S.; Hamon, M. A.; Hu, H.; Zhao, B.; Bhowmik, P.; Sen, R.; Itkis, M. E.; Haddon, R. C. Chemistry of Single-Walled Carbon Nanotubes. *Accounts of Chemical Research* **2002**, *35*, 1105-1113.

(41) Ajayan, P. M. Nanotubes from Carbon. *Chemical Reviews* **1999**, *99*, 1787-1800.

(42) Bhatt, A.; Jain, A.; Gurnany, E.; Jain, R.; Modi, A.; Jain, A.: 17 - Carbon Nanotubes: A Promising Carrier for Drug Delivery and Targeting A2 - Holban, Alina Maria. In *Nanoarchitectonics for Smart Delivery and Drug Targeting*; Grumezescu, A. M., Ed.; William Andrew Publishing, 2016; pp 465-501.

(43) Smalley, R. E.: *Carbon nanotubes: synthesis, structure, properties, and applications*; Springer Science & Business Media, 2003; Vol. 80.

(44) Popov, V. N. Carbon nanotubes: properties and application. *Materials Science and Engineering: R: Reports* **2004**, *43*, 61-102.

(45) Rafique, M. M. A.; Iqbal, J. Production of carbon nanotubes by different routes-a review. *Journal of encapsulation and adsorption sciences* **2011**, *1*, 29.

(46) Shi, D.; Mi, G.; Webster, T. J.: Chapter 11 - The Synthesis, Application, and Related Neurotoxicity of Carbon Nanotubes A2 - Jiang, Xinguo. In *Neurotoxicity of Nanomaterials and Nanomedicine*; Gao, H., Ed.; Academic Press, 2017; pp 259-284.

(47) Su, M.; Zheng, B.; Liu, J. A scalable CVD method for the synthesis of single-walled carbon nanotubes with high catalyst productivity. *Chemical Physics Letters* **2000**, *322*, 321-326.

(48) Serp, P.; Corrias, M.; Kalck, P. Carbon nanotubes and nanofibers in catalysis. *Applied Catalysis A: General* **2003**, *253*, 337-358.

(49) Trojanowicz, M. Analytical applications of carbon nanotubes: a review. *TrAC Trends in Analytical Chemistry* **2006**, *25*, 480-489.

(50) Yang, Q.-H.; Hou, P.-X.; Bai, S.; Wang, M.-Z.; Cheng, H.-M. Adsorption and capillarity of nitrogen in aggregated multi-walled carbon nanotubes. *Chemical Physics Letters* **2001**, *345*, 18-24.

(51) Chetty, R.; Xia, W.; Kundu, S.; Bron, M.; Reinecke, T.; Schuhmann, W.; Muhler, M. Effect of Reduction Temperature on the Preparation and Characterization of Pt−Ru Nanoparticles on Multiwalled Carbon Nanotubes. *Langmuir* **2009**, *25*, 3853-3860.

(52) Xu, G.; Zhang, J.; Wang, S.; Zhao, Y.; Ma, X. A well fabricated PtSn/SiO2 catalyst with enhanced synergy between Pt and Sn for acetic acid hydrogenation to ethanol. *RSC Advances* **2016**, *6*, 51005-51013.

(53) Schwarz, J. A.; Contescu, C.; Contescu, A. Methods for Preparation of Catalytic Materials. *Chemical Reviews* **1995**, *95*, 477-510.

(54) Cherubini, F. The biorefinery concept: using biomass instead of oil for producing energy and chemicals. *Energy Conversion and Management* **2010**, *51*, 1412-1421.

(55) Anderson, T. R.; Hawkins, E.; Jones, P. D. CO2, the greenhouse effect and global warming: from the pioneering work of Arrhenius and Callendar to today's Earth System Models. *Endeavour* **2016**, *40*, 178-187.

(56) Liu, X.; Wang, X.; Liu, Q.; Xu, G.; Li, X.; Mu, X. A sustainable process for the production of 2-methyl-1,4-butanediol by hydrogenation of biomass-derived itaconic acid. *Catalysis Today* **2016**, *274*, 88-93.

(57) Arellano, J. S.; Molina, L. M.; Rubio, A.; López, M. J.; Alonso, J. A. *J. Chem. Phys.* **2002**, *117*, 2281.

(58) Hunter, P. Massing life. *EMBO reports* **2010**, *11*, 511-514.

(59) Alonso, D. M.; Wettstein, S. G.; Dumesic, J. A. Bimetallic catalysts for upgrading of biomass to fuels and chemicals. *Chemical Society Reviews* **2012**, *41*, 8075-8098.

(60) Sebayang, A. H.; Masjuki, H. H.; Ong, H. C.; Dharma, S.; Silitonga, A. S.; Mahlia, T. M. I.; Aditiya, H. B. A perspective on bioethanol production from biomass as alternative fuel for spark ignition engine. *RSC Advances* **2016**, *6*, 14964-14992.

(61) Mu, W.; Ben, H.; Ragauskas, A.; Deng, Y. Lignin pyrolysis components and upgrading—technology review. *BioEnergy Research* **2013**, *6*, 1183-1204.

(62) Ragauskas, A. J.; Williams, C. K.; Davison, B. H.; Britovsek, G.; Cairney, J.; Eckert, C. A.; Frederick, W. J.; Hallett, J. P.; Leak, D. J.; Liotta, C. L. The path forward for biofuels and biomaterials. *science* **2006**, *311*, 484-489.

(63) Corma, A.; Iborra, S.; Velty, A. Chemical routes for the transformation of biomass into chemicals. *Chem Rev* **2007**, *107*, 2411-2502.

(64) Werpy, T.; Petersen, G.; Aden, A.; Bozell, J.; Holladay, J.; White, J.; Manheim, A.; Eliot, D.; Lasure, L.; Jones, S. *Top value added chemicals from biomass. Volume 1-Results of screening for potential candidates from sugars and synthesis gas*2004.

(65) Li, Y.; Ma, L.; Liu, H.; He, D. Influence of pretreatment on the catalytic performance of Ru/SBA-15 catalysts for glycerol hydrogenolysis. *Chinese Journal of Catalysis* **2014**, *35*, 677-683.

(66) Cui, X.; Li, Y.; Topf, C.; Junge, K.; Beller, M. Direct Ruthenium-Catalyzed Hydrogenation of Carboxylic Acids to Alcohols. *Angewandte Chemie International Edition* **2015**, *54*, 10596-10599.

(67) Song, H.; Lee, S. Y. Production of succinic acid by bacterial fermentation. *Enzyme and Microbial Technology* **2006**, *39*, 352-361.

(68) Rao, P. S.; Srikanth, B.; Rao, V.; Sastry, C. K.; Rao, G. N. Protonation equilibria of L-aspartic, citric and succinic acids in anionic micellar media. *Journal of Chemistry* **2009**, *6*, 561-568.

(69) Nghiem, N.; Kleff, S.; Schwegmann, S. Succinic Acid: Technology Development and Commercialization. *Fermentation* **2017**, *3*, 26.

(70) Mazière, A.; Prinsen, P.; García, A.; Luque, R.; Len, C. A review of progress in (bio)catalytic routes from/to renewable succinic acid. *Biofuels, Bioproducts and Biorefining*, n/a-n/a.

(71) Cao, Y.; Zhang, R.; Sun, C.; Cheng, T.; Liu, Y.; Xian, M. Fermentative succinate production: An emerging technology to replace the traditional petrochemical processes. *BioMed research international* **2013**, *2013*.

(72) Becker, J.; Lange, A.; Fabarius, J.; Wittmann, C. Top value platform chemicals: bio-based production of organic acids. *Current Opinion in Biotechnology* **2015**, *36*, 168-175.

(73) Tan, J. P.; Jahim, J. M.; Harun, S.; Wu, T. Y. Overview of the Potential of Bio-Succinic Acid Production from Oil Palm Fronds. *Journal of Physical Science* **2017**, *28*, 53.

(74) BIOAMBER AND CJ CHEILJEDANG PLAN JV FOR SUCCINIC ACID PRODUCTION IN ASIA. http://investor.bio-amber.com/2016-12-19-BioAmber-and-CJ-CheilJedang-Plan-JV-for-Succinic-Acid-Production-in-Asia (accessed 11/05/2017.

(75) Beerthuis, R.; Rothenberg, G.; Shiju, N. R. Catalytic routes towards acrylic acid, adipic acid and ?-caprolactam starting from biorenewables. *Green Chemistry* **2015**, *17*, 1341-1361.

(76) Lee, S. Y.; Kim, J. M.; Song, H.; Lee, J. W.; Kim, T. Y.; Jang, Y.-S. From genome sequence to integrated bioprocess for succinic acid production by Mannheimia succiniciproducens. *Applied microbiology and biotechnology* **2008**, *79*, 11-22.

(77) Chang, P.-C.; Hsu, H.-Y.; Jang, G.-W. Biological routes to itaconic and succinic acids. *Physical Sciences Reviews* **2016**, *2016*.

(78) Zeikus, J.; Jain, M.; Elankovan, P. Biotechnology of succinic acid production and markets for derived industrial products. *Applied Microbiology and Biotechnology* **1999**, *51*, 545-552.

(79) Cukalovic, A.; Stevens, C. V. Feasibility of production methods for succinic acid derivatives: a marriage of renewable resources and chemical technology. *Biofuels Bioproducts & Biorefining-biofpr* **2008**, *2*, 505-529.

(80) Berezina, N.; Martelli, S. M.: CHAPTER 1 Bio-based Polymers and Materials. In *Renewable Resources for Biorefineries*; The Royal Society of Chemistry, 2014; pp 1-28.

(81) Minh, D. P.; Besson, M.; egrave; le; Pinel, C.; Fuertes, P.; Petitjean, C.; Minh, D.; Besson, M.; egrave; le; Pinel, C.; Fuertes, P.; Petitjean, C.; Minh, D. P.; Besson, M.; egrave; le; Pinel, C.; Fuertes, P.; Petitjean, C. Aqueous-Phase Hydrogenation of Biomass-Based Succinic Acid to 1,4-Butanediol Over Supported Bimetallic Catalysts. *Top Catal* **2010**, *53*, 1270.

(82) Efe, C.; Straathof, A. J.; van der Wielen, L. A. Options for biochemical production of 4-hydroxybutyrate and its lactone as a substitute for petrochemical production. *Biotechnology and bioengineering* **2008**, *99*, 1392-1406.

(83) Parsons, B. A.; Dragojlovic, V. Demonstration of a Runaway Exothermic Reaction: Diels–Alder Reaction of (2 E, 4 E)-2, 4-Hexadien-1-ol and Maleic Anhydride. *Journal of Chemical Education* **2011**, *88*, 1553-1557.

(84) Bertone, M. E.; Meyer, C. I.; Regenhardt, S. A.; Sebastian, V.; Garetto, T. F.; Marchi, A. J. Highly selective conversion of maleic anhydride to γ-butyrolactone over Ni-supported catalysts prepared by precipitation–deposition method. *Applied Catalysis A: General* **2015**, *503*, 135-146.

(85) Di, X.; Shao, Z.; Li, C.; Li, W.; Liang, C. Hydrogenation of succinic acid over supported rhenium catalysts prepared by the microwave-assisted thermolytic method. *Catalysis Science & Technology* **2015**, *5*, 2441-2448.

(86) Kang, K. H.; Hong, U. G.; Bang, Y.; Choi, J. H.; Kim, J. K.; Lee, J. K.; Han, S. J.; Song, I. K. Hydrogenation of succinic acid to 1,4-butanediol over Re–Ru bimetallic catalysts supported on mesoporous carbon. *Applied Catalysis A: General* **2015**, *490*, 153-162.

(87) Hong, U. G.; Park, H. W.; Lee, J.; Hwang, S.; Song, I. K. Hydrogenation of succinic acid to γ-butyrolactone (GBL) over ruthenium catalyst supported on surfactant-templated mesoporous carbon. *Journal of Industrial and Engineering Chemistry* **2012**, *18*, 462-468.

(88) Zhang, C.; Cao, W.; Cheng, H.; Chen, L.; Qi, Z. Regenerable Subnanometer Pd Clusters on Zirconia for Highly Selective Hydrogenation of Biomass-Derived Succinic Acid in Water. *Catalysts* **2016**, *6*, 100.

(89) Chung, S.-H.; Park, Y.-M.; Kim, M.-S.; Lee, K.-Y. The effect of textural properties on the hydrogenation of succinic acid using palladium incorporated mesoporous supports. *Catalysis Today* **2012**, *185*, 205-210.

(90) You, C.; Zhang, C.; Chen, L.; Qi, Z. Highly dispersed palladium nanoclusters incorporated in amino-functionalized silica spheres for the selective hydrogenation of succinic acid to γ-butyrolactone. *Applied Organometallic Chemistry* **2015**, *29*, 653-660.

(91) Fu, J.; Sheng, D.; Lu, X. Hydrogenation of Levulinic Acid over Nickel Catalysts Supported on Aluminum Oxide to Prepare γ-Valerolactone. *Catalysts* **2015**, *6*, 6.

(92) Blaser, H.-U.; Indolese, A.; Schnyder, A.; Steiner, H.; Studer, M. Supported palladium catalysts for fine chemicals synthesis. *Journal of Molecular Catalysis A: Chemical* **2001**, *173*, 3-18.

(93) Arai, H.; Fukuzawa, H. Research and development on high temperature catalytic combustion. *Catalysis Today* **1995**, *26*, 217-221.

(94) Hong, U.; Lee, J.; Hwang, S.; Song, I. Hydrogenation of Succinic Acid to γ-Butyrolactone (GBL) Over Palladium-Alumina Composite Catalyst Prepared by a Single-Step Sol–Gel Method. *Catalysis Letters* **2011**, *141*, 332-338.

(95) Pallassana, V.; Neurock, M.; Coulston, G. Towards understanding the mechanism for the selective hydrogenation of maleic anhydride to tetrahydrofuran over palladium. *Catalysis Today* **1999**, *50*, 589-601.

(96) Müller, S. P.; Kucher, M.; Ohlinger, C.; Kraushaar-Czarnetzki, B. Extrusion of Cu/ZnO catalysts for the single-stage gas-phase processing of dimethyl maleate to tetrahydrofuran. *Journal of catalysis* **2003**, *218*, 419-426.

(97) Jung, S. M.; Godard, E.; Jung, S. Y.; Park, K.-C.; Choi, J. U. Liquid-phase hydrogenation of maleic anhydride over Pd–Sn/SiO2. *Catalysis Today* **2003**, *87*, 171-177.

(98) Wildberger, M. D.; Maciejewski, M.; Grunwaldt, J.-D.; Mallat, T.; Baiker, A. Sol–gel bismuth–molybdenum–titanium mixed oxides: II. Oxidation of butadiene to furan. *Applied Catalysis A: General* **1999**, *179*, 189-202.

(99) Aghaziarati, M.; Kazemeini, M.; Soltanieh, M.; Sahebdelfar, S. Evaluation of Zeolites in Production of Tetrahydrofuran from 1,4-Butanediol: Performance Tests and Kinetic Investigations. *Industrial & Engineering Chemistry Research* **2007**, *46*, 726-733.

(100) Delhomme, C.; Weuster-Botz, D.; Kuhn, F. E. Succinic acid from renewable resources as a C4 building-block chemical-a review of the catalytic possibilities in aqueous media. *Green Chemistry* **2009**, *11*, 13-26.

(101) Global Tetrahydrofuran Market to Exceed 800 Thousand Tons by 2017, According to a New Report by Global Industry Analysts, Inc. http://www.prweb.com/releases/tetrahydrofuran/ptmeg_solvents/prweb8281771.htm 08/11/2017).

(102) Bechthold, I.; Bretz, K.; Kabasci, S.; Kopitzky, R.; Springer, A. Succinic Acid: A New Platform Chemical for Biobased Polymers from Renewable Resources. *Chemical Engineering & Technology* **2008**, *31*, 647-654.

(103) Hong, U. G.; Park, H. W.; Lee, J.; Hwang, S.; Kwak, J.; Yi, J.; Song, I. K. Hydrogenation of succinic acid to 1,4-butanediol over rhenium catalyst supported on copper-containing mesoporous carbon. *J Nanosci Nanotechnol* **2013**, *13*, 7448-7453.

(104) Luque, R.; Clark, J. H.; Yoshida, K.; Gai, P. L. Efficient aqueous hydrogenation of biomass platform molecules using supported metal nanoparticles on Starbons[registered sign]. *Chemical Communications* **2009**, 5305-5307.

(105) Hong, U. G.; Park, H. W.; Lee, J.; Hwang, S.; Yi, J.; Song, I. K. Hydrogenation of succinic acid to tetrahydrofuran (THF) over rhenium catalyst supported on H2SO4-treated mesoporous carbon. *Applied Catalysis A: General* **2012**, *415–416*, 141-148.

(106) Ly, B. K.; Minh, D. P.; Pinel, C.; Besson, M.; Tapin, B.; Epron, F.; Especel, C. Effect of Addition Mode of Re in Bimetallic Pd–Re/TiO2 Catalysts Upon the Selective Aqueous-Phase Hydrogenation of Succinic Acid to 1, 4-Butanediol. *Top Catal* **2012**, *55*, 466-473.

(107) Yim, H.; Haselbeck, R.; Niu, W.; Pujol-Baxley, C.; Burgard, A.; Boldt, J.; Khandurina, J.; Trawick, J. D.; Osterhout, R. E.; Stephen, R.; Estadilla, J.; Teisan, S.; Schreyer, H. B.; Andrae, S.; Yang, T. H.; Lee, S. Y.; Burk, M. J.; Van Dien, S. Metabolic engineering of Escherichia coli for direct production of 1,4-butanediol. *Nat Chem Biol* **2011**, *7*, 445-452.

(108) 1,4 Butanediol (BDO) Market Worth $12.6 Billion By 2025 | CAGR: 7.7%. http://www.grandviewresearch.com/press-release/global-1-4-butanediol-market 08/11/2017).

(109) Herrmann, U.; Emig, G. Kinetics and Mechanism in the Liquid-Phase Hydrogenation of Maleic Anhydride and Intermediates. *Chemical Engineering & Technology* **1998**, *21*, 285-295.

(110) Chen, L.-F.; Guo, P.-J.; Zhu, L.-J.; Qiao, M.-H.; Shen, W.; Xu, H.-L.; Fan, K.-N. Preparation of Cu/SBA-15 catalysts by different methods for the hydrogenolysis of dimethyl maleate to 1, 4-butanediol. *Applied Catalysis A: General* **2009**, *356*, 129-136.

(111) Lee, J.; Han, M.; Choi, S.; Yi, J.; Lee, T.; Lee, S. 3.15-Organic acids: succinic and malic acids. *in-Chief: Murray MY (ed) Comprehensive biotechnology, 2nd edn. Academic Press, Burlington* **2011**, 149-161.

(112) Kang, K. H.; Hong, U. G.; Jun, J. O.; Song, J. H.; Bang, Y.; Choi, J. H.; Han, S. J.; Song, I. K. Hydrogenation of succinic acid to γ-butyrolactone and 1,4-butanediol over mesoporous rhenium–copper–carbon composite catalyst. *Journal of Molecular Catalysis A: Chemical* **2014**, *395*, 234-242.

(113) Dharaiya, D.; Jana, S. C.; Shafi, A. A study on the use of phenoxy resins as compatibilizers of polyamide 6 (PA6) and polybutylene terephthalate (PBT). *Polymer Engineering & Science* **2003**, *43*, 580-595.

(114) Szmant, H. H.: *Organic building blocks of the chemical industry*; John Wiley & Sons, 1989.

(115) Ly, B.; Minh, D.; Pinel, C.; Besson, M.; Tapin, B.; Epron, F.; Especel, C. Effect of Addition Mode of Re in Bimetallic Pd–Re/TiO2 Catalysts Upon the Selective Aqueous-Phase Hydrogenation of Succinic Acid to 1,4-Butanediol. *Top Catal* **2012**, *55*, 466-473.

(116) Torres, C. C.; Alderete, J. B.; Mella, C.; Pawelec, B. Maleic anhydride hydrogenation to succinic anhydride over mesoporous Ni/TiO2 catalysts: Effects of Ni loading and temperature. *Journal of Molecular Catalysis A: Chemical* **2016**, *423*, 441-448.

(117) Tapin, B.; Epron, F.; Especel, C.; Ly, B. K.; Pinel, C.; Besson, M. Study of Monometallic Pd/TiO2 Catalysts for the Hydrogenation of Succinic Acid in Aqueous Phase. *ACS Catalysis* **2013**, *3*, 2327-2335.

(118) Tapin, B.; Epron, F.; Especel, C.; Ly, B.; Pinel, C.; Besson, M. Performances of bimetallic Pd-Re/TiO2 catalysts for the selec-tive hydrogenation of succinic acid in aqueous-phase: influence of the Re introduction method and the Re loading. **2013**.

(119) Minh, D. P.; Besson, M.; Pinel, C.; Fuertes, P.; Petitjean, C. Aqueous-phase hydrogenation of biomass-based succinic acid to 1, 4-butanediol over supported bimetallic catalysts. *Top Catal* **2010**, *53*, 1270-1273.

(120) Sun, D.; Sato, S.; Ueda, W.; Primo, A.; Garcia, H.; Corma, A. Production of C4 and C5 alcohols from biomass-derived materials. *Green Chemistry* **2016**, *18*, 2579-2597.

(121) Beamson, G.; Papworth, A. J.; Philipps, C.; Smith, A. M.; Whyman, R. Selective hydrogenation of amides using bimetallic Ru/Re and Rh/Re catalysts. *Journal of Catalysis* **2011**, *278*, 228-238.

(122) Liu, X.; Wang, X.; Xu, G.; Liu, Q.; Mu, X.; Liu, H. Tuning the catalytic selectivity in biomass-derived succinic acid hydrogenation on FeO x-modified Pd catalysts. *Journal of Materials Chemistry A* **2015**, *3*, 23560-23569.

(123) Levulinic Acid Market Size to Reach $19.65 Million by 2020: Grand View Research, Inc. http://www.marketwired.com/press-release/levulinic-acid-market-size-to-reach-1965-million-by-2020-grand-view-research-inc-2078508.htm (accessed 10 12 2017.

(124) Su, J.; Shen, F.; Qiu, M.; Qi, X. High-Yield Production of Levulinic Acid from Pretreated Cow Dung in Dilute Acid Aqueous Solution. *Molecules* **2017**, *22*, 285.

(125) Corma, A.; Garcia, H.; Leyva, A. Catalytic activity of palladium supported on single wall carbon nanotubes compared to palladium supported on activated carbon: Study of the Heck and Suzuki couplings, aerobic alcohol oxidation and selective hydrogenation. *Journal of Molecular Catalysis A: Chemical* **2005**, *230*, 97-105.

(126) Piskun, A. S.; de Haan, J. E.; Wilbers, E.; van de Bovenkamp, H. H.; Tang, Z.; Heeres, H. J. Hydrogenation of Levulinic Acid to γ-Valerolactone in Water Using Millimeter Sized Supported Ru Catalysts in a Packed Bed Reactor. *ACS Sustainable Chemistry & Engineering* **2016**, *4*, 2939-2950.

(127) Albani, D.; Li, Q.; Vile, G.; Mitchell, S.; Almora-Barrios, N.; Witte, P. T.; Lopez, N.; Perez-Ramirez, J. Interfacial acidity in ligand-modified ruthenium nanoparticles boosts the hydrogenation of levulinic acid to gamma-valerolactone. *Green Chemistry* **2017**.

(128) Balla, P.; Perupogu, V.; Vanama, P. K.; Komandur, V. R. C. Hydrogenation of biomass-derived levulinic acid to γ-valerolactone over copper catalysts supported on ZrO2. *Journal of Chemical Technology & Biotechnology* **2015**, n/a-n/a.

(129) Ren, D.; Wan, X.; Jin, F.; Song, Z.; Liu, Y.; Huo, Z. Selective hydrogenation of levulinate esters to 1, 4-pentanediol using a ternary skeletal CuAlZn catalyst. *Green Chemistry* **2016**, *18*, 5999-6003.

(130) Corbel-Demailly, L.; Ly, B. K.; Minh, D. P.; Tapin, B.; Especel, C.; Epron, F.; Cabiac, A.; Guillon, E.; Besson, M.; Pinel, C. Heterogeneous catalytic hydrogenation of biobased levulinic and succinic acids in aqueous solutions. *ChemSusChem* **2013**, *6*, 2388-2395.

(131) Li, M.; Li, G.; Li, N.; Wang, A.; Dong, W.; Wang, X.; Cong, Y. Aqueous phase hydrogenation of levulinic acid to 1, 4-pentanediol. *Chemical Communications* **2014**, *50*, 1414-1416.

(132) Mizugaki, T.; Nagatsu, Y.; Togo, K.; Maeno, Z.; Mitsudome, T.; Jitsukawa, K.; Kaneda, K. Selective hydrogenation of levulinic acid to 1, 4-pentanediol in water using a hydroxyapatite-supported Pt–Mo bimetallic catalyst. *Green Chemistry* **2015**, *17*, 5136-5139.

(133) Draths, K. M.; Frost, J. W. Environmentally compatible synthesis of adipic acid from D-glucose. *Journal of the American Chemical Society* **1994**, *116*, 399-400.

(134) Vardon, D. R.; Franden, M. A.; Johnson, C. W.; Karp, E. M.; Guarnieri, M. T.; Linger, J. G.; Salm, M. J.; Strathmann, T. J.; Beckham, G. T. Adipic acid production from lignin. *Energy & Environmental Science* **2015**, *8*, 617-628.

(135) Matthiesen, J. E.; Carraher, J. M.; Vasiliu, M.; Dixon, D. A.; Tessonnier, J.-P. Electrochemical Conversion of Muconic Acid to Biobased Diacid Monomers. *ACS Sustainable Chemistry & Engineering* **2016**, *4*, 3575-3585.

(136) Isikgor, F. H.; Becer, C. R. Lignocellulosic biomass: a sustainable platform for the production of bio-based chemicals and polymers. *Polymer Chemistry* **2015**, *6*, 4497-4559.

(137) Cyclohexane (CX) Uses and Market Data. https://www.icis.com/resources/news/2007/11/01/9075207/cyclohexane-cx-uses-and-market-data/ (accessed 12 12 2017.

(138) Cavani, F.; Centi, G.; Perathoner, S.; Trifirò, F.: *Sustainable Industrial Chemistry: Principles, Tools and Industrial Examples*; John Wiley & Sons, 2009.

(139) Scelfo, S.; Pirone, R.; Russo, N. Highly efficient catalysts for the synthesis of adipic acid from cis,cis-muconic acid. *Catalysis Communications* **2016**, *84*, 98-102.

(140) Zhang, H.; Li, X.; Su, X.; Ang, E. L.; Zhang, Y.; Zhao, H. Production of Adipic Acid from Sugar Beet Residue by Combined Biological and Chemical Catalysis. *ChemCatChem* **2016**, *8*, 1500-1506.

(141) Scelfo, S.; Pirone, R.; Russo, N. Thermodynamics of cis,cis-muconic acid solubility in various polar solvents at low temperature range. *Journal of Molecular Liquids* **2016**, *222*, 823-827.

(142) Niu, W.; Draths, K. M.; Frost, J. W. Benzene-Free Synthesis of Adipic Acid. *Biotechnology Progress* **2002**, *18*, 201-211.

(143) Vardon, D. R.; Rorrer, N. A.; Salvachúa, D.; Settle, A. E.; Johnson, C. W.; Menart, M. J.; Cleveland, N. S.; Ciesielski, P. N.; Steirer, K. X.; Dorgan, J. R. cis, cis-Muconic acid: separation and catalysis to bio-adipic acid for nylon-6, 6 polymerization. *Green Chemistry* **2016**, *18*, 3397-3413.

(144) Woodruff, M. A.; Hutmacher, D. W. The return of a forgotten polymer—polycaprolactone in the 21st century. *Progress in Polymer Science* **2010**, *35*, 1217-1256.

(145) Buntara, T.; Noel, S.; Phua, P. H.; Melián-Cabrera, I.; de Vries, J. G.; Heeres, H. J. Caprolactam from Renewable Resources: Catalytic Conversion of 5-Hydroxymethylfurfural into Caprolactone. *Angewandte Chemie International Edition* **2011**, *50*, 7083-7087.

(146) TAKAHASHI, K.; MATSUDA, T.; TAKADA, Y. Reaction of ε-Caprolactone in aqueous Ammonia. *Journal of Synthetic Organic Chemistry, Japan* **1974**, *32*, 372-374.

(147) Thomas, J. M.; Raja, R. Design of a "green" one-step catalytic production of ε-caprolactam (precursor of nylon-6). *Proceedings of the National Academy of Sciences of the United States of America* **2005**, *102*, 13732-13736.

(148) Silva, A. M.; Morales, M. A.; Baggio-Saitovitch, E. M.; Jordão, E.; Fraga, M. A. Selective hydrogenation of dimethyl adipate on titania-supported RuSn catalysts. *Applied Catalysis A: General* **2009**, *353*, 101-106.

(149) Mormul, J.; Breitenfeld, J.; Trapp, O.; Paciello, R.; Schaub, T.; Hofmann, P. Synthesis of Adipic Acid, 1, 6-Hexanediamine, and 1, 6-Hexanediol via Double-n-Selective Hydroformylation of 1, 3-Butadiene. *ACS Catalysis* **2016**, *6*, 2802-2810.

(150) Buntara, T.; Noel, S.; Phua, P. H.; Melián-Cabrera, I.; de Vries, J. G.; Heeres, H. J. From 5-Hydroxymethylfurfural (HMF) to Polymer Precursors: Catalyst Screening Studies on the Conversion of 1,2,6-hexanetriol to 1,6-hexanediol. *Top Catal* **2012**, *55*, 612-619.

(151) Takahashi, K.; Yamashita, M.; Nozaki, K. Tandem hydroformylation/hydrogenation of alkenes to normal alcohols using Rh/Ru dual catalyst or Ru single component catalyst. *Journal of the American Chemical Society* **2012**, *134*, 18746-18757.

(152) Tuteja, J.; Choudhary, H.; Nishimura, S.; Ebitani, K. Direct Synthesis of 1, 6-Hexanediol from HMF over a Heterogeneous Pd/ZrP Catalyst using Formic Acid as Hydrogen Source. *ChemSusChem* **2014**, *7*, 96-100.

(153) Yuan, P.; Liu, Z.; Hu, T.; Sun, H.; Liu, S. Highly efficient Cu–Zn–Al catalyst for the hydrogenation of dimethyl adipate to 1,6-hexanediol: influence of calcination temperature. *Reaction Kinetics, Mechanisms and Catalysis* **2010**, *100*, 427-439.

(154) Xiao, B.; Zheng, M.; Li, X.; Pang, J.; Sun, R.; Wang, H.; Pang, X.; Wang, A.; Wang, X.; Zhang, T. Synthesis of 1, 6-hexanediol from HMF over double-layered catalysts of Pd/SiO 2+ Ir–ReO x/SiO 2 in a fixed-bed reactor. *Green Chemistry* **2016**, *18*, 2175-2184.

(155) Wirth, C. T.; Bayer, B. C.; Gamalski, A. D.; Esconjauregui, S.; Weatherup, R. S.; Ducati, C.; Baehtz, C.; Robertson, J.; Hofmann, S. The Phase of Iron Catalyst Nanoparticles during Carbon Nanotube Growth. *Chem. Mater.* **2012**, *24*, 4633-4640.

(156) Mai, E. F.; Machado, M. A.; Davies, T. E.; Lopez-Sanchez, J. A.; Teixeira da Silva, V. Molybdenum carbide nanoparticles within carbon nanotubes as superior catalysts for [gamma]-valerolactone production via levulinic acid hydrogenation. *Green Chemistry* **2014**, *16*, 4092-4097.

(157) Wang, Y.; Rong, Z.; Wang, Y.; Zhang, P.; Wang, Y.; Qu, J. Ruthenium nanoparticles loaded on multiwalled carbon nanotubes for liquid-phase hydrogenation of fine chemicals: An exploration of confinement effect. *Journal of Catalysis* **2015**, *329*, 95-106.

(158) Wang, C.; Guo, S.; Pan, X.; Chen, W.; Bao, X. Tailored cutting of carbon nanotubes and controlled dispersion of metal nanoparticles inside their channels. *Journal of Materials Chemistry* **2008**, *18*, 5782-5786.

(159) X-ray Powder Diffraction (XRD). http://serc.carleton.edu/research_education/geochemsheets/techniques/XRD.html (accessed 13/09/2017.

(160) Bragg's Law of Diffraction. http://www.microscopy.ethz.ch/bragg.htm (accessed 08/10/2017.

(161) Campos, D.; Sisler, G. M.: Platinum-rhenium-tin catalyst for hydrogenation in aqueous solution. Google Patents, 2003.

(162) X-ray in Characterization Techniques. http://www.science20.com/mei/blog/xray_characterization_techniques (accessed 08/10/2017.

(163) Kerber, S.; Barr, T.; Mann, G.; Brantley, W.; Papazoglou, E.; Mitchell, J. The complementary nature of x-ray photoelectron spectroscopy and angle-resolved x-ray diffraction Part I: Background and theory. *Journal of materials engineering and performance* **1998**, *7*, 329-333.

(164) Gao, X.; Zhu, Y.-P.; Luo, Z.-h. CFD modeling of gas flow in porous medium and catalytic coupling reaction from carbon monoxide to diethyl oxalate in fixed-bed reactors. *Chemical Engineering Science* **2011**, *66*, 6028-6038.

(165) MUKHOPADHYAY, S. M. SAMPLE PREPARATION FOR MICROSCOPIC AND SPECTROSCOPIC CHARACTERIZATION OF SOLID SURFACES AND FILMS.

(166) Comparison between light microscope and electron microscope. https://www.pinterest.com/pin/50313720815744718/ (accessed 09 12 2017.

(167) Chaudhari, R.; Rode, C.; Deshpande, R.; Jaganathan, R.; Leib, T.; Mills, P. Kinetics of hydrogenation of maleic acid in a batch slurry reactor using a bimetallic Ru–Re/C catalyst. *Chemical engineering science* **2003**, *58*, 627-632.

(168) Pillai, U. R.; Sahle-Demessie, E. Selective hydrogenation of maleic anhydride to γ-butyrolactone over Pd/Al 2 O 3 catalyst using supercritical CO 2 as solvent. *Chemical Communications* **2002**, 422-423.

(169) Catalyst characterization-Chemisorption. http://nptel.ac.in/courses/103103026/module2/lec13/1.html (accessed 07/10/2017.

(170) Canton, P.; Fagherazzi, G.; Battagliarin, M.; Menegazzo, F.; Pinna, F.; Pernicone, N. Pd/CO Average Chemisorption Stoichiometry in Highly Dispersed Supported Pd/γ-Al2O3 Catalysts. *Langmuir* **2002**, *18*, 6530-6535.

(171) Merlo, A. B.; Vetere, V.; Ruggera, J. F.; Casella, M. L. Bimetallic PtSn catalyst for the selective hydrogenation of furfural to furfuryl alcohol in liquid-phase. *Catalysis Communications* **2009**, *10*, 1665-1669.

(172) Coman, S. M.; Tudorache, M.; Parvulescu, V. I. Green catalysis methods: catalysis for lignocellulosic biomass capitalization into chemicals. **2013**.

(173) Fadoni, M.; Lucarelli, L. Temperature programmed desorption, reduction, oxidation and flow chemisorption for the characterisation of heterogeneous catalysts. Theoretical aspects, instrumentation and applications. *Studies in Surface Science and Catalysis* **1999**, *123*, 289-342.

(174) Robertson, S. D.; McNicol, B. D.; De Baas, J. H.; Kloet, S. C.; Jenkins, J. W. Determination of reducibility and identification of alloying in copper-nickel-on-silica catalysts by temperature-programmed reduction. *Journal of Catalysis* **1975**, *37*, 424-431.

(175) Webb, P. A. Introduction to chemical adsorption analytical techniques and their applications to catalysis. *Micromeritics Instrument Corp. Technical Publications* **2003**.

(176) Weidenthaler, C. Pitfalls in the characterization of nanoporous and nanosized materials. *Nanoscale* **2011**, *3*, 792-810.

(177) Castiglioni, G. L.; Ferrari, M.; Guercio, A.; Vaccari, A.; Lancia, R.; Fumagalli, C. Chromium-free catalysts for selective vapor phase hydrogenation of maleic anhydride to γ-butyrolactone. *Catalysis today* **1996**, *27*, 181-186.

(178) PIEROTTI, R.; ROUQUEROL, J. REPORTING PHYSISORPTION DATA FOR GAS/SOLID SYSTEMS with Special Reference to the Determination of Surface Area and Porosity. **1985**.

(179) Thommes, M.; Kaneko, K.; Neimark, A. V.; Olivier, J. P.; Rodriguez-Reinoso, F.; Rouquerol, J.; Sing, K. S. Physisorption of gases, with special reference to the evaluation of surface area and pore size distribution (IUPAC Technical Report). *Pure and Applied Chemistry* **2015**, *87*, 1051-1069.

(180) BET Surface Area Analysis of Nanoparticles. https://cnx.org/contents/9cBY4EHy@1/BET-Surface-Area-Analysis-of-N (accessed 16/10/2017.

(181) Bianchi, M.; Menchi, G.; Francalanci, F.; Piacenti, F.; Matteoli, U.; Frediani, P.; Botteghi, C. Homogeneous catalytic hydrogenation of free carboxylic acids in the presence of cluster ruthenium carbonyl hydrides. *Journal of Organometallic Chemistry* **1980**, *188*, 109-119.

(182) Anastas, P.; Eghbali, N. Green Chemistry: Principles and Practice. *Chemical Society Reviews* **2010**, *39*, 301-312.

(183) Dallinger, D.; Kappe, C. O. Microwave-Assisted Synthesis in Water as Solvent. *Chemical Reviews* **2007**, *107*, 2563-2591.

(184) Lu, X.; He, J.; Jing, R.; Tao, P.; Nie, R.; Zhou, D.; Xia, Q. Microwave-activated Ni/carbon catalysts for highly selective hydrogenation of nitrobenzene to cyclohexylamine. *Scientific Reports* **2017**, *7*, 2676.

(185) Anwar, J.; Shafique, U.; Waheed uz, Z.; Rehman, R.; Salman, M.; Dar, A.; Anzano, J. M.; Ashraf, U.; Ashraf, S. Microwave chemistry: Effect of ions on dielectric heating in microwave ovens. *Arabian Journal of Chemistry* **2015**, *8*, 100-104.

(186) Yoshida, K.; Sonobe, T.; Zen, H.; Hachiya, K.; Okumura, K.; Mishima, K.; Inukai, M.; Negm, H.; Torgasin, K.; Omer, M.; Kinjo, R.; Kii, T.; Masuda, K.; Ohgaki, H. Effect of microwave irradiation on the electronic structure of ZnO. *Journal of Physics and Chemistry of Solids* **2015**, *83*, 47-51.

(187) Microwave-assisted synthesis. http://wiki.anton-paar.com/microwave-assisted-synthesis/ (accessed 24/09/2017.

(188) Zeng, J.; Su, F.; Lee, J. Y.; Zhou, W.; Zhao, X. Methanol oxidation activities of Pt nanoparticles supported on microporous carbon with and without a graphitic shell. *Carbon* **2006**, *44*, 1713-1717.

(189) Gaba, M.; Passi, N.: *Microwave Chemistry: General Features and Applications*, 2010.

(190) Werpy, T.; Frye, J.; Holladay, J. Succinic acid–a model building block for chemical production from renewable resources. *Biorefineries-Industrial Processes and Products: Status Quo and Future Directions* **2006**, 367-379.

(191) Brewster, T. P.; Miller, A. J. M.; Heinekey, D. M.; Goldberg, K. I. Hydrogenation of Carboxylic Acids Catalyzed by Half-Sandwich Complexes of Iridium and Rhodium. *Journal of the American Chemical Society* **2013**, *135*, 16022-16025.

(192) Capello, C.; Fischer, U.; Hungerbühler, K. What is a green solvent? A comprehensive framework for the environmental assessment of solvents. *Green Chemistry* **2007**, *9*, 927-934.

(193) Figoli, A.; Marino, T.; Simone, S.; Di Nicolo, E.; Li, X. M.; He, T.; Tornaghi, S.; Drioli, E. Towards non-toxic solvents for membrane preparation: a review. *Green Chemistry* **2014**, *16*, 4034-4059.

(194) Richter, T.; Vogel, H. The Dehydration of 1,4-Butanediol to Tetrahydrofuran in Supercritical Water. *Chemical Engineering & Technology* **2001**, *24*, 340-343.

(195) Teunissen, H. T. Homogeneous ruthenium catalyzed hydrogenation of esters to alcohols. *Chemical Communications* **1998**, 1367-1368.

(196) Kluson, P.; Cerveny, L. Selective hydrogenation over ruthenium catalysts. *Applied Catalysis A: General* **1995**, *128*, 13-31.

(197) Michel, C.; Gallezot, P. Why Is Ruthenium an Efficient Catalyst for the Aqueous-Phase Hydrogenation of Biosourced Carbonyl Compounds? *ACS Catalysis* **2015**, *5*, 4130-4132.

(198) Rodríguez-Reinoso, F. The role of carbon materials in heterogeneous catalysis. *Carbon* **1998**, *36*, 159-175.

(199) Hong, U. G.; Kim, J. K.; Lee, J.; Lee, J. K.; Song, J. H.; Yi, J.; Song, I. K. Hydrogenation of succinic acid to tetrahydrofuran over ruthenium-carbon composite catalysts: Effect of HCl concentration in the preparation of the catalysts. *Journal of Industrial and Engineering Chemistry* **2014**, *20*, 3834-3840.

(200) Dresselhaus, M. S.; Dresselhaus, G.; Eklund, P. C.; Rao, A. M.: Carbon Nanotubes. In *The Physics of Fullerene-Based and Fullerene-Related Materials*; Andreoni, W., Ed.; Springer Netherlands: Dordrecht, 2000; pp 331-379.

(201) Serp, P.; Castillejos, E. Catalysis in Carbon Nanotubes. *ChemCatChem* **2010**, *2*, 41-47.

(202) Giordano, R.; Serp, P.; Kalck, P.; Kihn, Y.; Schreiber, J.; Marhic, C.; Duvail, J.-L. Preparation of Rhodium Catalysts Supported on Carbon Nanotubes by a Surface Mediated Organometallic Reaction. *European Journal of Inorganic Chemistry* **2003**, *2003*, 610-617.

(203) Li, Y.; Lai, G.-H.; Zhou, R.-X. Carbon nanotubes supported Pt–Ni catalysts and their properties for the liquid phase hydrogenation of cinnamaldehyde to hydrocinnamaldehyde. *Applied surface science* **2007**, *253*, 4978-4984.

(204) Yan, K.; Lafleur, T.; Liao, J. Facile synthesis of palladium nanoparticles supported on multi-walled carbon nanotube for efficient hydrogenation of biomass-derived levulinic acid. *Journal of Nanoparticle Research* **2013**, *15*, 1906.

(205) Selva, M.; Gottardo, M.; Perosa, A. Upgrade of Biomass-Derived Levulinic Acid via Ru/C-Catalyzed Hydrogenation to γ-Valerolactone in Aqueous–Organic–Ionic Liquids Multiphase Systems. *ACS Sustainable Chemistry & Engineering* **2013**, *1*, 180-189.

(206) Kang, J.; Zhang, S.; Zhang, Q.; Wang, Y. Ruthenium Nanoparticles Supported on Carbon Nanotubes as Efficient Catalysts for Selective Conversion of Synthesis Gas to Diesel Fuel. *Angewandte Chemie* **2009**, *121*, 2603-2606.

(207) Vu, H.; Gonçalves, F.; Philippe, R.; Lamouroux, E.; Corrias, M.; Kihn, Y.; Plee, D.; Kalck, P.; Serp, P. Bimetallic catalysis on carbon nanotubes for the selective hydrogenation of cinnamaldehyde. *Journal of Catalysis* **2006**, *240*, 18-22.

(208) Yin, S.-F.; Zhang, Q.-H.; Xu, B.-Q.; Zhu, W.-X.; Ng, C.-F.; Au, C.-T. Investigation on the catalysis of COx-free hydrogen generation from ammonia. *Journal of Catalysis* **2004**, *224*, 384-396.

(209) Oresmaa, L.; Moreno, M. A.; Jakonen, M.; Suvanto, S.; Haukka, M. Catalytic activity of linear chain ruthenium carbonyl polymer [Ru(CO)4]n in 1-hexene hydroformylation. *Applied Catalysis A: General* **2009**, *353*, 113-116.

(210) Takeda, Y.; Shoji, T.; Watanabe, H.; Tamura, M.; Nakagawa, Y.; Okumura, K.; Tomishige, K. Inside Back Cover: Selective Hydrogenation of Lactic Acid to 1,2-Propanediol over Highly Active Ruthenium–Molybdenum Oxide Catalysts (ChemSusChem 7/2015). *ChemSusChem* **2015**, *8*, 1287-1287.

(211) Chen, L.; Zhu, Y.; Zheng, H.; Zhang, C.; Zhang, B.; Li, Y. Aqueous-phase hydrodeoxygenation of carboxylic acids to alcohols or alkanes over supported Ru catalysts. *Journal of Molecular Catalysis A: Chemical* **2011**, *351*, 217-227.

(212) Guo, S.; Pan, X.; Gao, H.; Yang, Z.; Zhao, J.; Bao, X. Probing the electronic effect of carbon nanotubes in catalysis: NH3 synthesis with Ru nanoparticles. *Chemistry–A European Journal* **2010**, *16*, 5379-5384.

(213) Ran, M.; Liu, Y.; Chu, W.; Borgna, A. Enhanced Conversion of Cellobiose to Sugar Alcohols by Controlled Dispersion of Ruthenium Nanoparticles Inside Carbon Nanotube Channels. *Catalysis Letters* **2013**, *143*, 1139-1144.

(214) Guan, Z.; Lu, S.; Li, C. Enantioselective hydrogenation of α,β-unsaturated carboxylic acid over cinchonidine-modified Pd nanoparticles confined in carbon nanotubes. *Journal of Catalysis* **2014**, *311*, 1-5.

(215) Ma, H.; Wang, L.; Chen, L.; Dong, C.; Yu, W.; Huang, T.; Qian, Y. Pt nanoparticles deposited over carbon nanotubes for selective hydrogenation of cinnamaldehyde. *Catalysis Communications* **2007**, *8*, 452-456.

(216) Castillejos, E.; Debouttière, P.-J.; Roiban, L.; Solhy, A.; Martinez, V.; Kihn, Y.; Ersen, O.; Philippot, K.; Chaudret, B.; Serp, P. An Efficient Strategy to Drive Nanoparticles into Carbon Nanotubes and the Remarkable Effect of Confinement on Their Catalytic Performance. *Angewandte Chemie* **2009**, *121*, 2567-2571.

(217) Rossi, M. P.; Ye, H.; Gogotsi, Y.; Babu, S.; Ndungu, P.; Bradley, J.-C. Environmental Scanning Electron Microscopy Study of Water in Carbon Nanopipes. *Nano Letters* **2004**, *4*, 989-993.

(218) Park, Y. S.; Choi, Y. C.; Kim, K. S.; Chung, D.-C.; Bae, D. J.; An, K. H.; Lim, S. C.; Zhu, X. Y.; Lee, Y. H. High yield purification of multiwalled carbon nanotubes by selective oxidation during thermal annealing. *Carbon* **2001**, *39*, 655-661.

(219) Hou, P.-X.; Liu, C.; Cheng, H.-M. Purification of carbon nanotubes. *Carbon* **2008**, *46*, 2003-2025.

(220) Hou, P. X.; Bai, S.; Yang, Q. H.; Liu, C.; Cheng, H. M. Multi-step purification of carbon nanotubes. *Carbon* **2002**, *40*, 81-85.

(221) Ko, C.-J.; Lee, C.-Y.; Ko, F.-H.; Chen, H.-L.; Chu, T.-C. Highly efficient microwave-assisted purification of multiwalled carbon nanotubes. *Microelectronic Engineering* **2004**, *73–74*, 570-577.

(222) Belin, T.; Epron, F. Characterization methods of carbon nanotubes: a review. *Materials Science and Engineering: B* **2005**, *119*, 105-118.

(223) Akbayrak, S.; Özkar, S. Ruthenium(0) Nanoparticles Supported on Multiwalled Carbon Nanotube As Highly Active Catalyst for Hydrogen Generation from Ammonia–Borane. *ACS Applied Materials & Interfaces* **2012**, *4*, 6302-6310.

(224) Sun, Z.; Zhang, X.; Na; Liu, Z.; Han, B.; An, G. Synthesis of ZrO2−Carbon Nanotube Composites and Their Application as Chemiluminescent Sensor Material for Ethanol. *The Journal of Physical Chemistry B* **2006**, *110*, 13410-13414.

(225) Liu, J.; Bai, P.; Zhao, X. Ruthenium nanoparticles embedded in mesoporous carbon microfibers: preparation, characterization and catalytic properties in the hydrogenation of D-glucose. *Physical Chemistry Chemical Physics* **2011**, *13*, 3758-3763.

(226) Li, S.; Wang, X.; Liu, X.; Xu, G.; Han, S.; Mu, X. Aqueous-phase hydrogenation of biomass-derived itaconic acid to methyl-γ-butyrolactone over Pd/C catalysts: Effect of pretreatments of active carbon. *Catalysis Communications* **2015**, *61*, 92-96.

(227) Kim, M.-C.; Kim, T.-W.; Kim, H. J.; Kim, C.-U.; Bae, J. W. Aqueous phase reforming of polyols for hydrogen production using supported PtFe bimetallic catalysts. *Renewable Energy* **2016**, *95*, 396-403.

(228) Checa, M.; Marinas, A.; Marinas, J. M.; Urbano, F. J. Deactivation study of supported Pt catalyst on glycerol hydrogenolysis. *Applied Catalysis A: General* **2015**, *507*, 34-43.

(229) Soni, K.; Shekar, S. C.; Singh, B.; Agrawal, A. Catalytic oxidation of CO in presence of ozone over supported palladium catalysts. **2014**.

(230) Verboekend, D.; Thomas, K.; Milina, M.; Mitchell, S.; Perez-Ramirez, J.; Gilson, J.-P. Towards more efficient monodimensional zeolite catalysts: n-alkane hydro-isomerisation on hierarchical ZSM-22. *Catalysis Science & Technology* **2011**, *1*, 1331-1335.

(231) Wang, L.; Chen, J.; Rudolph, V.; Zhu, Z. Nanotubules-supported Ru nanoparticles for preferential CO oxidation in H2-rich stream. *Advanced Powder Technology* **2012**, *23*, 465-471.

(232) Yang, X.; Wang, X.; Qiu, J. Aerobic oxidation of alcohols over carbon nanotube-supported Ru catalysts assembled at the interfaces of emulsion droplets. *Applied Catalysis A: General* **2010**, *382*, 131-137.

(233) Machado, B. F.; Oubenali, M.; Axet, M. R.; Nguyen, T. T.; Tunckol, M.; Girleanu, M.; Ersen, O.; Gerber, I. C.; Serp, P. Understanding the surface chemistry of carbon nanotubes: Toward a rational design of Ru nanocatalysts. *Journal of Catalysis* **2014**, *309*, 185-198.

(234) Betancourt, P.; Rives, A.; Hubaut, R.; Scott, C. E.; Goldwasser, J. A study of the ruthenium–alumina system. *Applied Catalysis A: General* **1998**, *170*, 307-314.

(235) Li, G.; Li, W.; Zhang, H.; Pu, Y.; Sun, M.; Zhang, J. Non-mercury catalytic acetylene hydrochlorination over Ru catalysts enhanced by carbon nanotubes. *RSC Advances* **2015**, *5*, 9002-9008.

(236) Priecel, P.; Endot, N. A.; Carà, P. D.; Lopez-Sanchez, J. A. Fast Catalytic Hydrogenation of 2,5-Hydroxymethylfurfural to 2,5-Dimethylfuran with Ruthenium on Carbon Nanotubes. *Industrial & Engineering Chemistry Research* **2018**, *57*, 1991-2002.

(237) Martin-Martinez, M.; Gómez-Sainero, L. M.; Bedia, J.; Arevalo-Bastante, A.; Rodriguez, J. J. Enhanced activity of carbon-supported Pd–Pt catalysts in the hydrodechlorination of dichloromethane. *Applied Catalysis B: Environmental* **2016**, *184*, 55-63.

(238) Li, F.; Cao, B.; Zhu, W.; Song, H.; Wang, K.; Li, C. Hydrogenation of Phenol over Pt/CNTs: The Effects of Pt Loading and Reaction Solvents. *Catalysts* **2017**, *7*, 145.

(239) Li, C.; Shao, Z.; Pang, M.; Williams, C. T.; Zhang, X.; Liang, C. Carbon Nanotubes Supported Mono- and Bimetallic Pt and Ru Catalysts for Selective Hydrogenation of Phenylacetylene. *Industrial & Engineering Chemistry Research* **2012**, *51*, 4934-4941.

(240) Morgan, D. J. Resolving ruthenium: XPS studies of common ruthenium materials. *Surface and Interface Analysis* **2015**, *47*, 1072-1079.

(241) Larichev, Y. V.; Moroz, B. L.; Bukhtiyarov, V. I. Electronic state of ruthenium deposited onto oxide supports: an XPS study taking into account the final state effects. *Applied Surface Science* **2011**, *258*, 1541-1550.

(242) Li, J.; Tian, W.-p.; Shi, L. Hydrogenation of Maleic Anhydride to Succinic Anhydride over Ni/HY-Al2O3. *Industrial & Engineering Chemistry Research* **2010**, *49*, 11837-11840.

(243) Wiebe, R.; Gaddy, V. L. The Solubility of Hydrogen in Water at 0, 50, 75 and 100° from 25 to 1000 Atmospheres. *Journal of the American Chemical Society* **1934**, *56*, 76-79.

(244) Murahashi, S.-I.: *Ruthenium in organic synthesis*; John Wiley & Sons, 2006.

(245) Brunner, E. Solubility of hydrogen in 10 organic solvents at 298.15, 323.15, and 373.15 K. *Journal of Chemical & Engineering Data* **1985**, *30*, 269-273.

(246) Gevantman, L. Solubility of selected gases in water. *Nitric oxide (NO)* **2000**, *308*, 10-14.

(247) d Angelo, J.; Francesconi, A. Salt effect in the solubility of hydrogen in n-alcohols at pressures up to 10 MPa and temperatures up to 498.15 K. *Brazilian Journal of Chemical Engineering* **2000**, *17*, 497-506.

(248) Wypych, G.: *Handbook of solvents*; ChemTec Publishing, 2001.

(249) Galvagno, S.; Capannelli, G.; Neri, G.; Donato, A.; Pietropaolo, R. Hydrogenation of cinnamaldehyde over Ru/C catalysts: effect of Ru particle size. *Journal of molecular catalysis* **1991**, *64*, 237-246.

(250) Guldi, D. M.; Martín, N.: *Carbon nanotubes and related structures: synthesis, characterization, functionalization, and applications*; John Wiley & Sons, 2010.

(251) Pan, X.; Bao, X. The Effects of Confinement inside Carbon Nanotubes on Catalysis. *Acc. Chem. Res.* **2011**, *44*, 553-562.

(252) Zhang, H.; Wang, J.; Zhang, Y.; Jiao, Y.; Ren, C.; Gong, M.; Chen, Y. A study on H2-TPR of Pt/Ce0.27Zr0.73O2 and Pt/Ce0.27Zr0.70La0.03Ox for soot oxidation. *Applied Surface Science* **2016**, *377*, 48-55.

(253) Priecel, P.; Endot, N. A.; Carà, P. D.; Lopez-Sanchez, J. A. Fast catalytic hydrogenation of 2,5-hydroxymethylfurfural to 2,5-dimethylfuran with ruthenium on carbon nanotubes. *Ind. Eng. Chem. Res.* **2018**.

(254) Englisch, M.; Jentys, A.; Lercher, J. A. Structure Sensitivity of the Hydrogenation of Crotonaldehyde over Pt/SiO2and Pt/TiO2. *J. Catal.* **1997**, *166*, 25-35.

(255) Koningsberger, D. C.; de Graaf, J.; Mojet, B. L.; Ramaker, D. E.; Miller, J. T. The metal–support interaction in Pt/Y zeolite: evidence for a shift in energy of metal d-valence orbitals by Pt–H shape resonance and atomic XAFS spectroscopy. *Appl. Catal. A Gen.* **2000**, *191*, 205-220.

(256) Mojet, B. L.; Miller, J. T.; Ramaker, D. E.; Koningsberger, D. C. A New Model Describing the Metal–Support Interaction in Noble Metal Catalysts. *J. Catal.* **1999**, *186*, 373-386.

(257) Ramaker, D. E.; de Graaf, J.; van Veen, J. A. R.; Koningsberger, D. C. Nature of the Metal–Support Interaction in Supported Pt Catalysts: Shift in Pt Valence Orbital Energy and Charge Rearrangement. *J. Catal.* **2001**, *203*, 7-17.

(258) Toebes, M. L.; Prinsloo, F. F.; Bitter, J. H.; van Dillen, A. J.; de Jong, K. P. Influence of oxygen-containing surface groups on the activity and selectivity of carbon nanofiber-supported ruthenium catalysts in the hydrogenation of cinnamaldehyde. *J. Catal.* **2003**, *214*, 78-87.

(259) Nieto, E.; Ruiz, A.; Rodriguez-Ramos, I.: *Modification of the stereoselectivity in the citral hydrogenation by application of carbon nanotubes as support of the Pt particles*, 2006; Vol. 44.

(260) Bagheri, S.; Muhd Julkapli, N.; Bee Abd Hamid, S. Titanium Dioxide as a Catalyst Support in Heterogeneous Catalysis. *The Scientific World Journal* **2014**, *2014*.

(261) Zhu, Z.; Lu, G.; Guo, Y.; Guo, Y.; Zhang, Z.; Wang, Y. Influences of Pd precursors and preparation method on the catalytic performances of Pd-only close-coupled catalysts. *Journal of Industrial and Engineering Chemistry* **2012**, *18*, 2135-2140.

(262) Zhang, C.; Chen, L.; Cheng, H.; Zhu, X.; Qi, Z. Atomically dispersed Pd catalysts for the selective hydrogenation of succinic acid to γ-butyrolactone. *Catalysis Today* **2016**, *276*, 55-61.

(263) Bartholomew, C. H. Mechanisms of catalyst deactivation. *Applied Catalysis A: General* **2001**, *212*, 17-60.

(264) Su, F.; Lv, L.; Lee, F. Y.; Liu, T.; Cooper, A. I.; Zhao, X. S. Thermally Reduced Ruthenium Nanoparticles as a Highly Active Heterogeneous Catalyst for Hydrogenation of Monoaromatics. *Journal of the American Chemical Society* **2007**, *129*, 14213-14223.

(265) Dani, M.; RUGGIERO, G.; PERINI, D.; BIANCHI, A.; Novamont S.P.A.; Genomatica Inc. Process for the production of 1,4-butanediol. *Process for the production of 1,4-butanediol* **2015**, *WO2015158716 A1*.

(266) Burgard, A.; Burk, M. J.; Osterhout, R.; Van Dien, S.; Yim, H. Development of a commercial scale process for production of 1,4-butanediol from sugar. *Current Opinion in Biotechnology* **2016**, *42*, 118-125.

(267) Huang, J.; Dai, W.-L.; Li, H.; Fan, K. Au/TiO2 as high efficient catalyst for the selective oxidative cyclization of 1,4-butanediol to γ-butyrolactone. *Journal of Catalysis* **2007**, *252*, 69-76.

(268) Hunter, S. E.; Ehrenberger, C. E.; Savage, P. E. Kinetics and Mechanism of Tetrahydrofuran Synthesis via 1,4-Butanediol Dehydration in High-Temperature Water. *The Journal of Organic Chemistry* **2006**, *71*, 6229-6239.

(269) Küksal, A.; Klemm, E.; Emig, G. Reaction kinetics of the liquid-phase hydrogenation of succinic anhydride on CuZnO-catalysts with varying copper-to-zinc ratios in a three-phase slurry reactor. *Applied Catalysis A: General* **2002**, *228*, 237-251.

(270) Ichikawa, N.; Sato, S.; Takahashi, R.; Sodesawa, T.; Inui, K. Dehydrogenative cyclization of 1,4-butanediol over copper-based catalyst. *Journal of Molecular Catalysis A: Chemical* **2004**, *212*, 197-203.

(271) Carnahan, J.; Ford, T.; Gresham, W.; Grigsby, W.; Hager, G. Ruthenium-catalyzed hydrogenation of acids to alcohols. *Journal of the American Chemical Society* **1955**, *77*, 3766-3768.

(272) Deshpande, R.; Buwa, V.; Rode, C.; Chaudhari, R.; Mills, P. Tailoring of activity and selectivity using bimetallic catalyst in hydrogenation of succinic acid. *Catalysis Communications* **2002**, *3*, 269-274.

(273) Hong, U. G.; Hwang, S.; Seo, J. G.; Yi, J.; Song, I. K. Hydrogenation of Succinic Acid to γ-Butyrolactone over Palladium Catalyst Supported on Mesoporous Alumina Xerogel. *Catalysis letters* **2010**, *138*, 28-33.

(274) Hong, U. G.; Hwang, S.; Seo, J. G.; Lee, J.; Song, I. K. Hydrogenation of succinic acid to γ-butyrolactone (GBL) over palladium catalyst supported on alumina xerogel: Effect of acid density of the catalyst. *Journal of Industrial and Engineering Chemistry* **2011**, *17*, 316-320.

(275) Croy, J. R.; Mostafa, S.; Hickman, L.; Heinrich, H.; Cuenya, B. R. Bimetallic Pt-Metal catalysts for the decomposition of methanol: Effect of secondary metal on the oxidation state, activity, and selectivity of Pt. *Applied Catalysis A: General* **2008**, *350*, 207-216.

(276) Jordão, M. H.; Simões, V.; Cardoso, D. Zeolite supported Pt-Ni catalysts in n-hexane isomerization. *Applied Catalysis A: General* **2007**, *319*, 1-6.

(277) Shao, Z.; Li, C.; Di, X.; Xiao, Z.; Liang, C. Aqueous-Phase Hydrogenation of Succinic Acid to γ-Butyrolactone and Tetrahydrofuran over Pd/C, Re/C, and Pd–Re/C Catalysts. *Industrial & Engineering Chemistry Research* **2014**, *53*, 9638-9645.

(278) Coloma, F.; Sepúlveda-Escribano, A.; Fierro, J.; Rodriguez-Reinoso, F. Crotonaldehyde hydrogenation over bimetallic Pt· Sn catalysts supported on pregraphitized carbon black. Effect of the preparation method. *Applied Catalysis A: General* **1996**, *148*, 63-80.

(279) Torres, G. C.; Ledesma, S. D.; Jablonski, E. L.; de Miguel, S. R.; Scelza, O. A. Hydrogenation of carvone on Pt–Sn/Al 2 O 3 catalysts. *Catalysis today* **1999**, *48*, 65-72.

(280) Recchia, S.; Dossi, C.; Poli, N.; Fusi, A.; Sordelli, L.; Psaro, R. Outstanding performances of magnesia-supported platinum–tin catalysts for citral selective hydrogenation. *Journal of Catalysis* **1999**, *184*, 1-4.

(281) De la Hoz, A.; Diaz-Ortiz, A.; Moreno, A. Microwaves in organic synthesis. Thermal and non-thermal microwave effects. *Chemical Society Reviews* **2005**, *34*, 164-178.

(282) Zhang, S.; Duan, X.; Ye, L.; Lin, H.; Xie, Z.; Yuan, Y. Production of ethanol by gas phase hydrogenation of acetic acid over carbon nanotube-supported Pt–Sn nanoparticles. *Catalysis Today* **2013**, *215*, 260-266.

(283) Mendes, M. J.; Santos, O. A. A.; Jordão, E.; Silva, A. M. Hydrogenation of oleic acid over ruthenium catalysts. *Applied Catalysis A: General* **2001**, *217*, 253-262.

(284) dos Santos, S. M.; Silva, A. M.; Jordão, E.; Fraga, M. A. Performance of RuSn catalysts supported on different oxides in the selective hydrogenation of dimethyl adipate. *Catalysis Today* **2005**, *107*, 250-257.

(285) Coq, B.; Kumbhar, P.; Moreau, C.; Moreau, P.; Warawdekar, M. Liquid phase hydrogenation of cinnamaldehyde over supported ruthenium catalysts: influence of particle size, bimetallics and nature of support. *Journal of molecular catalysis* **1993**, *85*, 215-228.

(286) Pouilloux, Y.; Autin, F.; Guimon, C.; Barrault, J. Hydrogenation of Fatty Esters over Ruthenium–Tin Catalysts; Characterization and Identification of Active Centers. *Journal of Catalysis* **1998**, *176*, 215-224.

(287) Ito, Y.; Kawamoto, H.; Saka, S. Efficient and selective hydrogenation of aqueous acetic acid on Ru–Sn/TiO2 for bioethanol production from lignocellulosics. *Fuel* **2016**, *178*, 118-123.

(288) Musci, J. J.; Merlo, A. B.; Casella, M. L. Aqueous phase hydrogenation of furfural using carbon-supported Ru and RuSn catalysts. *Catalysis Today* **2017**, *296*, 43-50.

(289) Galvagno, S.; Donato, A.; Neri, G.; Pietropaolo, R.; Capannelli, G. Selective hydrogenation of cinnamaldehyde over Ru—Sn catalysts. *Journal of Molecular Catalysis* **1993**, *78*, 227-236.

(290) KLUSOŇ, P.; ČERVENÝ, L. Ru-Sn CATALYST-A NEW PROMISING SYSTEM FOR SELECTIVE HVDROr^ FNATTON OF A TARRONVT íiROTTP. *Chem. Listy* **1997**, *91*, 100-104.

(291) Lee, J.-M.; Upare, P. P.; Chang, J.-S.; Hwang, Y. K.; Lee, J. H.; Hwang, D. W.; Hong, D.-Y.; Lee, S. H.; Jeong, M.-G.; Kim, Y. D.; Kwon, Y.-U. Direct Hydrogenation of Biomass-Derived Butyric Acid to n-Butanol over a Ruthenium–Tin Bimetallic Catalyst. *ChemSusChem* **2014**, *7*, 2998-3001.

(292) Wettstein, S. G.; Bond, J. Q.; Alonso, D. M.; Pham, H. N.; Datye, A. K.; Dumesic, J. A. RuSn bimetallic catalysts for selective hydrogenation of levulinic acid to γ-valerolactone. *Applied Catalysis B: Environmental* **2012**, *117–118*, 321-329.

(293) Echeverri, D. A.; Marín, J. M.; Restrepo, G. M.; Rios, L. A. Characterization and carbonylic hydrogenation of methyl oleate over Ru-Sn/Al 2 O 3: Effects of metal precursor and chlorine removal. *Applied Catalysis A: General* **2009**, *366*, 342-347.

(294) Xu, T.; Zhang, Q.; Cen, J.; Xiang, Y.; Li, X. Selectivity tailoring of Pd/CNTs in phenol hydrogenation by surface modification: Role of CO oxygen species. *Applied Surface Science* **2015**, *324*, 634-639.

(295) Tahara, K.; Nagahara, E.; Itoi, Y.; Nishiyama, S.; Tsuruya, S.; Masai, M. Liquid-phase hydrogenation of car□ylic acid on supported bimetallic RuSn-Alumina catalysts. *Applied Catalysis A: General* **1997**, *154*, 75-86.

(296) Chantaravitoon, P.; Chavadej, S.; Schwank, J. Pt–Sn/Al2O3 catalysts: effect of catalyst preparation and chemisorption methods on H2 and O2 uptake. *Chemical Engineering Journal* **2004**, *98*, 99-104.

(297) Zhu, Z.; Lu, Z.; Li, B.; Guo, S. Characterization of bimetallic Ru-Sn supported catalysts and hydrogenation of 1,4-cyclohexanedicarboxylic acid. *Applied Catalysis A: General* **2006**, *302*, 208-214.

(298) Iqbal, S.; Kondrat, S. A.; Jones, D. R.; Schoenmakers, D. C.; Edwards, J. K.; Lu, L.; Yeo, B. R.; Wells, P. P.; Gibson, E. K.; Morgan, D. J.; Kiely, C. J.; Hutchings, G. J. Ruthenium Nanoparticles Supported on Carbon: An Active Catalyst for the Hydrogenation of Lactic Acid to 1,2-Propanediol. *ACS Catalysis* **2015**, *5*, 5047-5059.

(299) Luo, Z.; Bing, Q.; Kong, J.; Liu, J.-y.; Zhao, C. Mechanism of supported Ru3Sn7 nanocluster-catalyzed selective hydrogenation of coconut oil to fatty alcohols. *Catalysis Science & Technology* **2018**.

(300) Patt, J.; Moon, D. J.; Phillips, C.; Thompson, L. Molybdenum carbide catalysts for water–gas shift. *Catalysis Letters* **2000**, *65*, 193-195.

(301) Bariås, O. A.; Holmen, A.; Blekkan, E. A. Propane Dehydrogenation over Supported Pt and Pt–Sn Catalysts: Catalyst Preparation, Characterization, and Activity Measurements. *Journal of Catalysis* **1996**, *158*, 1-12.

(302) Arason, K. M.; Bergmeier, S. C. The synthesis of succinic acids and derivatives. A review. *Organic preparations and procedures international* **2002**, *34*, 337-366.

(303) Serrano-Ruiz, J. C.; Sepúlveda-Escribano, A.; Rodríguez-Reinoso, F.; Duprez, D. Pt–Sn catalysts supported on highly-dispersed ceria on carbon: Application to citral hydrogenation. *Journal of Molecular Catalysis A: Chemical* **2007**, *268*, 227-234.

(304) Hara, Y.; Endou, K. The drastic effect of platinum on carbon-supported ruthenium-tin catalysts used for hydrogenation reactions of carboxylic acids. *Applied Catalysis A: General* **2003**, *239*, 181-195.

(305) Mitsui, T.; Tsutsui, K.; Matsui, T.; Kikuchi, R.; Eguchi, K. Support effect on complete oxidation of volatile organic compounds over Ru catalysts. *Applied Catalysis B: Environmental* **2008**, *81*, 56-63.

(306) Murphy, V. J.; Dias, E. L.; Shoemaker, J. A.: Production of 1, 6-hexanediol from adipic acid. Google Patents, 2014.

(307) Cavani, F.; Albonetti, S.; Basile, F.; Gandini, A.: *Chemicals and Fuels from Bio-Based Building Blocks*; John Wiley & Sons, 2016.

(308) Van de Vyver, S.; Roman-Leshkov, Y. Emerging catalytic processes for the production of adipic acid. *Catalysis Science & Technology* **2013**, *3*, 1465-1479.

(309) Bos, A. N. R.; Westerterp, K. R. Mechanism and kinetics of the selective hydrogenation of ethyne and ethene. *Chemical Engineering and Processing: Process Intensification* **1993**, *32*, 1-7.

(310) Liao, H.-G.; Xiao, Y.-J.; Zhang, H.-K.; Liu, P.-L.; You, K.-Y.; Wei, C.; Luo, H. a. Hydrogenation of nitrocyclohexane to cyclohexanone oxime over Pd/CNT catalyst under mild conditions. *Catalysis Communications* **2012**, *19*, 80-84.

(311) He, T.; Liu, L.; Wu, G.; Chen, P. Covalent triazine framework-supported palladium nanoparticles for catalytic hydrogenation of N-heterocycles. *Journal of Materials Chemistry A* **2015**, *3*, 16235-16241.

(312) Eslava, J. L.; Sun, X.; Gascon, J.; Kapteijn, F.; Rodriguez-Ramos, I. Ruthenium particle size and cesium promotion effects in Fischer-Tropsch synthesis over high-surface-area graphite supported catalysts. *Catalysis Science & Technology* **2017**, *7*, 1235-1244.

(313) Manyar, H. G.; Paun, C.; Pilus, R.; Rooney, D. W.; Thompson, J. M.; Hardacre, C. Highly selective and efficient hydrogenation of carboxylic acids to alcohols using titania supported Pt catalysts. *Chemical Communications* **2010**, *46*, 6279-6281.

(314) Nomanbhay, S.; Ong, M. Y. A review of microwave-assisted reactions for biodiesel production. *Bioengineering* **2017**, *4*, 57.

(315) Chemat, F.; Esveld, D. C.; Poux, M.; Di-Martino, J. L. The Role of Selective Heating in the Microwave Activation of Heterogeneous Catmnsis Reactions Using a Continuous Microwave Reactor. *Journal of Microwave Power and Electromagnetic Energy* **1998**, *33*, 88-94.

(316) Girisuta, B.; Heeres, H. J.: Levulinic Acid from Biomass: Synthesis and Applications. In *Production of Platform Chemicals from Sustainable Resources*; Fang, Z., Smith, J. R. L., Qi, X., Eds.; Springer Singapore: Singapore, 2017; pp 143-169.

(317) Galletti, A. M. R.; Antonetti, C.; De Luise, V.; Martinelli, M. A sustainable process for the production of [gamma]-valerolactone by hydrogenation of biomass-derived levulinic acid. *Green Chemistry* **2012**, *14*, 688-694.

(318) Yan, K.; Jarvis, C.; Gu, J.; Yan, Y. Production and catalytic transformation of levulinic acid: A platform for speciality chemicals and fuels. *Renewable and Sustainable Energy Reviews* **2015**, *51*, 986-997.

(319) Piskun, A.; de Haan, J.; Wilbers, E.; van de Bovenkamp, H.; Tang, Z.; Heeres, H. Hydrogenation of levulinic acid to γ-valerolactone in water using millimeter sized supported Ru catalysts in a packed bed reactor. *Acs Sustainable Chemistry & Engineering* **2016**, *4*, 2939-2950.

(320) Upare, P. P.; Lee, J.-M.; Hwang, D. W.; Halligudi, S. B.; Hwang, Y. K.; Chang, J.-S.; Upare, P. P.; Lee, J.-M.; Hwang, D. W.; Halligudi, S. B.; Hwang, Y. K.; Chang, J.-S. Selective hydrogenation of levulinic acid to γ-valerolactone over carbon-supported noble metal catalysts. *Journal of Industrial and Engineering Chemistry* **2011**, *17*, 287.

(321) Bermudez, J. M.; Menendez, J. A.; Romero, A. A.; Serrano, E.; Garcia-Martinez, J.; Luque, R. Continuous flow nanocatalysis: reaction pathways in the conversion of levulinic acid to valuable chemicals. *Green Chemistry* **2013**, *15*, 2786-2792.

(322) Lu, F.; Yu, C.; Meng, X.; Chen, G.; Zhao, P. Degradation of highly concentrated organic compounds over a supported Ru-Cu bimetallic catalyst. *New Journal of Chemistry* **2017**, *41*, 3280-3289.

(323) Lian, J.; Ma, J.; Duan, X.; Kim, T.; Li, H.; Zheng, W. One-step ionothermal synthesis of [gamma]-Al2O3 mesoporous nanoflakes at low temperature. *Chemical Communications* **2010**, *46*, 2650-2652.

(324) Li, Z. Q.; Lu, C. J.; Xia, Z. P.; Zhou, Y.; Luo, Z. X-ray diffraction patterns of graphite and turbostratic carbon. *Carbon* **2007**, *45*, 1686-1695.

(325) Guo, Z.; Chen, Y.; Li, L.; Wang, X.; Haller, G. L.; Yang, Y. Carbon nanotube-supported Pt-based bimetallic catalysts prepared by a microwave-assisted polyol reduction method and their catalytic applications in the selective hydrogenation. *Journal of Catalysis* **2010**, *276*, 314-326.

(326) Pan, J.; Li, J.; Wang, C.; Yang, Z. Multi-wall carbon nanotubes supported ruthenium for glucose hydrogenation to sorbitol. *Reaction Kinetics and Catalysis Letters* **2007**, *90*, 233-242.

(327) Li, B.; Wang, C.; Yi, G.; Lin, H.; Yuan, Y. Enhanced performance of Ru nanoparticles confined in carbon nanotubes for CO preferential oxidation in a H2-rich stream. *Catalysis Today* **2011**, *164*, 74-79.

(328) Burch, R.; Paun, C.; Cao, X. M.; Crawford, P.; Goodrich, P.; Hardacre, C.; Hu, P.; McLaughlin, L.; Sá, J.; Thompson, J. M. Catalytic hydrogenation of tertiary amides at low temperatures and pressures using bimetallic Pt/Re-based catalysts. *Journal of Catalysis* **2011**, *283*, 89-97.

(329) Ge, C.; Li, Y.; Zhao, J.; Zhou, R. Carbon nanotubes supported palladium catalysts for selective hydrogenation of cinnamaldehyde under atmospheric pressure. **2010**.

(330) Tidahy, H. L.; Siffert, S.; Lamonier, J. F.; Zhilinskaya, E. A.; Aboukaïs, A.; Yuan, Z. Y.; Vantomme, A.; Su, B. L.; Canet, X.; De Weireld, G.; Frère, M.; N'Guyen, T. B.; Giraudon, J. M.; Leclercq, G. New Pd/hierarchical macro-mesoporous ZrO2, TiO2 and ZrO2-TiO2 catalysts for VOCs total oxidation. *Applied Catalysis A: General* **2006**, *310*, 61-69.

(331) Roth, W. J.; Gil, B.; Makowski, W.; Marszalek, B.; Eliášová, P. Layer like porous materials with hierarchical structure. *Chemical Society Reviews* **2016**, *45*, 3400-3438.

(332) Ingham, D. B.; Pop, I.: *Transport phenomena in porous media III*; Elsevier, 2005; Vol. 3.

(333) Ribeiro, L. S.; Delgado, J. J.; de Melo Orfao, J. J.; Ribeiro Pereira, M. F. A one-pot method for the enhanced production of xylitol directly from hemicellulose (corncob xylan). *RSC Advances* **2016**, *6*, 95320-95327.

(334) Sing, K. S. Reporting physisorption data for gas/solid systems with special reference to the determination of surface area and porosity (Recommendations 1984). *Pure and applied chemistry* **1985**, *57*, 603-619.

(335) Ribeiro, L. S.; Delgado, J. J.; de Melo Órfão, J. J.; Pereira, M. F. R. Direct conversion of cellulose to sorbitol over ruthenium catalysts: Influence of the support. *Catalysis Today* **2017**, *279*, 244-251.

(336) Liu, X.; Zeng, J.; Wang, J.; Shi, W.; Zhu, T. Catalytic oxidation of methyl bromide using ruthenium-based catalysts. *Catalysis Science & Technology* **2016**, *6*, 4337-4344.

(337) García-García, F. R.; Álvarez-Rodríguez, J.; Rodríguez-Ramos, I.; Guerrero-Ruiz, A. The use of carbon nanotubes with and without nitrogen doping as support for ruthenium catalysts in the ammonia decomposition reaction. *Carbon* **2010**, *48*, 267-276.

(338) Escandón, L. S.; Ordóñez, S.; Vega, A.; Díez, F. V. Oxidation of methane over palladium catalysts: effect of the support. *Chemosphere* **2005**, *58*, 9-17.

(339) Toebes, M. L.; Nijhuis, T. A.; Hájek, J.; Bitter, J. H.; Van Dillen, A. J.; Murzin, D. Y.; de Jong, K. P. Support effects in hydrogenation of cinnamaldehyde over carbon nanofiber-supported platinum catalysts: Kinetic modeling. *Chemical Engineering Science* **2005**, *60*, 5682-5695.

(340) Agostini, G.; Groppo, E.; Piovano, A.; Pellegrini, R.; Leofanti, G.; Lamberti, C. Preparation of Supported Pd Catalysts: From the Pd Precursor Solution to the Deposited Pd2+ Phase. *Langmuir* **2010**, *26*, 11204-11211.

(341) Jiang, Z.; Lan, G.; Liu, X.; Tang, H.; Li, Y. Solid state synthesis of Ru-MC with highly dispersed semi-embedded ruthenium nanoparticles in a porous carbon framework for benzoic acid hydrogenation. *Catalysis Science & Technology* **2016**, *6*, 7259-7266.

(342) Wang, M.; Li, F.; Zhang, R. Study on catalytic hydrogenation properties and thermal stability of amorphous NiB alloy supported on carbon nanotubes. *Catalysis Today* **2004**, *93-95*, 603-606.

(343) Jahjah, M.; Kihn, Y.; Teuma, E.; Gómez, M. Ruthenium nanoparticles supported on multi-walled carbon nanotubes: Highly effective catalytic system for hydrogenation processes. *Journal of Molecular Catalysis A: Chemical* **2010**, *332*, 106-112.

(344) He, L.; Weniger, F.; Neumann, H.; Beller, M. Synthesis, Characterization, and Application of Metal Nanoparticles Supported on Nitrogen-Doped Carbon: Catalysis beyond Electrochemistry. *Angewandte Chemie International Edition* **2016**, *55*, 12582-12594.

(345) Bell, T. E.; Zhan, G.; Wu, K.; Zeng, H. C.; Torrente-Murciano, L. Modification of Ammonia Decomposition Activity of Ruthenium Nanoparticles by N-Doping of CNT Supports. *Top Catal* **2017**, *60*, 1251-1259.

(346) Amadou, J.; Chizari, K.; Houllé, M.; Janowska, I.; Ersen, O.; Bégin, D.; Pham-Huu, C. N-doped carbon nanotubes for liquid-phase CC bond hydrogenation. *Catalysis Today* **2008**, *138*, 62-68.